# THEORY OF STOCHASTIC LOCAL AREA CHANNEL MODELING FOR WIRELESS COMMUNICATIONS

by

Gregory D. Durgin

Final Dissertation submitted to the Faculty of the
Virginia Polytechnic Institute and State University
in partial fulfillment of the requirements for the degree of

DOCTOR OF PHILOSOPHY
in
Electrical Engineering

Theodore S. Rappaport(Chairman)
David A. de Wolf
Gary S. Brown
Jeffrey H. Reed
Werner Kohler
Robert J. Boyle

December 2000
Blacksburg, Virginia

Keywords: Fading, Mobile Radio Propagation, Wireless Communications

# THEORY OF STOCHASTIC LOCAL AREA CHANNEL MODELING FOR WIRELESS COMMUNICATIONS

Gregory D. Durgin

## (ABSTRACT)

This report was written to satisfy the **final dissertation** requirements toward a doctoral degree in electrical engineering. The dissertation outlines work accomplished in the pursuit of this degree. This report is also designed to be a general introduction to the concepts and techniques of small-scale radio channel modeling. At the present time, there does not exist a comprehensive introduction and overview of basic concepts in this field. Furthermore, as the wireless industry continues to mature and develop technology, the need is now greater than ever for more sophisticated channel modeling research.

Each chapter of this preliminary report is, in itself, a stand-alone topic in channel modeling theory. Culled from original reports and journal papers, each chapter makes a unique contribution to the field of channel modeling. Original contributions in this report include

- joint characterization of time-varying, space-varying, and frequency-varying channels under the rubric of *duality*
- rules and definitions for constructing channel models that solve *Maxwell's equations*
- overview of *probability density functions* that describe random small-scale fading
- techniques for modeling a small-scale radio channel using an *angle spectrum*
- overview of techniques for describing fading statistics in wireless channels
- results from a wideband spatio-temporal measurement campaign

Together, the chapters provide a cohesive overview of basic principles. The discussion of the wideband spatio-temporal measurement campaign at 1920 MHz makes an excellent case study in applied channel modeling and ties together much of the theory developed in this dissertation.

# Contents

# List of Tables

# List of Figures

# Acknowledgements

Any endeavor as large as a Ph.D. dissertation requires numerous contributions by people other than the Ph.D. candidate. This dissertation is no exception, as there are a number of organizations and people that must be acknowledged before a single technical detail can be discussed.

First, there is a long list of generous sponsors and contributors. The research in this dissertation was sponsored by a Bradley Fellowship in Electrical and Computer Engineering, the MPRG Industrial Affiliates Program, and ITT Defense & Electronics, Inc. The peer-to-peer measurement campaign could not have been performed without the generous assistance of MPRG students Vikas Kukshya, Jiun Siew, Erica Lau, Christopher Steger, Paulo Cardieri, Jason Aaron, and Bruce Puckett.

I also owe an extreme debt of gratitude to everyone on my Ph.D. committee. Three members in particular – Ted Rappaport, David de Wolf, and Gary Brown – contributed numerous technical criticisms, ideas, and suggestions that found their way into the final dissertation. I could not have asked for a more supportive (and knowledgeable) Ph.D. committee.

An equal debt of gratitude is owed to the extremely talented students and staff of the Mobile and Portable Radio Research Group of Virginia Tech. What wonderful people I have worked with over the years! There are three students I would like to single out for their help and devoted friendship throughout my dissertation: Neal Patwari, Hao Xu, and Bruce Puckett.

Finally, my deepest gratitude and sincerest love is owed to these three people: my mother Lisa, my father Dave, and my Lord and Savior Jesus Christ. A deep, loving relationship with each has provided all inspiration and direction in life.

# Chapter 1

# Introduction

There are few things in nature more unwieldy than the power-limited, space-varying, time-varying, frequency-varying *wireless channel*. Yet there is great reward for engineers who can overcome these limitations and transmit data through such a harsh environment. The explosive worldwide growth of personal communications services through the 1990's is a testament to the business opportunities that result from conquering the wireless channel. However, given the emergence of newer wireless systems that require more and more bandwidth, the task of conquering the wireless channel is becoming more difficult. This task requires a thorough background in wireless channel modeling.

The main purpose of this dissertation is to present a foundational, physically-based approach to modeling random behavior in wireless channels. Using sound principles in stochastic process theory, electromagnetic wave propagation, and wireless communications, this report develops a theoretical framework for characterizing stochastic local area radio channels. The theory is applicable to *any* type of wireless data transmission, regardless of bandwidth, carrier frequency, or environment of operation.

The final chapters of the dissertation deal with applied statistics and channel measurements. Specifically, results from a wideband spatio-temporal measurement campaign are presented that illuminate many of the concepts discussed in the previous chapters. The wideband channel measurement campaign was performed in the 1850-1990 MHz frequency bands on the campus of Virginia Tech. Using peer-to-peer configurations for transmitter and receiver antennas (height of 1.5m above ground), this measurement campaign produced results that characterize both frequency and spatial selectivity of locations. The results not only validate research concepts developed in this report, but will assist industry in developing wireless modems for peer-to-peer networks.

## 1.1 The Need for Improvement in Channel Modeling Theory

The theory that engineers use to measure and model wireless communications has changed very little over the last 30 years. The main reason for this stagnation of development may be summed up as follows: the current theory still works for wireless systems that have been deployed to date. Do not expect this statement to hold much longer. There are 6 current trends in wireless communications which emphasize the need for improved and expanded channel modeling theory.

### 1.1.1 Higher and Higher Data Rates

The capacity for data transmission of current wireless systems is still tiny when compared to wired forms of communications. But wireless data rates continue to increase. To understand the push for higher and higher data rates, it is useful to consider an analogy involving the trends of memory size and processor speed in the personal computer market.

In the early 1980's, a typical personal computer had about 64 kilobytes of RAM and operated with a processor that clocked at speeds less than 1 MHz. At the time, the perception of future computer hardware needs was best summarized by a famous industry magnate:

> 640 kilobytes [of RAM] ought to be enough for anybody.
>
> *-Bill Gates, 1981*

In the year 2000, the typical personal computer has a processor that operates at a clock frequency close to 1 GHz and requires as much as 100 MB of RAM – *and this capability continues to increase*. In short, as soon as computer hardware is enhanced, new commercial software applications are developed which exploit the new-found capacity for storing and manipulating data.

The computer hardware illustration provides a valuable lesson for the wireless industry. There is a basic rule that applies to all information technology: new hardware that increases the capacity to store or manipulate data is quickly followed by new applications that exhaust the resources. For wireless, this means that the current technology will continue to gravitate towards higher transmitted data rates.

Of course, higher data rates translate into wireless systems that operate with wider bandwidths. Future wireless systems will operate with bandwidths that greatly exceed conventional channel models. New systems will require new channel models and measurements.

### 1.1.2 Ubiquity of Wireless Devices

Wireless personal communications has permeated nearly every environment on earth. It is now possible to use a wireless handset in a city, in a car, in the home, in an office building, on a boat – the list goes on. Future applications will involve wireless sensors and impersonal communications between engines, machinery, and appliances.

The wireless channel is heavily dependent on the environment in which it operates. Since future wireless applications will operate in nearly every imaginable environment, there will be an incredibly diverse variety of channels that require characterization. In fact, many of these new environments will defy characterization by the older paradigms of wireless channel modeling.

### 1.1.3 Smart Antennas

Adaptive arrays and other types of smart antenna techniques are emerging technologies for improving the wireless link and mitigating interference in a multiple access system [1, 2]. Many multi-user communication systems such as cellular radio networks have, until now, operated well below their designed capacity. As the market for these systems has grown and matured over the years, the network traffic has grown as well. Smart antenna technology is seen as a cheap and effective solution for mitigating the problem of excess network traffic.

A directional antenna at a receiver or transmitter drastically changes the channel characteristics. Channel models that once applied to omnidirectional antennas must be modified and improved to account for the new spatio-temporal distortion of the channel by the directional antenna.

### 1.1.4 Faster, Smaller, Cheaper Hardware

Over the years, basic research in wireless communications has produced a plethora of modulation, multiple access, and signal processing innovations that combat the distortions introduced by a wireless channel. Only a small subset of these innovations are used in practice, since many algorithms and techniques do not have a feasible realization in hardware.

Radio frequency and digital signal processing technology continues to develop, however. The computational power of baseband chip sets is increasing. The radio frequency (RF) integrated circuits are operating at higher power levels and at higher frequencies. Above all, these transmitter and receiver components are becoming cheaper and cheaper to fabricate. As a result, many algorithms and techniques which are not feasible to implement today, will become feasible tomorrow.

The added capabilities of future radio receivers, therefore, will be able to combat the detrimental effects of the multipath channel in new and innovative ways. With added functionality, receivers of the future need more than just an ad-hoc approximation about the radio channel. Future receiver designs will require models that mimic the detailed dispersion, time-varying, and space-varying characteristics of a realistic wireless channel.

### 1.1.5 Frequency Congestion

Bandwidth is a finite resource. As wireless systems with wider and wider bandwidths continue to deploy, frequency congestion becomes a problem. One solution is to move outside of common frequency bands and into higher, uncrowded frequency in the upper microwave and mm-wave bands. Propagation at these higher frequencies presents an entirely different set of problems. Clearly, channel models developed around the 1 GHz microwave bands are inadequate to characterize wireless systems where both the carrier frequency and signal bandwidth are orders-of-magnitude greater.

### 1.1.6 Multiple-Input, Multiple-Output Systems

Perhaps one of the most interesting trends in wireless communications is the proposed use of multiple-input, multiple-output (MIMO) systems. A MIMO system uses multiple transmitter antennas *and* multiple receiver antennas to break a multipath channel into several individual spatial channels. The resulting system then employs *space-time coding* to increase the link capacity [3].

New MIMO systems represent a huge philosophical change in how wireless communications systems are designed. This change reflects how we view multipath in a wireless system:

> **The Old Perspective:** The ultimate goal of wireless communications is to combat the distortion caused by multipath in order to approach the theoretical limit of capacity for a band-limited channel.
>
> **The New Perspective:** Since multipath propagation actually represents *multiple channels* between a transmitter and receiver, the ultimate goal of wireless communications is to *use* multipath to provide higher total capacity than the theoretical limit for a conventional band-limited channel.

This philosophical reversal implies that many of the engineering design rules-of-thumb that were based on pessimistic, worst-case scenario channel models have now become unrealistically optimistic. Design of such systems will require new space-frequency channel models.

## 1.2 Key Topics in Small-Scale Channel Modeling

Each chapter of this report addresses a key shortcoming in conventional channel modeling theory. Each also builds on knowledge accumulated in the previous chapter, so that the entire report may be read as a coherent, foundational development of wireless channel modeling concepts. The various topics addressed by each of the chapters are discussed below.

### 1.2.1 Spatial, Temporal, and Frequency Coherence

The linear time-invariant channel is well-understood by most engineers. Unfortunately, the wireless channel is *time-varying* and *space-varying* as well as *frequency selective*. A general approach to channel modeling must consider all three possible variations – frequency, time, and three-dimensional space – in order to characterize the end-to-end performance of wireless communication systems.

Typically, the wireless research community relies on theory developed by Bello in [4] to characterize random time-varying, frequency-selective channels. In doing so, the spatial dimension is often neglected; for mobile receivers, it is "lumped" together with the temporal variations using some type of $\textit{space} = \textit{velocity} \times \textit{time}$ substitution. For complete generality, it must be viewed as a separate phenomenon.

Chapter 2 presents a foundational overview of baseband channel modeling, emphasizing the distinct temporal, frequency, and spatial *coherence* of a wireless channel. The concept of *duality* between the three dependencies is stressed in the development. This powerful concept states that if one understands the characterization of a single dependency, then channel characterization of other dependencies may be understood by analogy.

### 1.2.2 Rigorous Application of Physics to Channel Models

In the research literature, many stochastic wireless channel models are simply ad-hoc mixtures of random variables that supposedly generate realistic radio channels. But channel models of arbitrary construction are not always true-to-life because a wireless channel must result from propagation that obeys *Maxwell's equations*. In other words, electromagnetic propagation will only produce communications channels of a certain type.

Chapter 3 discusses the basic form that a stochastic local area channel model must take. Great care is taken in defining a *local area* and a *stochastic local area channel*, clearly stating the assumptions associated with each term. This chapter also categorizes the local area channel models and discusses conditions for stationarity.

### 1.2.3 Physically-Based Small-Scale Fading Distributions

The use of a probability density function (PDF) to characterize the distributions of received envelope with respect to space or frequency is a common practice in wireless. In fact, *dozens* of these probabilistic distributions exist in the literature and there is always great debate as to which PDF applies for various situations [5, 6, 7].

Chapter 4 uses the fundamental development in the introductory chapters to construct a method for generating envelope PDF's given a distribution of arriving multipath power. The resulting PDF's exhibit a remarkably diverse range of behavior without resorting to empirical distributions that disguise the physics of propagation.

### 1.2.4 Characterization and Analysis of Angle Spectra

A *wavevector spectrum* is the most appropriate method for characterizing the second-order statistics of a wide-sense stationary stochastic space-varying channel. Engineers do not typically view spatial propagation in terms of a wavevector spectrum. Rather, it is more common to use an *angle spectrum* which represents the angle-of-arrival of multipath power. While use of an angle spectrum is common, the rationale and assumptions involved in this concept are often ignored.

Chapter 5 rigorously defines the angle spectrum, describing the exact class of channel models for which this spectrum is valid. Furthermore, this chapter introduces one of the most original contributions of this report – the use of multipath *shape factors* to describe the geometrical properties of angle spectrum. The shape factors allow engineers to gauge spatial selectivity characteristics without ever having to resort to a wavevector spectrum.

### 1.2.5 Channel Statistics of Rayleigh Fading

The theory in this dissertation may be used to calculate a number of useful channel statistics. Chapter 6 focuses on calculating channel statistics – level-crossing rates, average fade duration, correlation behavior, and coherence definitions – for *Rayleigh* fading channels. Rayleigh channels, with their diffusely propagating multipath, are useful case studies since their statistics are often analytically tractable. Indeed, this chapter shows that duality may be applied liberally to the channel analysis to generate statistics for temporal, spatial, and frequency statistics. Such a unified approach to channel statistical analysis does not exist in the literature to date.

### 1.2.6 Spatio-Temporal Peer-to-Peer Measurements

Chapter 7 discusses a measurement campaign which measures both frequency and spatial selectivity in 1920 MHz wideband channels. In the process, much of the small-scale fading theory that has been developed in this report will be used and tested to describe the channel characteristics.

The results not only apply theory, but they also have a great deal of research value to the wireless industry. Few publications to date have been made on joint statistics involving space and dispersion in the microwave bands. Furthermore, the transmitter and receiver locations in the measurement campaign are chosen to model a *peer-to-peer* wireless network. The full spatio-temporal channel for such a configuration is virtually unknown, but of interest to industry, which sees a great commercial and military future for mobile radio units that communicate directly to one another.

## 1.3 How to Read This Dissertation

The primary purpose of this dissertation is to provide a foundational research reference for wireless researchers that require knowledge of the dispersive, space-varying, time-varying channel. The target reader is a researcher with basic exposure to stochastic processes, electromagnetic propagation, and communications. A first-year graduate student should have little difficulty understanding the mathematics and physics presented throughout the work.

Since communications, stochastic process theory, and electromagnetic wave theory are, by themselves, very difficult and vast subjects, advanced topics are introduced with thorough background information. Extensive mathematical derivations have been removed from the main text and placed in appendices at the end of the chapters. Important *theorems* are proven with pragmatic methods that emphasize understanding instead of mathematical rigor. *Examples* are used to illustrate concepts, wherever possible.

> *Note: Supplemental Information*
>
> Throughout this report there are *noteboxes* (like this one) that contain information that supplements the technical concepts in the main text. These noteboxes are used to clarify possible points of confusion, to justify a certain type of notation, to alert the reader to misconceptions that exist in the research literature, or even to provide some history behind a useful concept and its inventor. Such "editorials-in-miniature" are crucial for understanding how propagation, stochastic, and communication theory fit together to form the field of wireless channel modeling.

Overall, the report is intended to be a readable introduction to channel modeling theory. It may be used as a springboard into all sorts of theoretical and applied research in wireless communications.

# Chapter 2

# Foundations of Stochastic Channel Modeling

A grove of trees rustling in the wind scrambles received power from one second to the next in a point-to-point microwave link. Or a cellular handset drops a call after moving just a few centimeters from an operable location. Or the tap-delay line filter of a linear equalizer becomes unstable, incapable of canceling the intersymbol interference experienced by a wireless receiver. While the causes and effects of each channel-related problem are varied, the channel analysis is nearly identical for each case – *if rigorous stochastic channel modeling is employed*.

The goal of this chapter is to develop the terminology, definitions, and basic concepts of modeling a wireless channel that can be a function of time, frequency, and receiver position in space. The chapter is broken into the following sections:

- Section 2.1: basic definitions for representing a complex baseband wireless channel
- Section 2.2: introduction to channel coherence and selectivity
- Section 2.3: discussion of complex baseband channel usage
- Section 2.4: concepts for stochastic channel modeling such as autocorrelation, power spectrum, and RMS spectral spread
- Section 2.5: summary of important concepts

As a whole, this chapter represents a stepping stone to every subsequent concept developed in this work.

## 2.1 Baseband Representation

Development of a baseband representation for modulated functions is a cornerstone of channel modeling and analysis. A baseband representation essentially removes the dependence of a passband radio channel from its carrier frequency, which both generalizes and simplifies channel modeling. This section discusses the mathematics behind switching between passband and baseband representations of radio signals and channels.

### 2.1.1 Signal Modulation

One of the most fundamental operations in radio communications is the act of modulating a carrier wave by a band-limited data signal. Thus, modulation converts a *baseband* signal to a *passband* signal. To represent the act of modulation, we will use the modulation operator $\mathcal{M}\{\cdot\}$ to denote transformation of a baseband signal, $\tilde{x}(t)$, to a passband signal, $x(t)$, that modulates a carrier wave. Thus, using notation we write

$$x(t) = \mathcal{M}\{\tilde{x}(t)\} \tag{2.1}$$

The tilde, $\tilde{}$, above a function will be the convention used throughout this work to denote baseband representation of a signal or channel.

It is easiest to view modulation in the frequency domain using the Fourier transforms or *spectra* of $\tilde{x}(t)$ and $x(t)$:

$$\tilde{X}(f) = \int_{-\infty}^{+\infty} \tilde{x}(t) \exp(-j2\pi f t)\, dt \tag{2.2}$$

$$X(f) = \int_{-\infty}^{+\infty} x(t) \exp(-j2\pi f t)\, dt \tag{2.3}$$

The Fourier transform of the passband signal may be calculated from the baseband signal as follows:

$$X(f) = \frac{1}{2}\tilde{X}(f + f_c) + \frac{1}{2}\tilde{X}^*(-f - f_c) \tag{2.4}$$

where * denotes complex conjugate. In the frequency domain, $X(f)$ is simply a copy of the spectrum $\tilde{X}(f)$ shifted to a center frequency of $f = +f_c$ and a mirror copy of $\tilde{X}(f)$ shifted to a center frequency of $f = -f_c$.

The operation of modulation can be defined directly in the time domain. Given a carrier frequency, $f_c$,

$$\mathcal{M}\{\tilde{x}(t)\} \doteq \underbrace{\text{Real}\{}_{\substack{\text{mirror}\\\text{image}}}\ \tilde{x}(t)\ \underbrace{\exp(j2\pi f_c t)}_{\substack{\text{frequency}\\\text{shift}}}\ \} \tag{2.5}$$

where $f_c$ is the carrier frequency. The complex exponential in Eqn (2.5) shifts the baseband signal, $\tilde{x}(t)$ up to a carrier frequency of $f_c$ and the Real$\{\cdot\}$ operator produces the conjugate mirror-image spectrum at $-f_c$.

At this point, it is necessary to define the *bandwidth*, $B$, of a baseband signal. There are many different ways to define bandwidth, as illustrated in Figure 2.1. In this work, unless noted otherwise, we will use the largest-valued definition of bandwidth, *non-zero bandwidth*.

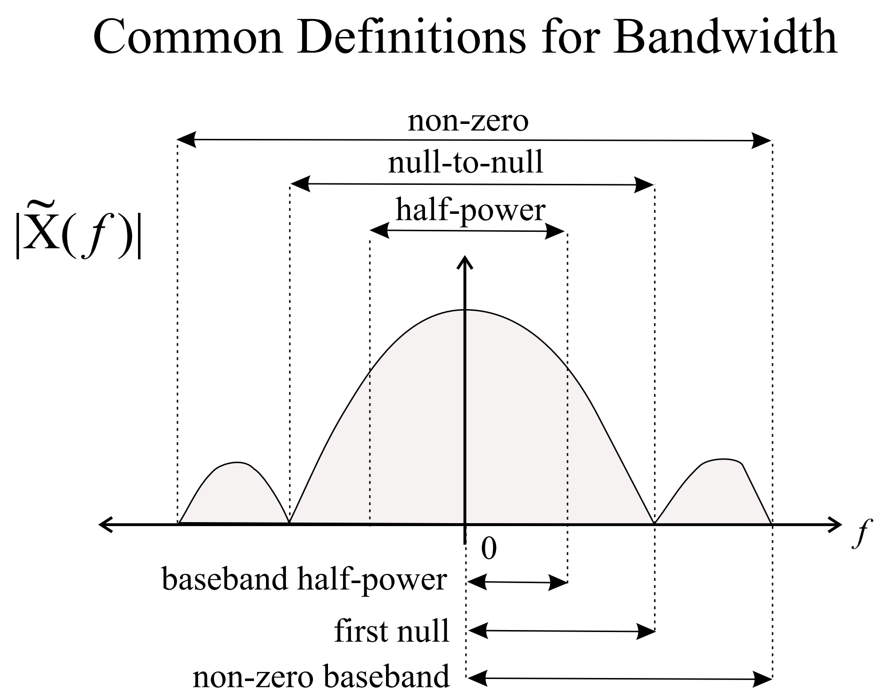


Figure 2.1: The many different bandwidths defined for a baseband signal.

The inverse operation of modulation – converting a passband signal, $x(t)$, back to a baseband signal, $\tilde{x}(t)$ – also has a time domain definition:

$$\mathcal{M}^{-1}\{x(t)\} = \underbrace{[x(t)\,\exp(-j2\pi f_c t)]}_{\substack{\text{frequency}\\ \text{shift}}} \otimes \underbrace{[2B\text{sn}(Bt)]}_{\substack{\text{low-pass}\\ \text{filter}}} \tag{2.6}$$

$$= 2B\int_{-\infty}^{+\infty} x(\zeta)\exp(-j2\pi f_c\zeta)\,\text{sn}(B[t-\zeta])\,d\zeta \tag{2.7}$$

where $\otimes$ denotes convolution and sn$(\cdot)$ is the sinc function, $\text{sn}(x) = \frac{\sin(\pi x)}{\pi x}$. The complex exponential term in Eqn (2.6) shifts the passband signal spectrum, $H(f)$, by an amount $f_c$ so that the copy of $\tilde{X}(f)$ lies centered at $f = 0$ and its mirror image lies at $f =$

$-2f_c$. The convolution with the sinc function – a low-pass filter – then removes the high-frequency mirror image so that only $\tilde{X}(f)$ remains. The complete operation of modulation and demodulation is shown in Figure 2.2.

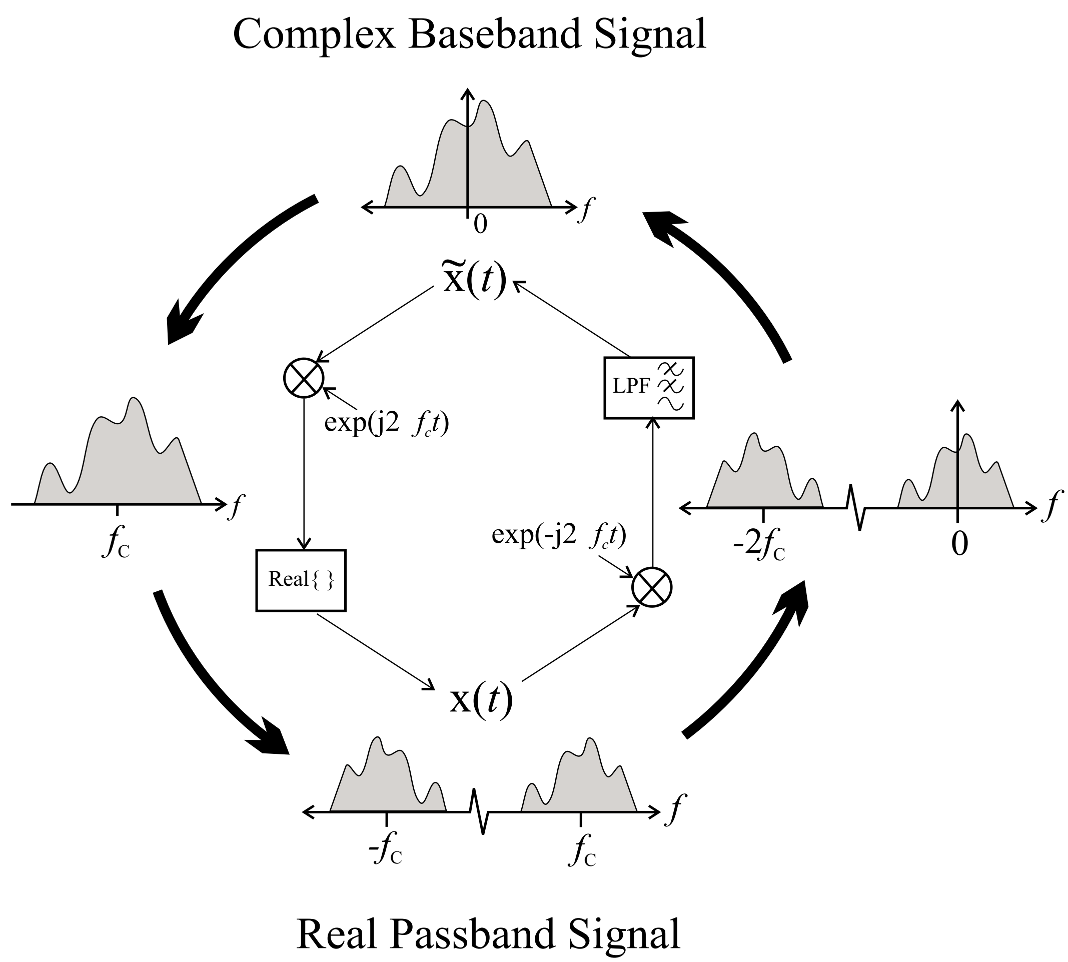


Figure 2.2: Baseband-Passband transformations in the time domain (inner cycle) and the frequency domain (outer cycle).

If the modulated signal, $x(t)$, is to represent a physically realizeable transmission, then it must be a real-valued function. No such restriction is placed on the baseband signal, as *any* complex-valued function that modulates a carrier according to Eqn (2.5) will produce a real-valued function. This difference between baseband and passband representations stems from the conjugate mirror image in the passband spectrum, $X(f)$. Thus, $X(f)$ has twice as much non-zero bandwidth as the baseband signal. A *complex* function, which is actually two real-valued functions (one for the real component and one for the imaginary component), is the easiest way to accommodate this extra information so that nothing is lost in the baseband representation of a modulated signal. Consider the following example:

**Example 2.1: Amplitude and Phase**

**Problem:** Passband signals are commonly written in the form

$$x(t) = V(t)\cos[2\pi f_c t + \varphi(t)]$$

where $V(t)$ is a real amplitude and $\varphi(t)$ is a real phase, both of which are band-limited functions. Find an expression for the baseband representation, $\tilde{x}(t)$, of this type of signal.

**Solution:** The first step is to plug the expression for $x(t)$ into the demodulation operation of Eqn (2.7):

$$\tilde{x}(t) = 2B \int_{-\infty}^{+\infty} V(\zeta)\cos[2\pi f_c \zeta + \varphi(\zeta)]\exp(-j2\pi f_c \zeta)\,\mathrm{sn}(B[t-\zeta])\,d\zeta$$

Using the Euler relation for $\cos(\cdot)$, it is possible to rewrite this integral as

$$\tilde{x}(t) = \int_{-\infty}^{+\infty} \frac{\{\overbrace{V(\zeta)\exp[j\varphi(\zeta)]}^{\substack{\text{low}\\ \text{frequency}}} + \overbrace{V(\zeta)\exp[-j4\pi f_c \zeta + \varphi(\zeta)]}^{\substack{\text{high}\\ \text{frequency}}}\}\sin(\pi B[t-\zeta])\,d\zeta}{\pi(t-\zeta)}$$

which may be evaluated by inspection. The left term inside the braces is a low-frequency component which passes through the integration unchanged. The right term inside the braces is a high-frequency component which evaluates to zero upon integration. Thus,

$$\tilde{x}(t) = V(t)\exp[j\varphi(t)]$$

which is the complex baseband representation of the real-valued transmitted signal.

---

*Note: Removing the Carrier*

From Example 2.1, it is clear that inverse modulation simply removes the oscillations of the carrier wave while retaining amplitude and phase information. The act of removing carrier oscillations is a staple of applied sciences. For example, when amplitude and phase are constant with respect to time ($V(t) = V_0$ and $\varphi(t) = \varphi_0$), the passband signal is said to be *time-harmonic*. The definitions for modulation and inverse modulation then degenerate into the commonly-used *Phasor transforms*.

### 2.1.2 The Baseband Channel

Three passband functions are required to represent the operation of the simplest wireless communication system: a transmitted signal, $x(t)$, a received signal, $y(t)$, and a channel, $H(t)$. If the channel is linear and time-invariant, then it is possible to relate these three quantities using convolution:

$$y(t) = x(t) \otimes H(t) \tag{2.8}$$

However, it is more convenient to analyze these functions using their baseband representation, since they become independent of carrier frequency. Using the following relationships for baseband and passband signals,

$$x(t) = \mathcal{M}\{\tilde{x}(t)\} \tag{2.9}$$

$$y(t) = \mathcal{M}\{\tilde{y}(t)\} \tag{2.10}$$

$$H(t) = \mathcal{M}\left\{\tilde{H}(t)\right\} \tag{2.11}$$

it is possible to write Eqn (2.8) as a convolution of baseband signals:

$$\tilde{y}(t) = \tilde{x}(t) \otimes \tilde{H}(t) \tag{2.12}$$

Keep in mind that, while Eqn (2.12) captures all of the behavior of the passband channel, it is a convenient representation and is *not* a physical process. An engineer must always return to Eqn (2.9)-Eqn (2.11) to get the actual functions for the transmitted and received signals and the radio channel. However, all theory and development presented in this work will deal with the baseband representation of signals and channels.

The baseband and passband channel models for *single input, single output* (SISO) transmission are pictured in Figure 2.3. The *single input* is the transmitted signal and the *single output* is the received signal. Of course, a realistic communication system must contend with additive noise, $n(t)$. This noise can be thermal noise, impulsive noise, multiple-access interference, jamming – virtually any type of undesired signal that coexists in the passband of the desired signal. Additive noise modeling is a well-understood practice. For the purposes of this work, the additive noise function, $n(t)$ or $\tilde{n}(t)$, will be ignored until we develop an application where the effects of noise or interference is important.

### 2.1.3 Time-Invariant vs. Time-Varying Channels

It is a hallmark of linear, time-invariant systems that the convolution of a transmitted signal and a channel may be written as a product in the frequency domain. Consider the following

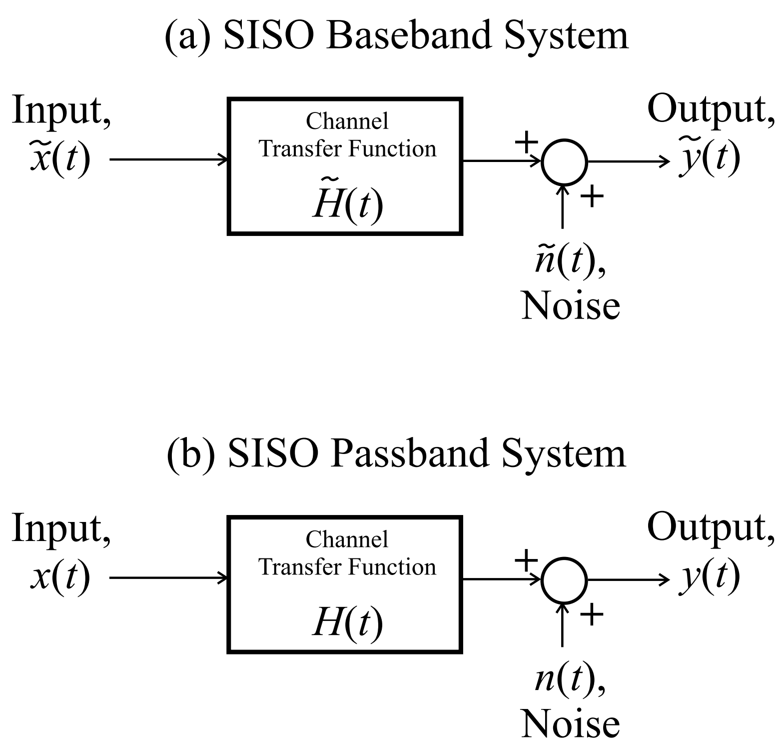


Figure 2.3: Block diagram of baseband and passband channel models for SISO transmission.

Fourier transform pairs:

$$\begin{aligned}
\tilde{x}(t) &\iff \tilde{X}(f) \\
\tilde{y}(t) &\iff \tilde{Y}(f) \\
\tilde{H}(t) &\iff \tilde{h}(f)
\end{aligned}$$

Using these definitions, Eqn (2.8) and Eqn (2.12) may be written, respectively, as

$$Y(f) = X(f)\,h(f) \tag{2.13}$$

$$\tilde{Y}(f) = \tilde{X}(f)\,\tilde{h}(f) \tag{2.14}$$

These equations provide insight into the equivalence of dealing with passband signals and their baseband representations. Figure 2.4 illustrates the parallel nature of these operations in baseband and passband.

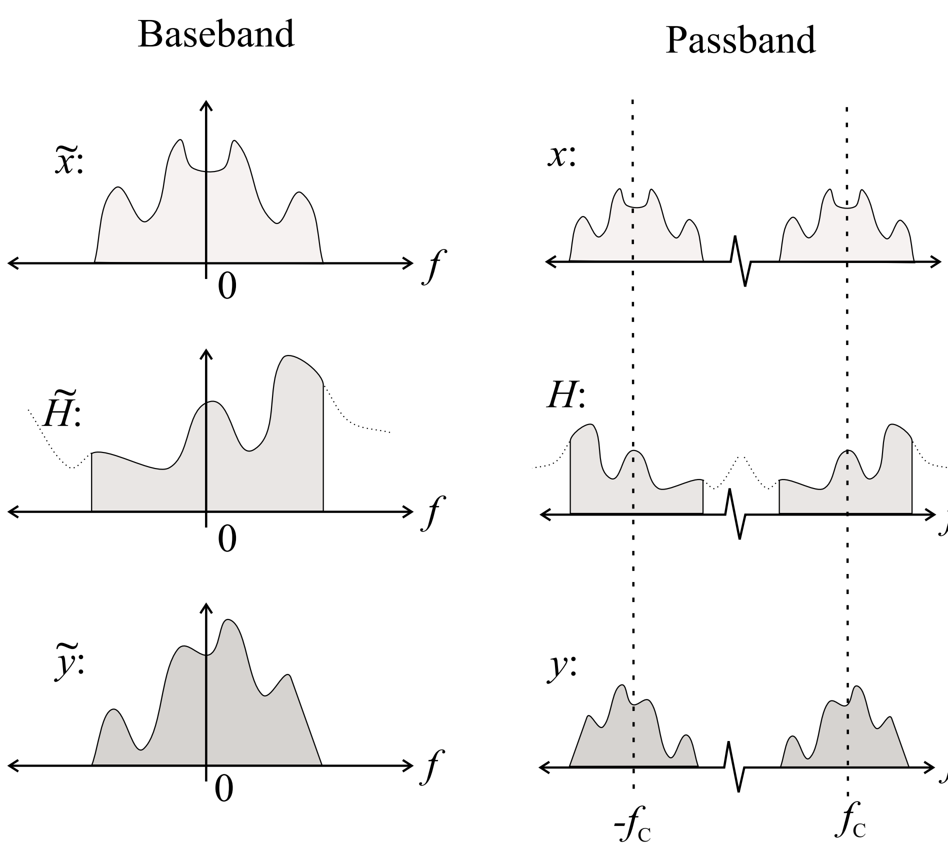


Figure 2.4: Spectral diagram of baseband and passband signals and channel.

*Note: Communications vs. Channel Modeling*

In communications theory, the time domain is always the base domain in which all transforms are referenced. In channel modeling theory, for reasons that will become clear later, it is much more powerful and convenient to view the *frequency* domain as the base domain. To avoid confusion between the conventions of communications and channel modeling, the same Fourier transform definitions are used to move back and forth between time and frequency for both signals and channels. However, *frequency* is chosen as the base domain for channels, which receive the lower-case function designation, $\tilde{h}$.

If a channel is time-varying, then neither convolution nor frequency-domain multiplication can be used to calculate signal transmission through the channel. For baseband transmission in a time-varying channel, the following input-output relationship must be used:

$$\tilde{y}(t) = \int_{-\infty}^{+\infty} \tilde{X}(f)\, \tilde{h}(f,t)\, \exp(j2\pi f t)\, df \tag{2.15}$$

Eqn (2.15) is basically the inverse Fourier transform of Eqn (2.14) with a frequency-domain transfer function, $\tilde{h}(f,t)$, that is now also a function of time.

The input-output relationship of Eqn (2.15) causes a new problem in the characterization of $\tilde{h}(f,t)$: the values of frequency, $f$, and time, $t$ are no longer valid transform domain pairs as they were in the time-invariant system. For example, using the inverse Fourier transform on $\tilde{h}(f,t)$ produces a pure time domain function that is useless for calculating the transmitted signal, $\tilde{y}(t)$:

**Incorrect:** $\tilde{h}(t) = \int_{-\infty}^{+\infty} \tilde{h}(f,t)\, \exp(j2\pi f t)\, df$

To circumvent this problem, the frequency and time dependencies of the channel must always be kept separate, even when performing spectral analysis on one or the other. This separation is discussed in greater detail in Section 2.3 on page 26.

### 2.1.4 Detection

*Detection* is the operation performed by a receiver as it demodulates a passband signal. There are many ways to actually implement detection. For example, noncoherent receivers essentially take the magnitude of the received complex voltage signal, $\tilde{y}(t)$ and throw away the phase information. Coherent receivers simultaneously detect the real and imaginary components of $\tilde{y}(t)$ so that both are available for baseband signal processing. Regardless of technique, detection is usually described in terms of four real-valued functions, based on the complex baseband representation of a signal. Summarized in Table 2.1, they are

**In-Phase Component:** This is the real part of a complex baseband voltage signal. Physically, the in-phase component arises by mixing the passband signal with $\cos(2\pi f_c t)$ and then low-pass filtering the result.

**Quadrature Component:** This is the imaginary part of a complex baseband voltage signal. The quadrature component arises by mixing the passband signal with $\sin(2\pi f_c t)$ and then low-pass filtering the result. Many modern receivers demodulate in-phase and quadrature components simultaneously. This type of receiver is called an IQ detector [8].

**Voltage Envelope:** The voltage envelope is defined to be the magnitude of the complex baseband signal. A receiver operating on this principle is called a *noncoherent* receiver and uses an *envelope detector* to strip away the carrier and phase information from the signal.

**Received Power:** Similar to voltage envelope, the received power is defined to be the magnitude-squared of the complex baseband signal. Defined this way, received power has units of $Volts^2$. Received power is used in the calculation of a signal-to-noise or signal-to-interference ratio, which ultimately determines the theoretical limit of wireless channel capacity [9].

Table 2.1: Received signal functions used in complex baseband analysis.

| | | | |
|---|---|---|---|
| In-Phase Component: | $I(t)$ | $=$ | $\text{Real}\{\tilde{y}(t)\}$ |
| Quadrature Component: | $Q(t)$ | $=$ | $\text{Imag}\{\tilde{y}(t)\}$ |
| Voltage Envelope: | $R(t)$ | $=$ | $\lvert\tilde{y}(t)\rvert$ |
| Received Power: | $P(t)$ | $=$ | $\lvert\tilde{y}(t)\rvert^2$ |

## 2.2 Channel Coherence

The most important concept in describing the wireless channel is *channel coherence*. This section presents an overview of the many types of coherence that a wireless channel exhibits.

### 2.2.1 Coherence vs. Selectivity

*Fading* is a general term used to describe a wireless channel affected by some type of *selectivity*. A channel has selectivity if it varies as a function of either time, frequency, or space. The opposite of selectivity is *coherence*. A channel has coherence if it does not change as a function of time, frequency, or space over a specified "window" of interest.

Indeed, wireless channels may be functions of both time, frequency, *and* space. The most fundamental concept in channel modeling is classifying the three possible channel dependencies of time, frequency, and space as either coherent or selective. In order to keep track of these dependencies in the wireless channel, it is important to speak of each individually before developing the mathematics of joint characterization. The next sections discuss each type of coherence.

### 2.2.2 Temporal Coherence

A wireless channel has temporal coherence if the envelope of the unmodulated carrier wave does not change over a time window of interest. Mathematically, we express this condition in terms of a narrowband (no frequency dependence), fixed (no spatial dependence) channel, $\tilde{h}(t)$:

$$\left|\tilde{h}(t)\right| \approx V_0, \qquad \text{for } |t_0 - t| \leq \frac{T_c}{2} \tag{2.16}$$

where $V_0$ is some constant voltage, $T_c$ is the size of the time window of interest, and $t_0$ is some arbitrary moment in time. The largest value of $T_c$, on average, for which Eqn (2.16) holds is called the *coherence time* and is the approximate time window over which the channel appears static. Figure 2.5 illustrates these definitions.

Note that the received voltage in Eqn (2.16) is in complex phasor form and is independent of carrier frequency. Naturally, a transmitted wave will produce sinusoidal oscillations as a function of time, but the definition of temporal coherence is concerned with the *envelope* of those oscillations.

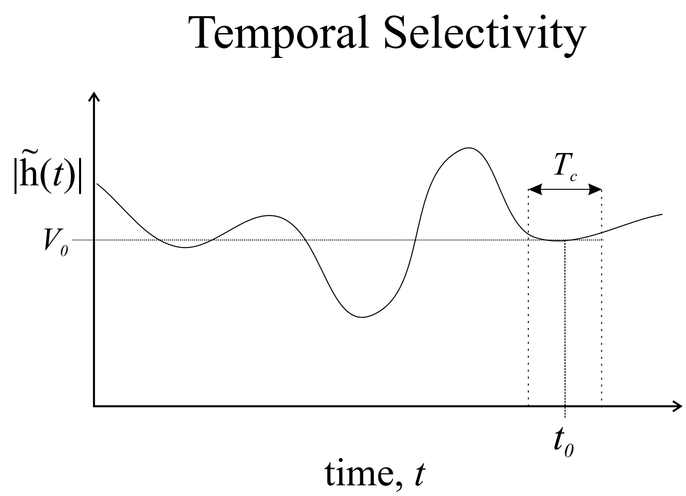


Figure 2.5: Example of a time-varying channel.

*Note: Formal Definitions of Coherence*

As is the case for each type of coherence defined in this chapter, the definition in Eqn (2.16) is subjective since the condition $\left|\tilde{h}(t)\right| \approx V_0$ is open to interpretation; it neither defines a formal metric for channel selectivity nor does it present a threshold for characterizing a truly coherent channel. A formal treatment of coherence, however, requires much more background in stochastic channel modeling than has been presented thus far.

In the microwave and millimeter frequency regime the most common cause of temporal incoherence is motion by either the transmitter or the principle scatterers in the propagation environment. Temporal channel coherence can degrade the performance of a wireless communication system. If the transmitted data rate is comparable to the temporal coherence, it becomes extremely difficult for the receiver to demodulate the transmitted signal reliably. Fluctuations due to data modulation and fluctuations due to the time-varying channel occur at the same time scale, causing catastrophic distortion.

One method for reliable communications in a time-varying channel is to transmit data using symbols that are much larger than the channel coherence time and rely on long-period averaging to filter out the fluctuations of the carrier from each symbol. When the envelope of the carrier wave fluctuates at a rate faster than the transmitted symbol rate, the channel is said to be *fast fading*. Another method for reliable communications in a time-varying channel is to transmit data using symbols that are much smaller than the channel coherence time. For this case, the time-varying channel appears static over the short symbol period. When the envelope of the carrier wave fluctuates at a rate slower than the transmitted symbol rate, the channel is said to be *slow fading*.

### 2.2.3 Frequency Coherence

A wireless channel has frequency coherence if the magnitude of the carrier wave does not change over a frequency window of interest. This window of interest is usually the bandwidth of the transmitted signal. Mathematically, we express the condition of frequency coherence in terms of the static (no time dependence), fixed channel, $\tilde{h}(f)$:

$$\left|\tilde{h}(f)\right| \approx V_0, \qquad \text{for } |f_c - f| \leq \frac{B_c}{2} \tag{2.17}$$

where $V_0$ is some constant amplitude, $B_c$ is the size of the frequency window of interest, and $f_c$ is the center carrier frequency. The largest value of $B_c$ for which Eqn (2.17) holds is called the *coherence bandwidth* and is the approximate range of frequencies over which the channel appears static. Figure 2.6 illustrates these definitions.

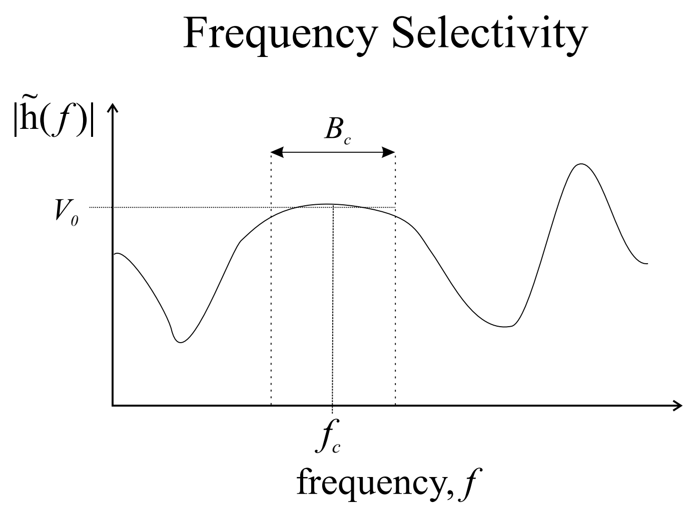


Figure 2.6: Example of a frequency-varying channel.

The loss of frequency coherence in a wireless communications system is caused by the dispersion of multipath propagation. Since each received multipath wave has traveled a different path from the transmitter, the same transmitted signal will arrive at the receiver as a cluster of symbols, each with a unique time delay. Thus, in the time domain, a dispersive channel introduces *intersymbol interference*. In the frequency domain, a dispersive channel has peaks and valleys across the bandwidth of interest. This behavior in the frequency domain gives rise to two distinct classifications of fading in wireless communications. A wireless channel with a coherence bandwidth that is less than the bandwidth of a transmitted signal is said to have *frequency-selective fading*. A channel with a coherence bandwidth that is greater than the transmitted signal bandwidth is said to have *frequency-flat fading*.

### 2.2.4 Spatial Coherence

A wireless channel has spatial coherence if the magnitude of the carrier wave does not change over a spatial displacement of the receiver. Once again, we express the condition of spatial coherence in terms of the static narrowband channel, $\tilde{h}(\vec{r})$, which is a function of three-dimensional (3D) position vector, $\vec{r}$:

$$\left|\tilde{h}(\vec{r})\right| \approx V_0, \qquad \text{for } |\vec{r}_0 - \vec{r}| \leq \frac{D_c}{2} \tag{2.18}$$

where $V_0$ is some constant amplitude, $D_c$ is the size of the position displacement, and $\vec{r}_0$ is an arbitrary position in space. The largest value of $D_c$ for which Eqn (2.18) holds is called the *coherence distance* and is the approximate distance that a wireless receiver can move with the channel appearing to be static. Figure 2.7 illustrates these definitions.

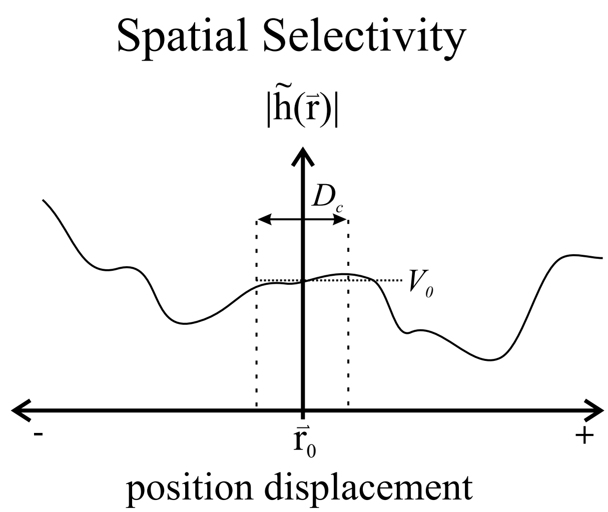


Figure 2.7: Example of a space-varying channel (one-dimensional cut).

Note that for a wireless receiver moving in three-dimensional space, the coherence distance is a function of the direction that the receiver travels, since $\vec{r}$ in Eqn (2.18) is a 3D position vector. The three dimensions of free space make the study of spatial coherence more difficult than the scalar quantities of temporal or frequency coherence.

While frequency incoherence is caused by multipath arriving with many different time delays, spatial incoherence is caused by multipath arriving from many different directions in space. These multipath waves create pockets of constructive and destructive interference so that the received signal power does not appear to be constant over small changes in receiver position. Thus, this type of channel exhibits *spatial selectivity.* If the distance traversed by a receiver is greater than the coherence distance of the channel, we say that the channel experiences *small-scale fading.*

### Large-Scale vs. Small-Scale Fading

The converse of small-scale fading, *large-scale fading*, refers to fluctuations in spatially-averaged received power due to shadowing and scattering of objects in the propagation environment. Typically, small-scale fluctuations occur when a receiver moves a distance comparable to the size of the electromagnetic wavelength of the carrier. Large-scale fluctuations occur when the receiver moves over many wavelengths. An example of small-scale and large-scale fading for a received signal level as a function of position is illustrated in Figure 2.8.

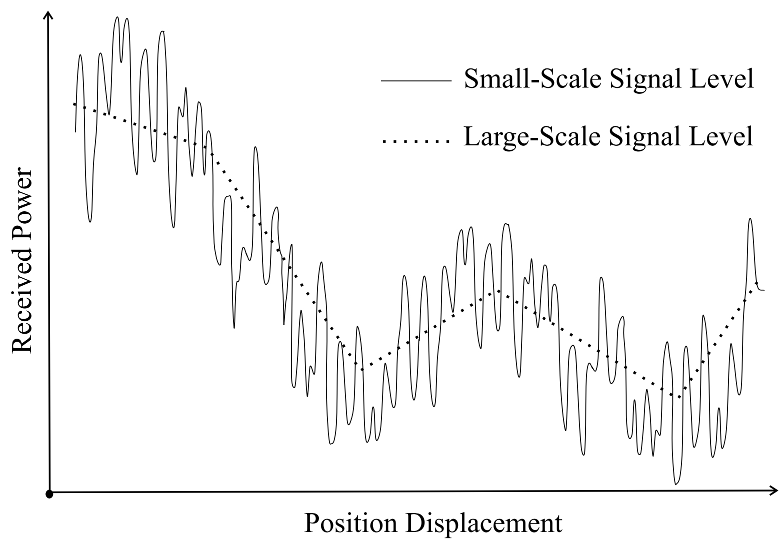


Figure 2.8: Example of small-scale and large-scale fading.

It is quite possible in a small-scale fading channel to experience near-zero received power levels at points in space even if the large-scale power level is high. This type of dip in the power level is called a *null*. Conversely, a point in space which leads to maxima in the received power levels is called a *peak*.

### Mobile Fading

For *mobile* wireless communications, spatial incoherence in a channel leads directly to temporal incoherence. As a receiver moves through space, the fading may treated as a function of time instead of space by relating the position $\vec{r}$ and the time $t$ by a simple equation of motion:

$$\vec{r}(t) = \vec{r}(0) + \vec{v}t \tag{2.19}$$

where $\vec{v}$ is the velocity vector of the receiver. Thus, small-scale fading causes temporal incoherence for wireless systems with mobile receivers.

*Note: Not-So-Fast Fading*

Some authors have confused the terms used for temporal and spatial incoherence and will refer to small-scale fading as *fast fading*. This is particularly unfortunate since the motion-induced temporal fading that arises from small-scale fading is almost never really fast fading: the coherence time of the temporal fades is *always* larger than the symbol period of modern communications systems with useful data rates.

## 2.3 Using the Complete Baseband Channel

The complete wireless baseband channel, $\tilde{h}(f, \vec{r}, t)$, is a function of frequency, position, and time. This section discusses the basic representations of the baseband channel and how they related to the wireless transmission of signals.

### 2.3.1 Spectral Domain Representations

The definitions of Fourier transforms are useful tools in channel analysis. Since the full channel representation, $\tilde{h}(f, \vec{r}, t)$, is a function of frequency, space, and time, transforms may be defined for each of these domains. The three possible spectral domains are listed below:

**delay domain:** The spectral domain of frequency, $f$, is the *delay* domain, with dependence denoted by $\tau$. Since $f$ has units of *frequency*, the reciprocal units of delay, $\tau$, must be *time*.

**wavevector domain:** The spectral domain of a position vector, $\vec{r}$, is the *wavevector* domain, with dependence denoted by $\vec{k}$. Tranformations between position and wavevector domains are perhaps the most difficult to visualize, since there are actually three variable dependencies in a position vector that must be transformed (one for each dimension of space). Since the components of position vector $\vec{r}$ have units of *distance*, the components of wavevector $\vec{k}$ must have reciprocal units of *radians per unit distance*.

**Doppler domain:** The spectral domain of time, $t$, is the *Doppler frequency* domain, or just the *Doppler* domain. This dependence is denoted by Doppler frequency $\omega$.

The three spectral domains are summarized in Table 2.2 along with the mathematical definitions for their Fourier transformations. To perform a transformation into a spectral domain, insert the channel function into the brackets of the expression in the column of Table 2.2 marked *Transform*. To transform out of the spectral domain, insert the channel function into the brackets of the expression in the column marked *Inverse Transform*.

Table 2.2: Fourier transform definitions for each channel dependency.

| Domain Pairs | Transform | Inverse Transform |
|---|---|---|
| frequency, $f$ $\Longleftrightarrow$ delay, $\tau$ | $\int_{-\infty}^{+\infty} \{\} \exp(j2\pi\tau f)df$ | $\int_{-\infty}^{+\infty} \{\} \exp(-j2\pi\tau f)d\tau$ |
| position, $\vec{r}$ $\Longleftrightarrow$ wavevector, $\vec{k}$ | $\int_{-\infty}^{+\infty} \{\} \exp(-j\vec{k}\cdot\vec{r})d\vec{r}$ | $\frac{1}{(2\pi)^3}\int_{-\infty}^{+\infty} \{\} \exp(j\vec{k}\cdot\vec{r})d\vec{k}$ |
| time, $t$ $\Longleftrightarrow$ Doppler, $\omega$ | $\int_{-\infty}^{+\infty} \{\} \exp(-j\omega t)dt$ | $\frac{1}{2\pi}\int_{-\infty}^{+\infty} \{\} \exp(j\omega t)d\omega$ |

*Note: $2\pi$ or not $2\pi$?*

A keen observer will note that the frequency-delay Fourier pairs ($f$ and $\tau$), are defined differently than either time-Doppler ($t$ and $\omega$) or space-wavevector ($\vec{r}$ and $\vec{k}$). While the latter are *units* and *radian units*$^{-1}$ Fourier pairs, frequency and delay are defined as *units* and *units*$^{-1}$ Fourier pairs. This definition was chosen, not only to follow conventions in the wireless literature, but also to emphasize the difference between delay-frequency and time-Doppler relationships which are easily confused.

The transformations of Table 2.2 may operate on $\tilde{h}(f,\vec{r},t)$ in any order and combination. When one or more of the channel dependencies have been transformed into the spectral domain, a *transfer function* has been created. A transfer function will be written in the following form throughout this work:

$$\tilde{H}(\text{transformed dependencies; untransformed dependencies})$$

where the transformed dependencies are either $\tau$, $\vec{k}$, or $\omega$ and the untransformed dependencies are either $f$, $\vec{r}$, or $t$. For example, the transfer function $\tilde{H}(\tau,\omega;\vec{r})$ represents a Fourier transform of the channel, $\tilde{h}(f,\vec{r},t)$, with respect to both frequency, $f$, and time, $t$.

Various types of transfer functions are commonly used in the wireless literature and have developed specific terminology. Several of these specific transfer functions are listed below:

- $\tilde{H}(\tau;\vec{r},t)$: This transfer function is called the *channel impulse response*. It is the received baseband signal after sending a very short modulated pulse at the transmitter [10].

- $\tilde{H}(\vec{k}; f, t)$: This transfer function is called the *radio channel* by the International Telecommunications Union (ITU). It is the formal definition used by the organization to characterize wireless propagation [11].
- $\tilde{H}(\tau, \vec{k}, \omega)$: This transfer function is a Fourier transform of $\tilde{h}(f, \vec{r}, t)$ for all three dependencies. We define this to be the *complete transfer function.* Complete transfer functions are useful in stochastic channel modeling when defining power spectra.

### 2.3.2 General Signal Transmission

Armed with the complete definition of the baseband spatio-temporal channel, it is now possible to study the wireless transmission of a signal, $\tilde{x}(t)$, through a channel that varies with space, time, and frequency. For a linear, time-varying channel, the received signal as a function of time and space is the result of the following integration:

$$\tilde{y}(t, \vec{r}) = \int_{-\infty}^{+\infty} \tilde{H}(\tau; \vec{r}, t)\tilde{x}(t - \tau)\, d\tau \tag{2.20}$$

The result in Eqn (2.20) may also be calculated using the untransformed channel, $\tilde{h}(f, \vec{r}, t)$, rather than its delay transform, $\tilde{H}(\tau; \vec{r}, t)$:

$$\tilde{y}(t, \vec{r}) = \int_{-\infty}^{+\infty} \tilde{h}(f, \vec{r}, t)\tilde{X}(f) \exp(j2\pi f t)\, df \tag{2.21}$$

These equations are the most general input-output relationships for signal transmission through a wireless channel with a single transmitter.

### 2.3.3 Static Channel Transmission

In a linear time-invariant wireless channel (or, simply, a *static* channel) there are no moving scatterers within the propagation environment. Such a channel may be represented as a function of only frequency, $f$, and position, $\vec{r}$. For such a channel, the general transmission equation of Eqn (2.20) reduces to

$$\tilde{y}(t, \vec{r}) = \int_{-\infty}^{+\infty} \tilde{H}(\tau; \vec{r})\tilde{x}(t - \tau)\, d\tau \tag{2.22}$$

Note that Eqn (2.22) is in the form of a convolution integral. Therefore, the relationship for the received signal, $\tilde{y}(t, \vec{r})$, may be written as the convolution of transmitted signal and channel:

$$\tilde{y}(t, \vec{r}) = \tilde{H}(\tau; \vec{r})\Big|_{\tau = t} \otimes \tilde{x}(t) \tag{2.23}$$

Of course, this convolution may also be written as the product of the Fourier pairs of Eqn (2.23):

$$\tilde{Y}(f;\vec{r}) = \tilde{h}(f,\vec{r})\tilde{X}(f) \tag{2.24}$$

The static channel arises repeatedly in channel analysis when either the significant scatterers in the propagation environment are genuinely static or when the time-variations are present, but occur on a scale that does not affect the operation of the receiver.

### 2.3.4 Mobile Receiver Transmission

Another special case of the basic channel input-output relationships is the case of a mobile receiver. The motion of a receiver at any given instant, may be characterized by a velocity vector, $\vec{v}$, which represents the speed and direction of the receiver. Now vector position, $\vec{r}$, becomes a function of scalar time, $t$, according to the simple equation of constant-velocity motion: $\vec{r} = \vec{v}t$. Therefore, the *mobile* received voltage signal is expressed solely as a function of time, $t$:

$$\tilde{y}(t) = \tilde{y}(t,\vec{r})\Big|_{\vec{r}=\vec{v}t} \tag{2.25}$$

which may be calculated by

$$\tilde{y}(t) = \int\limits_{-\infty}^{+\infty} \tilde{H}(\tau;\vec{r},t)\Big|_{\vec{r}=\vec{v}t}\tilde{x}(t-\tau)\,d\tau \tag{2.26}$$

The mobile case emphasizes the flexibility of the full-dependency baseband channel representation, $\tilde{h}(f,\vec{r},t)$. As a function of position, the channel representation may be used to study receivers that operate with antenna arrays with elements at various positions in space. After the time-velocity substitution, however, the channel representation may be used to study single-antenna receivers moving through space.

## 2.4 Stochastic Channel Characterization

This section introduces the fundamental concepts behind stochastic channel characterization. Autocorrelation functions and power spectra are defined for the channel in frequency, time, and space. The RMS spectral spread is introduced as an informal measure of channel coherence. The idea of duality between the three basic dependencies is also discussed.

### 2.4.1 Autocorrelation Relationships

The most common way to characterize the evolution of a stochastic process is by calculating the *autocorrelation* of a function. The definition for an autocorrelation of a time-varying stochastic channel, $\tilde{h}(t)$, is

$$C_{\tilde{h}}(t_1, t_2) \doteq \mathrm{E}\left\{\tilde{h}(t_1)\tilde{h}^*(t_2)\right\} \tag{2.27}$$

where $\mathrm{E}\{\cdot\}$ denotes ensemble averaging. Eqn (2.27) captures the time-evolution of $\tilde{h}(t)$ by averaging products of the function values at two different points in time, $t_1$ and $t_2$.

Most of the stochastic processes studied in this work are *wide-sense stationary* (WSS). The autocorrelation of a WSS stochastic process, by definition, only depends on the difference in time between $t_1$ and $t_2$. In other words, the correlation behavior is invariant of time:

$$C_{\tilde{h}}(t_1, t_2) = C_{\tilde{h}}(t_0 + t_1, t_0 + t_2) \quad \text{for all } t_0 \tag{2.28}$$

Therefore, a WSS autocorrelation is usually written as the function of one time variable, $\Delta t$, which is equal to $t_2 - t_1$. This WSS definition for autocorrelation is shown below:

$$C_{\tilde{h}}(\Delta t) = \mathrm{E}\left\{\tilde{h}(t)\tilde{h}^*(t + \Delta t)\right\} \tag{2.29}$$

Similar autocorrelation definitions exist for stochastic channels that are functions of frequency, $f$, and space, $\vec{r}$.

*Note: The Second Condition for WSS*

There is a second condition which must hold for a stochastic process to be truly WSS. In addition to being *autocorrelation stationary*, a stochastic process must also be *mean stationary*. Using the time-varying baseband channel as an example, mean stationarity holds if the value $\mathrm{E}\left\{\tilde{h}(t)\right\}$ is *not* a function of time, $t$. Most processes encountered in real-life modeling fail the WSS test due to their autocorrelation statistics. But be aware that pathological processes exist having nonstationary means *and* stationary autocorrelations.

### Autocovariance

There are several useful variations on the definition of an autocorrelation function. First, if the process is a zero-mean process, then the autocorrelation is said to be an *autocovariance*. Using the time-varying channel as an example, if $\mathrm{E}\{\tilde{h}(t)\} = 0$, then the function $C_{\tilde{h}}(\Delta t)$ is an autocovariance function. Otherwise, the following definition for autocovariance may be used which removes the mean value of the WSS process:

$$\begin{aligned} \bar{C}_{\tilde{h}}(\Delta t) &= \mathrm{E}\left\{\left[\tilde{h}(t_0) - \mu\right]\left[\tilde{h}^*(t_0 + \Delta t) - \mu^*\right]\right\}, \qquad \text{where } \mu = \mathrm{E}\left\{\tilde{h}(t)\right\} \\ &= C_{\tilde{h}}(\Delta t) - |\mu|^2 \end{aligned} \tag{2.30}$$

For many autocorrelation functions of the complex baseband channel, $\mu = 0$ and the autocorrelation *is* an autocovariance. The definition in Eqn (2.30) is most useful when studying random processes of envelope and power, which have a positive mean value.

### Unit Autocovariance

A second useful definition, the *unit autocovariance*, is an autocovariance function that has been normalized against the mean power of the process. In terms of the time-varying stochastic channel, mean power is equal to $C_{\tilde{h}}(0)$:

$$C_{\tilde{h}}(0) = \mathrm{E}\left\{\tilde{h}(t)\tilde{h}^*(t)\right\} = \mathrm{E}\left\{|\tilde{h}(t)|^2\right\} \tag{2.31}$$

Thus, the full definition for a unit autocovariance, hereafter denoted $\varrho_{\tilde{h}}(\Delta t)$, is given in terms of the autocorrelation by

$$\varrho_{\tilde{h}}(\Delta t) = \frac{C_{\tilde{h}}(\Delta t) - \left|\mathrm{E}\left\{\tilde{h}(t)\right\}\right|^2}{C_{\tilde{h}}(0) - \left|\mathrm{E}\left\{\tilde{h}(t)\right\}\right|^2} \tag{2.32}$$

The definition of unit autocovariance will arise in the study of random *envelope* processes; most formalized definitions of channel coherence are based on the unit autocovariance of received voltage envelope.

### Joint Autocorrelation

Finally, to accommodate all the random dependencies of a channel, it is possible to define a joint autocorrelation as a function of frequency, space, and time separation. The definition follows logically from the single-dependency autocorrelation of Eqn (2.29):

$$C_{\tilde{h}}(\Delta f, \Delta\vec{r}, \Delta t) = \mathrm{E}\left\{\tilde{h}(f, \vec{r}, t)\tilde{h}^*(f + \Delta f, \vec{r} + \Delta\vec{r}, t + \Delta t)\right\} \tag{2.33}$$

provided that the channel is WSS with respect to time, position, and frequency.

### 2.4.2 Power Spectrum

Another convenient method for characterizing a WSS stochastic process is the use of a power spectrum. The power spectrum is defined by using the Fourier transform of the WSS process. Once again using the time-varying channel $\tilde{h}(t)$ as an example, the power spectrum is defined as

$$S_{\tilde{h}}(\omega) \doteq \mathrm{E}\left\{\left|\tilde{H}(\omega)\right|^2\right\} \tag{2.34}$$

where $\tilde{H}(\omega)$ and $\tilde{h}(t)$ are Fourier pairs. A power spectrum that describes temporal selectivity is specifically called a *Doppler spectrum*. Power spectra are also defined for frequency selectivity (delay spectrum) and spatial selectivity (wavevector spectrum).

The usefulness of a power spectrum arises from the Wiener-Khintchine theorem [8, p. 70]. This theorem states that the power spectrum and the autocorrelation are Fourier transform pairs:

$$S_{\tilde{h}}(\omega) = \int_{-\infty}^{+\infty} C_{\tilde{h}}(\Delta t) \exp(-j\omega\Delta t)\, d\Delta t \tag{2.35}$$

$$C_{\tilde{h}}(\omega) = \frac{1}{2\pi} \int_{-\infty}^{+\infty} S_{\tilde{h}}(\Delta t) \exp(j\omega\Delta t)\, d\omega \tag{2.36}$$

The Wiener-Khintchine theorem is a very powerful result which is used often in spectral modeling of stochastic systems.

For the complete radio channel, it is possible to define a joint power spectrum that is a function of delay, wavevector, and Doppler:

$$S_{\tilde{h}}(\tau, \vec{k}, \omega) \doteq \mathrm{E}\left\{\left|\tilde{H}(\tau, \vec{k}, \omega)\right|^2\right\} \tag{2.37}$$

The Wiener-Khintchine theorem also holds between the joint power spectrum, $S_{\tilde{h}}(\tau, \vec{k}, \omega)$, and the joint autocorrelation, $C_{\tilde{h}}(\Delta f, \Delta\vec{r}, \Delta t)$:

$$C_{\tilde{h}}(\Delta f, \Delta\vec{r}, \Delta t) \Longleftrightarrow S_{\tilde{h}}(\tau, \vec{k}, \omega)$$

$$S_{\tilde{h}}(\tau, \vec{k}, \omega) = \iiint_{-\infty}^{+\infty} C_{\tilde{h}}(\Delta f, \Delta\vec{r}, \Delta t) \exp\left(j\left[2\pi f\Delta\tau - \vec{k}\cdot\Delta\vec{r} - \omega\Delta t\right]\right) d\Delta f\, d\Delta\vec{r}\, d\Delta t \tag{2.38}$$

$$C_{\tilde{h}}(\Delta f, \Delta\vec{r}, \Delta t) = \frac{1}{(2\pi)^4} \iiint_{-\infty}^{+\infty} S_{\tilde{h}}(\tau, \vec{k}, \omega) \exp\left(-j\left[2\pi f\Delta\tau - \vec{k}\cdot\Delta\vec{r} - \omega\Delta t\right]\right) d\tau\, d\vec{k}\, d\omega \tag{2.39}$$

The actual relationships between joint spectrum and joint autocorrelation can be difficult to grasp. The following presentation clarifies how joint spectrum-autocorrelations work together to characterize a channel.

### Time-Frequency Transform Map

To truly understand the concept of joint spectra and autocorrelations, it is best to eliminate some of the dependencies from the full space-time-frequency channel model. Consider the case of a fixed, single-antenna receiver operating in a channel that is only a function of time, $t$, and frequency, $f$. For this type of channel, Figure 2.9 is a roadmap through the various stochastic relationships [4, 12]. The stochastic, second-order behavior of this channel may be characterized by its joint autocorrelation, $C_{\tilde{h}}(\Delta t, \Delta f)$, or its power spectrum, $S_{\tilde{h}}(\omega, \tau)$. In a WSS channel, only knowledge of one is necessary since they are two-dimensional Fourier transform pairs.

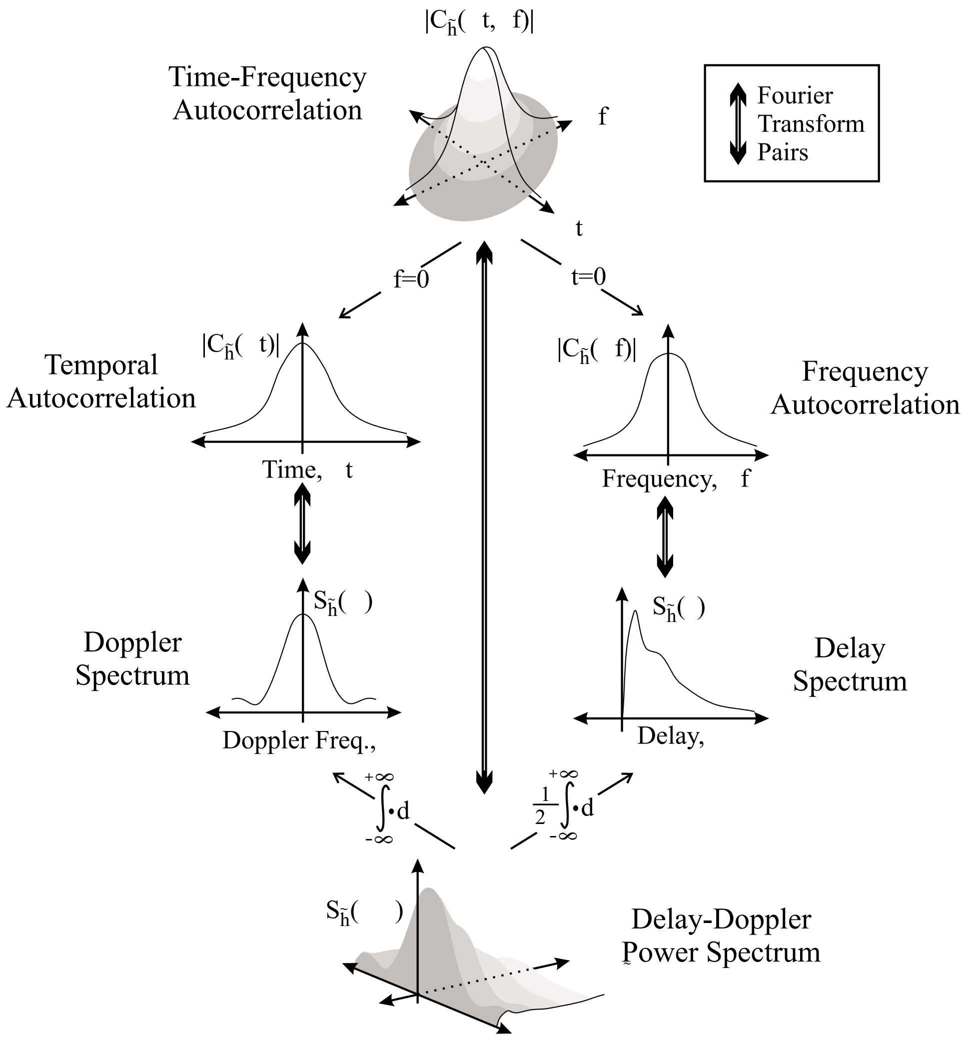


Figure 2.9: Autocorrelation and power spectrum relationships for time and frequency.

If the channel is *narrowband* (signal bandwidth is less than the coherence bandwidth), then the fading is flat about the carrier frequency and it suffices to characterize the stochastic channel with an autocorrelation that is only a function of time or a power spectrum that is only a function of Doppler. These one-dimensional functions may be calculated from their two-dimensional counterparts as

$$C_{\tilde{h}}(\Delta t) = C_{\tilde{h}}(\Delta t, \Delta f)\big|_{\Delta f=0} \tag{2.40}$$

$$S_{\tilde{h}}(\omega) = \int_{-\infty}^{+\infty} S_{\tilde{h}}(\omega, \tau)\, d\tau \tag{2.41}$$

This calculation is shown on the left side of Figure 2.9. The remaining one-dimensional functions – the temporal autocorrelation and Doppler spectrum – are Fourier transform pairs.

The right-hand side of Figure 2.9 represents characterization of a *static* channel that does not vary with time. A one-dimensional frequency autocorrelation is calculated from the joint time-frequency autocorrelation by setting $\Delta t$ equal to 0. A one-dimensional delay spectrum is calculated from the joint Doppler-delay spectrum by integrating out the Doppler frequency, $\omega$. And, of course, the resulting frequency autocorrelation and delay spectrum are Fourier transform pairs.

Many researchers have used Figure 2.9 to understand and characterize the stochastic behavior of linear, time-varying channels. It was first presented by [12] in the context of radio astronomy measurements. For this application, an antenna dish is located in a fixed position and receives signals that vary with time and frequency from the heavens. The concept may be extended to include spatial relationships as well.

### Space-Frequency Transform Map

For a static channel, we may extend the time-frequency transform map in Figure 2.9 for the space-frequency relationships shown in Figure 2.10. In this diagram, joint space-frequency autocorrelation and joint wavevector-delay spectrum are shown to be two-dimensional Fourier transform pairs. One-dimensional spatial or frequency autocorrelations may be calculated by zeroing out $\Delta f$ or $\Delta\vec{r}$, respectively, in the joint autocorrelation. One-dimensional wavevector or delay spectra may be calculated by integrating out $\tau$ or $\vec{k}$, respectively, in the joint power spectrum.

The only key difference between Figure 2.10 and Figure 2.9 is to recognize that position and wavevector are *vector* dependencies. Thus, there are actually three scalar values represented by $\vec{r}$ and $\vec{k}$.

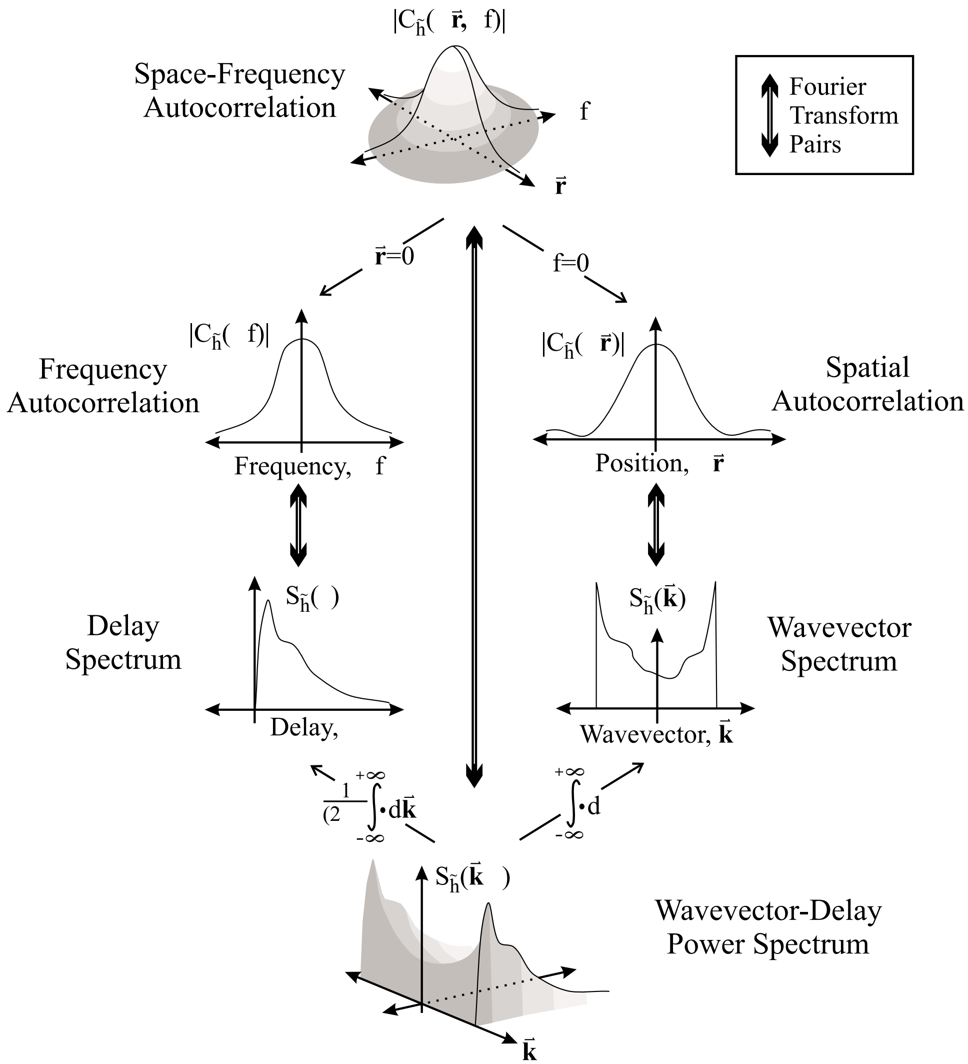


Figure 2.10: Autocorrelation and power spectrum relationships for space and frequency.

**Complete Transform Map**

Of course, all three dependencies – space, time, and frequency – may be studied jointly. The combined relationships of Figure 2.9 and Figure 2.10 are shown in one complete transform map, Figure 2.11. This figure is best viewed as a single "tile" in a transform map that continues with identical tiles in all directions. For example, the conversion from a joint spatial-temporal autocorrelation to a one-dimensional temporal autocorrelation is made by wrapping around from the right edge of Figure 2.11 to the left edge. Likewise, the complete autocorrelation of the stochastic channel is shown to be the three-dimensional Fourier transform pair of the complete power spectrum by wrapping around from the top edge of Figure 2.11 to the bottom edge. Although Figure 2.11 contains numerous channel dependencies and definitions, navigation through the relationships is crucial for understanding the stochastic characterization of the multivariable wireless channel.

### 2.4.3 RMS Power Spectrum Width

It is a basic principle in Fourier analysis that as function becomes narrower in one domain, its Fourier transform becomes wider in the transform domain. Therefore, the RMS width of a power spectrum can provide insight into the coherence of a channel: as the power spectrum widens in the transform domain, its autocorrelation becomes narrower and coherence decreases. RMS widths may be defined for channel power spectrum as a function of delay, Doppler, and wavenumber.

**RMS Delay Spread**

The RMS delay spread is defined from the delay spectrum of a stochastic channel. Mathematically, this delay spread is the second centered moment of this spectrum, defined as

$$\sigma_\tau^2 = \overline{\tau^2} - (\overline{\tau})^2, \quad \text{where } \overline{\tau^n} = \frac{\int\limits_{-\infty}^{+\infty} \tau^n S_{\tilde{h}}(\tau) d\tau}{\int\limits_{-\infty}^{+\infty} S_{\tilde{h}}(\tau) d\tau} \tag{2.42}$$

A larger delay spread implies increased frequency selectivity and a smaller coherence bandwidth. Many wireless engineers calculate the coherence bandwidth using the rule-of-thumb $B_C \approx \frac{1}{5\sigma_\tau}$.

**Example 2.2: Exponential Delay Spectrum**

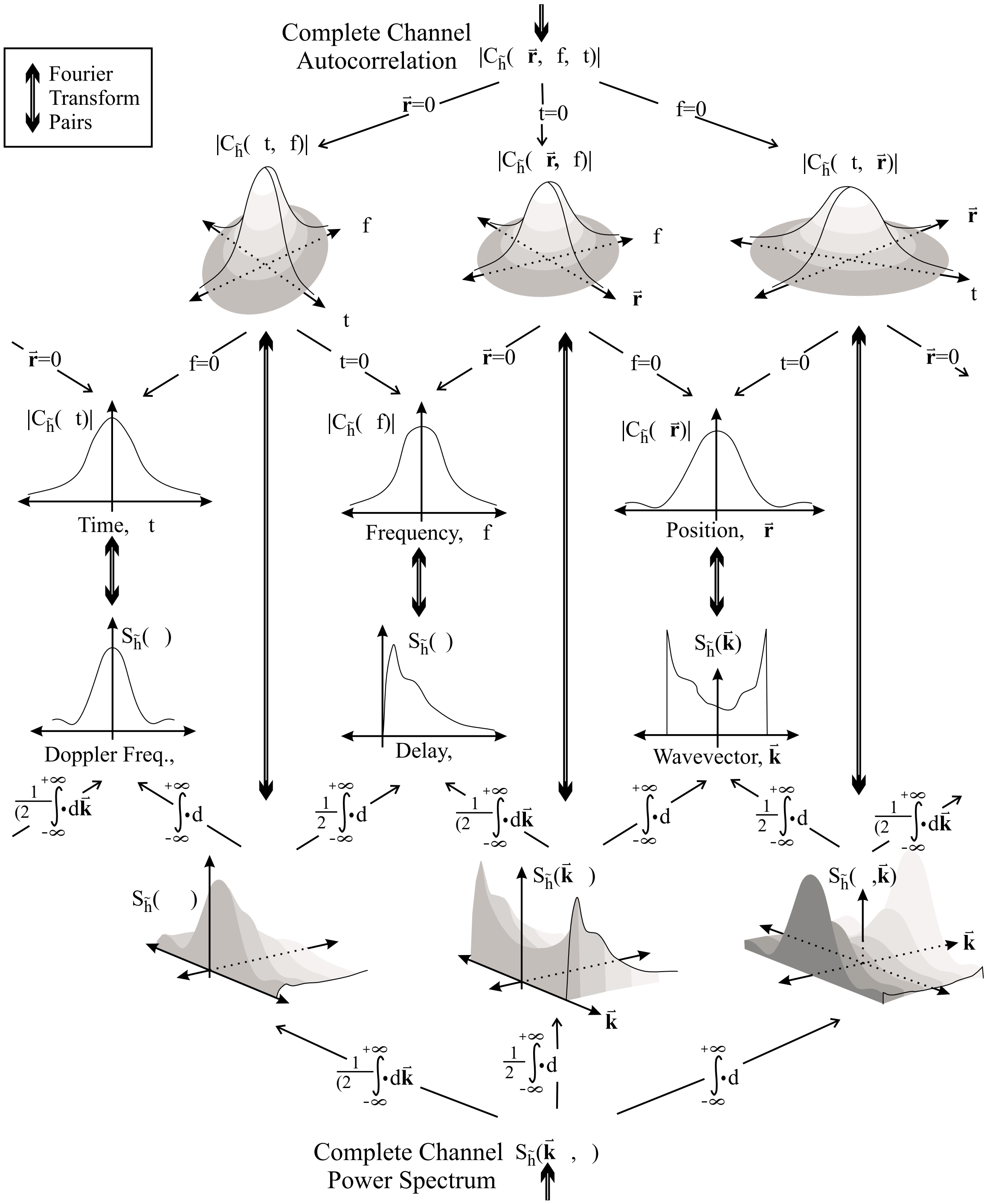


Figure 2.11: Autocorrelation and power spectrum relationships for space, time, and frequency.

**Problem:** The received power of multipath components typically decreases exponentially as a function of time delay. As a result, many engineers approximate the delay spectrum as an exponential-shaped function. Develop expressions for delay spectrum and autocorrelation as a function of RMS delay spread, $\sigma_\tau$.

**Solution:** If the RMS delay spread of an exponential-shaped spectrum is $\sigma_\tau$, then the delay spectrum must take the form

$$S_{\tilde{h}}(\tau) = S_0 \exp\left(-\frac{\tau}{\sigma_\tau}\right) u(\tau)$$

where $S_0$ is an arbitrary constant and $u(\tau)$ is the unit step function. Computing the inverse Fourier transform of this function produces the frequency autocorrelation:

$$C_{\tilde{h}}(\Delta f) = \frac{S_0 \sigma_\tau}{1 + j2\pi \Delta f \sigma_\tau}$$

The shape and widths of the delay spectrum and frequency autocorrelation are shown below:

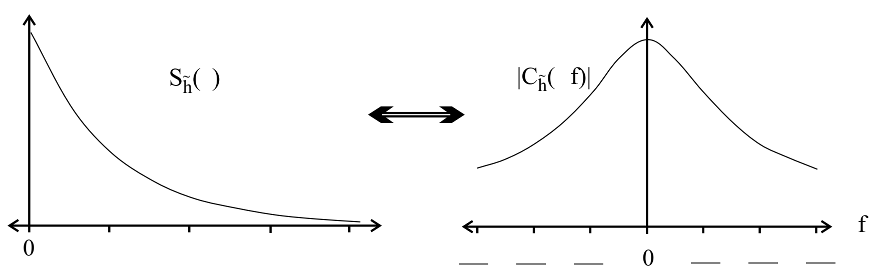


Note the inverse proportionality between the widths of the spectrum and the autocorrelation as the RMS delay spread, $\sigma_\tau$, increases.

---

**RMS Doppler Spread**

In definition, the RMS Doppler spread is nearly identical to RMS delay spread. This delay spread is calculated as the second centered moment of the Doppler spectrum:

$$\sigma_\omega^2 = \overline{\omega^2} - (\overline{\omega})^2, \quad \text{where } \overline{\omega^n} = \frac{\int_{-\infty}^{+\infty} \omega^n S_{\tilde{h}}(\omega) d\omega}{\int_{-\infty}^{+\infty} S_{\tilde{h}}(\omega) d\omega} \tag{2.43}$$

An increased Doppler spread implies a channel with wilder temporal fluctuations and a smaller coherence time.

**Example 2.3: Gaussian Doppler Spectrum**

**Problem:** The power in the Doppler spectrum of many types of time-varying channels is concentrated heavily at $\omega = 0$ and quickly diminishes for larger values of $|\omega|$. One model for this type of behavior is a Gaussian-shaped Doppler spectrum. Develop expressions for Doppler spectrum and autocorrelation as a function of Doppler spread, $\sigma_\omega$.

**Solution:** If the RMS Doppler spread of a Gaussian-shaped spectrum is $\sigma_\omega$, then the Doppler spectrum must take the following form:

$$S_{\tilde{h}}(\omega) = S_0 \exp\left(-\frac{\omega^2}{2\sigma_\omega^2}\right)$$

where $S_0$ is some arbitrary constant. The temporal autocorrelation, $C_{\tilde{h}}(\Delta t)$, is the inverse Fourier transform:

$$C_{\tilde{h}}(\Delta t) = \frac{S_0 \sigma_\omega}{\sqrt{2\pi}} \exp\left(-\frac{\Delta t^2 \sigma_\omega^2}{2}\right)$$

The shape and relative widths of the Doppler spectrum and temporal autocorrelation are shown below:

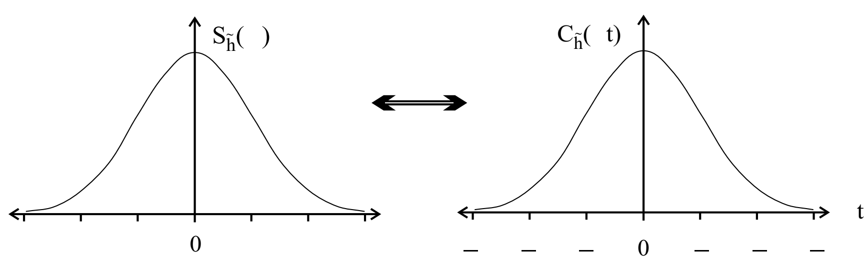


Note the inverse proportionality between the widths of the spectrum and the autocorrelation as the RMS Doppler spread, $\sigma_\omega$, increases.

### RMS Wavenumber Spread

The definition for RMS wavenumber spread follows immediately from the definitions of the previous RMS spreads, with one important exception: since the wavevector spectrum is a function of a vector, not a scalar, a direction in space must be specified before calculating the wavenumber spread. We will begin by expressing the wavevector spectrum as a function of radial coordinates: $S_{\tilde{h}}(k, \theta, \varphi)$, where

$$\vec{k} = k \left[\cos\varphi \cos\theta \hat{x} + \cos\varphi \sin\theta \hat{y} + \sin\varphi \hat{z}\right]$$

See Appendix 2.A.2 for an explanation of this geometry. If azimuthal angle, $\theta$, and elevation angle, $\varphi$, have been selected, then we shall write the wavevector spectrum as a function of wavenumber alone: $S_{\tilde{h}}(k)$. The definition for wavenumber spread is then given by

$$\sigma_k^2 = \overline{k^2} - (\overline{k})^2, \quad \text{where } \overline{k^n} = \frac{\int\limits_{-\infty}^{+\infty} k^n S_{\tilde{h}}(k) dk}{\int\limits_{-\infty}^{+\infty} S_{\tilde{h}}(k) dk} \tag{2.44}$$

This value must be recalculated if the orientation, $\theta$ and $\varphi$, changes.

### Example 2.4: Omnidirectional Wavenumber Spectrum

**Problem:** Spatial selectivity often is studied as a function of scalar position, $r$, which is characterized by a one-dimensional *wavenumber* (instead of wavevector) spectrum. A common model for wavenumber spectrum is the Clarke omnidirectional spectrum, which arises in cluttered outdoor environments when multipath power arrives from the horizon in every direction [13]. The wavenumber spectrum for this case is

$$S_{\tilde{h}}(k) = \frac{S_0}{\sqrt{k_{\max}^2 - k^2}} \quad \text{for } |k| \leq k_{\max}$$

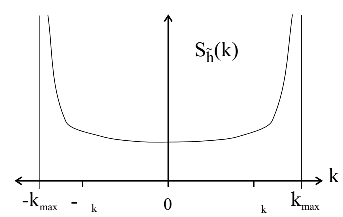


where $k$ is wavenumber, $S_0$ is an arbitrary constant, and $k_{\max}$ is the maximum free space wavenumber. Find expressions for the RMS wavenumber spread and spatial autocorrelation.

**Solution:** The wavenumber spread may be calculated in terms of $k_{\max}$ using Eqn (2.44):

$$\sigma_k = \frac{k_{\max}}{\sqrt{2}}$$

The spatial autocorrelation of this wavenumber spectrum is

$$C_{\tilde{h}}(\Delta r) = \frac{S_0}{2}\, \mathrm{J}_0(k_{\max}\Delta r)$$

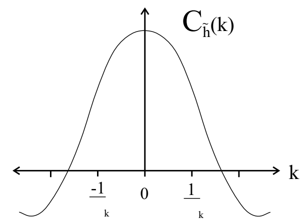

where $\mathrm{J}_0(\cdot)$ is a zero-order Bessel function.

---

### 2.4.4 Channel Duality Principle

By now it is obvious that a tremendous amount of similarity exists in the stochastic characterization of time, frequency, and space. An analytical technique developed for one dependency is equally applicable to the others. This is the principle of *duality* in channel modeling [14].

The time, frequency, and spatial *duals* of the basic stochastic concepts discussed in this section are summarized by Table 2.3. Despite the fact that each dependency characterizes a completely different aspect of the wireless channel, the concepts and terminology used to study each are the same. A generic summary of Section 2.4 might go something like this:

> *The stochastic wireless channel as a function of* **(time, frequency, space)** *displacement may be characterized by an autocorrelation function. The Fourier transform of the autocorrelation produces a* **(Doppler, delay, wavevector)** *spectrum. The width of this spectrum is characterized by its RMS* **(Doppler, delay, wavenumber)** *spread. As this spread increases, the* **(temporal, frequency, spatial)** *selectivity of the channel increases and the coherence* **(time, bandwidth, distance)** *decreases.*

As this work develops further concepts in channel modeling, the duality principle will be revisited extensively.

**Example 2.5: Coherence Time Duality**

**Problem:** The RMS Doppler spread, $\sigma_\omega$, of a time-varying, narrowband channel is known. Estimate the coherence time, $T_c$.

Table 2.3: Channel duality relationships between time, frequency, and space.

| | *Time* | *Frequency* | *Space* |
|---|---|---|---|
| Dependency | time, $t$ | frequency, $f$ | position, $\vec{r}$ |
| Coherence Window | time, $T_c$ | bandwidth, $B_c$ | distance, $D_c$ |
| Spectral Domain | Doppler, $\omega$ | delay, $\tau$ | wavevector, $\vec{k}$ |
| RMS Spectral Width | Doppler spread, $\sigma_\omega$ | delay spread, $\sigma_\tau$ | wavenumber spread, $\sigma_k$ |

**Solution:** We have yet to define a formal definition for coherence time. However, it was stated in Section 2.4.3 that the coherence bandwidth, $B_c$, for a dispersive channel is inversely proportional to $5\sigma_\tau$. It follows by duality that a similar rule-of-thumb should work for time-varying channels. The following substitutions are made: $B_c \Longrightarrow T_c$ and $\sigma_\tau \Longrightarrow \frac{1}{2\pi}\sigma_\omega$ (the $2\pi$ is the difference between Fourier transform definitions of the Doppler and delay domains). The "new" coherence time rule-of-thumb is now:

$$T_c \approx \frac{2\pi}{5\sigma_\omega}$$

which agrees with rule-of-thumb estimates presented in [10].

## 2.5 Chapter Summary

This chapter is an introduction to the terminology and mathematics used in the analysis of wireless channels. The following topics were discussed:

- Complex baseband representation allows for the study of radio channel effects on transmitted signals without dealing directly with the oscillating carrier wave.
- A channel may vary as a function of time, space, or frequency. Fluctuations as a function of each dependency may be characterized as follows:
  - A channel that does not change significantly has *coherence*.
  - A channel that changes significantly has *selectivity*.
  - A channel having selectivity that affects communications is a *fading* channel.
- There are three Fourier pairs which assist in channel analysis:
  - Frequency, $f \Longleftrightarrow$ Delay, $\tau$
  - Position, $\vec{r} \Longleftrightarrow$ Wavevector, $\vec{k}$
  - Time, $t \Longleftrightarrow$ Doppler Frequency, $\omega$
- In stochastic channel modeling, the channel is a stochastic random process with respect to time, frequency, and position.
  - Autocorrelation functions describe evolution over time, space, and frequency.
  - Power spectrum is the Fourier transform of autocorrelation for WSS processes.
  - A transform map is helpful when studying joint autocorrelations and power spectra.
  - The RMS spread measures the width of the power spectrum in one dimension.
  - Analysis used in one stochastic dependency may often be applied to the others (channel duality).

Up until this point, the theory presented thus far has been mathematical and generic. Save for the space-varying analysis, the concepts in this chapter are valid for analyzing *any* communications system with a stochastic time-varying channel. However, the wireless channel has additional characteristics and structure related to the physics of free space radio wave propagation. Chapter 3 creates a link between generic channel modeling theory and the physics of the small-scale channel.

## 2.A Functions of Three-Dimensional Space

This appendix discusses several concepts in analysis of functions that depend on three-dimensional position vectors and wavevectors.

### 2.A.1 Vector Notation for Fourier Transforms

The Fourier transform of a function of three-dimensional position is actually a three-fold transform over scalar coordinates. Thus, we write the transform pairs as

$$\tilde{h}(x, y, z) \Longleftrightarrow \tilde{H}(k_x, k_y, k_z)$$

where $x$, $y$, and $z$ are the Cartesian position coordinates and $k_x$, $k_y$, and $k_z$ are their corresponding wavenumbers in the spectral domain. The three-fold Fourier transform, therefore, requires three integrations which are written as

$$\tilde{H}(k_x, k_y, k_z) = \int_{-\infty}^{+\infty}\int_{-\infty}^{+\infty}\int_{-\infty}^{+\infty} \tilde{h}(x, y, z) \exp\left(-j\left[k_x x + k_y y + k_z z\right]\right)\, dx\, dy\, dz \tag{2.45}$$

The notation of Eqn (2.45) is cumbersome. Throughout this work, a set of vector shorthand notation is used to simplify the equations and emphasize the concepts rather than the raw mathematics.

First, the dependencies of both position and wavevector are collapsed into three-dimensional vectors as follows:

$$\vec{r} \doteq x\hat{x} + y\hat{y} + z\hat{z}$$

$$\vec{k} \doteq k_x\hat{x} + k_y\hat{y} + k_z\hat{z}$$

Next, the three-fold integrations over position variables or wavenumber variables is abbreviated into one integration over a vector partial, $d\vec{r}$ or $d\vec{k}$. These single integrations are defined to be

$$\int_{-\infty}^{+\infty} d\vec{r} \doteq \int_{-\infty}^{+\infty}\int_{-\infty}^{+\infty}\int_{-\infty}^{+\infty} dx\, dy\, dz$$

$$\int_{-\infty}^{+\infty} d\vec{k} \doteq \int_{-\infty}^{+\infty}\int_{-\infty}^{+\infty}\int_{-\infty}^{+\infty} dk_x\, dk_y\, dk_z$$

With these substitutions, the set of forward and inverse Fourier transforms for functions of vector position is given by the following:

$$\tilde{H}(\vec{k}) = \int_{-\infty}^{+\infty} \tilde{h}(\vec{r}) \exp(-j\vec{k}\cdot\vec{r})\, d\vec{r} \tag{2.46}$$

$$\tilde{h}(\vec{r}) = \frac{1}{(2\pi)^3} \int_{-\infty}^{+\infty} \tilde{H}(\vec{k}) \exp(j\vec{k} \cdot \vec{r})\, d\vec{k} \tag{2.47}$$

where $(\cdot)$ is a scalar product.

### 2.A.2 Scalar Collapse of Position Vectors

A function that depends on a three-dimensional position vector may be treated as a function of a scalar position variable by fixing the angular orientation of the spatial dependence. Thus, a full spatial channel, $\tilde{h}(\vec{r})$, may be expressed as a function of scalar position, $r$, by sacrificing two degrees of freedom in the representation. This reduction is useful for applications only requiring one degree of spatial freedom, such as a linear array of receiver antennas or constant-velocity motion in space.

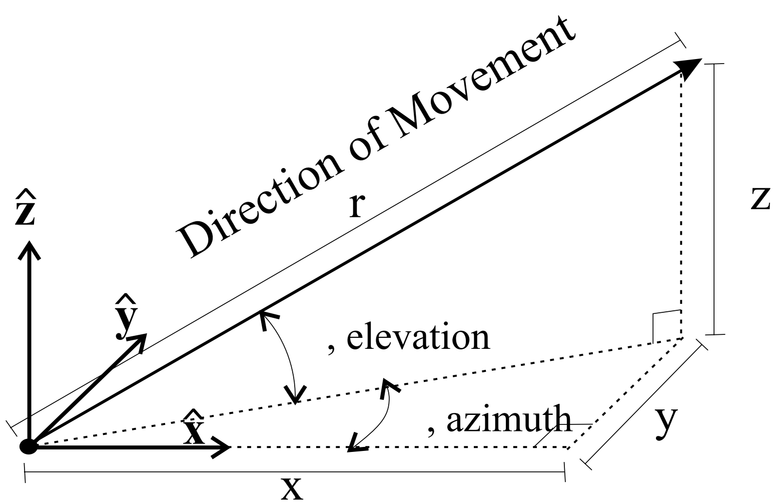


Figure 2.12: Relationship between $(x, y, z)$ and $(r, \theta, \varphi)$ coordinates.

The first step to reduce the spatial dependence of $\tilde{h}(\vec{r})$ is to break down the position variable $\vec{r}$ into its constituent Cartesian coordinates:

$$\vec{r} = x\hat{x} + y\hat{y} + z\hat{z}$$

where $\hat{x}$, $\hat{y}$, and $\hat{z}$ are the orthonormal Cartesian basis vectors for three-dimensional free space. We desire to fix the orientation of the movement in space as a function of a scalar value $r$, constraining movement on a line that points towards a direction in azimuth, $\theta$, and an elevation angle above the horizon, $\varphi$. In terms of these polar coordinates ($r$, $\theta$, and $\varphi$), the Cartesian coordinates become

$$x = r\cos\varphi\cos\theta$$

$$y = r\cos\varphi\sin\theta$$
$$z = r\sin\varphi$$

These relationships are graphed in Figure 2.12. Therefore, we can write:

$$\tilde{h}(\vec{r}) = \tilde{h}(r;\theta,\varphi) \tag{2.48}$$

where $\theta$ and $\varphi$ are fixed constants in all subsequent analysis. To avoid cumbersome notation, the scalar-distance channel is written as $\tilde{h}(r)$, implying that $\theta$ and $\varphi$ have been set to some arbitrary direction. This vector-to-scalar collapse may be applied to any function that has 3D space as one of its dependencies (spatio-temporal channels, received signals, and autocorrelations, for example).

**Example 2.6: Plane Wave Channel**

**Problem:** A static, narrowband channel of the form $\tilde{h}(\vec{r}) = V_0\exp(-jk_0\vec{r}\cdot\hat{x})$ is a function of 3D space. If azimuth, $\theta$, and elevation, $\varphi$, angles are known, calculate the scalar representation, $\tilde{h}(r)$.

**Solution:** The vector, $\vec{r}$, may be expressed as $r\hat{r}$, where $r$ is the scalar position and $\hat{r}$ is a unit vector given by

$$\hat{r} = \cos\varphi\cos\theta\,\hat{x} + \cos\varphi\sin\theta\,\hat{y} + \sin\varphi\,\hat{z}$$

Substituting $\vec{r} = r\hat{r}$ into the given function of $\tilde{h}(\vec{r})$ produces the scalar representation:

$$\tilde{h}(r) = V_0\exp(-jk_0 r\cos\varphi\cos\theta)$$

### 2.A.3 Scalar Collapse of Wavevectors

A scalar distance dependence implies a scalar Fourier transform dependence as well. For a channel, $\tilde{h}(r)$, the Fourier transform is given by $\tilde{H}(k)$ where $k$ is a wavenumber instead of a wavevector. We then use the standard scalar definition to define the Fourier pairs, $\tilde{h}(r) \Longleftrightarrow \tilde{H}(k)$:

$$\tilde{H}(k) = \int_{-\infty}^{+\infty}\tilde{h}(r)\exp(-jkr)\,dr \tag{2.49}$$

$$\tilde{h}(r) = \frac{1}{2\pi} \int_{-\infty}^{+\infty} \tilde{H}(k) \exp(-jkr) \, dk \tag{2.50}$$

which is simpler than the relationship between the Fourier transform pairs defined for functions of 3D position.

The relationship between scalar wavenumber Fourier transforms, $\tilde{H}(k)$, and wavevector Fourier transforms, $\tilde{H}(\vec{k})$, is not as simple as the relationship between scalar position and vector position channels. For example, it is tempting to write a wavevector as function of polar coordinates:

$$\vec{k} = k \left[\cos\varphi \cos\theta \, \hat{x} \, + \, \cos\varphi \sin\theta \, \hat{y} \, + \, \sin\varphi \, \hat{z}\right] \tag{2.51}$$

and then treat the orientation of azimuth angle $\theta$ and elevation angle $\varphi$ as fixed. This is incorrect, because the scalar Fourier Transform, is *not* given by

**Incorrect:** $H(k) = H(k; \theta, \varphi)$

since this is inconsistent with the definitions of Eqn (2.48) and Eqn (2.49).

The appropriate definition is derived from the vector Fourier relationship after making the substitution $\vec{r} = r\hat{r}$, where $\hat{r}$ is a constant unit vector that points in the direction of scalar position displacement:

$$\tilde{h}(r) = \frac{1}{(2\pi)^3} \int_{-\infty}^{+\infty} \tilde{H}(\vec{k}) \exp(jr\vec{k} \cdot \hat{r}) \, d\vec{k} \tag{2.52}$$

Eqn (2.52) is then substituted into Eqn (2.49) to produce

$$\begin{aligned} \tilde{H}(k) &= \frac{1}{(2\pi)^3} \int_{-\infty}^{+\infty} \int_{-\infty}^{+\infty} \tilde{H}(\vec{k}) \exp\left(-jr \left[k - \vec{k} \cdot \hat{r}\right]\right) dr \, d\vec{k} \\ &= \frac{1}{(2\pi)^2} \int_{-\infty}^{+\infty} \tilde{H}(\vec{k}) \, \delta(k - \vec{k} \cdot \hat{r}) \, d\vec{k} \end{aligned} \tag{2.53}$$

Eqn (2.53) is the correct way to convert a wavevector Fourier transform to a wavenumber Fourier transform.

Geometrically, the integration over the delta function of Eqn (2.53) collects all of the components from the 3D Fourier transform, $\tilde{H}(\vec{k})$, which satisfy

$$k = \vec{k} \cdot \hat{r} \tag{2.54}$$

Eqn (2.54) represents a collection of wavevectors, $\vec{k}$, whose tips lie in a geometrical plane that is perpendicular to the direction of scalar position displacement, $\hat{r}$, and a distance, $k$, from the origin. Thus, for a given $k$, all of the values of $\tilde{H}(\vec{k})$ associated with this plane integrate and collapse to a single Fourier transform value in $\tilde{H}(k)$.

The relationship of Eqn (2.53) also holds for wavevector spectrum, $S_{\tilde{h}}(\vec{k})$, and wavenumber spectrum, $S_{\tilde{h}}(k)$. An example of the vector-to-scalar mapping in the wavevector domain follows.

**Example 2.7: Spherical Shell Spectrum**

**Problem:** For a channel wavevector spectrum that takes the form of a "spherical shell", the spectrum is zero everywhere except for values of $\vec{k}$ that lie on a sphere of radius $k_0$; the value of the power spectrum on this sphere is constant. Mathematically, this wavevector spectrum takes the form

$$S_{\tilde{h}}(\vec{k}) = \frac{2\pi S_0}{k_0}\delta(|\vec{k}| - k_0)$$

Calculate the *wavenumber* spectrum for any arbitrary orientation in space.

**Solution:** Start by inserting the 3D wavevector spectrum into Eqn (2.53) using Cartesian coordinates ($k_x$, $k_y$, $k_z$). Recognize that the wavevector spectrum is *isotropic* (identical regardless of orientation), so that the wavenumber spectrum is identical for all possible values of $\hat{r}$. We set $\hat{r} = \hat{z}$ for convenience:

$$\begin{aligned} S_{\tilde{h}}(k) &= \frac{S_0}{2\pi k_0} \iiint\limits_{-\infty}^{+\infty} \delta\left(\sqrt{k_x^2 + k_y^2 + k_z^2} - k_0\right) \delta(k - k_z)\, dk_x\, dk_y\, dk_z \\ &= \iint\limits_{-\infty}^{+\infty} \delta\left(\sqrt{k_x^2 + k_y^2 + k^2} - k_0\right) dk_x\, dk_y \end{aligned}$$

This double integration is best performed in polar coordinates ($k'$, $\theta'$). After substituting $k'^2 = k_x^2 + k_y^2$ and $dk_x\, dk_y = k'\, dk'\, d\theta'$, the final wavenumber spectrum results:

$$\begin{aligned} S_{\tilde{h}}(k) &= \frac{S_0}{2\pi k_0} \int\limits_0^{+\infty} \int\limits_0^{2\pi} k'\delta\left(\sqrt{k'^2 + k^2} - k_0\right) d\theta'\, dk' \\ &= S_0 u(k_0 - |k|) \end{aligned}$$

The wavenumber spectrum is a constant value, $S_0$, over the range $-k_0 \leq k \leq +k_0$ and is zero elsewhere.

# Chapter 3

# The Physics of Small-Scale Fading

This chapter addresses a subject which is too often overlooked in the analysis of small-scale radio channels: *a realization of a radio channel must obey Maxwell's equations for free space propagation.* People often use stochastic process theory – such as that presented in Chapter 2 – and apply it to arbitrarily constructed channel models. Such channel models do not necessarily represent realistic propagation and will yield deceptive and incorrect results when applied to problems in wireless communications.

The principle goal of this chapter is to develop a fundamental understanding of what constitutes realistic small-scale channels. The following outline summarizes the topics of this chapter:

- Section 3.1: overview of plane wave propagation in free space
- Section 3.2: definition of a *local area*
- Section 3.3: classification of wave components into specular, non-specular, and diffuse
- Section 3.4: presentation of the *stochastic local area channel model*
- Section 3.5: summary of important concepts

The analysis focuses on the frequency-selective and spatially-selective behavior of the channel, $\tilde{h}(f, \vec{r})$. Scatterers in the propagation environment produce multipath waves with different time delays and wavevectors, causing both spatial and frequency selectivity. Temporal selectivity, on the other hand, is caused by the *motion* of scatters and lacks the close relationship shared by spatial and frequency selectivity.

## 3.1 Plane Wave Representation

This section describes the plane wave representations used in the analysis of small-scale wireless channels.

### 3.1.1 Electromagnetic Fields and Received Signals

The propagation of electromagnetic waves in space must be described using vector quantities such as electric or magnetic fields. However, a radio receiver does not "see" a vector signal. Rather, the input of a radio receiver is a scalar *voltage* emanating from the terminals of the receiver antenna. In essence, an antenna is a device which maps a space-varying, vector field quantity (with units of *Volts* $m^{-1}$) to a scalar voltage quantity (with units of *Volts*). This mapping is illustrated in Figure 3.1.

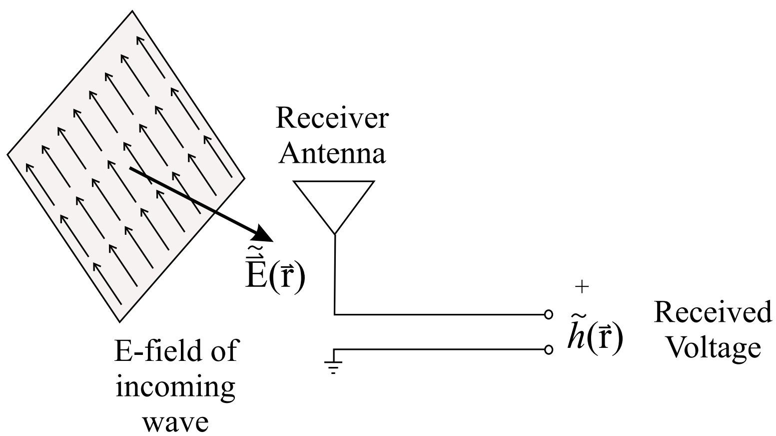


Figure 3.1: An antenna maps the complex electric field vector, $\tilde{\vec{E}}(\vec{r})$, to a scalar baseband channel voltage, $\tilde{h}(\vec{r})$.

To avoid the complications of vector notation, all channel modeling and measurement theory presented in this work will study the scalar voltage of the antenna instead of the vector fields of free space. This implies that the effects of the antenna – gain, phase change, and polarization mismatch – have already been accounted in the voltage representation. All of these antenna effects for a propagating wave may be accounted for by a single *polarization vector*, $\tilde{\vec{a}}$. If the propagation of a single time-harmonic electromagnetic wave is described by an electric field vector, $\tilde{\vec{E}}(\vec{r})$, then the baseband voltage, $\tilde{h}(\vec{r})$, results from the following operation:

$$\tilde{h}(\vec{r}) = \tilde{\vec{E}}(\vec{r}) \cdot \tilde{\vec{a}} \tag{3.1}$$

Thus, the dot product of the electric field and the polarization vector of the antenna produces the baseband voltage at the terminals of the receiver antenna.

> *Note: The Physical Channel Convention*
>
> The channel in Eqn (3.1) has units of *Volts* and, as defined, represents the physical voltage excited by waves at the terminals of the antenna. With this definition the terms *channel* and *received voltage* may be used interchangeably. This physical channel convention is convenient. If a unitless information signal, $\tilde{x}(t)$, is sent through the channel according to Figure 2.3, then the received baseband signal, $\tilde{y}(t)$, has the units of *Volts* and represents the actual signal processed by receiver hardware.

The polarization vector, $\tilde{\vec{a}}$, of Eqn (3.1) must have units of distance (meters) to be dimensionally correct. The magnitude of the polarization vector is proportional to the gain of the antenna. Since the polarization vector is complex, it is capable of modeling phase change of the incoming signal. The orientation of the vector is capable of modeling polarization mismatch. The only limitation regarding the polarization vector notation is that $\tilde{\vec{\mathrm{a}}}$ changes as the incident angle of the impinging wave changes. For example, if multiple waves from different directions impinge upon the antenna, then a polarization vector must be calculated for each wave:

$$\tilde{h}(\vec{r}) = \underbrace{\tilde{\vec{\mathrm{E}}}_1(\vec{r}) \cdot \tilde{\vec{\mathrm{a}}}_1}_{\tilde{V}_1(\vec{r})} + \underbrace{\tilde{\vec{\mathrm{E}}}_2(\vec{r}) \cdot \tilde{\vec{\mathrm{a}}}_2}_{\tilde{V}_2(\vec{r})} + \underbrace{\tilde{\vec{\mathrm{E}}}_3(\vec{r}) \cdot \tilde{\vec{\mathrm{a}}}_3}_{\tilde{V}_3(\vec{r})} + \ldots \tag{3.2}$$

Since much of our analysis requires breaking complicated propagating wave solutions into individual wave components, this aspect of polarization vectors is not restrictive.

### 3.1.2 The Maxwellian Basis

In order to describe complicated propagation in a bounded region of linear free space, it is useful to break down the complicated received voltage levels as a function of space into a *solution basis*. A solution basis is a set of elementary functions whose linear combinations span every possible solution. For example, we may postulate that a solution basis for any baseband received voltage is the set of all complex sinusoidal waves:

$$\tilde{h}(\vec{r}) = \sum_i V_i \exp(j[\phi_i - \vec{k}_i \cdot \vec{r}]) \tag{3.3}$$

where $\{V_i\}$ are real amplitudes, $\{\phi_i\}$ are real phases, and $\{\vec{k}_i\}$ are real vectors. According to basic Fourier analysis, *any* 3D function such as complex voltage, $\tilde{h}(\vec{r})$, may be written in the form of Eqn (3.3).

The basis of Eqn (3.3) is purely mathematical. In radio wave propagation, the solution basis for a channel must satisfy Maxwell's equations in addition to spanning all possible functions of received voltage. In fact, only a select few terms of the summation in Eqn (3.3) will obey the fundamental laws of propagation. A complete solution basis in which every term solves Maxwell's equations is called a *Maxwellian basis* [15].

One Maxwellian basis which may be used to construct any realizeable set of received voltages in bounded free space is the set of all plane waves. This basis is very similar to Eqn (3.3):

$$\tilde{h}(\vec{r}) = \sum_i V_i \exp(j[\phi_i - \vec{k}_i \cdot \vec{r}]) \qquad \text{where } \vec{k}_i \cdot \vec{k}_i = k^2 \tag{3.4}$$

where $\{V_i\}$ are real amplitudes, $\{\phi_i\}$ are real phases, and $\{\vec{k}_i\}$ are constant wavevectors [16, p. 562]. The terms of Eqn (3.4) are called *plane wave* due to the geometry of the equi-phase surfaces. An equi-phase surface of a propagating wave is defined as the set of points, $\vec{r}$, in 3D space which satisfy the following equation:

$$\arg\{\tilde{h}(\vec{r})\} = \phi_0 \tag{3.5}$$

where $\phi_0$ is some arbitrary phase constant. The equi-phase surfaces of each term in Eqn (3.4) form planes in 3D space.

At first glance, Eqn (3.4) appears to be a small subset of the Fourier basis in Eqn (3.3). The condition $\vec{k}_i \cdot \vec{k}_i = k^2$ restricts the solution set to plane waves with wavevectors of a certain magnitude (see Appendix 3.A for the derivation of this condition). But unlike the Fourier basis, *the wavevectors of Eqn (3.4) may be complex-valued.* A complex $\vec{k}_i$ still solves Maxwell's time-harmonic equations and is needed to describe every possible instance of received voltage in free space.

To facilitate discussion, it is best to classify the terms of the Maxwellian plane wave basis into two different types. The first group consists of *homogeneous* plane waves with strictly real-valued wavevectors. The second group consists of *homogeneous* plane waves with complex-valued wavevectors. Thus, Eqn (3.4) may be rewritten as

$$\tilde{h}(\vec{r}) = \underbrace{\sum_l V_l \exp(j[\phi_l - \vec{k}_l \cdot \vec{r}])}_{\substack{\text{Homogeneous,} \\ \text{Real } \vec{k}_l}} + \underbrace{\sum_m V_m \exp(j[\phi_m - \vec{k}_m \cdot \vec{r}])}_{\substack{\text{Inhomogeneous,} \\ \text{Complex } \vec{k}_m}} \tag{3.6}$$

Each classification of plane wave is discussed below.

> *Note: Definition of Free Space*
>
> The term *free space* in propagation implies the following three characteristics:
>
> 1. There are no current sources or charges present in the medium.
> 2. The propagation medium is *linear*, *isotropic*, and *lossless*.
> 3. The material parameters of permittivity and permeability are constants and are equal to that of vaccuous space ($\epsilon = \epsilon_0$ and $\mu = \mu_0$).
>
> It is generally accepted that the atmosphere – despite the presence of gases – behaves as a free-space medium for short-range propagation.

### 3.1.3 Homogeneous Plane Waves

Homogeneous plane waves are also called *uniform* plane waves because their envelope is a constant value that does not depend on position in space. Since the wavevector of a homogeneous plane wave, $\vec{k}$, is real-valued and satisfies the restriction noted in Eqn (3.4), the plane wave may be written as

$$V(\vec{r}) = V_0 \exp(j[\phi_0 - k\hat{k} \cdot \vec{r}]) \tag{3.7}$$

where $\hat{k}$ is a unit vector that points in the direction of propagation and $k$ is the free-space wavenumber. In a time-harmonic free space analysis, $k$ is related to the wavelength of radiation, $\lambda$:

$$k = \frac{2\pi}{\lambda} \tag{3.8}$$

Regardless of the direction of travel, all homogeneous plane waves propagate at the same speed with the same wavenumber. This is not true of inhomogeneous plane waves.

### 3.1.4 Inhomogeneous Plane Waves

Inhomogeneous plane waves are only slightly more difficult to understand than homogeneous plane waves. First, it helps to break the complex wavevector into a real and imaginary part:

$$\vec{k} = \beta\hat{\beta} - j\alpha\hat{\alpha} \tag{3.9}$$

where $\hat{\beta}$ is a unit vector pointing in the direction of the real part of $\vec{k}$ and $\hat{\alpha}$ is a unit vector pointing in the direction of the imaginary part of $\vec{k}$.

The form of Eqn (3.9) illuminates some basic properties of inhomogeneous plane waves.

Imposing the wavevector restriction of the Maxwellian basis leads to two descriptive conditions for a vector of this form:

$$\vec{k} \cdot \vec{k} = k^2 \quad \longrightarrow \quad \begin{array}{l} \hat{\alpha} \cdot \hat{\beta} = 0 \\ k^2 = \beta^2 - \alpha^2 \end{array}$$

First, we see that the unit vectors $\hat{\alpha}$ and $\hat{\beta}$ must be orthogonal to one another (their dot products are zero). Second, while $\alpha$ and $\beta$ may take on any positive value, they are dependent on one another. Specifically, the value $\sqrt{\beta^2 - \alpha^2}$ must be equal to the free space wavenumber, $k$.

Armed with this information, it is now useful to introduce the split wavevector of Eqn (3.9) into the expression for a propagating plane wave:

$$\tilde{h}(\vec{r}) = V_0 \overbrace{\exp(-\alpha[\hat{\alpha} \cdot \vec{r}])}^{\text{Attenuation}} \underbrace{\exp\left(j[\phi_0 - \beta(\hat{\beta} \cdot \vec{r})]\right)}_{\text{Phase Progression}} \tag{3.10}$$

Now the physical meanings of $\alpha$ and $\beta$ are apparent. The value of $\beta$ is the actual wavenumber of the inhomogeneous plane wave, determining the rate of phase progression through space in the direction $\hat{\beta}$. The value of $\alpha$ represents the rate of amplitude decay. As Eqn (3.10) shows, the amplitude of the plane wave attenuates in the direction of $\hat{\alpha}$. The direction of amplitude attenuation must always be orthogonal to the direction of propagation.

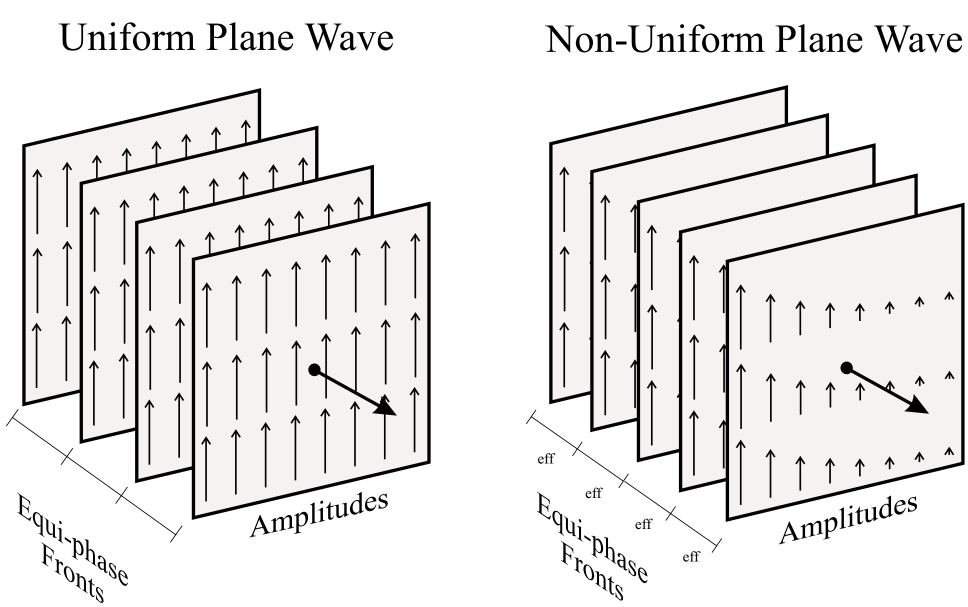


Figure 3.2: Homogeneous and inhomogeneous plane waves.

Figure 3.2 illustrates a comparison of homogeneous and inhomogeneous plane waves. Notice the two key differences between the types of plane waves. The wavenumber, $\beta$, of the inhomogeneous plane wave is always greater than the free space wavenumber, $k$. It is useful to refer to an "effective wavelength", $\lambda_{\text{eff}}$, for inhomogeneous plane waves, defined as

$$\lambda_{\text{eff}} = \frac{2\pi}{\beta} \tag{3.11}$$

The effective wavelength of an inhomogeneous plane wave is always smaller than the free space wavelength of radiation. As a result the equi-phase fronts of the inhomogeneous plane wave are more densely packed than the homogeneous plane wave.

The second key difference between homogeneous and inhomogeneous plane waves is the exponential decay of amplitudes perpendicular to the direction of propagation. If the decay rate, $\alpha$, is small, then the wavenumber, $\beta$, approaches the homogeneous free space wavenumber, $k$. If the decay rate, $\alpha$, is large, then the wavenumber, $\beta$, is much larger than $k$. This principle is foundational for later sections in this chapter that develop physically-based small-scale channel models.

### 3.1.5 Physics of Homogeneous vs. Inhomogeneous Plane Waves

If free space were unbounded, having infinite extent in every direction, then inhomogeneous plane waves would not exist. A quick study of Eqn (3.10) tells us why. A wave that decays exponentially in one direction actually grows exponentially in the opposite direction. Thus, in unbounded free space, the power density of an inhomogeneous plane wave becomes infinite towards one side of space – clearly a non-physical result. Homogeneous waves have no such imbalance, having a constant, finite power density in all of space.

Although inhomogeneous plane waves solve Maxwell's equations in bounded free space, these waves are caused by scatterers or sources in the propagation medium *outside* the bounded free-space region. The larger wavenumbers of inhomogeneous plane waves help meet the boundary conditions of electromagnetic fields close to material surfaces with fine spatial structure [16, p. 563]. This physical characteristic leads to a rule-of-thumb for inhomogeneous plane wave propagation:

> *Boundary conditions near large scatterers typically introduce inhomogeneous plane waves into a region of bounded free space. The direction of decay, $\hat{\alpha}$, for these waves tends to point away from the scatterers.*

The homogeneous waves follow a different rule-of-thumb:

> *The direction of propagation, $\hat{k}$, for homogeneous plane waves is typically away from the scatterers.*

These two rules-of-thumb are illustrated in Figure 3.3.

### An Analogy From Circuit Theory

A useful analogy exists between free space propagation and linear circuit theory which aids in understanding the nature of homogeneous and inhomogeneous plane waves. Consider as an example the linear circuit of Figure 3.4. This circuit contains an AC voltage source which switches on at $t = 0$. To solve for an output voltage, $V(t)$, as a function of time, we must solve the governing differential equation of the system. The order of a circuit differential equation is equal to the total number of inductors and capacitors. Thus, the example in Eqn (3.4) has a 7th-order differential equation governing the input-output relationships.

While the source of Figure 3.4 is a time-harmonic AC source, the closing switch at time $t = 0$ introduces transient behavior into the circuit. The solution of this circuit for $t \geq 0$ may be written in the following form:

$$V(t) = \text{Steady-State Solution} + \text{Transient Solutions} \quad \text{for } t \geq 0$$

A *stead-state solution* is a time-harmonic, sinusoidal voltage that eventually becomes the dominant solution for large values of $t$. The transient solution is an exponentially decaying set of voltages that transfers the circuit from its zero-excited state ($t < 0$) to its steady state ($t >> 0$). The concept of steady-state and transient solutions are illustrated in Figure 3.5. If we make several modifications in terminology, then the linear circuit becomes a powerful analogy for understanding free space propagation.

### Drawing Parallels to Plane Waves

The key difference between free space propagation and the linear circuit example is that the plane wave propagation is a function of space rather than time. Homogeneous plane waves are like the steady-state solutions in the linear circuit. These plane waves are periodic with respect to space just as the steady-state solution is periodic with respect to time. Inhomogeneous plane waves are like the transient solutions in the linear circuit. The amplitudes of these plane waves decay exponentially with respect to space just as the transient solution decays in time.

In the propagation problem, the electromagnetic scatterer is like a "switch in space". The position of the scatterer in space is like the time that the circuit switch is thrown. Solutions for fields that are very close to the scatterer must pay attention to the behavior of inhomogeneous plane waves, just as the transient circuit solutions dominate for times close to the switching time of $t = 0$. Solutions for fields that are further from the scatterer may

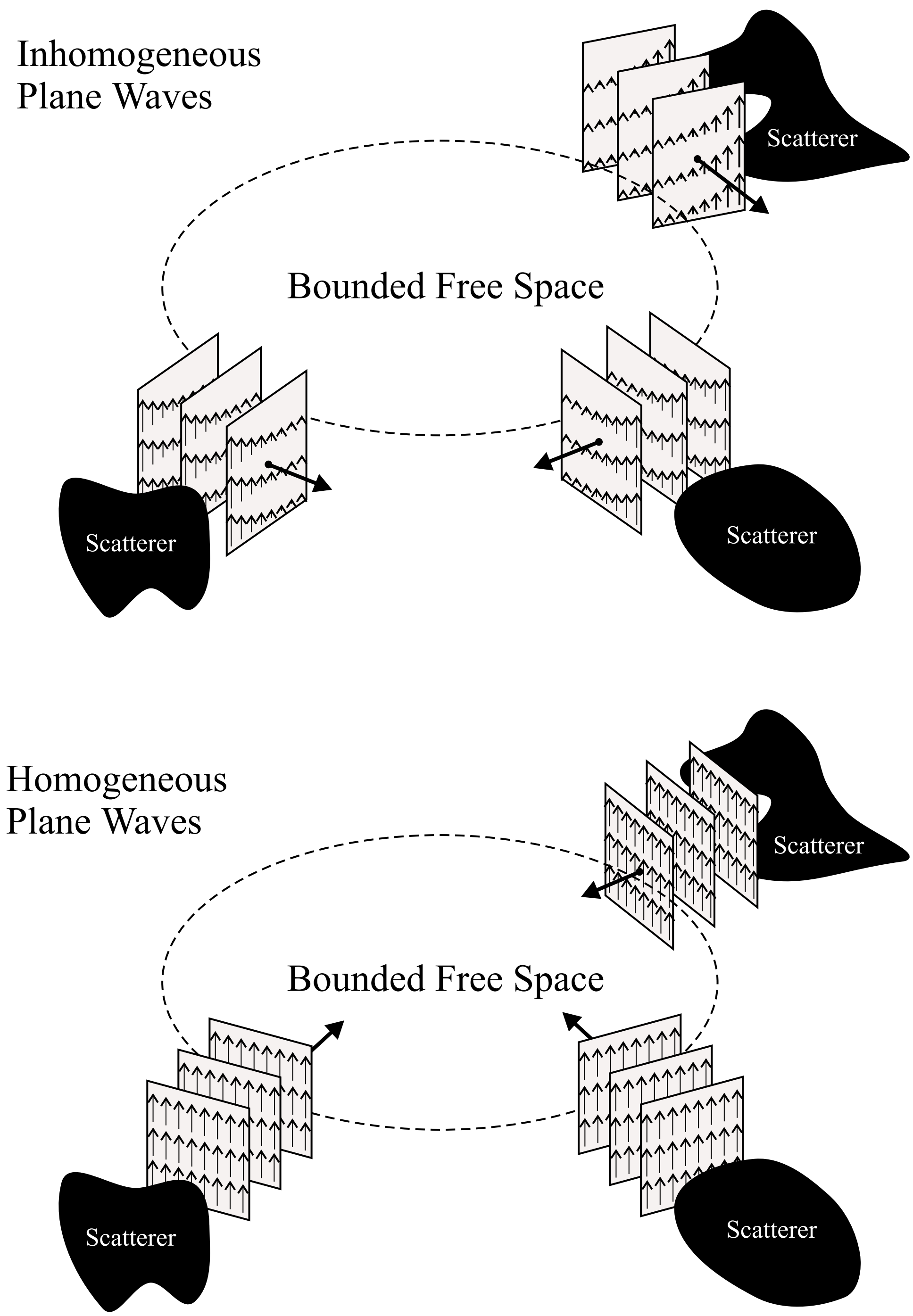


Figure 3.3: Rules-of-thumb for homogeneous and inhomogeneous plane wave propagation.

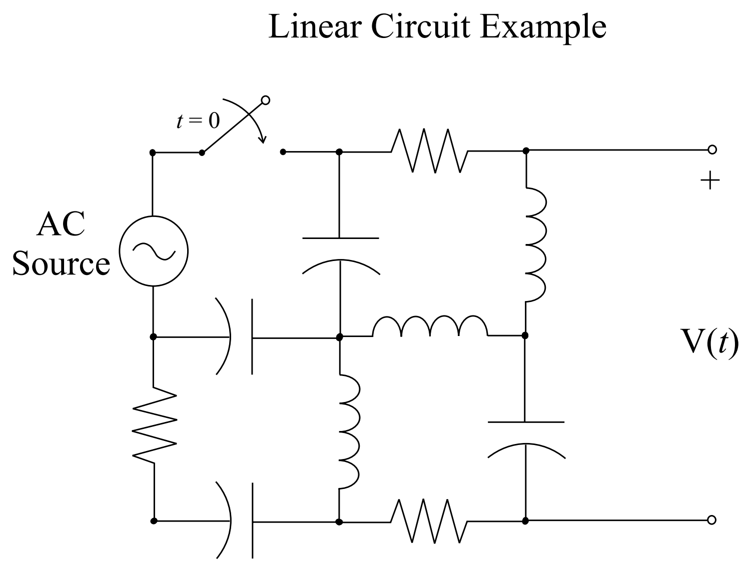


Figure 3.4: An example linear circuit contains capacitors, inductors, resistors and an AC source.

ignore the inhomogeneous plane waves, since they decay exponentially like the transient circuit solution.

There are numerous analogies to be made between the linear circuit of Figure 3.4 and the free space propagation of plane wave solutions. Below is a summary of many of these parallel concepts:

| Linear Circuit Concept | Free Space Propagation Concept |
|---|---|
| time | position |
| switch | scatterer |
| $t > 0$ | bounded free space |
| time elapsed since switch | distance from scatterer |
| stead-state solution | homogeneous plane waves |
| transient solution | inhomogeneous plane waves |

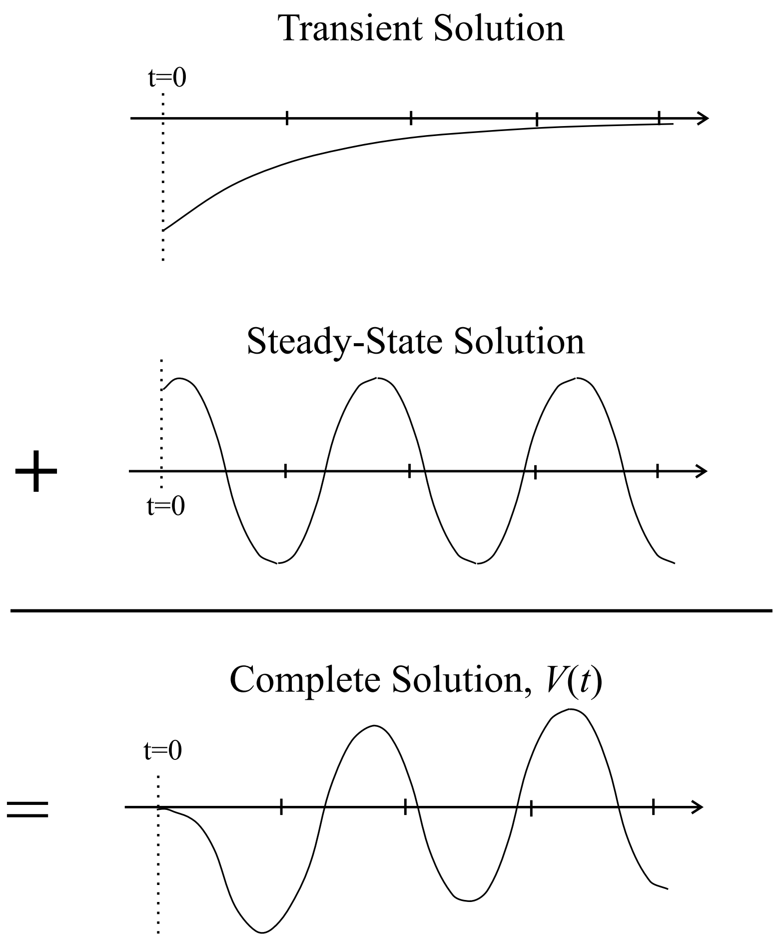


Figure 3.5: A linear circuit solution may be broken into a steady-state and transient solution.

## 3.2 The Local Area

Used often in the wireless literature without definition, the term *local area* is one of the most important concepts in small-scale channel modeling. This section presents a definition of the local area and analyzes its usefulness and validity.

### 3.2.1 Definition of a Local Area

Small-scale fading due to spatial selectivity is the focus of a *local area* propagation analysis. Characterization of a channel autocorrelation function is just one example of a local area propagation analysis. This is in contrast to a *macro area* analysis, which focuses on the differences in propagation from one environment to the next. A comparison of average power received in the front of a shopping mall to average power received on the top story of a parking garage is an example of a macro area analysis.

Before proceeding, it is crucial to define exactly what is meant by a local area, since the definition can be quite arbitrary. There is no magical distance quantity that can be applied to any region of space and called a local area. Rather, the following definition will be applied throughout this work:

> A *local area* is the largest volume of free space about a specified point in which the radio channel can be modeled accurately as the sum of homogeneous plane waves of the form
>
> $$\tilde{h}(f,\vec{r}) = \sum_i V_i \exp\left(j\left[\phi_i - \vec{k}_i \cdot \vec{r} - 2\pi f \tau_i\right]\right)$$

The justification for this definition of the local area channel is discussed next.

*Note: A Multipath Wave*

The term *multipath* is used by wireless engineers to describe the multiple wave components, each traveling different paths, that impinge on a receiver antenna. Hence, *multi*ple + *path*s = *multipath*. When the term *multipath wave* is used in this work, we are speaking of a single wave term in the local area representation. With this definition, it is possible that a single scatterer may produce more than one *multipath wave*. Therefore, be aware that the *multi* in multipath refers to the number of waves and not the number of scatterers.

### 3.2.2 Scatterer Proximity

First note that the local area definition does not include inhomogeneous plane waves in the description of the propagation. For the local area definition to be valid, all inhomogeneous plane waves must be either ignored or approximated by homogeneous plane waves. To rationalize this restriction, first group the inhomogeneous waves into two types:

**Abruptly Decaying:** The direction of decay for the inhomogeneous plane waves typically points into the local area (see Figure 3.3). If the decay rate is high, then the power carried by the plane wave extinguishes after the wave penetrates the local area by only one or two wavelengths. Thus, when one considers the total power carried by the fast-decaying wave with respect to all other multipath waves in the local area, it becomes insignificant and may be ignored.

**Gently Decaying:** For slowly decaying inhomogeneous plane waves, the value of decay rate $\alpha$ is small. As a result, the wavenumber $\beta$ is approximately equal to the free-space wavenumber $k$:

$$\beta = \sqrt{k^2 + \alpha^2} \approx k$$

Thus, a slowly-decaying inhomogeneous plane wave moves in space with the same phase progression as a homogeneous plane wave and has only a gradual taper to its amplitude. A homogeneous plane wave is a valid approximation to this wave over a small region of space.

Of course, the size of the free-space region that satisfies these approximations varies from case to case and is largely a function of *scatterer proximity*. We know that inhomogeneous plane waves are caused by scatterers in free space and that their contribution to propagation diminishes in regions away from the significant scatterer. Thus, the proximity of the local area to significant scatterers usually determines the acceptable size of the local area.

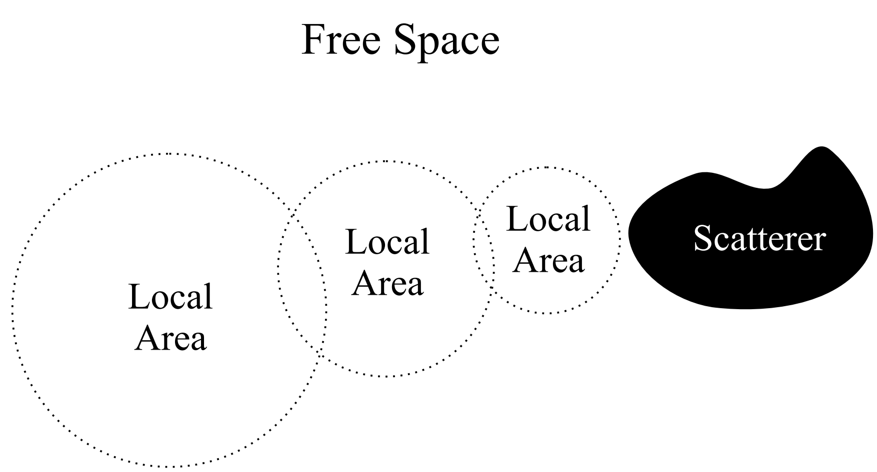


Figure 3.6: The size of a local area decreases closer to significant scatterers.

This concept is illustrated in Figure 3.6. When the local area is not close to a large scatterer, then the "steady-state" homogeneous plane waves dominate the description of propagation and the size of the region over which inhomogeneous plane waves may be ignored is large. When the local area is close to a large scatterer, then inhomogeneous plane waves contribute significant power to the total power propagating through the space. The size of the valid local area is small, since the abruptly- and gently-decaying approximations fall apart after a few wavelengths of displacement.

### 3.2.3 A Wideband Plane Wave

The ideal wireless channel, from the standpoint of simplicity, results from a single uniform plane wave propagating through space. This plane wave impinges upon a receiver antenna and excites a constant-amplitude voltage at the receiver that does not change in magnitude as a function of position. The resulting complex, time-harmonic voltage at the receiver is given by

$$\tilde{h}(\vec{r}) = V \exp\left(j[\phi - \vec{k}\cdot\vec{r} - kL]\right) \tag{3.12}$$

where $V$ is a constant, real-valued amplitude and $\phi$ is a constant, real-valued phase. If the homogeneous plane wave exciting the voltage in Eqn (3.12) satisfies Maxwell's equations for free space propagation, then the real vector $\vec{k}$ points in the direction of propagation and has magnitude $k$. The value $L$ is the total distance traveled from transmitter to receiver by the wave.

The phase terms in the complex exponential of Eqn (3.12) each represent a different physical contribution to the total phase of the incoming wave, as illustrated in Figure 3.7. The three phase terms and their physical causes are listed below:

$$\arg\{\tilde{h}(\vec{r})\} = \phi - \vec{k}\cdot\vec{r} - kL$$

| | |
|---|---|
| $\phi$ | phase change accumulated by antenna and scatterer interaction |
| $kL$ | phase change due to total distance traveled |
| $\vec{k}\cdot\vec{r}$ | phase change due to motion of the receiver |

For a single homogeneous plane wave, the phase term contains most of the interesting physical behavior.

Hidden in Eqn (3.12) is an inherent narrowband dependence on the carrier frequency, $f_c$. Since $k$ is related to wavelength, $\lambda$, and wavelength is related to carrier frequency ($\lambda = c/f_c$, where $c$ is the free space speed of light), it is possible to substitute $k = \frac{2\pi f_c}{c}$ into Eqn (3.12) to observe the carrier dependence:

$$\tilde{h}(\vec{r}) = V \exp\left(j\left[\phi - \frac{2\pi f_c}{c}\hat{k}\cdot\vec{r} - 2\pi f_c \tau\right]\right) \tag{3.13}$$

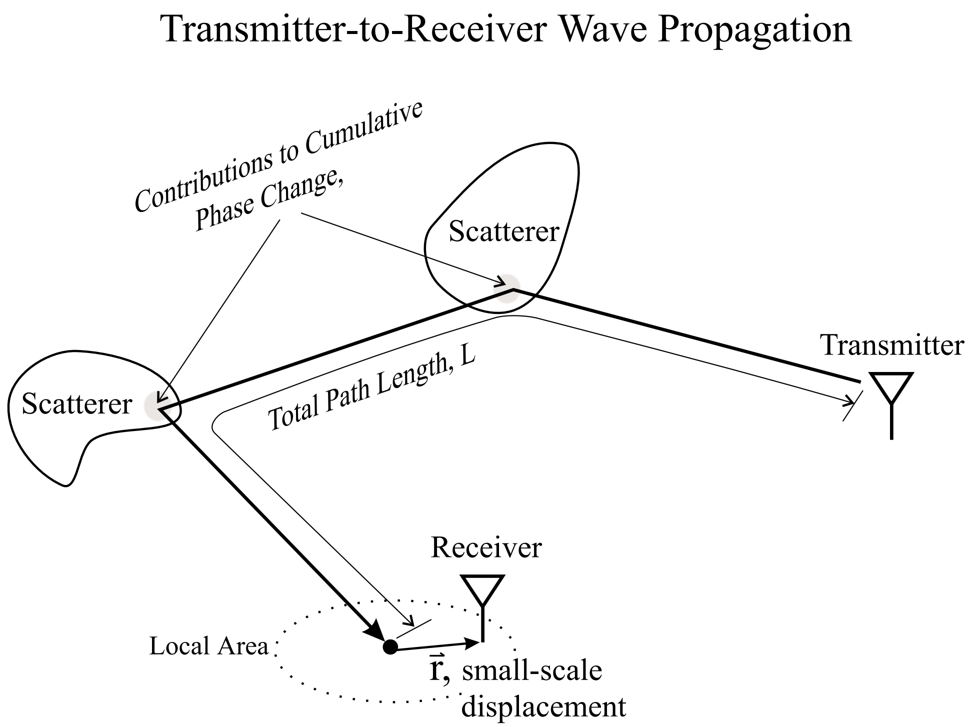


Figure 3.7: Illustration of the basic quantities of time-harmonic wave propagation through a scattering environment.

where $\tau = L/c$, which is the propagation delay of the wave, the time it takes to travel from transmitter to receiver. In Eqn (3.13), the value $\hat{k}$ is a unit vector that points into the direction of propagation.

### Adding Signal Bandwidth

If the plane wave has been modulated with a band-limited transmitted signal, then the narrowband characterization of Eqn (3.13) becomes insufficient to characterize the channel. For a small frequency displacement, $f$, about the carrier frequency, Eqn (3.13) may be rewritten as

$$\tilde{h}(\vec{r}, f) = V \exp\left(j\left[\phi - \frac{2\pi(f_c + f)}{c}\hat{k}\cdot\vec{r} - 2\pi(f_c + f)\tau\right]\right) \tag{3.14}$$

The phase term of Eqn (3.14) may be regrouped to produce

$$\tilde{h}(\vec{r}, f) = V \exp\left(j\left[\phi_0 - \vec{k}\cdot\vec{r} - 2\pi f\tau - \frac{2\pi f}{c}\hat{k}\cdot\vec{r}\right]\right) \tag{3.15}$$

where $\phi_0 = \phi - 2\pi f_c\tau$. Eqn (3.15) still retains the basic characteristics of a plane wave. The envelope of the channel is still a constant, independent of position, $\vec{r}$, *and* frequency, $f$.

### Adding More Bandwidth

The plane wave in Eqn (3.15) is actually a small-frequency expansion about the carrier frequency. If a wideband signal modulates the plane wave, then the amplitude and phase of the single wave may also become functions of frequency, $f$. This frequency dependence results from the fine scattering mechanisms in the environment and sometimes even the electromagnetic interations with receiver and transmitter antennas. Every interaction with a realistic material has some type of inherent frequency-dependence, which makes the excess phase change, $\phi_0$, and the amplitude, $V$, a function of frequency.

To treat this case analytically, simply expand the amplitude and excess phase change in terms of a Fourier series of an arbitrary number of terms:

$$V(f)\exp[j\phi_0(f)] = \sum_i V_i \exp(j\phi_i - 2\pi f\tau_i') \tag{3.16}$$

Inserting this expansion into Eqn (3.15), we arrive at

$$\tilde{h}(\vec{r}, f) = \sum_i V_i \exp(j\phi_i - 2\pi f\tau_i)\exp\left(-j\left[\vec{k}\cdot\vec{r} + \frac{2\pi f}{c}\hat{k}\cdot\vec{r}\right]\right) \tag{3.17}$$

where $\tau_i = \tau_i' + \tau$. Therefore, the full wideband expression of a modulated uniform plane wave will break the wave into the sum of smaller waves with various propagation delays, $\tau_i$. Note, however, that each wave component in Eqn (3.17) has the same form as a single homogeneous plane wave of the form:

$$V_i \exp\left(j\left[\phi_i - \vec{k}\cdot\vec{r} - 2\pi f\tau_i - \frac{2\pi f}{c}\hat{k}\cdot\vec{r}\right]\right) \tag{3.18}$$

The envelope of this wave is constant, independent of position, $\vec{r}$, and frequency, $f$.

## 3.2.4 The Bandwidth-Distance Threshold

If time-harmonic propagation in a region of free space may be broken into the sum of homogeneous plane waves, and each plane wave may be broken into components of the form Eqn (3.18) as bandwidth is added, then we have almost validated the usefulness of the local area definition. There is one key difference between the type of waves specified in the local area definition and the type of wave specified by Eqn (3.18). Consider the phase of the wave in Eqn (3.18):

$$\exp\left(j\left[\phi_i - \overbrace{\vec{k}\cdot\vec{r}}^{\substack{\text{Space}\\\text{Term}}} - \underbrace{2\pi f\tau_i}_{\substack{\text{Frequency}\\\text{Term}}} - \overbrace{\frac{2\pi f}{c}\hat{k}\cdot\vec{r}}^{\substack{\text{Cross}\\\text{Product}}}\right]\right) \tag{3.19}$$

The homogeneous wave terms in the local area definition contain the space and frequency terms, but do not contain the space-frequency cross-product term.

Thus, the local area representation makes the following approximation to the uniform plane wave equation:

$$\exp\left(-j\left[\vec{k}\cdot\vec{r}+2\pi f\tau_i+\frac{2\pi f}{c}\hat{k}\cdot\vec{r}\right]\right)\approx\exp\left(-j\left[\vec{k}\cdot\vec{r}+2\pi f\tau_i\right]\right) \tag{3.20}$$

The temptation is to justify this approximation by simply stating that the frequency and space terms are much larger than the cross-product term. After all, both frequency, $f$, and small-scale displacement, $\vec{r}$, must change substantially for the cross-product to affect the total phase.

Completely ignoring the cross-product term, however, is a poor approximation for a phase term. Phase terms *always* remain sensitive to small changes in a large net value due to the $2\pi$ periodicity. Therefore, an absolute limit on the contribution of the cross-product term must be imposed if the local area representation is accurate. We will restrict the cross-product term to always contribute less than a $\frac{\pi}{2}$-radian phase change in any single homogeneous plane wave component. This restriction may be written as

$$\frac{2\pi f}{c}\hat{k}\cdot\vec{r}<\frac{\pi}{2} \tag{3.21}$$

The maximum value for frequency displacement, $f$, in the basebamd channel is one-half the RF signal bandwidth, $B$. The maximum value for the small-scale position displacement is one-half the size of the local area, $L_A$:

$$\hat{k}\cdot\vec{r}<|\hat{k}||\vec{r}|<\frac{L_A}{2} \tag{3.22}$$

Therefore, the largest possible value for the left-hand side in Eqn (3.21) occurs when frequency and small-scale position displacement are at a maximum:

$$\frac{BL_A}{c}<1 \tag{3.23}$$

which may be re-written in terms of carrier frequency, $f_c$, and wavelength, $\lambda$:

$$\frac{L_A}{\lambda}<\frac{f_c}{B} \tag{3.24}$$

This relationship may be stated in words: the ratio of the local area size to the wavelength of radiation must be less than the ratio of the carrier frequency to the signal bandwidth.

> *Note: Narrowband and Fixed-Receiver Analysis*
>
> The cross-product term of Eqn (3.20) is unique to joint analysis of space-frequency channel selectivity. If the analysis were narrowband, then frequency displacement, $f$, about the carrier would always be 0 and the cross-product term would vanish. If the analysis were on a fixed receiver, the position vector, $\vec{r}$, would be $\mathbf{0}$ and the term would also vanish. Thus, the cross-product term and the resulting bandwidth-distance threshold is a unique artifact of full spatio-temporal channel modeling.

Along with scatterer proximity, the bandwidth-distance threshold limits the size of a valid local area. This threshold is typically less-restrictive than scatter proximity for the discussion of realistic wireless systems. Table 3.1 lists the carrier frequencies and bandwidths of several common wireless applications. The resulting local area size according to the bandwidth-distance threshold is large in terms of wavelengths – even for applications that the industry considers "wideband". Of course, the size of a wavelength decreases as the carrier frequency increases, so the absolute size of a local area does become small for mm-wave applications.

Table 3.1: Maximum size of a local area according to the bandwidth-distance threshold for example wireless applications.

| Wireless Application | Carrier Frequency | Signal Bandwidth | Local Area Size |
|---|---|---|---|
| Analog Cellular Channel | 840 MHz | 30 kHz | 28000 $\lambda$ |
| PCS Spread-Spectrum Channel | 1910 MHz | 1.25 MHz | 1528 $\lambda$ |
| NII Campus Link | 5.7 MHz | 100 MHz | 57 $\lambda$ |
| LMDS Link (proposed) | 28 GHz | 500 MHz | 56 $\lambda$ |

## 3.3 Wave Groupings

Ultimately, it is the properties of radio wave propagation that determine the temporal, spatial, and frequency coherence of a channel. Consequently, the terms specular and non-specular are also used to describe the electromagnetic waves propagating in a region of space.

### 3.3.1 Specular Wave Component

A *specular wave component* refers to a received multipath component that may be described by a single homogeneous plane wave. Mathematically, a specular wave component has the following form:

$$\tilde{h}(f, \vec{r}) = V_i \exp\left(j\left[\phi_i - \vec{k}_i \cdot \vec{r} - 2\pi f \tau_i\right]\right) \tag{3.25}$$

The envelope of a specular wave component does not change as a function of space and frequency. Clearly, if a local area wireless channel consisted of a single homogeneous plane wave component, then the channel would have perfect frequency coherence and perfect spatial coherence.

There are numerous propagation mechanisms that may give rise to large specular components propagating through a local area. Examples of specular components include the direct line-of-sight wave from a transmitter antenna, the specular reflection from a flat surface in the propagation environment, or even a far-field wave diffracted from the edge of an object.

### 3.3.2 Non-specular Wave Component

An *non-specular wave component* refers to a voltage that may be written as the sum of many differently-phased waves. For a local area, a non-specular wave component is a collection of homogeneous plane waves that either travel in different directions or arrive with different time delays. Mathematically, a non-specular wave component has the following form:

$$\tilde{h}(f, \vec{r}) = \sum_i V_i \exp\left(j\left[\phi_i - \vec{k}_i \cdot \vec{r} - 2\pi f \tau_i\right]\right) \tag{3.26}$$

Given a position in frequency, $f$, and space, $\vec{r}$, the envelope of such a channel is random and unknown unless every phase variable in Eqn (3.26) is known. The channel resulting from non-specular waves clearly has frequency selectivity and spatial selectivity.

The distinction between non-specular and specular wave components may seem arbitrary, since a non-specular wave component may be expressed as the sum of specular wave components in a local area. In actuality, the grouping of multipath waves into non-specular and specular components is quite useful. The scattering mechanisms in many wireless channel are so numerous and varied that characterizing each homogeneous plane wave may take thousands or even millions of terms. Often, it suffices to lump the majority of the waves into a non-specular term and analyze it as a single component.

### 3.3.3 Diffuse Wave Component

One more important type of wave component grouping is the *diffuse* wave component. In a local area, an non-specular wave component is said to be *diffuse* if its constituent homogeneous plane wave amplitudes, $\{V_i\}$, satisfy the following relationship:

$$[\max(V_1, V_2, V_3, \ldots)]^2 << \sum_i V_i^2 \tag{3.27}$$

In other words, a non-specular wave component is diffuse if each homogeneous plane wave carries power that is negligible compared to the total average power in the component.

Diffuse non-specular wave propagation is extremely common in a wireless environment. There are so many irregular, inhomogeneous objects in a realistic propagation environment that scatter power to the receiver and back-and-forth amongst each other. A wireless receiver is flooded with tiny waves that have negligible power, individually, but by sheer quantity contribute a large portion to the overall received signal strength. There is always a collection of diffuse, non-specular waves in every realistic wireless channel [17, 18].

### 3.3.4 Reduced Wave Grouping

Now that specular, non-specular, and diffuse wave components have been defined, it is possible to discuss the concept of a *reduced wave grouping*. In a local area, it is possible to write the channel as the sum of a finite number of specular waves and a non-specular component:

$$\tilde{h}(f, \vec{r}) = \sum_{i=1}^{N} \underbrace{V_i \exp\left(j\left[\phi_i - \vec{k}_i \cdot \vec{r} - 2\pi f \tau_i\right]\right)}_{\text{Specular Waves}} + \tilde{h}_{\text{dif}}(f, \vec{r}) \tag{3.28}$$

where $N$ is the number of specular waves.

The grouping in Eqn (3.28) is arbitrary. Any number of specular components may be lumped inside or outside the non-specular channel component, $\tilde{h}_{\text{dif}}(f, \vec{r})$. The *reduced wave grouping*, however, refers to a specific combination of specular and non-specular wave components. Specifically, the following definition will be used throughout this work:

> A *reduced wave grouping* of local area propagation is the representation of Eqn (3.28) with the smallest value of $N$ such that the non-specular component is diffuse.

In other words, a reduced wave grouping reduces a local area channel of any arbitrary complexity to the sum of a few large specular components and a single non-specular term of “left-over” components that are diffuse.

There is a simple recipe for constructing the reduced wave grouping of a channel if the voltage amplitudes of the constituent waves are known. The procedure for generating the reduced wave grouping is shown in Table 3.2. When this procedure is finished, the reduced wave grouping for the local area has been achieved. The grouping consists of $N$ specular components and a non-specular component. It is possible that, at the end of the procedure, there are no specular components ($N = 0$) or that nothing is left in the non-specular component. The reduced wave grouping is unique for every instance of local area propagation.

Table 3.2: Reduced Wave Grouping Algorithm

| | |
|---|---|
| **Step 1:** | Group *all* of the local area wave components into one single non-specular component and set $N = 0$. |
| **Step 2:** | Is the non-specular component diffuse? If so, then stop. |
| **Step 3:** | Remove the homogeneous plane wave from the non-specular component with the largest amplitude and increment $N$. |
| **Step 4:** | Go to Step 2. |

## 3.4 The Stochastic Local Area Channel (SLAC) Model

This section defines the stochastic local area channel (SLAC) model and explores several of its key properties. This model is a cornerstone of small-scale channel analysis.

### 3.4.1 Stochastic Model

Following from the definition of a local area, the stochastic model for small-scale propagation is written in the following form:

$$\tilde{h}(f,\vec{r}) = \sum_{i=1}^{N} V_i \exp\left(j\left[\Phi_i - \vec{k}_i \cdot \vec{r} - 2\pi f \tau_i\right]\right) \tag{3.29}$$

In this model, $\{V_i\}$, $\{\vec{k}_i\}$, and $\{\tau_i\}$ are all constants, determined by the propagation that characterizes the local area. The phases, $\{\Phi_i\}$, are the random variables which make Eqn (3.29) a stochastic model [19]. Eqn (3.29) will be referred to as the SLAC model throughout the rest of this work.

As written in the form of Eqn (3.29), the SLAC model appears to be a discrete sum of waves – but it would be incorrect to view this as a discrete model. No restriction is placed on the number of components, $N$, or the types of values assigned the amplitudes, $\{V_i\}$. It may be that some local area propagation requires an *infinite* number of terms, each with an infinitesimal amplitude values, in Eqn (3.29) to model propagation accurately.

#### Random Phases

Random phase makes the SLAC model useful for two types of small-scale analysis. First, the SLAC model may be considered an ensemble of representative cases for local area propagation. Amplitude, delay, and angle-of-arrival (related to wavevector) are the most typical inputs to a channel model. In contrast, the absolute phases of individual waves are difficult to measure with radio hardware or to estimate using deterministic propagation techniques. Eqn (3.29) is capable of generating any number of realistic channels without knowledge of individual phases.

Second, the SLAC model may be considered an ensemble of channels for a receiver that is *randomly placed* in a local area. Even if every quantity in Eqn (3.29) is known, the exact position reference for the model may not be known. For example, the position $\vec{r} = 0$ represents the reference position as shown in Figure 3.7. If the reference position is moved several wavelengths in any direction, the amplitudes, delays, and wavevectors of the local area plane waves do not change, but all of the phases will jumble with respect to one another. The end result is an ensemble of realizations that have the same collection of homogeneous plane waves, but with random phases with respect to each other.

### Other Random Quantities

In stochastic channel modeling, other quantities in Eqn (3.29) that are fixed constants in the SLAC model are sometimes treated as random variables. The physical implications of random amplitudes, wavevectors, or delays in Eqn (3.29) lead to a *stochastic macro area channel* (SMAC) model. For example, if the $\{V_i\}$ of Eqn (3.29) are random variables, then each channel realization in the ensemble will represent a set of plane waves with different amplitudes. Thus, each channel realization in the ensemble will represent a completely different local area.

*Note: SMAC or SLAC?*

The difference between SLAC and SMAC models is an endless source of confusion. The classical presentation of small-scale fading statistics by Jakes used a model similar to Eqn (3.29) with random phases *and* random amplitudes (a SMAC model) [20]. Such a model is valid for deriving small-scale fading statistics only when the receiver operates in a diffuse, high-scatter channel – the type presented by Jakes. Since then, however, many channel modeling researchers indiscriminately randomize variables in Eqn (3.29) with little regard to the physics of what is actually modeled.

## 3.4.2 Random Phase Models

For a SLAC model, the essence of the randomness boils down to the distribution of phases, $\{\Phi_i\}$, in Eqn (3.29). The distribution of phases is usually characterized by a *probability density function* (PDF). Without exception, the random phases in the SLAC model are considered to be uniformly distributed over the interval $[-\pi, \pi)$. Mathematically, the PDF for the $i$th phase, $\Phi_i$, is written as

$$f_{\Phi_i}(\phi_i) = \frac{1}{2\pi} \qquad -\pi \leq \phi_i < \pi \tag{3.30}$$

The justification for this distribution comes from a simple physical argument. A typical radio wave travels a long distance to reach a local area – usually the distance of hundreds or thousands of wavelengths. Since all effects of phase are periodic, only the $2\pi$-modulus of the phase is essential for characterizing a propagating wave. The $2\pi$-modulus of a very large absolute phase value is unpredictable and, therefore, may be treated as a uniformly-distributed random variable.

While the PDF of Eqn (3.30) is useful for describing the individual distribution of phase values, the true nature of any SLAC model relates to how random phases relate to one another in an ensemble of realizations. This behavior is described by the *joint PDF* of the random phases. Two useful joint characterizations for phases are discussed below.

### Uncorrelated Phases

If the phases of a SLAC model are *uncorrelated*, then we refer to this representation of local area propagation as a U-SLAC model. The mathematical definition for uncorrelated phase is slightly different than the conventional definition for uncorrelated random variables:

$$\begin{aligned} \text{Conventionally Uncorrelated:} \quad & \mathrm{E}\left\{\Phi_l \Phi_m\right\} = 0 \\ \text{Uncorrelated Phases:} \quad & \mathrm{E}\left\{\exp\left(j[\Phi_l - \Phi_m]\right)\right\} = 0 \end{aligned} \tag{3.31}$$

The former expression is the common definition for random variable decorrelation. Throughout this work, the term *uncorrelated phases* refers to the latter definition. This subtle distinction accounts for the periodic nature of phase that is absent in other types of random variables.

Formally, we state that a SLAC model is a U-SLAC model if the following condition holds for all values of phase in Eqn (3.29):

$$\mathrm{E}\left\{\exp\left(j[\Phi_l - \Phi_m]\right)\right\} = 0 \quad \text{for } l \neq m \tag{3.32}$$

The physical argument for uncorrelated phase is straightforward. Different phases describe the behavior of differently scattered waves. Therefore, a weak, uncorrelated relationship should govern the selection of random phases with respect to one another in the SLAC model.

As we will show, uncorrelated phases lead to very useful behavior in a SLAC model. The condition *uncorrelated* still does not produce an expression for the joint phase PDF, however.

### Independent Phases

If the random phases of a SLAC model are *independent*, then we refer to the channel model as an I-SLAC model. Imposing *independence* on the random variables of a SLAC model is much stronger than simply stating that the phases are uncorrelated. Thus, all I-SLAC models are U-SLAC models, but the converse is not true.

By definition, independence implies that a joint PDF may be written as the product of individual PDF's. For the case of random phases, the joint PDF is

$$f_{\vec{\Phi}}(\vec{\phi}) = f_{\Phi_1}(\phi_1)\, f_{\Phi_2}(\phi_2) \ldots f_{\Phi_N}(\phi_N), \qquad \vec{\phi} = \begin{bmatrix} \phi_1 \\ \phi_2 \\ \vdots \\ \phi_N \end{bmatrix} \tag{3.33}$$

Since the individual PDF's of each phase is a uniform distribution, the final form of the joint PDF for an I-SLAC model is

$$f_{\vec{\Phi}}(\vec{\phi}) = \frac{1}{(2\pi)^N} \quad 0 \le \vec{\phi} < 2\pi \tag{3.34}$$

Unlike the U-SLAC model, phase independence in the I-SLAC model leads to a specific joint PDF. This powerful feature of the I-SLAC model will make it the target of much of our subsequent analysis.

The independence of phases is justified in a manner similar the argument for uncorrelated phases in a channel model. The argument for independent phase simply states that each individual wave arrives from a different set of scattering mechanisms. As a result, a combination of wave phases in a realization of Eqn (3.29) is just as valid as any other in the ensemble.

### 3.4.3 Fourier Transforms

The Fourier transform of a SLAC model is simple to compute. Transformation of the position vector and frequency domains into the wavevector and delay domains, respectively, produces the following expression for $\tilde{H}(\tau, \vec{k})$:

$$\tilde{H}(\tau, \vec{k}) = (2\pi)^3 \sum_{i=1}^{N} V_i \exp(j\Phi_i)\, \delta(\tau - \tau_i)\, \delta(\vec{k} - \vec{k}_i) \tag{3.35}$$

Each discrete component in Eqn (3.29) produces a delta function in Eqn (3.35) at $\tau = \tau_i$ and $\vec{k} = \vec{k}_i$.

A delta function that appears in a Fourier transform or a power spectrum is called a *spectral line*. This term refers to the concentration of power about a single point in the spectral domain. Again, however, the discrete nature of Eqn (3.35) is misleading. By allowing $N$ to approach infinity and the amplitudes to become infinitesimally small, Eqn (3.35) could just as easily represent a continuous function.

At this point, it is useful to introduce a new type of spectral domain representation of a Fourier transform which eliminates spectral lines. Often, a Fourier transform is written as an integral:

$$F(\tau, \vec{k}) = \int_{-\infty}^{\tau} \int_{-\infty}^{\vec{k}} \tilde{H}(\tau', \vec{k}')\, d\vec{k}'\, d\tau' \tag{3.36}$$

The inverse Fourier transform may be written in terms of $F(\tau, \vec{k})$ in the form of a Riemann-Stieltjes integral:

$$\tilde{h}(f, \vec{r}) = \int_{-\infty}^{+\infty} \exp(j[2\pi f\tau + \vec{k}\cdot\vec{r}])\, dF(\tau, \vec{k}) \tag{3.37}$$

The Riemann-Stieltjes representation smoothes the Fourier transform, $\tilde{H}(\tau, \vec{k})$, and eliminates the need for delta functions. For the SLAC model, $F(\tau, \vec{k})$ may be written as

$$F(\tau, \vec{k}) = (2\pi)^3 \sum_{i=1}^{N} V_i \exp(j\Phi_i)\, \mathrm{u}(\tau - \tau_i)\, \mathrm{u}(\vec{k} - \vec{k}_i) \tag{3.38}$$

where $\mathrm{u}(\cdot)$ is the unit step function. Now, spectral lines are represented in Eqn (3.38) by discontinuities instead of spectral lines.

*Note: The Mythical Delta Function*

Mathematicians often remind engineers that the delta function is not really a function at all because it is defined by an irresolvable limit. The Riemann-Stieltjes integral representation of a Fourier transform or spectrum is used by mathematicians and physicists who wish to be rigorous and avoid the use of delta functions in their analysis. Engineers, however, unabashedly use the convenient delta function. Beware: engineering researchers working in the field of stochastic modeling will eventually encounter the Riemann-Stieltjes integral and should not be daunted by the notation.

### 3.4.4 Autocorrelation Functions

It is now possible to analyze some of the more sophisticated statistical properties of a SLAC model, such as the autocorrelation function. Since the distribution of phase plays such a critical role in the characteristics of a SLAC model, the type of SLAC model determines the nature of the autocorrelation function. Consider Theorem 3.1 – one of the most important and useful theorems in local area channel modeling.

**Theorem 3.1: U-SLAC Wide-Sense Stationarity**

**Statement:** A SLAC model, $\tilde{h}(f, \vec{r})$, is WSS with respect to space and frequency if and only if it is a U-SLAC model.

**Proof:** Start with the definition of an autocorrelation function , and substitute the inverse Fourier transforms of $\tilde{H}(\tau, \vec{k})$ for the channel $\tilde{h}(f, \vec{r})$.

$$
\begin{aligned}
C_{\tilde{h}}(f_1, f_2, \vec{r}_1, \vec{r}_2) \quad = \quad & \mathrm{E}\Bigg\{ \overbrace{\left[ \frac{1}{(2\pi)^3} \iint\limits_{-\infty}^{+\infty} \tilde{H}(\tau_1, \vec{k}_1) \exp(j[\vec{k}_1 \cdot \vec{r}_1 + 2\pi f_1 \tau_1])\, d\vec{k}_1\, d\tau_1 \right]}^{\tilde{h}(f_1, \vec{r}_1)} \times \\
& \overbrace{\left[ \frac{1}{(2\pi)^3} \iint\limits_{-\infty}^{+\infty} \tilde{H}^*(\tau_2, \vec{k}_2) \exp(-j[\vec{k}_2 \cdot \vec{r}_2 + 2\pi f_2 \tau_2])\, d\vec{k}_2\, d\tau_2 \right]}^{\tilde{h}^*(f_2, \vec{r}_2)} \Bigg\}
\end{aligned}
$$

$$
= \sum_{l=1}^{N} \sum_{m=1}^{N} V_l V_m \exp\left( j \left[ \vec{k}_l \cdot \vec{r}_1 - \vec{k}_m \cdot \vec{r}_2 + 2\pi(f_l \tau_1 - f_m \tau_2) \right] \right) \mathrm{E}\left\{ \exp(j[\Phi_l - \Phi_m]) \right\} \tag{3.39}
$$

If Eqn (3.39) is a U-SLAC model, by definition the phases, $\Phi_l$ and $\Phi_m$, are uncorrelated for $l \neq m$ and the autocorrelation function reduces to

$$
C_{\tilde{h}}(f_1, f_2, \vec{r}_1, \vec{r}_2) = \sum_{i=1}^{N} V_i^2 \exp(j[\vec{k}_i \cdot \underbrace{(\vec{r}_1 - \vec{r}_2)}_{\Delta \vec{r}} + 2\pi \tau_i \underbrace{(f_1 - f_2)}_{\Delta f}])
$$

which is WSS since the autocorrelation may be written in terms of $\Delta f$ and $\Delta \vec{r}$, only. Furthermore, $\vec{k}_l$ must equal $\vec{k}_m$ and $f_l$ must equal $f_m$ in Eqn (3.39) for the SLAC model to be WSS. The *only* way to force this condition for the general case is with uncorrelated random phase variables.

---

According to Theorem 3.1, SLAC models with uncorrelated phases always lead to WSS channels with respect to position and frequency. The autocorrelation for all U-SLAC models may be written as

$$
C_{\tilde{h}}(\Delta f, \Delta \vec{r}) = \sum_{i=1}^{N} V_i^2 \exp(j[\vec{k}_i \cdot \Delta \vec{r} + 2\pi \tau_i \Delta f]) \tag{3.40}
$$

Most of the models presented in this work from this point on are U-SLAC models. The WSS properties and convenient form of autocorrelation for these models make them powerful tools for illustrating channel behavior.

### 3.4.5 Heterogeneous Scattering

At this point, it is important to define a special case of SLAC models – one that results from *heterogeneous scattering*. A SLAC model is a result of heterogeneous scattering if the following condition holds:

$$\vec{k}_l \neq \vec{k}_m \quad \text{and} \quad \tau_l \neq \tau_m \quad \text{for all } l \neq m$$

In words, heterogeneous scattering describes a condition where no two multipath waves in Eqn (3.29) arrive with precisely the same time delays or wavevectors.

The condition of heterogeneous scattering is mentioned as a special type of SLAC model because it often leads to some powerful theorems in stochastic channel modeling. Consider, as an example, Theorem 3.2. The theorem shows that if heterogeneous scattering can be established in a SLAC model, *then wide-sense stationarity with respect to one channel dependency* **automatically** *implies wide-sense stationarity with respect to the other.*

**Theorem 3.2: WSS Heterogeneous Scattering**

**Statement:** A SLAC model, $\tilde{h}(f, \vec{r})$, with heterogeneous scattering is WSS with respect to position, $\vec{r}$, if and only if it is WSS with respect to frequency, $f$.

**Proof:** Using the proof in Theorem 3.1, it may be shown that a heterogeneous SLAC model is WSS with respect to position if and only if *all* phases, $\{\Phi_i\}$, are uncorrelated. Likewise, it is also true that the same model is WSS with respect to frequency if and only if all phases are uncorrelated. By transitivity, the theorem is proven.

---

Without the condition of heterogeneous scattering, Theorem 3.2 would not hold. If two delays, $\tau_i$ and $\tau_j$, were equal, then correlated phases $\Phi_i$ and $\Phi_j$ will cause non-stationarity with respect to position, $\vec{r}$, but will not effect the wide-sense stationarity with respect to frequency, $f$. The dual problem exists for matching wavevectors.

### 3.4.6 Power Spectrum

Since a U-SLAC model is WSS, it is possible to define a power spectrum using the Wiener-Khintchine theorem. The wavevector-delay spectrum for the U-SLAC model is

$$S_{\tilde{h}}(\tau, \vec{k}) = (2\pi)^3 \sum_{i=1}^{N} V_i^2 \, \delta(\tau - \tau_i) \, \delta(\vec{k} - \vec{k}_i) \tag{3.41}$$

Just as in the case of the Fourier transform, an integrated version of the power spectrum may be defined to eliminate the delta functions:

$$F_{\tilde{h}}(\tau, \vec{k}) \quad = \quad \int_{-\infty}^{\tau} \int_{-\infty}^{\vec{k}} S_{\tilde{h}}(\tau', \vec{k}') \, d\tau' \, d\vec{k}'$$

$$= \quad (2\pi)^3 \sum_{i=1}^{N} V_i^2 \, \mathrm{u}(\tau - \tau_i) \, \mathrm{u}(\vec{k} - \vec{k}_i) \tag{3.42}$$

The space-frequency autocorrelation function may then be written as a Riemann-Stieltjes integral:

$$C_{\tilde{h}}(\Delta f, \Delta \vec{r}) = \frac{1}{(2\pi)^3} \int_{-\infty}^{+\infty} \exp\left(j[2\pi\tau\Delta f + \vec{k} \cdot \Delta\vec{r}]\right) \, dF_{\tilde{h}}(\tau, \vec{k}) \tag{3.43}$$

Although this work will use the standard power spectrum, $S_{\tilde{h}}(\tau, \vec{k})$, whenever possible, there are certain types of analysis (usually involving the spectral lines caused by large specular components) that are best performed with the integrated power spectrum.

### Diffuse Non-specular Components

Often the power spectrum is a more flexible way of characterizing diffuse, non-specular power in a SLAC model. Specifically, a continuous power spectrum is a simple way to represent multipath waves that are diffusely spread over a range of delays and wavevectors – a case that would require an infinite number of terms in the SLAC model summation in Eqn (3.29).

The integrated power spectrum is a particularly useful method for characterizing diffuse non-specular power. A local area channel is *perfectly diffuse* if no discontinuities are present in the integrated power spectrum, $F_{\tilde{h}}(\tau, \vec{k})$. Mathematically, this condition may be expressed as

$$\lim_{\substack{\delta\tau \to 0 \\ |\delta\vec{k}| \to 0}} \left| F_{\tilde{h}}(\tau + \delta\tau, \vec{k} + \delta\vec{k}) - F_{\tilde{h}}(\tau - \delta\tau, \vec{k} - \delta\vec{k}) \right| = 0 \quad \text{for all } \tau \text{ and } \vec{k} \tag{3.44}$$

Figure 3.8 illustrates different types of delay spectra (only one dependency, delay, is shown for graphical simplicity). Notice how the discontinuities in the spectrum indicate the presence of a specular component.

### Specular Components

The integrated power spectrum allows us to formalize a definition for the presence of a specular component in a local area. A specular component with magnitude $V_i$, delay $\tau_i$, and wavevector $\vec{k}_i$ exists if a discontinuity is present in the integrated power spectrum, $F_{\tilde{h}}$. Mathematically, this condition may be stated as

$$\lim_{\substack{\delta\tau \to 0 \\ |\delta\vec{k}| \to 0}} \frac{1}{(2\pi)^3} \left| F_{\tilde{h}}(\tau_i + \delta\tau, \vec{k}_i + \delta\vec{k}) - F_{\tilde{h}}(\tau_i - \delta\tau, \vec{k}_i - \delta\vec{k}) \right| = V_i^2$$

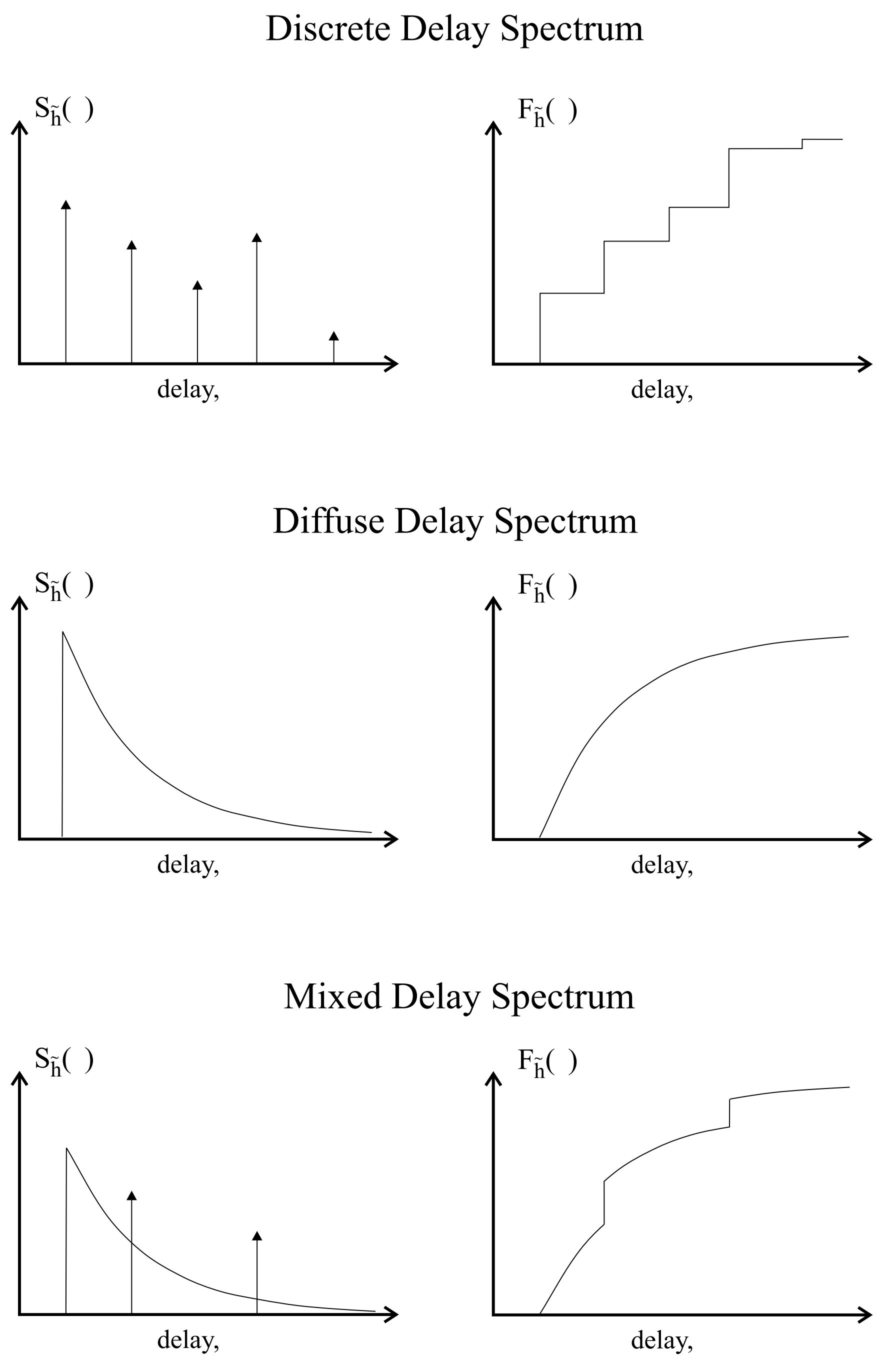


Figure 3.8: Examples of different delay spectra using the standard power spectrum, $S_{\tilde{h}}(\tau)$, and the integrated power spectrum, $F_{\tilde{h}}(\tau)$.

Examples of specular spectral components are illustrated in Figure 3.8.

## 3.5 Chapter Summary

This chapter presented an introduction to the physics behind local area modeling of the small-scale radio channel. Below is a useful outline of key points:

- Propagation in a region of free space may be expressed as the sum of two types of plane waves:
  - ▹ *Homogeneous* plane waves have constant amplitude.
  - ▹ *Inhomogeneous* plane waves have an exponentially-decaying amplitude.
- A *local area* is a region of free space in which the propagation is approximated by the sum of only homogeneous plane waves.
- Wave components may be characterized into three different groups:
  - ▹ A *specular* component is a single homogeneous plane wave.
  - ▹ A *non-specular* component is a collection of multiple waves.
  - ▹ A *diffuse* component is a non-specular component consisting of numerous individual waves with small amplitudes.
- A *reduced wave grouping* is a minimal collection of $N$ specular components and a diffuse, non-specular component. All local area propagation has a unique reduced wave grouping.
- The *stochastic local area channel* (SLAC) model represents propagation as the sum of randomly phased homogeneous plane waves. There are several types of SLAC models:
  - ▹ A *U-SLAC* model has uncorrelated random phases and is WSS.
  - ▹ An *I-SLAC* model has independent (as well as uncorrelated) random phases.
  - ▹ A SLAC model with *heterogeneous scattering* consists of homogeneous plane waves that have unique delays and wavevectors.

This chapter, when taken together with Chapter 2, represents the foundational theory and terminology behind stochastic modeling of the physical radio channel. All of the subsequent analysis in this work is simply an application of the terminology and theory presented in these chapters.

## 3.A Wavevector Criterion for Free Space Plane Waves

This section derives the wavevector condition of Eqn (3.4) for constructing a plane-wave basis in free space. The electric field of a plane wave propagating in free space takes the following form:

$$\tilde{\vec{\mathrm{E}}}(\vec{r}) = \tilde{\vec{\mathrm{E}}}_0 \exp(-j\vec{k}_0 \cdot \vec{r}) \tag{3.45}$$

where $\tilde{\vec{\mathrm{E}}}_0$ is a complex, constant electric field vector and $\vec{k}_0$ is a constant-valued wavevector. Any solution of Eqn (3.45) must solve the scalar wave equation for free-space:

$$(\nabla^2 + k^2)\tilde{\vec{\mathrm{E}}}(\vec{r}) = 0 \tag{3.46}$$

where $k$ is the free-space wavenumber of time-harmonic propagation. Inserting Eqn (3.45) into Eqn (3.46) produces the following result:

$$\begin{aligned} (\nabla^2 + k^2)\, \tilde{\vec{\mathrm{E}}}_0 \exp(-j\vec{k}_0 \cdot \vec{r}) &= 0 \\ \tilde{\vec{\mathrm{E}}}_0 \left[k^2 - \vec{k}_0 \cdot \vec{k}_0\right] \exp(-j\vec{k}_0 \cdot \vec{r}) &= 0 \end{aligned} \tag{3.47}$$

The following vector relationship was used to arrive at Eqn (3.47):

$$\nabla^2 \exp(-j\vec{k}_0 \cdot \vec{r}) = -\vec{k}_0 \cdot \vec{k}_0 \; \exp(-j\vec{k}_0 \cdot \vec{r})$$

Thus, in order for Eqn (3.47) to hold, the wavevector, $\vec{k}_0$, must satisfy the following relationship:

$$\vec{k}_0 \cdot \vec{k}_0 = k^2 \tag{3.48}$$

All plane waves must have wavevectors of this form in order to be a valid solution of Maxwell's equations in free space.

# Chapter 4

# First-Order Statistics of Small-Scale Channels

The performance of a wireless link operating in a small-scale fading channel can vary unpredictably. The received power in these channels fluctuates between maxima and minima as a function of space and frequency. A wireless engineer must accept the fact that, for certain regions in space or frequency, the receiver may have to operate with received signal strength below an acceptable *signal-to-noise* or *signal-to-interference* ratio. To quantify the effects of a fading channel on receiver performance, we must first quantify the distribution of received power or voltage envelope that a receiver experiences in a randomly selective channel.

This chapter develops the principles of first-order analysis for stochastic frequency-selective and spatially-selective radio channels. A topical summary is listed below:

- Section 4.1: discussion of mean received power
- Section 4.2: construction of envelope PDF's for I-SLAC models
- Section 4.3: analytical solutions to I-SLAC envelope PDF's
- Section 4.4: analysis of the Two-Wave with Incoherent Power (TIP) PDF
- Section 4.5: summary of important concepts

This chapter uses the definitions and concepts from the preceding chapters to develop many of the classical distributions used in wireless engineering to describe small-scale fading. Furthermore, new fading distributions are developed and discussed which augment the classical knowledge. Indeed, the SLAC model defined in Chapter 3 is shown to produce an incredible variety of channel behavior.

## 4.1 Mean Received Power

Of all first-order statistics to calculate for stochastic channel model, mean received power is perhaps the most common. Regardless of small-scale statistical properties, mean received power is an intuitive measure of receiver performance since, according to information theory, received power determines the fundamental limitations on the amount of information that can be sent through a noisy channel [9].

### 4.1.1 Stationarity

Stationarity is one of the most important and powerful attributes to determine in a stochastic model. There are many different types of stationarity (we have already discussed *wide sense stationarity* in previous chapters). In fact, the term *stationary* may be used to describe any type of statistic that is invariant of channel dependencies. For example, a time-varying process is *mean stationary* if its mean value does not change as a function of time.

Often, statistics of an entire *order* are said to be stationary. The *order* of a statistic refers to the number of stochastic process samples used in its calculation. For example, an autocorrelation function is a *second-order* statistic because it is calculated from two samples of the stochastic process:

$$C_{\tilde{h}}(t_1, t_2) = \mathrm{E}\left\{\tilde{h}(t_1)\tilde{h}^*(t_2)\right\} \tag{4.1}$$

One sample is taken at $t_1$ and the other sample is taken at $t_2$. Recall that Eqn (4.1) is WSS if the autocorrelation function is invariant of the values of $t_1$ and $t_2$ – only the difference between the two values matters.

In this chapter, it is useful to establish *first-order stationarity* in the stochastic channel models. A process is first-order stationary if all of its first-order statistics – mean, variance, PDF, etc. – are invariant of the dependencies, time and frequency. The U-SLAC model is a first-order stationary channel model, which makes it a convenient tool for analytical channel description. This trait of the U-SLAC model is proven in Theorem 4.1.

**Theorem 4.1: First-Order Stationarity**

**Statement:** The U-SLAC model is first-order stationary.

**Proof:** Consider the U-SLAC model of Eqn (3.29) evaluated at frequency $f = 0$ and position $\vec{r} = \mathbf{0}$. The resulting channel expression is shown below

$$\tilde{h}(0, \mathbf{0}) = \sum_{i=1}^{N} V_i \exp\left(j\left[\Phi_i - \vec{k}_i \cdot \vec{r} - 2\pi f \tau_i\right]\right)\Bigg|_{\substack{f=0 \\ \vec{r}=\mathbf{0}}} = \sum_{i=1}^{N} V_i \exp(j\Phi_i) \tag{4.2}$$

Now consider the case of the channel evaluated at any arbitrary point in frequency, $f$, and space, $\vec{r}$. By making the following substitution,

$$\Phi_i' = \left(\Phi_i - \vec{k}_i \cdot \vec{r} - 2\pi f \tau_i\right) \bmod 2\pi$$

we could express the U-SLAC model in the following form:

$$\tilde{h}(f, \vec{r}) = \sum_{i=1}^{N} V_i \exp(j\Phi_i') \tag{4.3}$$

The random phases, $\{\Phi_i'\}$, in Eqn (4.3) are simply the same set of random phases, $\{\Phi_i\}$, in Eqn (4.2) with arbitrary constants added. Otherwise, the two equations look identical. Since a uniform phase random variable remains uniformly distributed if any arbitrary constant is added to it, the expressions in Eqn (4.2) and Eqn (4.3) are identically-distributed random variables. Adding the constant does not change the cyclical correlation properties, either. Thus, the distribution of values for $\tilde{h}(f, \vec{r})$ is identical and independent of frequency, $f$, and position, $\vec{r}$ – the definition of first-order stationary.

---

The most sweeping type of stationarity is *strict-sense stationarity* (SSS). A stochastic process is SSS if it is stationary with respect to every order. While establishing strict-sense stationarity in a process is highly desireable, it is extremely difficult to prove in most types of stochastic processes. The I-SLAC model is an exception, as Theorem 4.2 demonstrates.

**Theorem 4.2: Strict-Sense Stationarity**

**Statement:** The I-SLAC model is strict-sense stationary.

**Proof:** Consider a simple stochastic channel consisting of a single wave term:

$$\tilde{h}_1(f, \vec{r}) = V_1 \exp\left(j\left[\Phi_1 - \vec{k}_1 \cdot \vec{r} - 2\pi f \tau_1\right]\right)$$

where $V_1$ is a constant amplitude and $\Phi_1$ is a random phase variable, uniformly distributed over the interval $[0, 2\pi)$. This process is SSS [21, p. 301]. Since the sum of two independent SSS processes will produce a SSS process, the following process

$$\tilde{h}_2(f, \vec{r}) = \tilde{h}_1(f, \vec{r}) + V_2 \exp\left(j\left[\Phi_2 - \vec{k}_2 \cdot \vec{r} - 2\pi f \tau_2\right]\right)$$

is SSS provided the random phase variable, $\Phi_2$, is independent of $\Phi_1$ (as it is in an I-SLAC model). An arbitrary number of independent wave components may be added in this manner and, by induction, any I-SLAC model may be constructed and shown to be a SSS process.

---

It is probably evident now why we draw a distinction between SLAC, U-SLAC, and I-SLAC models: the nature of the phase distributions in the model of Eqn (3.29) (arbitrary, uncorrelated, or independent) determines the level of stationarity. A SLAC model may be non-stationarity with respect to every statistic. A U-SLAC model, however, is guaranteed to be at least WSS (Theorem 3.1 and Theorem 4.1). And an I-SLAC model is guaranteed to be stationary with respect to *every* order and statistic (Theorem 4.2).

### 4.1.2 Mean U-SLAC Power

For a WSS U-SLAC model, it is possible to calculate a closed-form expression for the mean received power, $P(f, \vec{r})$. Inserting the SLAC model expression into the definition of mean received power produces

$$\begin{aligned} \mathrm{E}\left\{P(f,\vec{r})\right\} &= \mathrm{E}\left\{|\tilde{h}(f,\vec{r})|^2\right\} \\ &= \sum_{l=1}^{N}\sum_{m=1}^{N} V_l V_m \underbrace{\mathrm{E}\left\{\exp\left(j\left[\Phi_l - \Phi_m\right]\right)\right\}}_{=\,0 \text{ for } l\neq m} \exp\left(j\left[(\vec{k}_m - \vec{k}_l)\cdot\vec{r} + 2\pi(\tau_m - \tau_l)f\right]\right) \\ &= \sum_{i=1}^{N} V_i^2 \end{aligned} \tag{4.4}$$

The expectation in the second line of Eqn (4.4) is zero for $m \neq l$ by definition of a U-SLAC process. The end result of Eqn (4.4) may be stated in words as follows: the mean power in a U-SLAC model is equal to the sum of the powers carried by the individual multipath waves [10]. Stated this way, Eqn (4.4) can be considered a type of conservation-of-power law.

### 4.1.3 Frequency and Spatial Averaging

In the application of first-order statistics to real-life problems, it is important to speak of *averaging*. This is particularly true when attempting to measure the local area channel. In practice, it is not possible to generate an infinitum of realizations and calculate an ensemble. Rather, it is most feasible to average a measured statistic over a single example.

This averaging may occur over each dependency of the measured channel. For example, sweeping a narrowband transmitted carrier over a range of frequencies and measuring the received voltage is a form of *frequency averaging*. Mathematically, we will define the operation of frequency averaging as

$$\left\langle \ \cdot \ \right\rangle_f = \lim_{B\to\infty} \frac{1}{B} \int_{-B/2}^{B/2} (\ \cdot\ )\ df \tag{4.5}$$

In this definition, a statistic is calculated by averaging the value over the range of all allowable frequencies (in practice the integration of Eqn (4.5) cannot be taken over an infinite range).

A similar definition exists for spatial averaging. Mathematically, we will define the operation of spatial averaging as

$$\left\langle \ \cdot \ \right\rangle_{\vec{r}} = \lim_{L\to\infty} \frac{1}{L^3} \int_{-L/2}^{L/2} (\ \cdot\ )\ d\vec{r} \tag{4.6}$$

where the integration in Eqn (4.6) is a three-fold integration over the $x$, $y$, and $z$ coordinates as discussed in Section 2.A.1.

### 4.1.4 Ergodicity

Stochastic processes with statistics that exhibit *ergodicity* are particularly useful for measurements and analysis of real-world processes. A statistic is said to be ergodic if, when measured by averaging a single realization of a stochastic ensemble, it is equal to the ensemble average. For example, a process is *mean-ergodic* if the frequency- and spatially-averaged mean of a single realization equals the ensemble-averaged mean. We express mean ergodicity for a stochastic channel as

$$\text{Condition for Mean Ergodicity:} \ \left\langle \left\langle \tilde{h}(f,\vec{r}) \right\rangle_{\vec{r}} \right\rangle_f = \mathrm{E}\left\{ \tilde{h}(f,\vec{r}) \right\}$$

Of course, this property must hold for *all* realizations of $\tilde{h}(f,\vec{r})$ in the stochastic ensemble.

Since there are two dependencies in the SLAC model – frequency and space – it is convenient to describe ergodicity with respect to each individual dependency. For example, it is possible that a statistic is ergodic with respect to frequency but not space. The converse is also possible. The basic principles governing the frequency and spatial ergodicity of mean received power are summarized in Theorem 4.3.

**Theorem 4.3: Power Ergodicity**

**Statement:**

1. A U-SLAC model is power-ergodic with respect to frequency if its scattering is heterogeneous with respect to frequency.
2. A U-SLAC model is power-ergodic with respect to space if its scattering is heterogeneous with respect to space.
3. All U-SLAC models with heterogeneous scattering are power-ergodic with respect to both space and frequency.

**Proof:**

1. The frequency averaged power of any SLAC model is given by inserting Eqn (3.29) into the frequency-averaging operation defined in Eqn (4.5):

$$\begin{aligned} \langle P(f,\vec{r})\rangle_f &= \left\langle |\tilde{h}(f,\vec{r})|^2 \right\rangle_f \\ &= \sum_{l=1}^{N}\sum_{m=1}^{N} V_l V_m \exp\left(j\left[\Phi_l - \Phi_m + (\vec{k}_m - \vec{k}_l)\cdot\vec{r}\right]\right) \\ &\quad \times \underbrace{\langle \exp\left(j2\pi[\tau_m - \tau_l]f\right)\rangle_f}_{=0 \text{ for } \tau_m \neq \tau_l} \end{aligned} \tag{4.7}$$

If all delays, $\{\tau_i\}$, in the SLAC model are heterogeneous (dissimilar), then the result in Eqn (4.7) reduces to

$$\langle P(f,\vec{r})\rangle_f = \sum_{i=1}^{N} V_i^2 \tag{4.8}$$

which is the ensemble average for power in a U-SLAC model.

2. The spatially averaged power of any SLAC model is given by inserting Eqn (3.29) into the space-averaging operation defined in Eqn (4.6):

$$\begin{aligned} \langle P(f,\vec{r})\rangle_{\vec{r}} &= \left\langle |\tilde{h}(f,\vec{r})|^2 \right\rangle_{\vec{r}} \\ &= \sum_{l=1}^{N}\sum_{m=1}^{N} V_l V_m \exp\left(j\left[\Phi_l - \Phi_m + 2\pi(\tau_m - \tau_l)f\right]\right) \\ &\quad \times \underbrace{\left\langle \exp\left(j[\vec{k}_m - \vec{k}_l]\cdot\vec{r}\right)\right\rangle_{\vec{r}}}_{=0 \text{ for } \vec{k}_m \neq \vec{k}_l} \end{aligned} \tag{4.9}$$

If all wavevectors, $\{\vec{k}_i\}$, in the SLAC model are heterogeneous (dissimilar), then the result in Eqn (4.9) reduces to

$$\langle P(f,\vec{r})\rangle_{\vec{r}} = \sum_{i=1}^{N} V_i^2 \tag{4.10}$$

which is also the ensemble average for power in a U-SLAC model.

3. This result follows naturally from 1 and 2.

---

An immediate consequence of Theorem 4.3 is the equivalence of averaging received power with respect to frequency or space. If a SLAC model has heterogeneous scattering, then the following result holds:

$$\langle P(f,\vec{r})\rangle_f = \langle P(f,\vec{r})\rangle_{\vec{r}} \qquad (4.11)$$

In other words, received power averaged as a function of frequency produces the same result as received power averaged as a function of space. Both are equal to the ensemble-averaged power of the U-SLAC model that describes the location.

This equivalence is particularly powerful when *measuring* local area power in a real-life radio channel. The experimentalist has the freedom to calculate mean power in a channel measurement by using

(a) a wideband transmitted signal and a stationary receiver [10].

(b) a narrowband transmitted signal and a receiver moving in space [22].

For case (a), the mean power is calculated from the received power averaged over the frequencies in the wideband signal. For case (b), the mean power is calculated from the received power averaged at the different receiver positions in space. The two techniques are equivalent.

*Note: Importance of Heterogeneous Scattering*

The relationship between heterogeneous scattering and the ergodicity of a statistic will appear again in later chapters. By now it is clear why Chapter 3 introduced the concept of *heterogeneous scattering*. Heterogeneous scattering is the crucial property for determining ergodicity. Ergodicity is the crucial property for determining the "measurability" of a real-world channel. Hence, the property of heterogeneous scattering determines how statistics may be calculated from a real-world channel measurement.

## 4.2 Envelope Probability Density Functions

Mean received power is just one aspect of first order stochastic channel behavior. To understand the complete first order behavior, it is necessary to calculate the power or envelope *probability density function* (PDF). This section describes the generation of PDF's for a variety of I-SLAC models.

### 4.2.1 Notes and Concepts

The PDF's developed in this section are strictly for I-SLAC models. In order to derive a deterministic expression for the distribution of received power or voltage envelope, it is necessary to have a uniquely defined joint PDF on the phases of a SLAC model. A U-SLAC model, which only asserts uncorrelated phases, is not restrictive enough for this criterion. The I-SLAC model, with its independent, uniformly distributed phases, does have a specific joint PDF describing phases.

Futhermore, the envelope PDF's of this section are based on the *reduced wave grouping* (see Section 3.3.4). As will become apparent later, envelope PDF's involving a diffuse, non-specular component only depends on the mean-squared power of that component – not the fine multipath wave structure within the component. Thus, when constructing a PDF from an arbitrarily-complicated I-SLAC model, the reduced wave grouping may be used without loss of generality.

Finally, all of the PDF's presented in this chapter are with respect to received voltage envelope. If a distribution with respect to received power is desired, the envelope PDF may be converted to a power PDF. Since envelope, $R$, is simply equal to the square root of power, $P$, the following relationships hold:

$$\text{Converting envelope PDF to power PDF} \qquad f_P(\mathrm{p}) = \frac{1}{2\sqrt{\mathrm{p}}} f_R(\sqrt{\mathrm{p}}) \tag{4.12}$$

$$\text{Converting power PDF to envelope PDF} \qquad f_R(\rho) = 2\rho f_P(\rho^2) \tag{4.13}$$

Most wireless journal papers, as a convention, report envelope PDF's.

### 4.2.2 Characteristic Functions

Since the reduced wave grouping of Eqn (3.28) is a sum of independent random variables, the envelope PDF may be found by using a characteristic function approach. Recall from probability theory that if a real-valued random variable, $Z$, is the sum of a set of independent random variables, $\{W_i\}$:

$$Z = \sum_i W_i$$

then the characteristic function of $Z$ – the Fourier transform of the PDF – is equal to the product of the characteristic functions of each individual $W_i$ random variable [21].

The same characteristic function technique may be used for the independent, *complex* random variable terms that constitute an I-SLAC model. The diffuse, non-specular term and the $N$ specular terms of Eqn (3.28) are independent complex variables, each having a characteristic function, $\Phi_{XY}(\upsilon)$. The product of these individual characteristic functions may then be transformed into a PDF describing the envelope of Eqn (3.28).

The PDF of a scalar random variable and its characteristic function are Fourier transform pairs. Since fading PDF's are functions of *envelope* and since complex *voltages* must be summed as phasors, the transforms for an envelope PDF, $f_R(\rho)$, and its characteristic function, $\Phi_{XY}(\upsilon)$, are modified to the following expressions as shown in Appendix 4.A:

$$\Phi_{XY}(\upsilon) = \int_0^\infty f_R(\rho) J_0(\upsilon\rho)\, d\rho \tag{4.14}$$

$$f_R(\rho) = \rho \int_0^\infty \Phi_{XY}(\upsilon) J_0(\upsilon\rho)\, \upsilon\, d\upsilon \tag{4.15}$$

Mathematicians refer to Eqn (4.14) and Eqn (4.15) as the operations defining a *Fourier-Bessel transform* [23]. To solve the problem of constructing envelope PDF's for a reduced wave grouping, we must only find the characteristic functions of specular components and diffuse components.

### 4.2.3 Specular Characteristic Function

A specular voltage term of the form $V_0 \exp(j\Phi_0)$ has constant amplitude, $V_0$, and uniformly random phase, $\Phi_0$. The envelope of this term is always $V_0$, regardless of the phase. Therefore, the envelope PDF of a specular component is best described by a delta function:

$$f_R(\rho) = \delta(\rho - V_0) \tag{4.16}$$

Plugging this function into the transform in Eqn (4.14) produces the specular characteristic function:

$$\Phi_{XY}(\upsilon) = J_0(V_0\upsilon) \tag{4.17}$$

Thus, the characteristic function of a specular wave component is a zero-order Bessel function that depends only on the amplitude of the specular component [24].

### 4.2.4 Diffuse, Non-specular Characteristic Function

Diffuse, non-specular received voltage may be written as the sum of numerous small-valued wave components.

$$\begin{aligned}
\tilde{V}_{\text{dif}} &= \sum_{i=1}^{N} V_i \exp(j\Phi_i) \\
&= \sum_{i=1}^{N} V_i \cos\Phi_i \quad + \quad j\sum_{i=1}^{N} V_i \sin\Phi_i \\
&= X + jY
\end{aligned}$$

which may be grouped into in-phase, $X$, and quadrature, $Y$ random variables. In the limit of large $N$, the real and imaginary components of $\tilde{V}_{\text{dif}}$ follow the central limit theorem, each tending to zero-mean, identically distributed Gaussian distributions. Provided all the individual amplitudes, $\{V_i\}$, remain small relative to the total power, the distributions of $X$ and $Y$ will be uncorrelated. Thus, the joint distribution may be written as

$$f_{XY}(x,y) = \frac{1}{2\pi\sigma^2}\exp\left(-\frac{x^2+y^2}{2\sigma^2}\right) \tag{4.18}$$

where $\sigma^2$ is the variance of $X$ and $Y$.

The probability that the random envelope, $R$, of the diffuse, non-specular voltage is below a level $\rho$ is defined as the *cumulative density function* (CDF). The envelope CDF, $F_R(\rho)$, may be calculated from the joint distribution, $f_{XY}(x,y)$ by performing the following integration:

$$F_R(\rho) = \mathrm{P}\left[R < \rho\right] = \int_0^{2\pi}\int_0^{\rho} f_{XY}(\rho'\cos\phi, \rho'\sin\phi)\rho' d\rho' d\phi \tag{4.19}$$

Eqn (4.19) has a simple geometrical interpretation. If we view the in-phase component, $X$, and quadrature component, $Y$, as coordinates on a cartesian plane, then the envelope, $R$, is simply the pythagorean distance to the origin, $R = \sqrt{X^2+Y^2}$. Thus, the probability that the envelope will be less than a threshold value $\rho$ is equal to the integration of the joint PDF over a circular region centered at the origin with radius $\rho$. Eqn (4.19) performs this integration.

The PDF is simply the derivative of the CDF. Differentiating Eqn (4.19) produces

$$f_R(\rho) = \frac{dF_R(\rho)}{d\rho} = \rho\int_0^{2\pi} f_{XY}(\rho\cos\phi, \rho\sin\phi)d\phi \tag{4.20}$$

To obtain the PDF of the diffuse, non-specular voltage component, we insert the joint

Gaussian PDF of Eqn (4.18) into Eqn (4.20). This produces the following PDF:

$$\begin{aligned} f_R(\rho) &= \frac{\rho}{2\pi\sigma^2}\int_0^{2\pi} \exp\left(-\frac{(\rho\cos\phi)^2 + (\rho\sin\phi)^2}{2\sigma^2}\right) d\phi \\ &= \frac{\rho}{\sigma^2}\exp\left(-\frac{\rho^2}{2\sigma^2}\right) \\ &= \frac{2\rho}{P_{\text{dif}}}\exp\left(-\frac{\rho^2}{P_{\text{dif}}}\right) \end{aligned} \tag{4.21}$$

The substitution, $P_{\text{dif}} = 2\sigma^2$, was made to give the PDF more physical meaning. The value $P_{\text{dif}}$ is the mean power of the non-specular voltage component,

$$P_{\text{dif}} = \mathrm{E}\left\{\left|\tilde{V}_{\text{dif}}\right|^2\right\}$$

and is less nebulous than the value $\sigma$.

The final step simply involves plugging the diffuse, non-specular envelope PDF into Eqn (4.14) to produce the characteristic function

$$\Phi_{XY}(\upsilon) = \exp\left(-\frac{\upsilon^2 P_{\text{dif}}}{4}\right) \tag{4.22}$$

Thus, the characteristic function of a diffuse, non-specular voltage component is a Gaussian-shaped function that depends only on the average power of the voltage component, $P_{\text{dif}}$ [25, 26]. The distribution of amplitudes, $\{V_i\}$, is not important – only the mean-squared power affects the shape of this characteristic function.

### 4.2.5 The I-SLAC PDF Generator

Now that the characteristic functions for specular components and diffuse, non-specular components have been determined, it is now possible to construct an envelope PDF for the reduced wave grouping by chaining the characteristic functions together and inverting the product using Eqn (4.15). The general form for the I-SLAC envelope PDF of Eqn (3.28) is given by

$$f_R(\rho) = \rho\int_0^{\infty} J_0(\upsilon\rho)\exp\left(\frac{-\upsilon^2 P_{\text{dif}}}{4}\right)\left[\prod_{i=1}^{N} J_0(V_i\upsilon)\right]\upsilon\, d\upsilon \tag{4.23}$$

which is valid for $\rho \geq 0$. Eqn (4.23) allows for *any* combination of single, constant-amplitude voltage waves and a group of voltage waves that carry non-specular power. As the next section demonstrates, Eqn (4.23) has a number of closed-form solutions that result from standard definite integrals [27, 28].

## 4.3 Closed-Form PDF Solutions

There are 5 different types of reduced wave groupings that produce closed-form solutions for the envelope PDF generator in Eqn (4.23). This section describes the 5 PDF's and discusses their use in wireless communications. Table 4.1 summarizes these cases.

### 4.3.1 The One-Wave PDF

A trivial case of fading is the *One-Wave PDF*, in which only one constant-amplitude wave is present in a local area. Its characteristic function, however, is a building block for other canonical fading PDF's. Integrating Eqn (4.23) for $N = 1$ and $P_{\text{dif}} = 0$ produces a result of 0 for all values of $r$ except $r = V_1$, which is infinite [27, p. 485]. Thus, the PDF is represented by

$$f_R(\rho) = \delta(\rho - V_1) \tag{4.24}$$

where $\delta(\cdot)$ is an impulse function. The One-Wave PDF, therefore, results in no envelope fading.

### 4.3.2 The Two-Wave PDF

The *Two-Wave PDF* represents the envelope fading caused by the interference of only two constant-amplitude waves in a local area, corresponding to $N = 2$ and $P_{\text{dif}} = 0$ in Eqn (4.23). Integration of Eqn (4.23) under these conditions is a well understood result which produces the following PDF [28, p. 718]:

$$f_R(\rho) = \frac{2\rho}{\pi\sqrt{4V_1^2V_2^2 - (V_1^2 + V_2^2 - \rho^2)^2}}, \quad |V_1 - V_2| \leq \rho \leq V_1 + V_2 \tag{4.25}$$

Eqn (4.23) evaluates to zero for $\rho < |V_1 - V_2|$ and $\rho > V_1 + V_2$, leading to the limits placed on $\rho$ in Eqn (4.25).

Figure 4.1 plots several examples of the Two-Wave PDF and CDF (cumulative density function) using a convenient parameter, $\Delta$, which we have defined to relate the relative magnitudes of $V_1$ and $V_2$ to one another [29]. The $\Delta$-parameter ranges between 0 and 1 and is defined by

$$\Delta = \frac{\text{Peak Specular Power}}{\text{Average Specular Power}} - 1 = \frac{2V_1V_2}{V_1^2 + V_2^2} \tag{4.26}$$

As shown in Figure 4.1, when the magnitudes of two multipath waves are equal, $\Delta = 1$. In the absence of a second component ($V_1$ or $V_2 = 0$), $\Delta = 0$. For dissimilar voltage values, the Two-Wave PDF exhibits two prominent spikes which mark the interval over which the PDF is non-zero. For the limiting case of $\Delta = 1$ ($V_1 = V_2$), the lower spike disappears and the PDF permits envelope values of zero which correspond to complete destructive cancellation.

| PDF | Expression for Envelope PDF $f_R(\rho)$ | Characteristic Function $\Phi_{XY}(\upsilon)$ | $\mathrm{E}\{R\}$ (volts) | $\mathrm{E}\{R^2\}$ (volts$^2$) |
|---|---|---|---|---|
| ONE-WAVE<br>No Fading | $\delta(\rho - V_1)$ | $J_0(V_1\upsilon)$ | $V_1$ | $V_1^2$ |
| TWO-WAVE<br>Simple Fading | $\frac{2\rho}{\pi\sqrt{4V_1^2V_2^2-(V_1^2+V_2^2-\rho^2)^2}}$<br>$\lvert V_1 - V_2\rvert \leq \rho \leq V_1 + V_2$ | $J_0(V_1\upsilon)J_0(V_2\upsilon)$ | $\frac{2(V_1+V_2)}{\pi}\mathrm{E}\left[\frac{4V_1V_2}{(V_1+V_2)^2}\right]$ | $V_1^2+V_2^2$ |
| THREE-WAVE†<br>Max. Discrete Fading | $\frac{\rho^{\frac{1}{2}}}{\pi^2\sqrt{V_1V_2V_3}}K\left(\frac{\Delta_\rho^2}{V_1V_2V_3\rho}\right),\ \Delta_\rho^2 < V_1V_2V_3\rho^*$<br>$\frac{\rho}{\pi^2\Delta_\rho}K\left(\frac{V_1V_2V_3\rho}{\Delta_\rho^2}\right),\ \Delta_\rho^2 < V_1V_2V_3\rho^*$ | $J_0(V_1\upsilon)J_0(V_2\upsilon)J_0(V_3\upsilon)$ | no closed-form solution | $V_1^2+V_2^2+V_3^2$ |
| RAYLEIGH<br>Numerous Multipath | $\frac{2\rho}{P_{\mathrm{dif}}}\exp\left(\frac{-\rho^2}{P_{\mathrm{dif}}}\right)$ | $\exp\left(\frac{-\upsilon^2 P_{\mathrm{dif}}}{4}\right)$ | $\sqrt{\frac{\pi P_{\mathrm{dif}}}{4}}$ | $P_{\mathrm{dif}}$ |
| RICIAN<br>Dominant Component | $\frac{2\rho}{P_{\mathrm{dif}}}\exp\left(\frac{-\rho^2-V_1^2}{P_{\mathrm{dif}}}\right)\mathrm{I}_0\left(\frac{2V_1\rho}{P_{\mathrm{dif}}}\right)$ | $J_0(V_1\upsilon)\exp\left(\frac{-\upsilon^2 P_{\mathrm{dif}}}{4}\right)$ | no closed-form solution | $P_{\mathrm{dif}}+V_1^2$ |
| TIP‡<br>Two Dominant Components | $\frac{2\rho}{P_{\mathrm{dif}}}\exp\left(\frac{-\rho^2}{P_{\mathrm{dif}}}-K\right)\mathrm{I}_0\left\{\rho\sqrt{\frac{4K}{P_{\mathrm{dif}}}}\sqrt{1-\frac{d}{dK}}\right\}I_0(\Delta K)$ | $J_0(V_1\upsilon)J_0(V_2\upsilon)\exp\left(\frac{-\upsilon^2 P_{\mathrm{dif}}}{4}\right)$ | no closed-form solution | $P_{\mathrm{dif}}+V_1^2+V_2^2$ |

* also provided that $2\max(V_1, V_2, V_3)-V_1-V_2-V_3 \leq \rho \leq V_1+V_2+V_3$; otherwise $f_R(\rho) = 0$.

† $16\Delta_\rho^2 = \left[(\rho+V_1)^2-(V_2-V_3)^2\right]\left[(V_2+V_3)^2-(\rho-V_1)^2\right]$

‡ $K = \frac{V_1^2+V_2^2}{P_{\mathrm{dif}}}$ $\quad \Delta = \frac{2V_1V_2}{V_1^2+V_2^2}$

$K(x)$ – Complete 1st Kind Elliptical Integral

$E(x)$ – Complete 2nd Kind Elliptical Integral

$J_n(x)$ – Bessel Function

$I_n(x)$ – Modified Bessel Function

Table 4.1: Summary of envelope PDF's in different fading environments.

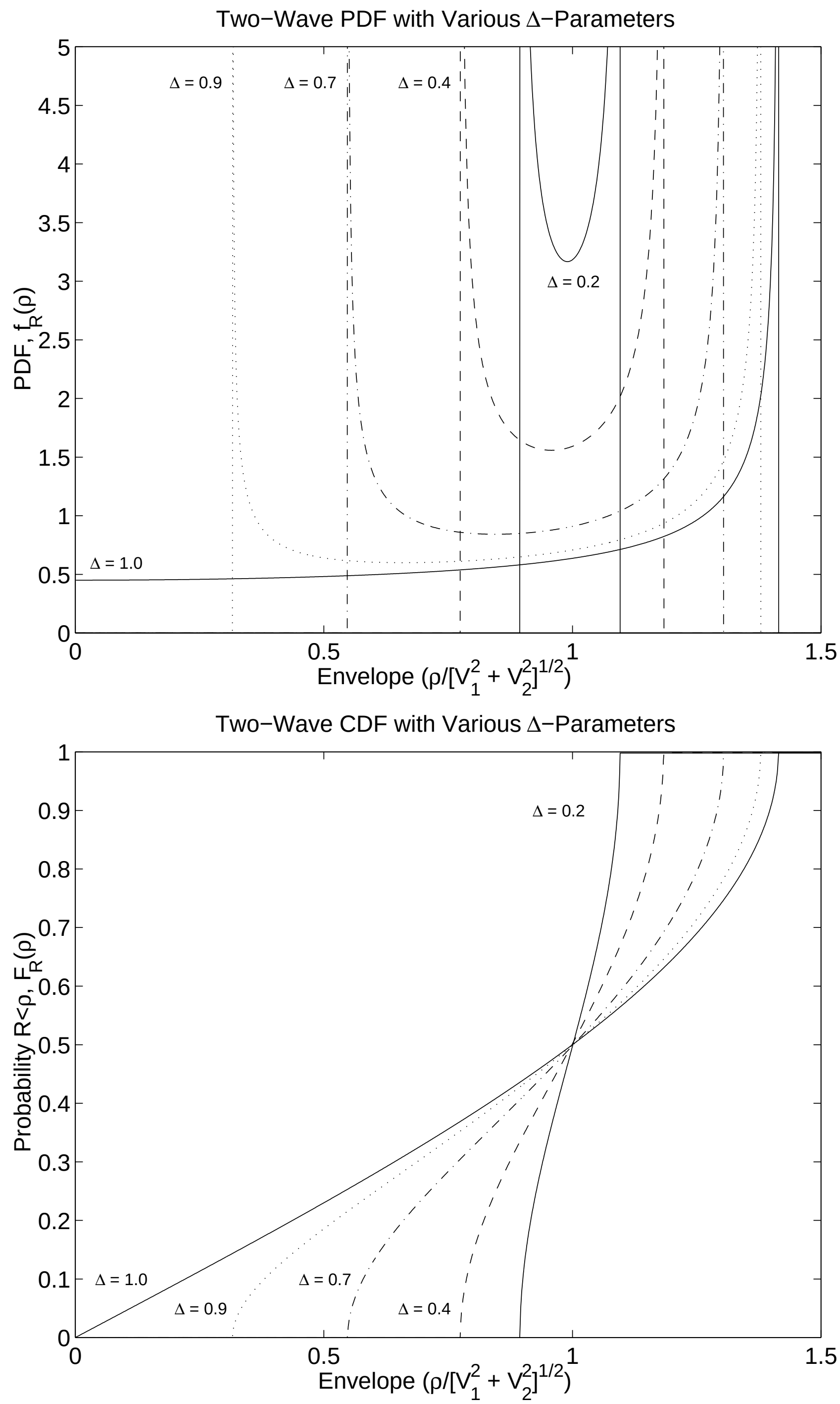


Figure 4.1: Evolution of a Two-Wave PDF and CDF with varying $\Delta$.

### 4.3.3 The Three-Wave PDF

Two- and Three-Wave models often are used to describe fading in microwave digital radio communications [30]. The *Three-Wave PDF* in Table 4.1 is the solution of Eqn (4.23) for $N = 3$ and $P_{\text{dif}} = 0$, a result formulated by Nicholson in 1920 [31] and given below:

$$f_R(\rho) = \begin{cases} 0, & \rho < \rho_{\min} \text{ or } \rho > \rho_{\max} \\ \frac{\rho^{\frac{1}{2}}}{\pi^2\sqrt{V_1V_2V_3}} K\left[\frac{\Delta_\rho^2}{V_1V_2V_3\rho}\right], & \Delta_\rho^2 < V_1V_2V_3\rho \\ \frac{r}{\pi^2\Delta_\rho} K\left[\frac{V_1V_2V_3\rho}{\Delta_\rho^2}\right], & \Delta_\rho^2 > V_1V_2V_3\rho \end{cases} \tag{4.27}$$

The function $K(\cdot)$ is an elliptic integral of the first kind. Note that $\Delta_\rho$ in Eqn (4.27) is a function of $\rho$. Here we have used the subscript $\rho$, which is appended to Nicholson's notation to avoid any confusion between this parameter and the $\Delta$-parameter used to describe the Two-Wave PDF. The values $\rho_{\min}$ and $\rho_{\max}$ define the interval over which the integration of Eqn (4.23) and, subsequently, the PDF is non-zero. They are given by

$$\rho_{\max} = V_1 + V_2 + V_3 \qquad \rho_{\min} = \max[2\max(V_1, V_2, V_3) - V_1 - V_2 - V_3, 0] \tag{4.28}$$

The expressions in Eqn (4.28) have an appealing geometric interpretation: the Three-Wave PDF is 0 for all $\rho$ such that four line segments of lengths $\rho$, $V_1$, $V_2$, and $V_3$ are incapable of forming a quadrilateral [31].

As one might expect, the behavior of the Three-Wave PDF is varied and complicated. Figure 4.2 plots just a few examples of the PDF and corresponding CDF. A comparison of the Three-Wave CDF's of Figure 4.2 and the Two-Wave CDF's of Figure 4.1 provides insight into the difference between specular and non-specular power. Unlike the Two-Wave case, the different plots of the Three-Wave CDF are much more similar to one another. This similarity is due to the central limit theorem: the addition of another constant-amplitude wave to Two-Wave propagation makes the *total* multipath power more non-specular. Despite the complex shape of the CDF, the general cases of Three-Wave propagation begin to approach the CDF for purely non-specular power. Thus, even if it were possible to analytically calculate a "Four-Wave PDF", its usefulness would be limited since the most general cases will appear to be even more Rayleigh-distributed than the Three-Wave PDF's.

### 4.3.4 The Rayleigh PDF

The Rayleigh PDF assumes that *all* multipath power is non-specular and occurs from the integration of Eqn (4.23) under the condition $N = 0$ and non-zero $P_{\text{dif}}$. This definite integral

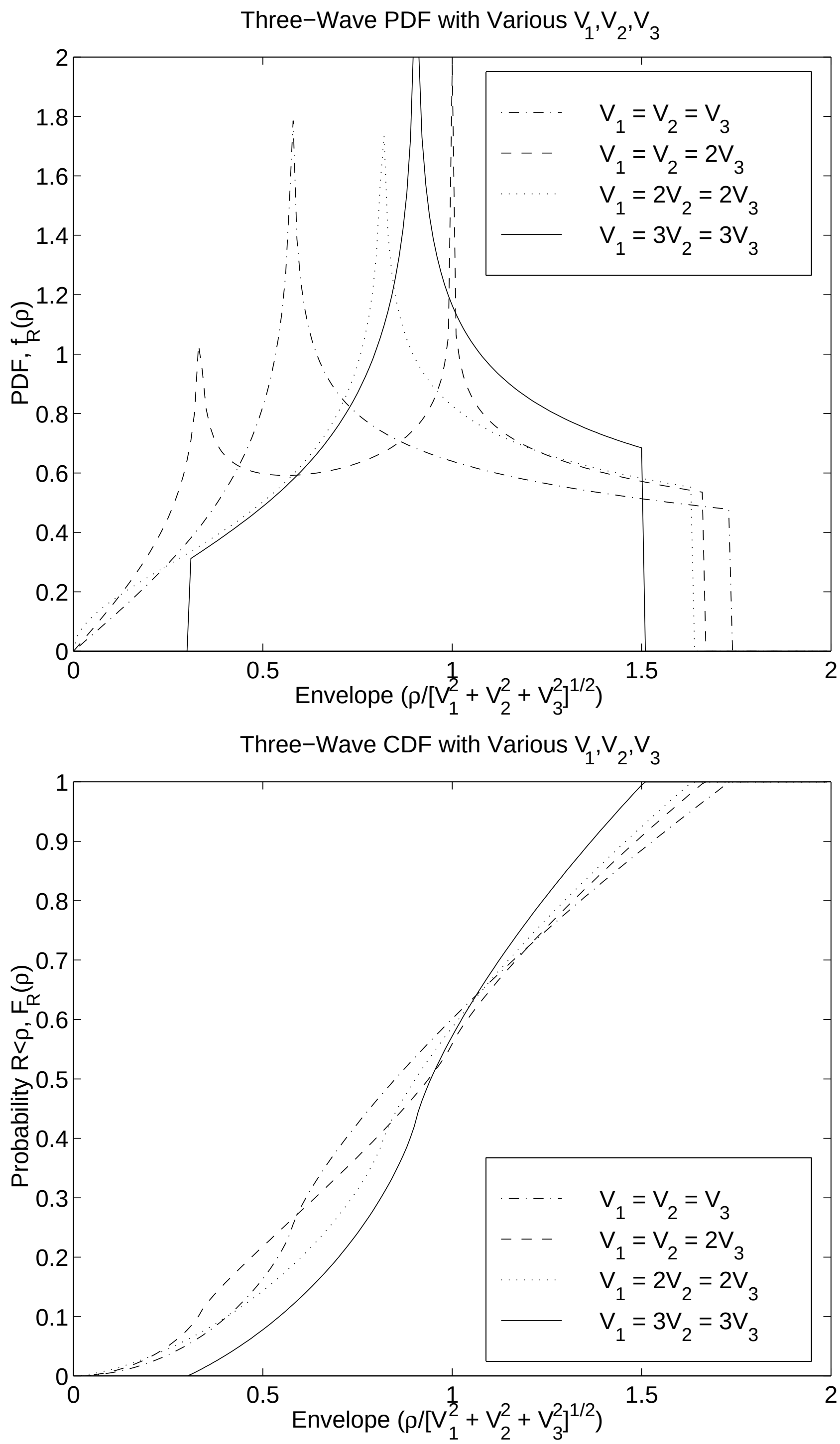


Figure 4.2: Several CDF's and PDF's for Three-Wave local area propagation.

is a standard result and produces the following PDF [28, p. 738]:

$$f_R(\rho) = \frac{2\rho}{P_{\text{dif}}} \exp\left(\frac{-\rho^2}{P_{\text{dif}}}\right), \quad \rho \geq 0 \tag{4.29}$$

Unlike the purely specular wave PDF's, the Rayleigh PDF is non-zero over the entire range of $0 \leq \rho < \infty$. The Rayleigh PDF has been used extensively to describe narrowband local area fading for mobile radio receivers [32, 33, 20].

### 4.3.5 The Rician PDF

The Rician PDF describes the fading of non-specular power in the presence of a dominant, non-fluctuating multipath component [33, 34]. The analytical expression for the Rician distribution results from the integration of Eqn (4.23) under the condition $N = 1$ and non-zero $P_{\text{dif}}$. After applying a well-understood definite integral relationship [28, p. 739], the resulting PDF is

$$f_R(\rho) = \frac{2\rho}{P_{\text{dif}}} \exp\left(\frac{-\rho^2 - V_1^2}{P_{\text{dif}}}\right) I_0\left(\frac{2\rho V_1}{P_{\text{dif}}}\right), \quad \rho \geq 0 \tag{4.30}$$

where $I_0(\cdot)$ is a 0-order modified Bessel function.

Figure 4.3 shows several different kinds of Rician PDF's and CDF's. The plots are labeled using a Rician $K$ factor, which is the ratio of the power of the dominant multipath component to the power of the remaining, non-specular multipath:

$$K = \frac{\text{Specular Power}}{\text{Non-specular Power}} = \frac{V_1^2}{P_{\text{dif}}} \tag{4.31}$$

In the literature, the parameter $K$ is often given as a dB value, which is $10\log_{10}$ of the quantity in Eqn (4.31). Notice from Figure 4.3 that $K = -\infty$ dB corresponds to the Rayleigh PDF and the complete disappearance of the specular power.

*Note: Rice or Nakagami*

The Rician distribution is also called the *Rice-Nakagami* distribution in the literature, to recognize the result which was independently formulated by outstanding Japanese researcher M. Nakagami. The term *Rician* is used in this work not to diminish Nakagami's contribution, but to avoid confusion with another popular PDF in wireless which bears his namesake: the *Nakagami-m* distribution [35]. This distribution was originally formulated for characterizing temporal fading measurements from upper-atmosphere propagation but has been applied liberally to the small-scale fading of terrestrial wireless systems as well [36, 7].

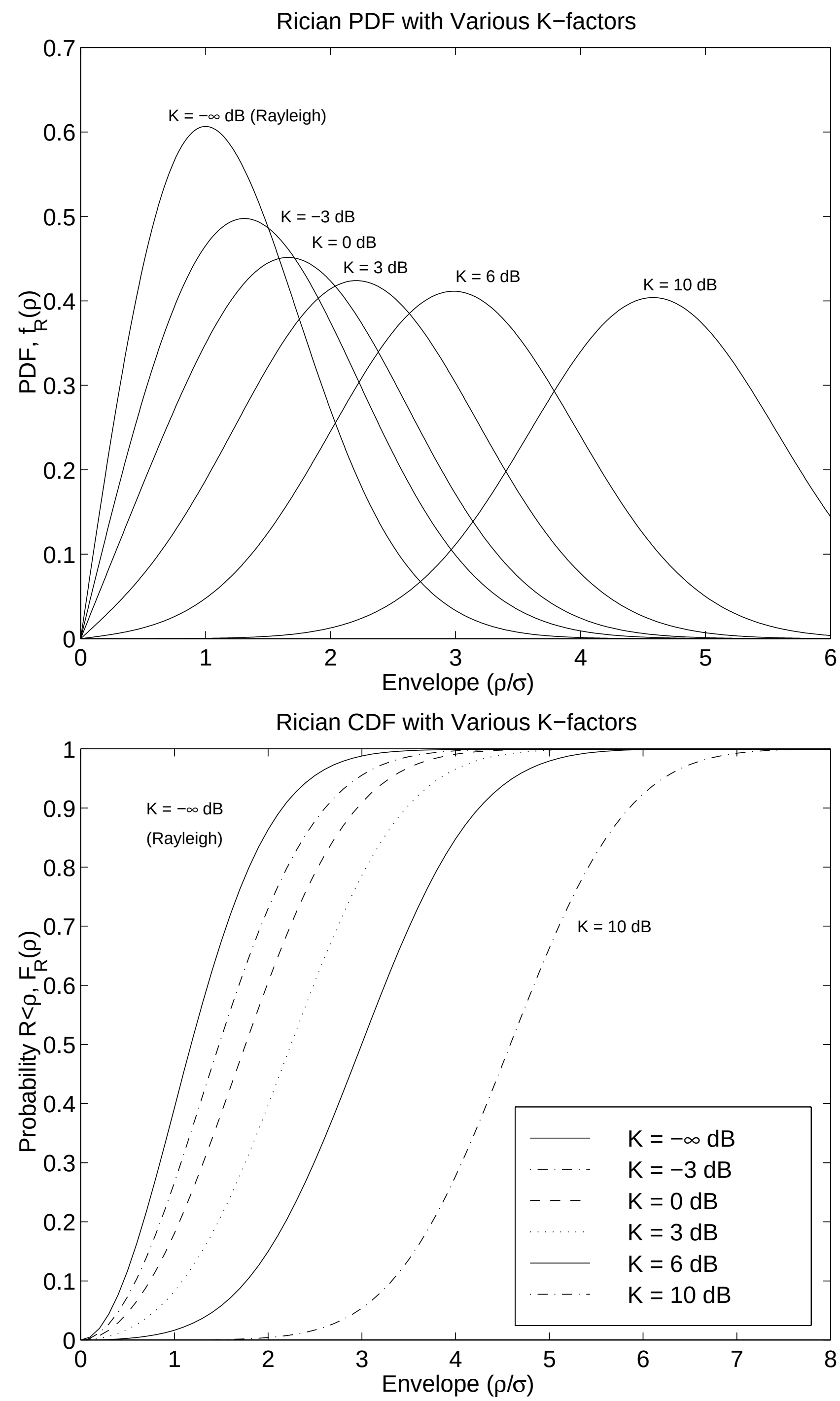


Figure 4.3: Evolution of a Rician PDF and CDF as the dominant multipath component increases. ($\sigma = \sqrt{P_{\mathrm{dif}}/2}$)

## 4.4 Two-Wave with Incoherent Power (TIP) PDF

If Eqn (4.23) is evaluated with $N = 2$ and non-zero $P_{\text{dif}}$, then the Two-Wave with Incoherent Power (TIP) PDF results. We will use parameters similar to the physical Rician $K$-parameter of Eqn (4.31) and the Two-Wave $\Delta$-parameter of Eqn (4.26) to classify the shape of the TIP PDF:

$$K = \frac{V_1^2 + V_2^2}{P_{\text{dif}}} \qquad \Delta = \frac{2V_1V_2}{V_1^2 + V_2^2} \tag{4.32}$$

There is no exact closed-form equation for TIP fading, but this section presents a family of closed-form PDF's that closely approximate the behavior of the exact TIP PDF.

### 4.4.1 Approximate Representation

Appendix 4.B derives the following *family* of PDF's that approximate the TIP PDF:

$$f_R(\rho) = \frac{2\rho}{P_{\text{dif}}} \exp\left(\frac{-\rho^2}{P_{\text{dif}}} - K\right) \sum_{i=1}^{M} a_i D\left(\frac{\rho}{\sqrt{P_{\text{dif}}/2}}; K, \Delta\cos\frac{\pi(i-1)}{2M-1}\right) \tag{4.33}$$

$$\text{where} \quad D\left(x; K, \alpha\right) = \frac{1}{2}\exp(\alpha K) I_0\left(x\sqrt{2K(1-\alpha)}\right) + \frac{1}{2}\exp(-\alpha K) I_0\left(x\sqrt{2K(1+\alpha)}\right)$$

We refer to the value $M$ in the summation as the *order* of the approximate TIP PDF. By increasing the order in Eqn (4.33), the approximate PDF becomes a more accurate representation of the true TIP PDF. However, using the first few orders ($M = 1$ through 5) yields accurate representations *over the most useful range of $K$ and $\Delta$ parameters.* Table 4.2 records the exact $\{a_i\}$ coefficients – derived in Appendix 4.B – for the first five orders of Eqn (4.33).

Table 4.2: Exact coefficients for the first five orders of the approximate Two-Wave with Incoherent Power (TIP) fading PDF.

| Order | $a_1$ | $a_2$ | $a_3$ | $a_4$ | $a_5$ |
|---|---|---|---|---|---|
| 1 | 1 | | | | |
| 2 | $\frac{1}{4}$ | $\frac{3}{4}$ | | | |
| 3 | $\frac{19}{144}$ | $\frac{25}{48}$ | $\frac{25}{72}$ | | |
| 4 | $\frac{751}{8640}$ | $\frac{3577}{8640}$ | $\frac{49}{320}$ | $\frac{2989}{8640}$ | |
| 5 | $\frac{2857}{44800}$ | $\frac{15741}{44800}$ | $\frac{27}{1120}$ | $\frac{1209}{2800}$ | $\frac{2889}{22400}$ |

The product of the parameters $K$ and $\Delta$ determines which order of Eqn (4.33) should be used when representing TIP fading. As the product of these two parameters increases, a higher-order approximation is needed to model the TIP PDF accurately. As a general rule of thumb, the minimum order is

$$\text{Order } (M) \geq \frac{1}{2} K\Delta \tag{4.34}$$

Eqn (4.34) is based on a graphical comparison between the approximate analytical functions and the true, numerical solution of the TIP PDF. The approximate PDF will only deviate from the exact TIP PDF if the specular power is much larger than the non-specular power (large $K$ value) *and* if the amplitudes of the specular voltage components are relatively equal in magnitude ($\Delta$ approaches 1).

**Example 4.1: Order-2 Approximate TIP PDF**

**Problem:** Using Table 4.2 and Eqn (4.33), calculate the order-2 approximate TIP PDF.

**Solution:** Plugging the coefficients $a_1$ and $a_2$ into Eqn (4.33) produces

$$f_R(\rho) = \frac{2\rho}{P_{\text{dif}}} \exp\left(\frac{-\rho^2}{P_{\text{dif}}} - K\right) \left[\frac{1}{4} D\left(\frac{\rho}{\sqrt{P_{\text{dif}}/2}}; K, \Delta\right) + \frac{3}{4} D\left(\frac{\rho}{\sqrt{P_{\text{dif}}/2}}; K, \frac{\Delta}{2}\right)\right]$$

which, in this form, is not much more complicated than a Rician PDF.

---

Despite being an approximate result, the family of PDF's in Eqn (4.33) have a number of extraordinary characteristics that are independent of order, $M$, and parameters, $K$ and $\Delta$:

- *They are mathematically exact PDF's.* They integrate to 1 over the range $0 \leq \rho < \infty$.
- *They are accurate over their upper and lower tails.* These regions are important for modeling noise-limited or interference-limited mobile communication systems [6].
- *They all exactly preserve the second moment of the true PDF.* The second moment is the most important moment to preserve since it physically represents the average local area power [10].
- *They can be entirely described with three physically intuitive parameters.* The physical parameters $P_{\text{dif}}$, $K$, and $\Delta$ – as defined in this paper – have straight-forward physical definitions.

- *They exhibit the proper limiting behavior.* All of the PDF's contain, as a special case of $\Delta = 0$, the exact Rician PDF and, as a special case of $K = 0$, the exact Rayleigh PDF.

Accurate analytical representation of these PDF's reveals interesting behavior in fading channels that goes unnoticed using Rician PDF's, which are capable of modeling the envelope fading of non-specular power in the presence of only *one* specular component.

### 4.4.2 Graphical Analysis

Figures 4.4 through 4.7 plot a series of PDF's and CDF's for TIP fading. As shown by Figure 4.4, there is little difference between the Rician PDF and the TIP PDF when $K$ is less than 3 dB. The difference gradually becomes more pronounced as $K$ increases, particularly when the specular power is divided equally between the two discrete components ($\Delta = 1$). The $K$=10 dB graph of Figure 4.7 illustrates these distortions most dramatically. In fact, as the product of parameters $K$ and $\Delta$ becomes large, the graph of the PDF becomes bimodal, exhibiting two maxima.

### 4.4.3 Rayleigh and Rician Approximations

For the limiting parameter cases of Table 4.3, the exact TIP PDF contains the Rayleigh, Rician, One-Wave, and Two-Wave PDF's. This demonstrates the generality of the exact and approximate TIP PDF's. It also shows the utility of the Three-Wave PDF, since it is the only analytical expression in Table 4.1 that is not a general case of the TIP PDF.

Table 4.3: The TIP PDF contains the Rayleigh, Rician, One-Wave, and Two-Wave PDF's as special cases.

| Parameter Value | | Type of Fading |
|---|---|---|
| $K = 0$ | – | Rayleigh |
| $K > 0$ | $\Delta = 0$ | Rician |
| $K \to \infty$ | $\Delta = 0$ | One-Wave |
| $K \to \infty$ | $\Delta > 0$ | Two-Wave |

Since the Rician and Rayleigh PDF's are special cases of the TIP PDF, it is useful to know the range of parameters over which TIP fading may be approximated by these simpler distributions. An inspection of the graphs of Figure 4.4-Figure 4.7 reveals the range of $K$ and $\Delta$ over which a Rician PDF approximates a TIP PDF. In general, the TIP PDF resembles a Rician PDF in shape for $K\Delta < 2$. Under this condition, the smallest of the two

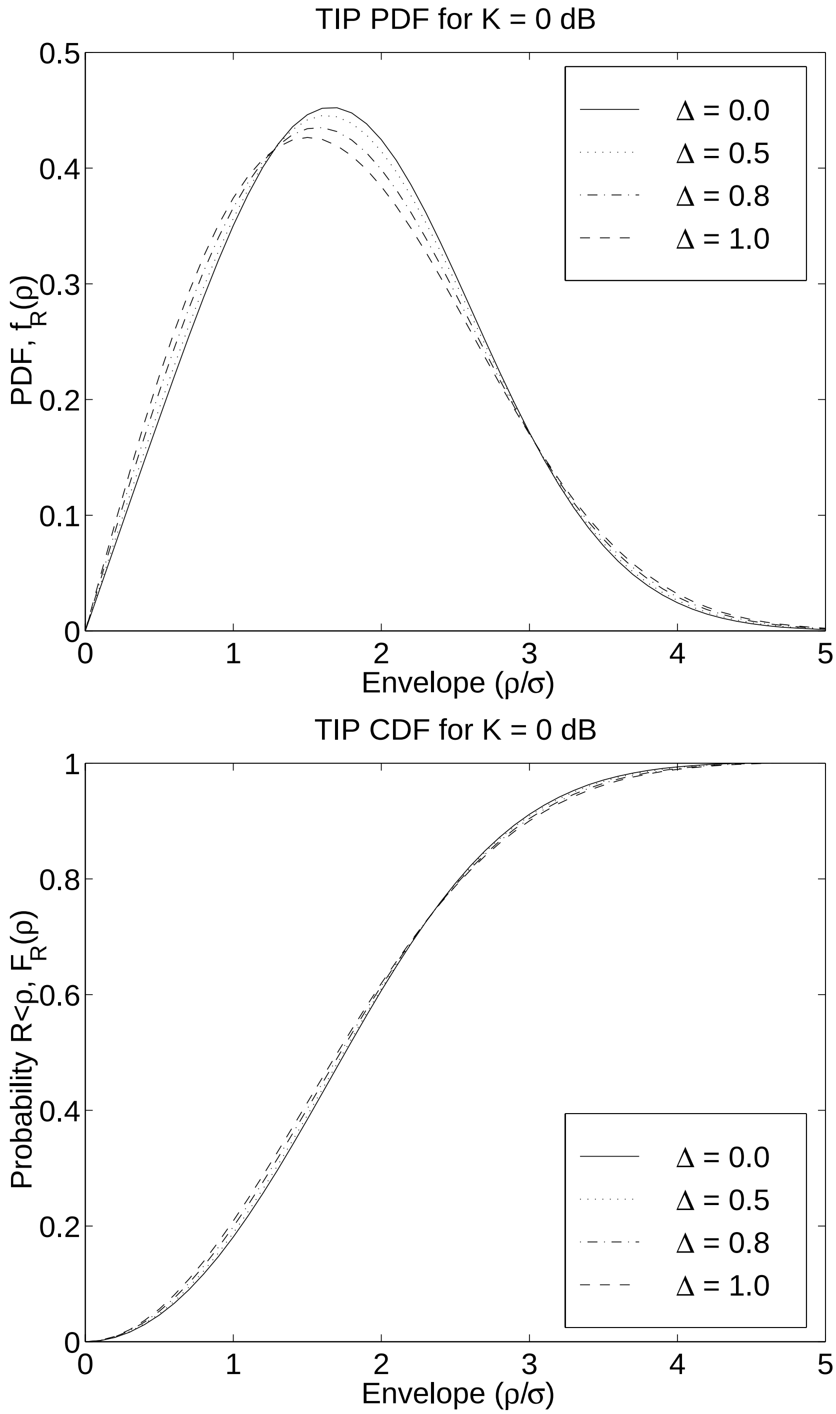


Figure 4.4: TIP PDF and CDF for $K = 0$ dB. ($\sigma = \sqrt{P_{\mathrm{dif}}/2}$)

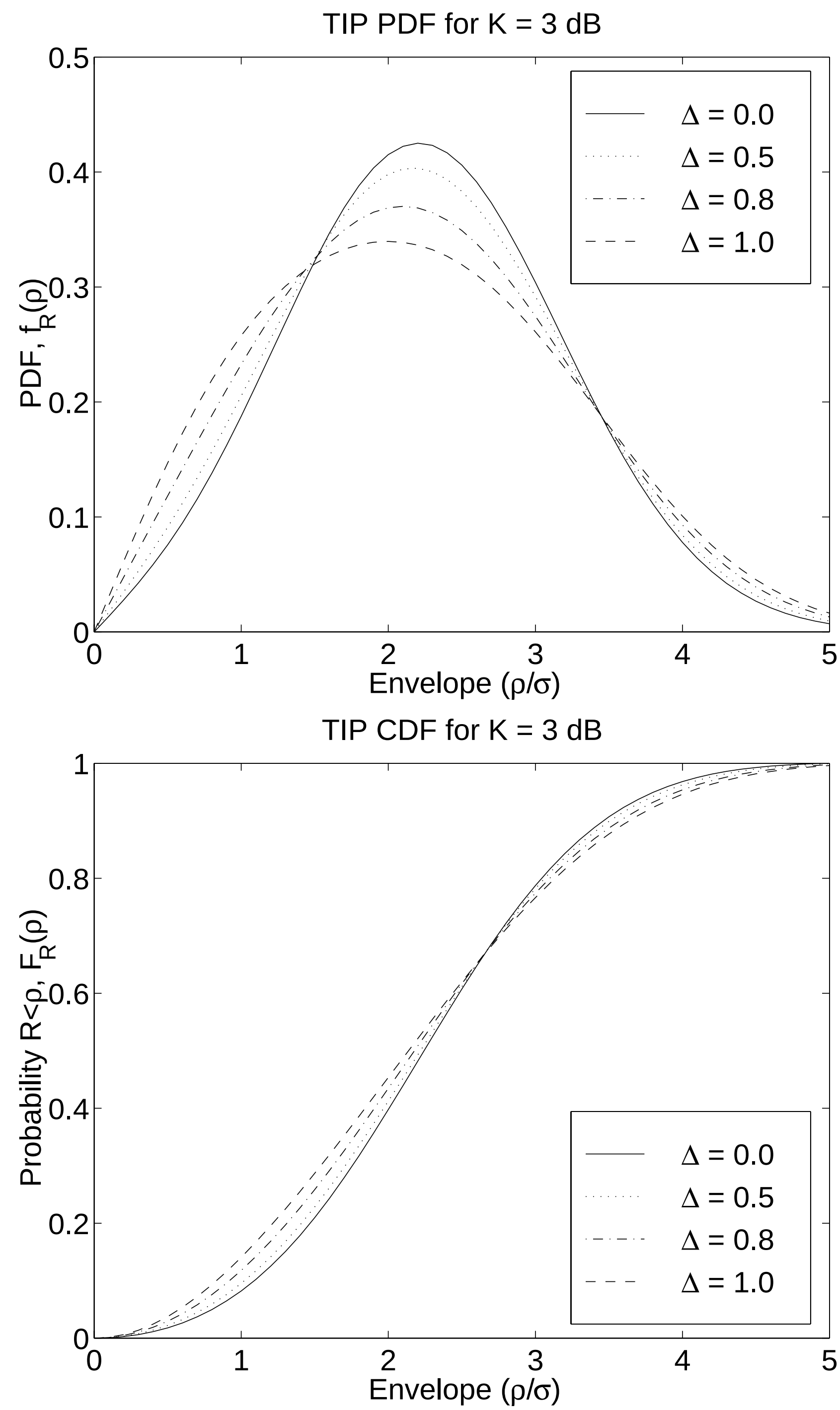


Figure 4.5: TIP PDF and CDF for $K = 3$ dB. ($\sigma = \sqrt{P_{\text{dif}}/2}$)

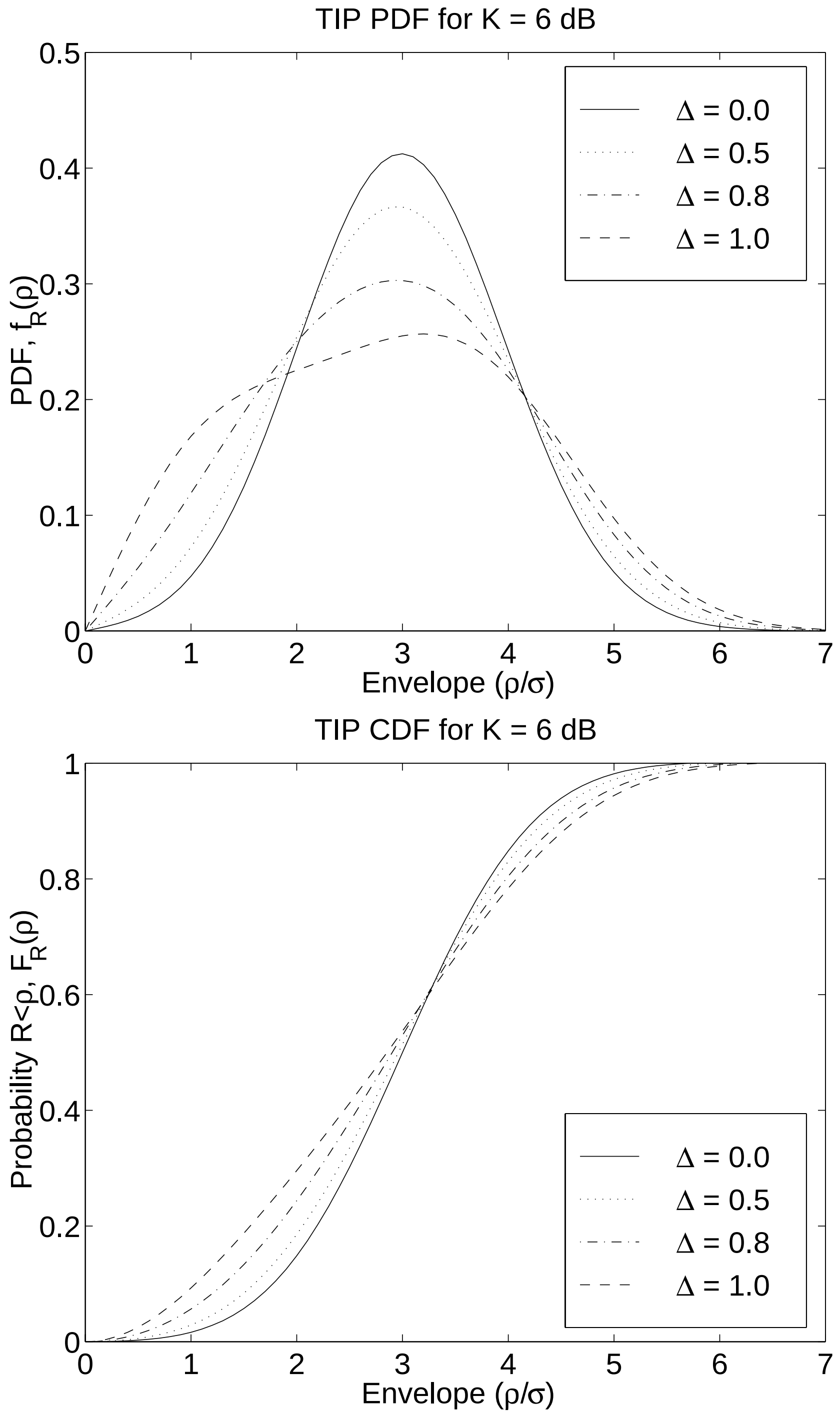


Figure 4.6: TIP PDF and CDF for $K = 6$ dB. ($\sigma = \sqrt{P_{\text{dif}}/2}$)

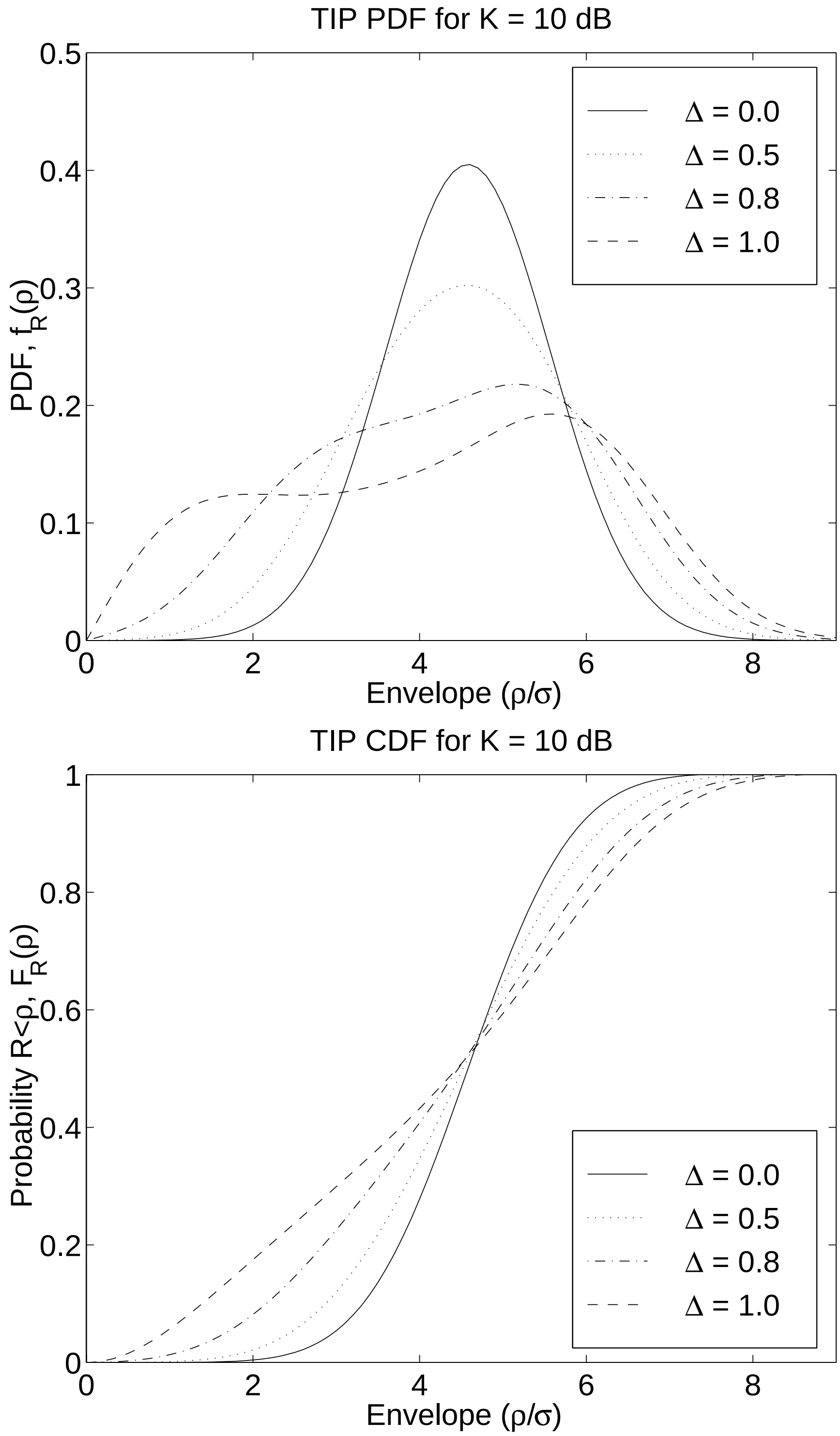


Figure 4.7: TIP PDF and CDF for $K = 10$ dB. ($\sigma = \sqrt{P_{\text{dif}}/2}$)

Table 4.4: Three examples of Two-Wave with Incoherent Power (TIP) fading that may simplify to Rayleigh or Rician PDF's.

| | Example TIP Voltage Values | | | | | |
|---|---|---|---|---|---|---|
| | 1st Specular | 2nd Specular | Non-specular RMS | TIP Parameters | | Simplest |
| Case | Voltage ($V_1$) | Voltage ($V_2$) | Voltage ($\sqrt{P_{\text{dif}}}$) | $K$ | $\Delta$ | PDF |
| A | 2 $\mu$V | 2 $\mu$V | 3 $\mu$V | 0.89 | 1.0 | Rayleigh |
| B | 4 $\mu$V | 2 $\mu$V | 3 $\mu$V | 2.22 | 0.8 | Rician |
| C | 4 $\mu$V | 4 $\mu$V | 3 $\mu$V | 3.56 | 1.0 | TIP |

specular components may be grouped with the non-specular power so that only one large specular component remains. After computing a Rician $K$-factor for this new grouping, the resulting Rician PDF will approximately describe the envelope of the TIP fading.

TIP fading may be further approximated by a Rayleigh PDF if, in addition to the above-mentioned criterion, the power of the largest specular component is less than the power of the smaller specular component *plus* the average non-specular power:

$$\begin{aligned} \max(V_1^2, V_2^2) &< \min(V_1^2, V_2^2) + P_{\text{dif}} \\ \frac{1}{2} + \frac{1}{2}\sqrt{1-\Delta^2} &< \frac{1}{2} - \frac{1}{2}\sqrt{1-\Delta^2} + \frac{1}{K+1} \end{aligned} \tag{4.35}$$

This condition derives from Figure 4.3, which shows that Rician PDF's resemble the shapes of Rayleigh PDF's (after scaling) for a Rician $K$-factor less than 0 dB. Under this condition, the entire sum of voltage components may be treated together as diffuse, non-specular power, despite the presence of two specular components.

The Rician and Rayleigh approximation conditions, therefore, are best summarized in terms of the TIP $K$ and $\Delta$ parameters by the following:

$$\text{Rician Condition:} \qquad K < \frac{2}{\Delta} \tag{4.36}$$

$$\text{Rayleigh Condition:} \qquad K < \min\left(\frac{2}{\Delta}, \frac{1}{\sqrt{1-\Delta^2}} - 1\right) \tag{4.37}$$

These conditions show the parameter range over which a TIP PDF may be approximated by an analytically simpler Rician or Rayleigh PDF. If these conditions are not met, then the only recourse is to use Eqn (4.33) or some other evaluation of Eqn (4.23) for $N = 2$ and non-zero $P_{\text{dif}}$.

Table 4.4 shows three examples of TIP fading and determines the simplest approximate PDF that describes the voltage envelope of each. Case A in Table 4.4 satisfies the Rayleigh condition of Eqn (4.37). Case B, on the other hand, satisfies only the Rician condition of Eqn (4.36). Case C satisfies neither condition and may not be approximated by a Rayleigh or Rician PDF. Note how the subtle changes in voltage amplitudes between the three cases drastically affects the overall shape and calculation of the PDF, emphasizing the need for careful and accurate representation of TIP PDF's.

### 4.4.4 Final Comments on Reduced Wave Groupings

Recall that, in the presentation of reduced wave groupings, a formal mathematical criterion for what constitutes an non-specular voltage component as *diffuse* was not presented. Although the criteria a researcher chooses to gauge diffuseness may depend on the application, the discussion in the previous section on approximating TIP and Rician PDF's as Rayleigh PDF's provides insight. For example, we now know that the shape of the Rician PDF is approximated well by a Rayleigh PDF when the specular component contains less power than the non-specular component (Rician $K$ is less than 1).

It is useful to have an algorithm for determining the optimal PDF – in terms of simplicity and accuracy – for representing the distribution of received voltage envelope for an aribtrary wave grouping. Figure 4.8 represents one such algorithm. Starting with any grouping of specular and non-specular power, Figure 4.8 finds the simplest and most accurate method for representing the envelope PDF based on the analytical expressions in Table 4.1 and the TIP approximations of Eqn (4.33).

**Example 4.2: PDF Grouping Algorithm**

**Problem:** It is known that an I-SLAC model is composed of 3 multipath waves with voltage amplitudes 4 $\mu$V, 3 $\mu$V, and 2 $\mu$V and a diffuse, non-specular component with $P_{\text{dif}} = (1\mu\text{V})^2$. Find the simplest analytical representation, if any, of this envelope PDF.

**Solution:** Following the grouping algorithm of Eqn (4.8):

1. The initial grouping of voltages is $[V_1 = 4,\ V_2 = 3,\ V_3 = 2,\ P_{\text{dif}} = 1]$ (units dropped for simplicity).
2. There is diffuse power ($P_{\text{dif}} \neq 0$) and there are more than two specular components ($N = 3$), so all but the two largest specular components must be grouped with the non-specular component. The new grouping is $[V_1 = 4,\ V_2 = 3,\ P_{\text{dif}} = 5]$.

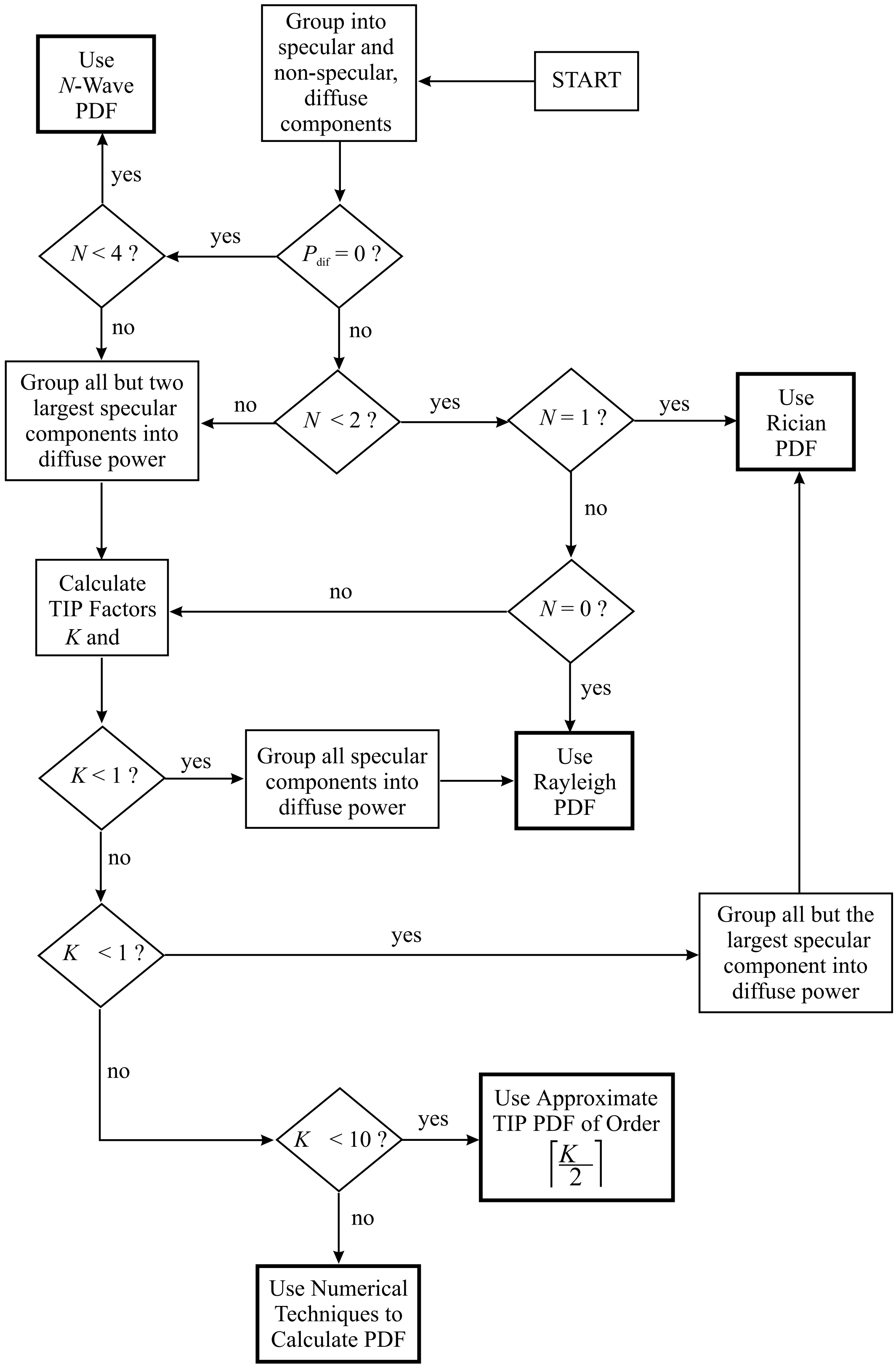


Figure 4.8: A flowchart for determining the simplest way to graph an I-SLAC PDF.

3. The TIP factors for this distribution are $K = 5$ and $\Delta = 0.96$. This TIP distribution is too complicated to simplify to a Rayleigh distribution ($K > 1$) or a Rician distribution ($K\Delta > 1$), but can be approximated accurately by Eqn (4.33) ($K\Delta < 10$).
4. The value of $\left\lceil \frac{K\Delta}{2} \right\rceil$ is 3, so an order 3 approximation of Eqn (4.33) should be used to represent the PDF.

---

### 4.4.5 TIP PDF Applications

The TIP PDF and its approximations are important for characterizing fading in a variety of propagation scenarios. Small-scale fading is characterized by the TIP PDF whenever the received signal contains two strong, specular multipath waves. While this may occur for typical narrowband receiver operation, directional antennas and wideband signals increase the likelihood of TIP small-scale fading.

The use of directive antennas or arrays at a receiver, for example, amplifies several of the strongest multipath waves that arrive in one particular direction while attenuating the remaining waves [1, 2]. This effectively increases the ratio of specular to non-specular received power, turning a Rayleigh or Rician fading channel into a TIP fading channel.

Wideband signal fading will likely exhibit TIP fading characteristics for similar reasons. A wideband receiver has the ability to reject multipath components that arrive with largely different propagation time delays [10, 37]. This property of a wideband receiver will naturally separate specular multipath components from other non-specular multipath waves. Under these circumstances, the ratio of specular to non-specular received power increases for a given propagation delay and a TIP fading channel may result.

### 4.4.6 Closing Remarks on TIP Fading

Beyond the TIP PDF, a "Three-Wave with Incoherent Power" (3IP) PDF is the next logical step. The value of such an analytically difficult PDF, however, is questionable. Much like the previously discussed "Four-Wave" PDF, the central-limit theorem would begin to dominate the behavior of an I-SLAC model, making it difficult to distinguish between the different cases of a 3IP PDF. For example, a 3IP PDF may be approximated by the TIP PDF if the smallest of the three specular voltage components is grouped with the non-specular power. This approximation would fail only if the non-specular power were small compared to the third smallest specular component – yet such a situation implies that the non-specular power is so small that it could be ignored: a 3IP PDF could then be approximated by the Three-Wave PDF. Therefore, it is safe to say that the analytical expressions of Eqn (4.33) and Table 4.1 provide a near-complete description of the possible envelope fading of complex voltages in an I-SLAC model.

## 4.5 Chapter Summary

In a randomly-varying small-scale channel, the distribution of received signal power or envelope will dramatically affect the performance of a receiver. These fluctuations are best described using a *probability density function* or PDF, which characterizes all of the first-order statistics of a channel. The following key points summarize the first-order analysis described in this chapter:

- Mean received power is one of the most fundamental first-order statistics in channel modeling and measurement.
  - For a U-SLAC model, the mean power of the channel is equal to the sum of the powers carried by individual multipath waves.
  - A U-SLAC model is ergodic.
  - For a U-SLAC model with heterogeneous scattering, spatial averaging and frequency averaging produce identical results for mean received power.
- The canonical PDF generator of Eqn (4.23) describes the distribution of received envelope voltages for I-SLAC models.
  - The generator is based on the reduced wave grouping and uses a characteristic function approach.
  - There are 5 closed-form solutions to the PDF generator.
  - The simplest solutions have become popular in wireless engineering.
- The Two-Wave with Incoherent Power (TIP) PDF models the most general type of fading behavior.
  - This PDF has no closed-form solution.
  - There are several techniques for approximating the TIP PDF.
  - The TIP PDF contains Rayleigh, Rician, One-Wave, and Two-Wave PDF's as special cases.
  - TIP behavior can deviate substantially from Rayleigh or Rician PDF's.

Determining the envelope PDF of a stochastic channel completely characterizes the first-order statistics of that channel. While useful, first-order statistics do not provide any information as to how processes develop as a function of frequency and space. To understand the frequency and space evolution of random channels, we must develop the concepts of power spectra and autocorrelations more thoroughly. This is the subject of Chapter 5.

## 4.A Derivation of Envelope Characteristic Functions

In the study of PDF's, it is convenient to define a characteristic function, which is the Fourier transform of the PDF [21]. The standard mathematical definitions for finding a characteristic function, $\Phi_X(\upsilon)$, from a PDF, $f_X(x)$, and vice versa are given below:

$$\Phi_X(\upsilon) = \int_{-\infty}^{+\infty} f_X(x)\exp(-j\upsilon x)\,dx \tag{4.38}$$

$$f_X(x) = \frac{1}{2\pi}\int_{-\infty}^{+\infty} \Phi_X(\upsilon)\exp(j\upsilon x)\,d\upsilon \tag{4.39}$$

Characteristic functions are useful for studying the addition of independent random variables. If random variables $A$, $B$, and $C$ satisfy the relationship $C = A + B$ and $A$ and $B$ are independent, then their characteristic functions satisfy the relationship $\Phi_C(\upsilon) = \Phi_A(\upsilon)\Phi_B(\upsilon)$ [38].

Characteristic functions are also useful for studying the superposition of two independent random voltages. Since voltage, $\tilde{V}$, is complex-valued, its characteristic function must be a *double* Fourier transform over the joint PDF of the random in-phase, $X$, and quadrature, $Y$, voltage components ($\tilde{V} = X + jY$). This transformation is demonstrated below:

$$\Phi_{XY}(\upsilon_x, \upsilon_y) = \int_{-\infty}^{+\infty}\int_{-\infty}^{+\infty} f_{XY}(x, y)\exp(-j\upsilon_x x)\exp(-j\upsilon_y y)\,dx\,dy \tag{4.40}$$

$$f_{XY}(x, y) = \frac{1}{4\pi^2}\int_{-\infty}^{+\infty}\int_{-\infty}^{+\infty} \Phi_{XY}(\upsilon_x, \upsilon_y)\exp(j\upsilon_x x)\exp(j\upsilon_y y)\,d\upsilon_x\,d\upsilon_y \tag{4.41}$$

Starting with the basic envelope PDF, $f_R(\rho)$, as a function of only envelope, $\rho$, it ispossible to extend this PDF into a joint PDF using the relationship

$$f_{R\Phi}(\rho, \phi) = \frac{1}{2\pi\rho} f_R(\rho) \tag{4.42}$$

Eqn (4.42) is a joint PDF, albeit in terms of envelope, $\rho$, and phase, $\phi$, variables instead of in-phase, $x$, and quadrature, $y$, variables. Eqn (4.42) assumes that the net phase, $\phi$, is uniformly-distributed, independent of $\rho$ – entirely consistent with the small-scale local area propagation model.

Rather than convert Eqn (4.42) into an $XY$ joint PDF, it is more convenient to make a change of variables in the transform definition of Eqn (4.40). With the polar-coordinate substitutions $x = -\rho\cos\phi$, $y = -\rho\sin\phi$, and $dx\,dy = \rho\,d\rho\,d\phi$, Eqn (4.40) becomes

$$\Phi_{XY}(\upsilon_x, \upsilon_y) = \frac{1}{2\pi}\int_{0}^{\infty}\int_{0}^{2\pi} f_R(\rho)\exp(j\upsilon_x\rho\cos\phi)\exp(j\upsilon_y\rho\sin\phi)\,d\phi\,d\rho \tag{4.43}$$

Eqn (4.43) may be regrouped:

$$\Phi_{XY}(\upsilon) = \int_0^\infty f_R(\rho) \left[ \frac{1}{2\pi} \int_0^{2\pi} \exp\left[-j\upsilon\rho\cos(\phi + \phi_0)\right] \, d\phi \right] d\rho \tag{4.44}$$

where $\upsilon = \sqrt{\upsilon_x^2 + \upsilon_y^2}$ and $\tan(\phi_0) = \upsilon_y/\upsilon_x$. The angle $\phi_0$ is unimportant since the integration of $\phi_0$ is over the entire period of the cosine function in Eqn (4.44). Thus, the characteristic function is solely dependent on the variable $\upsilon$.

The bracketed term in Eqn (4.44) is a standard definite integral that evaluates to a 0-order Bessel function of the first kind [28]. The final expression for the transformation from envelope PDF to characteristic function is Eqn (4.14). Using a similar set of reductions, the reverse transformation from characteristic function to envelope PDF becomes Eqn (4.15). The only assumption made in these transformations is the statistical independence and uniform distribution of the complex voltage phase.

## 4.B Derivation for TIP Fading PDF's

Following from Eqn (4.23), the TIP PDF results from the integration of

$$f_R(\rho) = \rho \int_0^\infty \exp\left(\frac{-\upsilon^2 P_{\text{dif}}}{4}\right) J_0(\upsilon\rho) J_0(V_1\upsilon) J_0(V_2\upsilon) \upsilon d\upsilon \tag{4.45}$$

The following relationship is used to transform the integration [28, p. 758]:

$$J_0(V_1\upsilon) J_0(V_2\upsilon) = \frac{1}{\pi} \int_0^\pi J_0\left(\upsilon\sqrt{V_1^2 + V_2^2 - 2V_1V_2\cos\theta}\right) d\theta \tag{4.46}$$

This result is substituted into Eqn (4.45) to produce

$$f_R(\rho) = \frac{r}{\pi} \int_0^\pi \left\{ \int_0^\infty \exp\left(\frac{-\upsilon^2 P_{\text{dif}}}{4}\right) J_0(\upsilon\rho) J_0\left(\upsilon\sqrt{V_1^2 + V_2^2 - 2V_1V_2\cos\theta}\right) \upsilon d\upsilon \right\} d\theta \tag{4.47}$$

Integration with respect to $\upsilon$ produces the following equation, in terms of the $K$ and $\Delta$ parameters of Eqn (4.31) and Eqn (4.26) [28, p. 739]:

$$f_R(\rho) = \frac{2r}{P_{\text{dif}}} \exp\left(\frac{-r^2}{P_{\text{dif}}} - K\right) \frac{1}{\pi} \int_0^\pi \exp(\Delta K \cos\theta)\, I_0\left[\frac{r}{\sqrt{P_{\text{dif}}/2}}\sqrt{2K(1 - \Delta\cos\theta)}\right] d\theta \tag{4.48}$$

Although still not in closed form, Eqn (4.48) is more intuitive and insightful than Eqn (4.45), somewhat resembling the Rician PDF. This form is useful for generating alternate or approximate representations for the TIP PDF.

### 4.B.1 Approximate Representation

The left side of Eqn (4.48) looks remarkably similar to the Rician PDF. The difficulty in evaluating this PDF lies in the integral term on the right side:

$$\boldsymbol{\mathcal{I}}(x; K, \Delta) = \frac{1}{\pi} \int_0^\pi \exp(\Delta K \cos\theta)\, I_0\left[x\sqrt{2K(1 - \Delta\cos\theta)}\right] d\theta \tag{4.49}$$

To generate the $M$th-order approximation to the TIP PDF, the integration of Eqn (4.49) is performed by representing the integrand as a Legendre polynomial with $2M$ terms. The Legendre polynomial representation for this integrand, assuming that the function is sampled at uniform $\theta$ increments, is

$$\begin{array}{c}\text{Integrand}\\ \text{of Eqn (4.49)}\end{array} \approx \sum_{i=1}^{2M} I_0\left(x\sqrt{2K(1 - \cos\theta_i)}\right) \exp(\Delta K \cos\theta_i) \prod_{\substack{k=1 \\ k \neq i}}^{2M} \left(\frac{\theta - \theta_k}{\theta_i - \theta_k}\right) \tag{4.50}$$

where

$$\theta_{i,k} = \frac{\pi(i, k-1)}{2M-1}$$

The integration of this result, $\boldsymbol{\mathcal{I}}_M$, may be written as

$$\boldsymbol{\mathcal{I}}_M(x; K, \Delta) = \sum_{i=1}^{2M} \frac{a_i}{2} I_0\left(x\sqrt{2K(1-\cos\theta_i)}\right)\exp(\Delta K\cos\theta_i) \tag{4.51}$$

$$\text{where } a_i = \frac{2(-1)^i}{(2M-1)(2M-i)!(i-1)!}\int_0^{2M-1}\prod_{\substack{k=1\\k\neq i}}^{2M}(u-k+1)du$$

The approximation turns the complicated integration of Eqn (4.49) into simple polynomial integrations of $a_i$.

To simplify the representation of this approximate PDF, it is useful to define the following helping function, $D(x; K, \alpha)$, which is defined in Eqn (4.33). Equipped with this relationship and the symmetrical property of $a_i$ ($a_i = a_{2M-i+1}$) it is now possible to write the approximated integration as

$$\boldsymbol{\mathcal{I}}_M(x; K, \Delta) = \sum_{i=1}^{M} a_i D\left(x; K, \Delta\cos\left[\frac{\pi(i-1)}{2M-1}\right]\right) \tag{4.52}$$

This leads to Eqn (4.33) and provides a simple method for approximating this complicated PDF to an arbitrary level of precision.

### 4.B.2 Property as a PDF

By making an approximation when constructing a PDF, it is often possible to destroy the mathematical properties of a PDF. Of principle concern, the PDF may no longer integrate to unity. It can be shown that

$$\int_0^{\infty} \frac{2\rho}{P_{\text{dif}}}\exp\left(\frac{-\rho^2}{P_{\text{dif}}} - K\right) D\left(\frac{\rho}{\sqrt{P_{\text{dif}}/2}}; K, \alpha\right) d\rho = 1 \tag{4.53}$$

which is valid for any combination of $K$ and $\alpha$. Mathematically, the integrand in Eqn (4.53) appears as two "half"-Rician distributions, which explains their integration to 1. The integration of the total approximated PDF is then given by

$$\int_0^{\infty} \frac{2r}{P_{\text{dif}}}\exp\left(\frac{-\rho^2}{P_{\text{dif}}} - K\right)\sum_{i=1}^{M} a_i D\left(\frac{\rho}{\sigma}; K, \Delta\cos\left[\frac{\pi(i-1)}{2M-1}\right]\right) d\rho = \sum_{i=1}^{M} a_i \tag{4.54}$$

Furthermore, the coefficients $a_i$ have the following property:

$$\sum_{i=1}^{M} a_i = 1 \tag{4.55}$$

*Regardless of order, each approximated PDF integrates exactly to 1 over the interval* $[0, \infty)$.

### 4.B.3 Proper Limiting Behavior

The exact distribution for TIP fading collapses to a Rician function as $\Delta$ approaches 0. Now notice how the *approximated* PDF behaves as $\Delta$ approaches 0. The function $D\left(x; K, \alpha\right)$ collapses to a 0-order modified Bessel function:

$$\boldsymbol{\mathcal{I}}_M(x; K, \Delta = 0) = \sum_{i=1}^{M} a_i D\left(x; K, 0\right) = \sum_{i=1}^{M} a_i I_0(x\sqrt{2K}) = I_0(x\sqrt{2K}) \tag{4.56}$$

When this result is substituted into Eqn (4.33), once again the Rician distribution results. *Regardless of order, each approximated PDF contains the exact Rician PDF as a special case.*

### 4.B.4 Preservation of the Second Moment

The second moment, $\mathrm{E}\{R^2\}$, of a fading envelope is essential to the calculation of mean power. It can be shown that

$$\int_0^\infty \frac{2\rho^3}{P_{\text{dif}}} \exp\left(\frac{-\rho^2}{P_{\text{dif}}} - K\right) D\left(\frac{\rho}{\sqrt{P_{\text{dif}}/2}}; K, \alpha\right) d\rho = P_{\text{dif}}(K+1) \tag{4.57}$$

which is valid for any combination of $K$ and $\Delta$. The integration of $\rho^2$ over the total approximated PDF is then given by

$$\begin{aligned}
\mathrm{E}\{R^2\} &= \int_0^\infty \frac{r^3}{P_{\text{dif}}} \exp\left(\frac{-\rho^2}{P_{\text{dif}}} - K\right) \sum_{i=1}^{M} a_i D\left(\frac{\rho}{\sqrt{P_{\text{dif}}/2}}; K, \Delta\cos\left[\frac{\pi(i-1)}{2M-1}\right]\right) d\rho \\
&= \sum_{i=1}^{M} 2a_i P_{\text{dif}}(K+1) = P_{\text{dif}}(K+1)
\end{aligned} \tag{4.58}$$

In terms of voltages, the value $P_{\text{dif}}(K+1)$ becomes $P_{\text{dif}} + V_1^2 + V_2^2$, which is the second moment of the true TIP PDF. *Regardless of order, each approximated PDF preserves the true second moment of the exact TIP PDF.*

# Chapter 5

# The Angle Spectrum

The concept of a delay spectrum is intuitive: multipath power arrives with different propagation delays, causing a smear of received power as a function of time delay. A Doppler spectrum is equally intuitive: moving objects in the channel introduce non-zero Doppler frequencies to selected multipath components.

The concept of a wavenumber spectrum is not as intuitive. Rather, most engineers characterize multipath in space using an *angle* spectrum rather than a wavenumber spectrum. The angle spectrum describes the angle-of-arrival of multipath power. The bulk of this chapter is dedicated to stochastic local area channel modeling using an angle spectrum. An outline of the contents appears below:

- Section 5.1 : presents definitions for angle spectrum
- Section 5.2 : defines fading rate variances
- Section 5.3 : introduces the concept of *shape factors*
- Section 5.4 : calculates shape factors for example channel models
- Section 5.5 : summarizes key concepts

This chapter emphasizes the use of an azimuthal angle spectrum and multipath *shape factors*. The use of shape factors is an original approach for characterizing spatial selectivity in a local area. This concept is useful for measurements and applications, as will be shown in future work.

## 5.1 Angle Spectrum Concepts

The *angle spectrum* is one of the most important concepts in spatial channel modeling since it provides a simpler, more intuitive way to characterize a wavevector spectrum. This section rigorously defines the angle spectrum and discusses its relationship to other spectra used in channel modeling.

### 5.1.1 Definition of the Angle Spectrum

Recall from Eqn (3.41) in Section 3.4.6 that, for the U-SLAC model, the wavevector spectrum for a static, narrowband channel may be written as

$$S_{\tilde{h}}(\vec{k}) = (2\pi)^3 \sum_{i=1}^{N} P_i \delta(\vec{k} - \vec{k}_i) \tag{5.1}$$

where $P_i$ is the power of the $i$th multipath component (units of $volts^2$). In fact, Eqn (5.1) *can only* represent the power spectrum of a U-SLAC model – power spectra are only defined for WSS processes and a SLAC model is WSS if and only if it is a U-SLAC model (Theorem 3.1).

By definition, if Eqn (5.1) represents a stochastic local area channel model, then all values of $\vec{k}_i$ must have a magnitude equal to the free-space wavenumber. For power spectrum analysis, we will denote the free-space wavenumber as $k_{\max}$, since this represents the magnitude of the maximum possible wavenumber for which a wavenumber spectrum has non-zero components. The reason for this will become apparent in the next section.

Now the vectors $\vec{k}_i$ and $\vec{k}$ in Eqn (5.1) may be expressed in terms of radial coordinates involving azimuth and elevation angles. The relationships between the radial coordinates and the vectors are given below:

$$\begin{aligned} \vec{k}_i &= k_{\max} \left(\cos\varphi_i \cos\theta_i \, \hat{x} + \cos\varphi_i \sin\theta_i \, \hat{y} + \sin\varphi_i \, \hat{z}\right) \\ \vec{k} &= |\vec{k}| \left(\cos\varphi \cos\theta \, \hat{x} + \cos\varphi \sin\theta \, \hat{y} + \sin\varphi \, \hat{z}\right) \end{aligned}$$

The azimuth angle, $\theta_i$, and the elevation angle, $\varphi_i$, may be thought of as the *angle-of-arrival* coordinates of the $i$th multipath. With these two expressions for $\vec{k}_i$ and $\vec{k}$, it is possible to rewrite the delta function term in Eqn (5.1) using the following identity:

$$\delta(\vec{k} - \vec{k}_i) = \frac{\delta(|\vec{k}| - k_{\max})\delta(\varphi - \varphi_i)\delta(\theta - \theta_i)}{k_{\max}^2 \cos\varphi_i} \tag{5.2}$$

Thus, the original wavevector spectrum may now be written as

$$S_{\tilde{h}}(\vec{k}) = \frac{(2\pi)^3 \delta(|\vec{k}| - k_{\max})}{k_{\max}^2} \underbrace{\sum_{i=1}^{N} \frac{P_i \delta(\varphi - \varphi_i)\delta(\theta - \theta_i)}{\cos\varphi_i}}_{p(\theta,\varphi)} \tag{5.3}$$

The underbraced term on the right-hand side of Eqn (5.3) is the *angle spectrum* of the multipath power.

There is a key principle in channel modeling that results from Eqn (5.3): *any U-SLAC wavevector spectrum may be completely described in terms of an angle spectrum,* $p(\theta, \varphi)$. To understand the advantages of an angle spectrum representation, consider the simplified form of Eqn (5.3):

$$S_{\tilde{h}}(\vec{k}) = \frac{(2\pi)^3 \delta(|\vec{k}| - k_{\max})}{k_{\max}^2} p(\theta, \varphi) \tag{5.4}$$

There are several key advantages to using an angle spectrum to represent spatial propagation:

- *The angle spectrum is physically intuitive.* The units of $p(\theta, \varphi)$ are *power per steradian.* The angles $\theta$ and $\varphi$ represent the respective azimuth and elevation angles-of-arrivals of radio waves that impinge upon the receiver antenna. Compared to a wavevector spectrum, the angle spectrum provides a closer physical representation to how engineers visualize radio wave propagation.

- *The full angle spectrum has only two dependencies.* The wavevector spectrum depends on a three-dimensional wavevector, $\vec{k}$. However, a U-SLAC model will only have spectral components for $|\vec{k}| = k_{\max}$, representing a sphere in $\vec{k}$-space. By casting the dependencies in terms of azimuth and elevation angles-of-arrival, the spatial propagation may be completely described with one fewer dependency – a convenient simplification.

- *Diffuse propagation is best represented with an angle spectrum.* Recall that, whenever a discrete sum of impulse functions were used to represent a spectrum in Chapter 3, we had to mention that a diffuse continuum of waves was possible if the summation contained an infinite number of terms and the amplitudes of each wave became infinitesimally small. We no longer require such a disclaimer. The angle spectrum representation, $p(\theta, \varphi)$, may contain impulses (specular components) and intervals of finite or continuous power (diffuse, non-specular components).

### 5.1.2 Mapping Angles to Wavenumbers

Recall from Appendix 2.A.3 that characterization of small-scale fading along a particular direction in space required a one-dimensional *wavenumber spectrum*, $S_{\tilde{h}}(k)$. Given a direction of characterization in space, $\hat{r}$, the wavenumber spectrum may be calculated from the wavevector spectrum using Eqn (2.53), which is repeated below for convenience:

$$S_{\tilde{h}}(k) = \frac{1}{(2\pi)^2} \int_{-\infty}^{+\infty} S_{\tilde{h}}(\vec{k})\delta(k - \vec{k}\cdot\hat{r})\, d\vec{k} \tag{5.5}$$

By substituting Eqn (5.4) and simplifying, the wavenumber spectrum may be calculated directly from the angle spectrum:

$$S_{\tilde{h}}(k) = 2\pi \int_{0}^{2\pi} \int_{-\frac{\pi}{2}}^{+\frac{\pi}{2}} p(\theta,\varphi)\, \delta(k - k_{\max}\hat{k}\cdot\hat{r}) \cos\varphi \, d\varphi \, d\theta \tag{5.6}$$

where

$$\hat{k} = \cos\varphi\cos\theta\,\hat{x} + \cos\varphi\sin\theta\,\hat{y} + \sin\varphi\,\hat{z}$$

Thus, Eqn (5.6) is a useful relationship for calculating a wavenumber spectrum from an angle spectrum. As Figure 5.1 illustrates, the mapping depends on the orientation, $\hat{r}$, in Eqn (5.6).

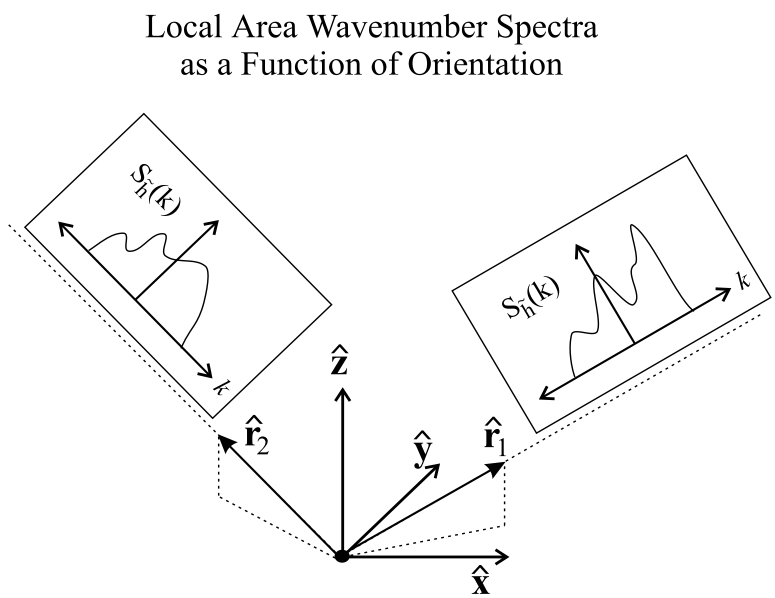


Figure 5.1: A local area characterized by an angle spectrum, $p(\theta, \varphi)$, will produce different wavenumber spectra, $S_{\tilde{h}}(k)$, depending on the orientation in space.

### 5.1.3 From-the-Horizon Propagation

An *azimuthal* channel model is of particular interest in wireless communications. Such a channel model consists of multipath that propagates from the horizon with zero elevation angle. The angle spectrum for this type of channel may be written as

$$p(\theta, \varphi) = p(\theta)\, \delta(\varphi) \tag{5.7}$$

where $p(\theta)$ is the azimuthal angle spectrum, with units of *power per radian*. Besides being a useful simplification, the azimuthal channel model of Eqn (5.7) is an excellent approximation to most terrestrial propagation scenarios [13].

Given an azimuthal angle spectrum, $p(\theta)$, it is possible to calculate a wavenumber spectrum by substituting Eqn (5.7) into Eqn (5.6) and integrating out the $\varphi$ variable:

$$S_{\tilde{h}} = 2\pi \int_{0}^{2\pi} p(\theta)\, \delta(k - k_{\max} \cos[\theta - \theta_R])\, d\theta \tag{5.8}$$

The resulting integration produces one of the most famous formulas in wireless communications, the Gans mapping for angle spectra [39]:

$$S_{\tilde{h}}(k) = \frac{2\pi}{\sqrt{k_{\max}^2 - k^2}} \left[ p\left(\theta_R + \cos^{-1}\frac{k}{k_{\max}}\right) + p\left(\theta_R - \cos^{-1}\frac{k}{k_{\max}}\right)\right], \quad |k| \le k_{\max} \tag{5.9}$$

where $\theta_R$ is the azimuthal direction of movement. The Gans mapping assumes that the orientation vector, $\hat{r}$, of Eqn (5.6) also points towards the horizon and may be written in the form

$$\hat{r} = \cos\theta_R\, \hat{x} + \sin\theta_R\, \hat{y} + 0\, \hat{z}$$

This assumption is not very restrictive. Most motion by a mobile receiver, for example, is going to be towards the horizon with virtually no vertical $\hat{z}$-component. In terrestrial systems, receivers with multiple antennas also tend to distribute their array or diversity antennas in the same azimuthal plane, eliminating the need to model the $\hat{z}$ dimension.

The mapping of Eqn (5.9) has a straight-forward physical interpretation from the geometry of propagation shown in Figure 5.2. A multipath wave arrives from the horizon at angle $\theta$ and the direction of azimuthal motion that we wish to map is $\theta_R$. The phase progression of this multipath wave is the free space wavenumber, $k_{\max}$. However, to a receiver moving along the $\theta_R$ direction, the actual wavenumber, $k$, appears to be foreshortened by a factor $\cos(\theta - \theta_R)$. Thus,

$$k = k_{\max}\cos(\theta - \theta_R) \quad \text{and} \quad \frac{dk}{d\theta} = -k_{\max}\sin(\theta - \theta_R) \tag{5.10}$$

We can arrive at Eqn (5.9), equivalently by, equating the wavevector spectrum power to the angle spectrum power: $S(k)|dk| = 2\pi p(\theta)|d\theta|$. The mapping of Eqn (5.9) provides a useful bridge between spatial selectivity and multipath angle-of-arrival characteristics.

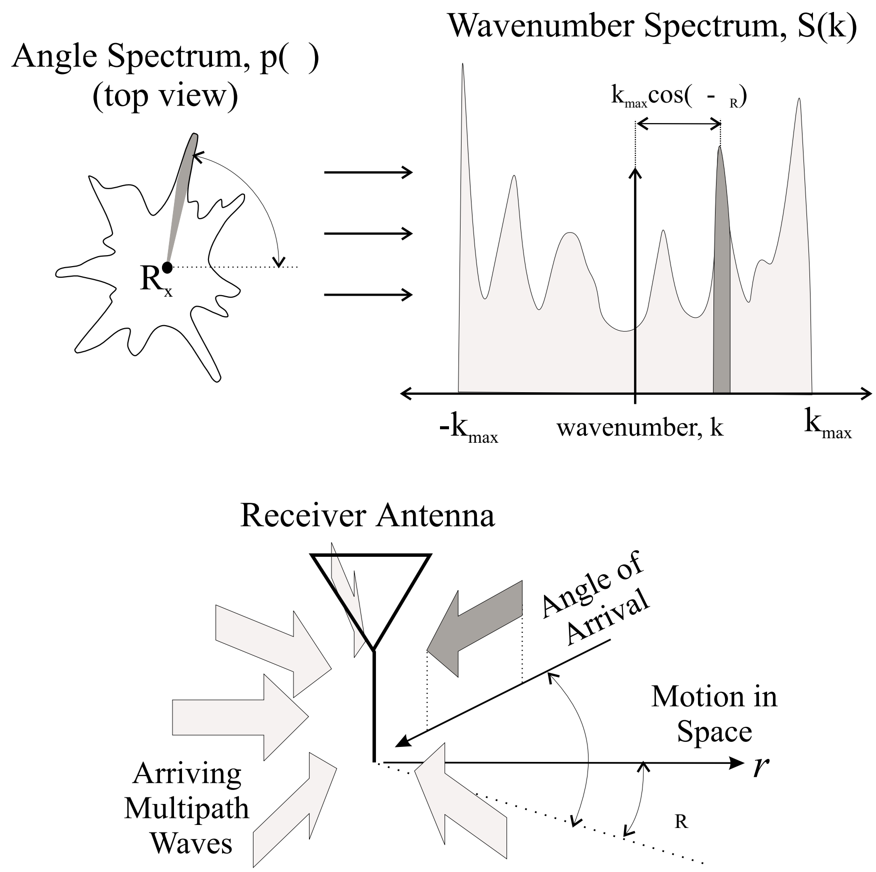


Figure 5.2: Multipath power is mapped from the angle spectrum, $p(\theta)$, to the wavenumber spectrum, $S_{\tilde{h}}(k)$, as a function of its angle-of-arrival.

**Example 5.1: Omnidirectional Mapping**

**Problem:** In a cluttered multipath environment it is common to approximate the angle spectrum of incoming multipath power as a uniform distribution:

$$p(\theta) = \frac{P_T}{2\pi} \tag{5.11}$$

where $P_T$ – the total average power – is a constant. Calculate the wavenumber spread for this angle spectrum.

**Solution:** Using Eqn (5.9), the wavenumber spectrum for this propagation scenario is

$$S(k) = \frac{2P_T}{\sqrt{k_{\max}^2 - k^2}}, \quad |k| \le k_{\max} \tag{5.12}$$

which is independent of orientation, $\theta_R$. The wavenumber spread is

$$\sigma_k^2 = \frac{k_{\max}^2 P_T}{2} \tag{5.13}$$

### 5.1.4 Summary of Angle Spectrum Concepts

To summarize the concepts of this section, Figure 5.3 shows a section of the space-frequency transform map of Figure 2.10 in Section 2.4.2. This mapping diagram has been modified to include angle spectra and wavenumber spectra, emphasizing how each relates to one another. An angle spectrum is simply an alternate way to represent a wavevector spectrum. Any local area channel model that has a wavevector spectrum can, by definition, be characterized by an angle spectrum. An angle spectrum is a simpler and more intuitive way to characterize spatial selectivity.

*Wavenumber* spectra may be calculated from the angle spectrum just as they are calculated from the wavevector spectrum. A direction in space, $\hat{r}$, must be assumed before a wavenumber spectrum can be calculated. The wavenumber spectrum is the Fourier transform of a one-dimensional spatial autocorrelation. This one-dimensional spatial autocorrelation may be calculated by fixing the orientation of the full spatial autocorrelation, $C_{\tilde{h}}(\Delta\vec{r}) \mid_{\Delta\vec{r}=\Delta r\hat{r}}$.

The only drawback in using an angle spectrum is that angle-of-arrival is not the natural domain for relating spectral properties to spatial selectivity in a channel. Therefore, the angle spectrum must be converted to a wavevector spectrum or wavenumber spectrum

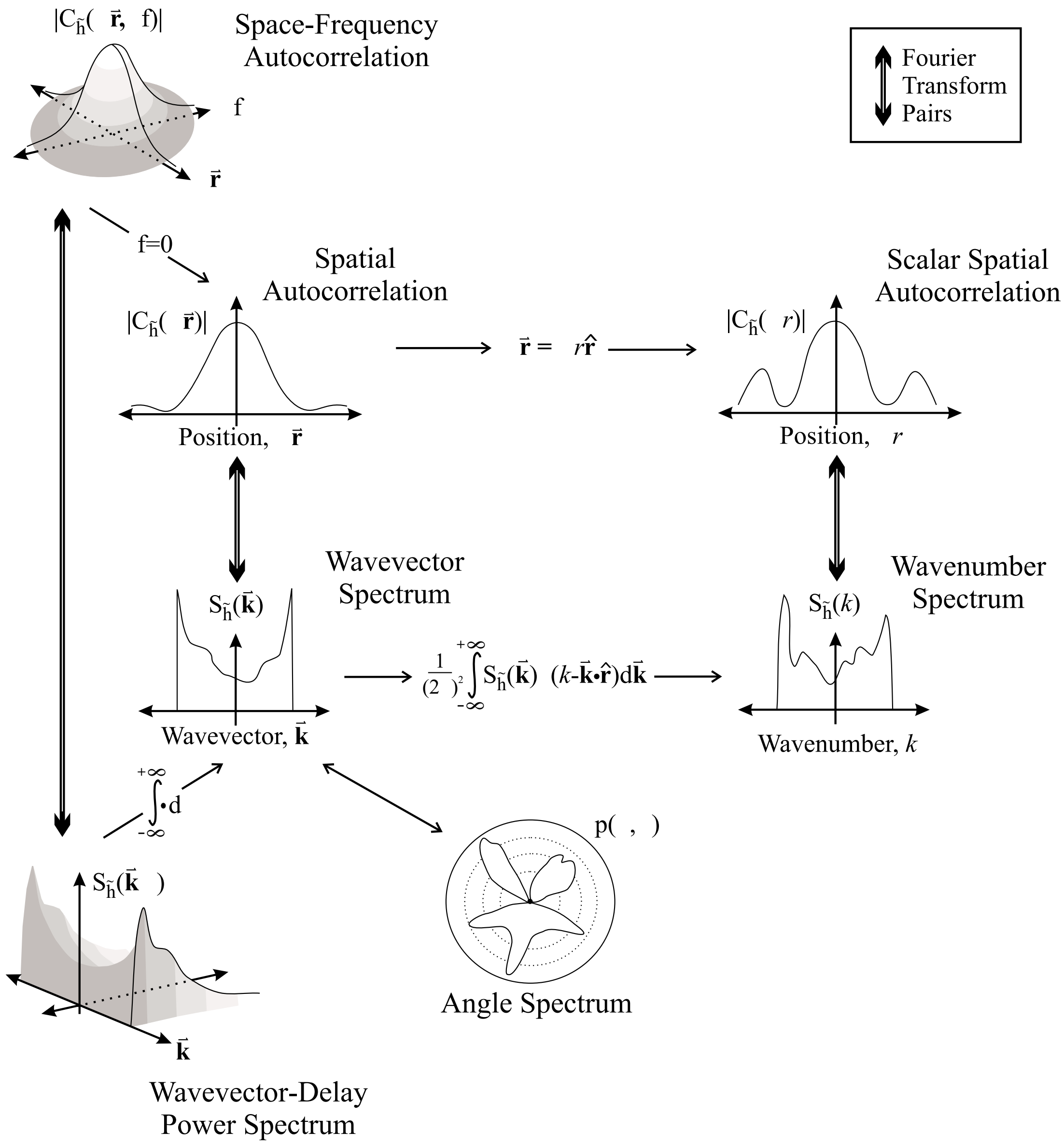


Figure 5.3: Autocorrelation and spectrum relationships for the space-varying channel.

whenever spatial autocorrelations, spectral spreads, or duality results are calculated. Remaining analysis in this work will mostly discuss the popular azimuthal channel model in detail. Indeed, for this channel model, it is possible to overcome the key drawback of an angle spectrum by using *shape factors* to relate the geometry of propagation to the properties of spatial selectivity.

## 5.2 Fading Rate Variance

Before continuing the discussion on angle spectra, it is important to introduce the concept of a *fading rate variance*. The fading rate variance is a key *second-order* statistic which determines how quickly a channel fluctuates as a function of time, space, or frequency.

### 5.2.1 Definition of a Rate Variance

Consider the snapshots of two stochastic processes in Figure 5.4. Both processes represent time-varying voltages and both follow a Rayleigh PDF. Clearly they are not the same process, as the process on the left fluctuates much faster than the process on the right. Their *second-order statistics*, which relate to evolution over time, are quite different.

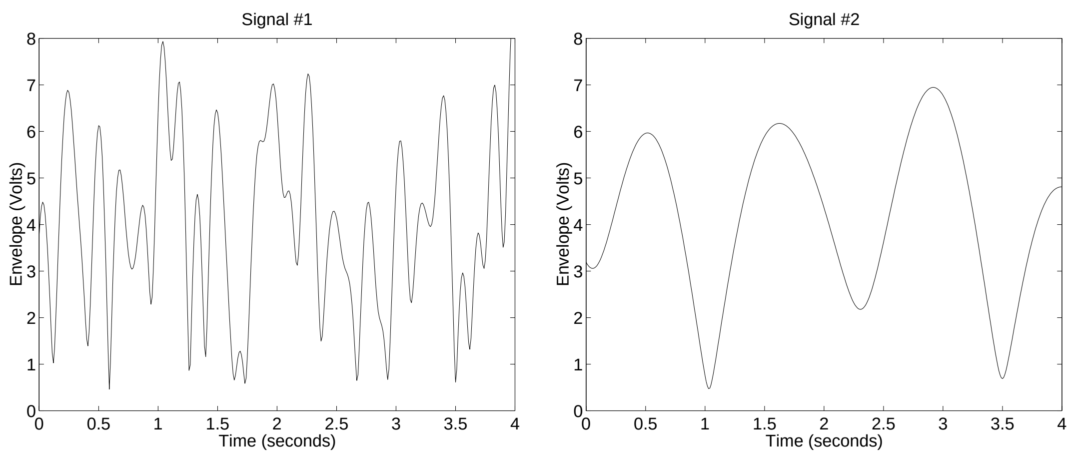


Figure 5.4: Two examples of time-varying, Rayleigh-distributed stochastic processes.

WSS second-order statistics are best characterized with either an autocorrelation or a power spectrum, one being the Fourier pair of the other. There exists simpler measures of how rapidly a process evolves over time, space, or frequency. One such measure may be based on the *derivative* of the channel. Consider the narrowband, fixed, time-varying channel, $\tilde{h}(t)$. A useful measure of fluctuations could be based on $\frac{d\tilde{h}(t)}{dt}$. Simply taking the ensemble average of this quantity is not useful, since the mean derivative of all WSS processes is 0. Rather, taking the ensemble average of $\left|\frac{d\tilde{h}(t)}{dt}\right|^2$ produces a result which, true to our intentions, measures the amount of fluctuation of the stochastic time-varying process, $\tilde{h}(t)$.

There is one final and subtle adjustment that must be made to our fluctuation measure. For a complex-valued process such as a baseband channel, we would like to measure the fluctuations of a process that has *stationary phase*. For example, a WSS stochastic channel has a phase that is, itself, a stochastic process. This process may be written as

$$\Phi(t) = \arg\{\tilde{h}(t)\}$$

If the centroid of the Doppler spectrum, $S_{\tilde{h}}(\omega)$, is not zero, then the stochastic phase process will not be mean-stationary. Instead, the mean phase will be a function of time:

$$\mathrm{E}\left\{\Phi(t)\right\} = \phi_0 + \bar{\omega}t$$

where $\bar{\omega}$ is the centroid of the Doppler spectrum. The solution to removing this non-stationary phase is to multiply the channel, $\tilde{h}(t)$, by a complex exponential of the form, $\exp(-j\bar{\omega}t)$.

After making the final adjustment for non-stationary phase, the final measure of temporal channel fluctuation becomes

$$\sigma_t^2 = \mathrm{E}\left\{\left|\frac{d\left[\tilde{h}(t)\exp(-j\bar{\omega}t)\right]}{dt}\right|^2\right\} \tag{5.14}$$

The measure, $\sigma_t^2$, is called a *fading rate variance* because the time-derivative of the channel represents the rate of fading and the mean-squared value represents the variance of that process [40]. Since the complex exponential term in Eqn (5.14) corrects the non-stationary phase, the fluctuations measured by the temporal fading rate variance are strictly related to the envelope fluctuations of $\tilde{h}(t)$, and not just the steady-state progression of phase.

Of course fading rate variances exist for other dependencies as well. For a measure of fluctuations as a function of frequency, it is possible to define a *frequency fading rate variance*, $\sigma_f^2$, for a static, fixed channel $\tilde{h}(f)$:

$$\sigma_f^2 = \mathrm{E}\left\{\left|\frac{d\left[\tilde{h}(f)\exp(-j2\pi\bar{\tau}f)\right]}{df}\right|^2\right\} \tag{5.15}$$

where $\bar{\tau}$ is the centroid of the delay spectrum. By duality, a *spatial fading rate variance*, $\sigma_r^2$, can be defined for a static, narrowband channel $\tilde{h}(r)$, where $r$ represents displacement in a fixed direction in space:

$$\sigma_r^2 = \mathrm{E}\left\{\left|\frac{d\left[\tilde{h}(r)\exp(-j\bar{k}r)\right]}{dr}\right|^2\right\} \tag{5.16}$$

The value of $\bar{k}$ is the centroid of the wavenumber spectrum, calculated for the direction of displacement in space. These fading rate variances are more than just an intuitive academic measure of fading fluctuations – there is a powerful relationship between fading rate variance and the RMS spread of a power spectrum.

### 5.2.2 Fundamental Spectral Spread Theorem

It is also possible to calculate the mean-squared derivative of a time-varying channel given its Doppler spectrum, $S_{\tilde{h}}(\omega)$. There is a basic theorem in stochastic process theory which relates the mean-squared derivatives of complex processes to power spectra [21]:

$$\mathrm{E}\left\{\left|\frac{d^n\tilde{h}(t)}{dt^n}\right|^2\right\} = \frac{1}{2\pi}\int_{-\infty}^{+\infty} \omega^{2n}\, S_{\tilde{h}}(\omega)\, d\omega \tag{5.17}$$

For the case of fading rate variance, we are interested in the case of $n = 1$:

$$\mathrm{E}\left\{\left|\frac{d\tilde{h}(t)}{dt}\right|^2\right\} = \frac{1}{2\pi}\int_{-\infty}^{+\infty} \omega^{2}\, S_{\tilde{h}}(\omega)\, d\omega \tag{5.18}$$

To account for the modulation of the process by the factor $\exp(-j\bar{\omega}t)$, it is possible to shift the spectrum in Doppler frequency by an amount $-\bar{\omega}$ and adjust the limits of integration:

$$\sigma_t^2 = \frac{1}{2\pi}\int_{-\infty}^{+\infty} (\omega-\bar{\omega})^2\, S_{\tilde{h}}(\omega)\, d\omega \tag{5.19}$$

This equation may be rearranged into the following form:

$$\sigma_t^2 = \underbrace{\frac{1}{2\pi}\int_{-\infty}^{+\infty} S_{\tilde{h}}(\omega)\, d\omega}_{\mathrm{E}\{P(t)\}}\ \underbrace{\frac{\int_{-\infty}^{+\infty} (\omega-\bar{\omega})^2\, S_{\tilde{h}}(\omega)\, d\omega}{\int_{-\infty}^{+\infty} S_{\tilde{h}}(\omega)\, d\omega}}_{\sigma_\omega^2} \tag{5.20}$$

Suddenly, the fading rate variance has become a simple function of two familiar measures: average power, $\mathrm{E}\{P(t)\}$, and RMS Doppler spread, $\sigma_\omega$.

The relationship in Eqn (5.20) is a very fundamental result and holds for any fading rate variance and spectral spread. Thus, for stochastic wireless channels, the following results hold:

$$\sigma_t^2 = \mathrm{E}\{P(t)\}\,\sigma_\omega^2 \tag{5.21}$$

$$\sigma_f^2 = (2\pi)^2\,\mathrm{E}\{P(f)\}\,\sigma_\tau^2 \tag{5.22}$$

$$\sigma_r^2 = \mathrm{E}\{P(r)\}\,\sigma_k^2 \tag{5.23}$$

It becomes clear from Eqn (5.21)-Eqn (5.23) why RMS spectral spreads provide such accurate measures of channel coherence. The RMS spectral spread, due to its direct relationship to fading rate variance, is an *excellent* measure of channel fluctuation. Eqn (5.21)-Eqn (5.23) are valuable starting points when applying stochastic channel theory to real-world problems.

## 5.3 Multipath Shape Factors

This section defines and describes multipath *shape factors* – geometrical characteristics of an azimuth angle spectrum that also describe small-scale spatial selectivity in a channel.

### 5.3.1 Definition of Shape Factors

This section presents the three multipath shape factors that characterize small-scale fading statistics in space. The shape factors are derived from the angular distribution of multipath power, $p(\theta)$, which is a general representation of from-the-horizon propagation in a local area. This representation of $p(\theta)$ includes antenna gains and polarization mismatch effects [40]. Shape factors are based on the complex Fourier coefficients of $p(\theta)$:

$$F_n = \int_0^{2\pi} p(\theta) \exp(jn\theta) d\theta \tag{5.24}$$

where $F_n$ is the $n$th complex Fourier coefficient.

#### Angular Spread

The shape factor *angular spread*, $\Lambda$, is a measure of how multipath concentrates about a single azimuthal direction. We define angular spread to be

$$\Lambda = \sqrt{1 - \frac{|F_1|^2}{F_0^2}} \tag{5.25}$$

where $F_0$ and $F_1$ are defined by Eqn (5.24). There are several advantages to defining angular spread in this manner. First, since angular spread is normalized by $F_0$ (the total amount of local average received power), it is invariant under changes in transmitted power. Second, $\Lambda$ is invariant under any series of rotational or reflective transformations of $p(\theta)$. Finally, this definition is intuitive; angular spread ranges from 0 to 1, with 0 denoting the extreme case of a single multipath component from a single direction and 1 denoting no clear bias in the angular distribution of received power.

It should be noted that other definitions exist in the literature for angular spread. These definitions involve either beamwidth or the second centered moment of $\theta$ and are often ill-suited for general application to periodic functions such as $p(\theta)$.

### Angular Constriction

The shape factor *angular constriction*, $\gamma$, is a measure of how multipath concentrates about *two* azimuthal directions. We define angular constriction to be

$$\gamma = \frac{|F_0 F_2 - F_1^2|}{F_0^2 - |F_1|^2} \tag{5.26}$$

where $F_0$, $F_1$, and $F_2$ are defined by Eqn (5.24). Much like the definition of angular spread, the measure for angular constriction is invariant under changes in transmitted power or any series of rotational or reflective transformations of $p(\theta)$. The possible values of angular constriction, $\gamma$, range from 0 to 1, with 0 denoting no clear bias in two arrival directions and 1 denoting the extreme case of exactly two multipath components arriving from different directions.

### Azimuthal Direction of Maximum Fading

A third shape factor, which may be thought of as an orientation parameter, is the *azimuthal direction of maximum fading*, $\theta_{\max}$. We define this parameter to be

$$\theta_{\max} = \frac{1}{2}\arg\left\{F_0 F_2 - F_1^2\right\} \tag{5.27}$$

The physical meaning of the parameter is presented in the next section.

## 5.3.2 Basic Wavenumber Spread Relationship

Shape factors have a particularly useful application when describing small-scale fading: the multipath angle-of-arrival dependence of wavenumber spread may be cast exclusively in terms of the three shape factors angular spread, angular constriction, and direction of maximum fading. It has been shown that the wavenumber spread for the complex voltage of a receiver traveling along the azimuthal direction $\theta_R$ is

$$\sigma_k^2 = \frac{2\pi^2\Lambda^2}{\lambda^2}\left(1 + \gamma\cos\left[2(\theta_R - \theta_{\max})\right]\right) \tag{5.28}$$

where $\lambda$ is the wavelength of the carrier frequency [41]. The value $\sigma_k^2$ describes the spatial selectivity of a channel in a local area for a receiver moving in the $\theta_R$ direction. Eqn (5.28) is valid for any channel in which multipath waves arrive at the receiver from the horizon – a common assumption when describing mobile radio propagation. The next section discusses the unique aspects of small-scale fading behavior described by each shape factor.

### 5.3.3 Comparison to Omnidirectional Propagation

Applying the three shape factors, $\Lambda$, $\gamma$, and $\theta_{\max}$, to the classical omnidirectional propagation model, we find that there is not a bias in either one or two directions of angle-of-arrival, leading to maximum angular spread ($\Lambda = 1$) and minimum angular constriction ($\gamma = 0$). The statistics of omnidirectional propagation are *isotropic*, exhibiting no dependence on the azimuthal direction of receiver travel, $\theta_R$.

If the rate variance relationship of Eqn (5.28) is normalized against their values for omnidirectional propagation, then they reduce to the following form:

$$\begin{aligned}\sigma^2(\theta_R) &= \frac{\sigma_k^2(\theta_R)}{\sigma_{k_{\text{omni}}}^2} \\ &= \Lambda^2\left(1 + \gamma\cos\left[2(\theta_R - \theta_{\max})\right]\right) \qquad (5.29)\end{aligned}$$

where $\sigma^2$ is a normalized wavenumber spread. Eqn (5.29) provides a convenient way to analyze the effects of the shape factors on the second-order statistics of small-scale fading.

First, notice that angular spread, $\Lambda$, describes the *average* fading rate within a local area. A convenient way of viewing this effect is to consider the fading rate variance taken along two perpendicular directions within the same local area. From Eqn (5.29), the average of the two fading rate variances, regardless of the orientation of the measurement, is always given by

$$\frac{1}{2}\left[\sigma^2(\theta_R) \ + \ \sigma^2(\theta_R + \pi/2)\right] = \Lambda^2 \qquad (5.30)$$

Eqn (5.30) shows that the typical fading rates within a local area decreases with respect to omnidirectional propagation as multipath power becomes more and more concentrated about a single azimuthal direction.

Second, notice that angular constriction, $\gamma$, does not affect the average fading rate within a local area, but describes the variability of fading rates taken along different azimuthal directions, $\theta_R$. From Eqn (5.29), fading rate variance $\sigma_r^2$ will change as a function of $\theta_R$, but will always fall within the following range:

$$\sqrt{1-\gamma} \leq \frac{\sigma(\theta_R)}{\Lambda} \leq \sqrt{1+\gamma} \qquad (5.31)$$

The upper limit of Eqn (5.31) corresponds to a receiver traveling in the azimuthal direction of maximum fading ($\theta_R = \theta_{\max}$) while the lower limit corresponds to travel in a perpendicular direction ($\theta_R = \theta_{\max} + \pi/2$). Eqn (5.31) clearly shows that the variability of fading rates within the same local area increases as the channel becomes more and more constricted.

It is interesting to note that the propagation mechanisms of a channel are not uniquely described by the three shape factors $\Lambda$, $\gamma$, and $\theta_{\max}$. An infinitum of propagation mechanisms exist which may have the same set of shape factors and, by extension, lead to channels which exhibit nearly the same end-to-end performance. In fact, Eqn (5.29) provides rigorous mathematical criteria for a multipath channel that may be treated as "pseudo-omnidirectional":

$$|F_1|, |F_2| \ll F_0 \tag{5.32}$$

Under the condition of Eqn (5.32), angular spread becomes approximately 1 and angular constriction becomes approximately 0. Thus, the second-order statistics of the channel behave nearly identical to the classical omnidirectional channel.

## 5.4 Illustrative Examples

This section presents four different analytical examples of directional propagation channels that provide insight into the shape factor definitions and how they describe spatial fading rate variances [42]. Each example is accompanied by a graph of the angular spread and angular constriction and a graph showing the average and limiting cases of fading rate variance with respect to omnidirectional propagation.

### 5.4.1 Two-Wave Channel Model

Consider the simplest small-scale fading situation where two constant amplitude multipath components, with individual powers defined by $P_1$ and $P_2$, arrive at a mobile receiver separated by an azimuthal angle $\alpha$. Figure 5.5 illustrates this angular distribution of power, which is mathematically defined as

$$p(\theta) = P_1\,\delta(\theta - \theta_o) + P_2\,\delta(\theta - \theta_o - \alpha) \tag{5.33}$$

where $\theta_o$ is an arbitrary offset angle and $\delta(\cdot)$ is an impulse function. By applying Eqn (5.25)-Eqn (5.27), the expressions for $\Lambda$, $\gamma$, and $\theta_{\max}$ for this distribution are

$$\Lambda = \frac{2\sqrt{P_1 P_2}}{P_1 + P_2}\sin\frac{\alpha}{2}, \qquad \gamma = 1, \qquad \theta_{\max} = \theta_0 + \frac{\alpha + \pi}{2} \tag{5.34}$$

The angular constriction, $\gamma$, is always 1 because the two-wave model represents perfect clustering about two directions. The limiting case of two multipath components arriving from the same direction ($\alpha = 0$) results in an angular spread, $\Lambda$, of 0. An angular spread of 1 results only when two multipath of identical powers ($P_1 = P_2$) are separated by $\alpha = 180°$. Figure 5.5 shows how the fading behavior changes as multipath separation angle, $\alpha$, increases for the case of two equal-powered waves. Thus, increasing $\alpha$ changes a channel with low spatial selectivity into a channel with high spatial selectivity that exhibits a strong dependence on the azimuthal direction of receiver motion.

### 5.4.2 Sector Channel Model

Consider another theoretical situation where multipath power is arriving continuously and uniformly over a range of azimuth angles. This model has been used to describe propagation for directional receiver antennas with a distinct azimuthal beam [39]. The function $p(\theta)$ will be defined by

$$p(\theta) = \begin{cases} \frac{P_T}{\alpha} & : \quad \theta_o \le \theta \le \theta_o + \alpha \\ 0 & : \quad \text{elsewhere} \end{cases} \tag{5.35}$$

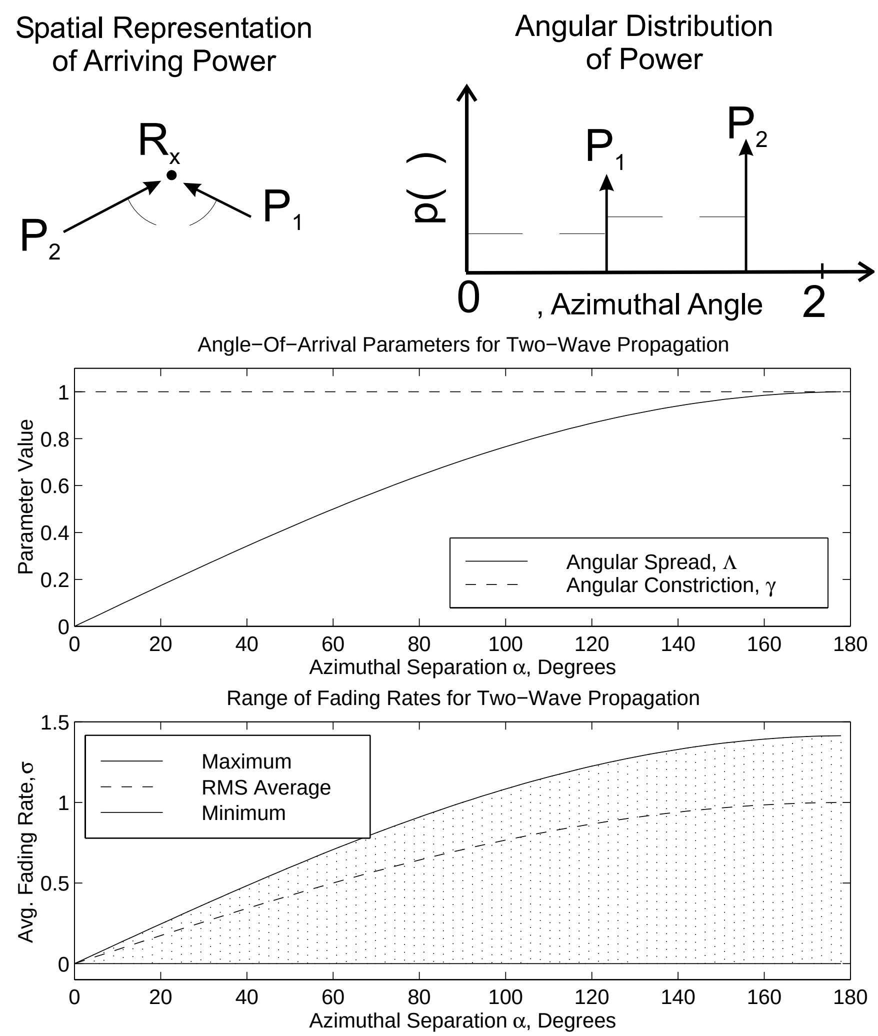


Figure 5.5: Two-wave propagation model. Graphs are for the special case of $P_1 = P_2$.

The angle $\alpha$ indicates the width of the sector (in radians) of arriving multipath power and the angle $\theta_o$ is an arbitrary offset angle, as illustrated by Figure 5.6. By applying Eqn (5.25)-Eqn (5.27), the expressions for $\Lambda$, $\gamma$, and $\theta_{\max}$ for this distribution are

$$\Lambda = \sqrt{1 - \frac{4\sin^2\frac{\alpha}{2}}{\alpha^2}}, \qquad \gamma = \frac{4\sin^2\frac{\alpha}{2} - \alpha\sin\alpha}{\alpha^2 - 4\sin^2\frac{\alpha}{2}}, \qquad \theta_{\max} = \theta_0 + \frac{\alpha+\pi}{2} \tag{5.36}$$

The limiting cases of these parameters and Eqn (5.28) provide deeper understanding of angular spread and constriction.

Figure 5.6 graphs the spatial channel parameters, $\Lambda$ and $\gamma$, as a function of sector width, $\alpha$. The limiting case of a single multipath arriving from precisely one direction corresponds to $\alpha = 0$, which results in the minimum angular spread of $\Lambda = 0$. The other limiting case of uniform illumination in all directions corresponds to $\alpha = 360°$ (omnidirectional Clarke model), which results in the maximum angular spread of $\Lambda = 1$. The angular constriction, $\gamma$, follows an opposite trend. It is at a maximum ($\gamma = 1$) when $\alpha = 0$ and at a minimum ($\gamma = 0$) when $\alpha = 360°$. The graph in Figure 5.6 shows that as the multipath angles of arrival are condensed into a smaller and smaller sector, the directional dependence of fading rates within the same local area increases. Overall, however, fading rates decrease with decreasing sector size $\alpha$.

### 5.4.3 Double Sector Channel Model

Another example of angular constriction may be studied using the Double Sector model of Figure 5.7. Diffuse multipath propagation over two equal and opposite sectors of azimuthal angles characterize the incoming power. The equation that describes this angular distribution of power is

$$p(\theta) = \begin{cases} \frac{P_T}{2\alpha} & : \quad \theta_o \le \theta \le \theta_o + \alpha, \quad \theta_o + \pi \le \theta \le \theta_o + \alpha + \pi \\ 0 & : \quad \text{elsewhere} \end{cases} \tag{5.37}$$

The angle $\alpha$ is the sector width and the angle $\theta_o$ is an arbitrary offset angle. By applying Eqn (5.25)-Eqn (5.27), the expressions for $\Lambda$, $\gamma$, and $\theta_{\max}$ for this distribution are

$$\Lambda = 1, \qquad \gamma = \frac{\sin\alpha}{\alpha}, \qquad \theta_{\max} = \theta_0 + \frac{\alpha}{2} \tag{5.38}$$

Note that the value of angular spread, $\Lambda$, is always 1. Regardless of the value of $\alpha$, an equal amount of power arrives from opposite directions, producing no clear bias in the direction of multipath arrival.

The limiting case of $\alpha = 180°$ (omnidirectional propagation) results in an angular constriction of $\gamma = 0$. As $\alpha$ decreases, the angular distribution of power becomes more and more

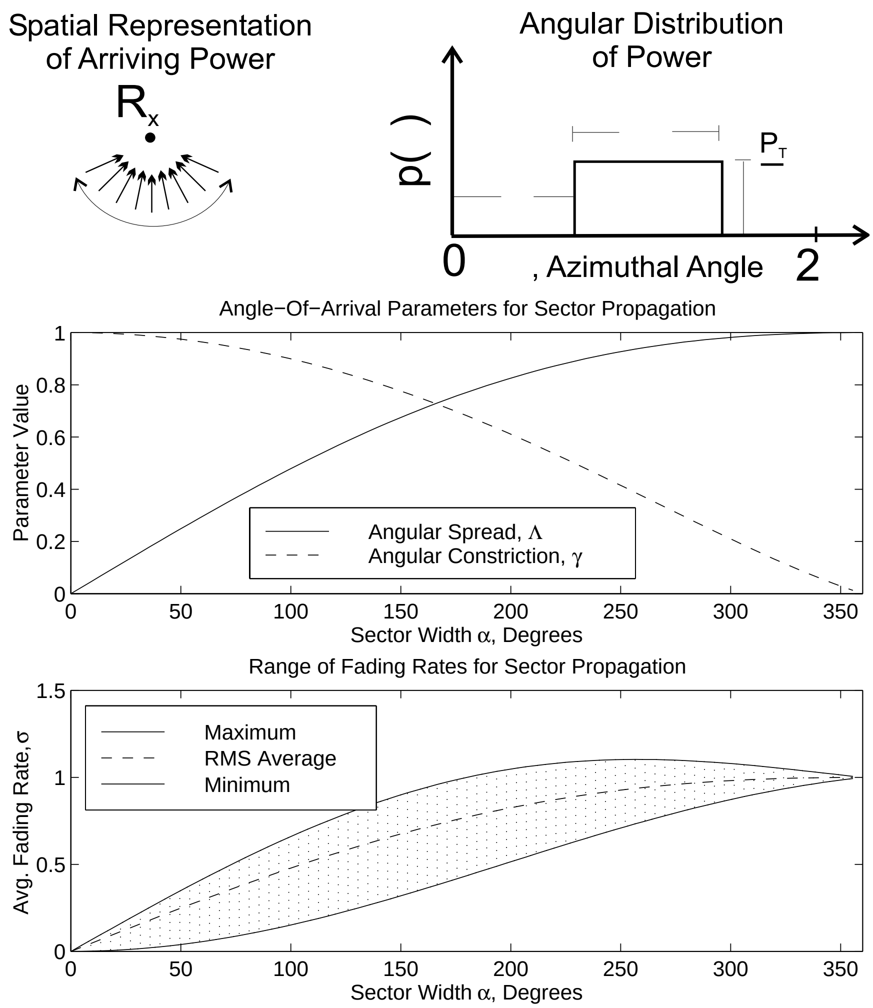


Figure 5.6: Multipath sector propagation model.

constricted. In the limit of $\alpha = 0$, the value of angular constriction reaches its maximum, $\gamma = 1$. This case corresponds to the above-mentioned instance of two-wave propagation. Figure 5.7 shows how the fading behavior changes as sector width $\alpha$ increases, making the fading rate more and more isotropic while the RMS average remains constant.

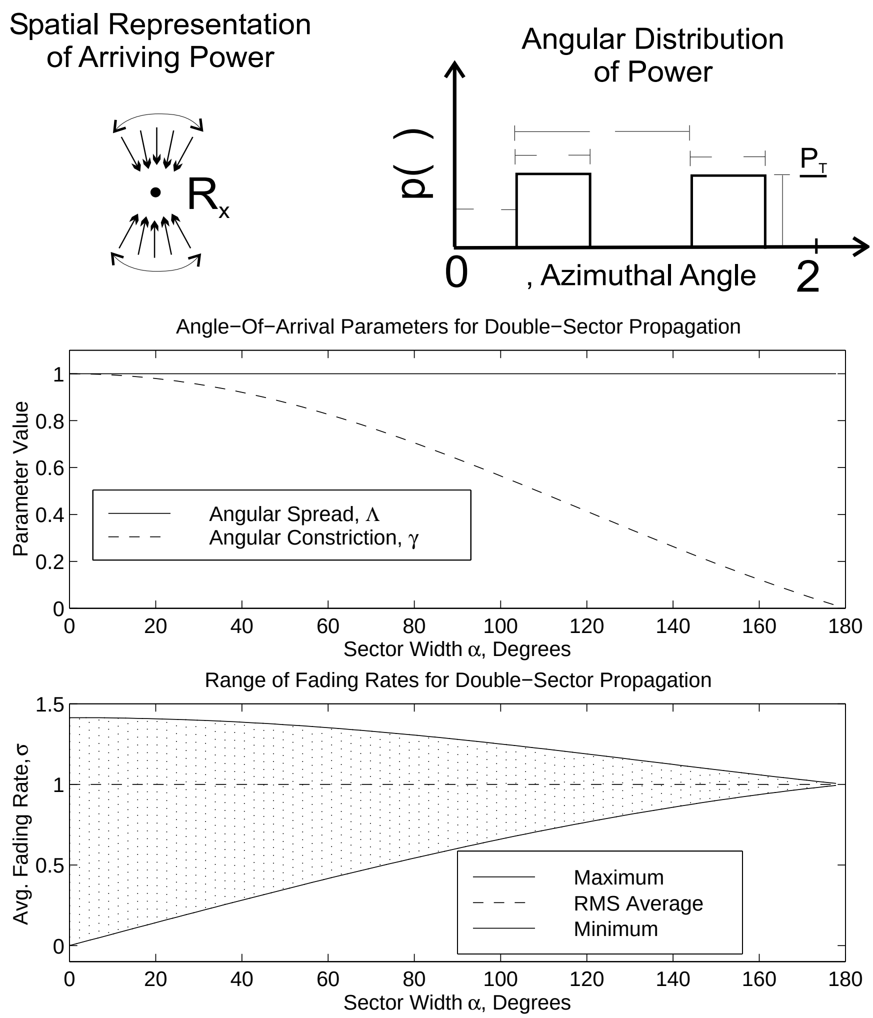


Figure 5.7: Multipath double sector propagation model.

### 5.4.4 Rician Channel Model

A Rician channel model results from the addition of a single plane wave and numerous diffusely scattered waves [34]. If the power of the scattered waves is assumed to be evenly distributed in azimuth, then the channel may be modeled by the following $p(\theta)$:

$$p(\theta) = \frac{P_T}{2\pi(K+1)}[1 + 2\pi K\delta(\theta - \theta_0)] \tag{5.39}$$

where $K$ is the ratio of specular to diffuse non-specular power, often referred to as the Rician $K$-factor. By applying Eqn (5.25)–Eqn (5.27), the expressions for $\Lambda$, $\gamma$, and $\theta_{\max}$ for this distribution are

$$\Lambda = \frac{\sqrt{2K+1}}{K+1}, \qquad \gamma = \frac{K}{2K+1}, \qquad \theta_{\max} = \theta_0 \tag{5.40}$$

Figure 5.8 depicts the spatial channel parameters, $\Lambda$ and $\gamma$, as a function of $K$-factor. For very small $K$-factors, the channel appears to be omnidirectional ($\Lambda = 1$ and $\gamma = 0$). As the $K$-factor increases, the angular spread of the Rician channel decreases and the angular constriction increases. This indicates that the overall fading rate in the Rician channel decreases and that the differences between the minimum and maximum fading rate variances within the same local area but different directions increases.

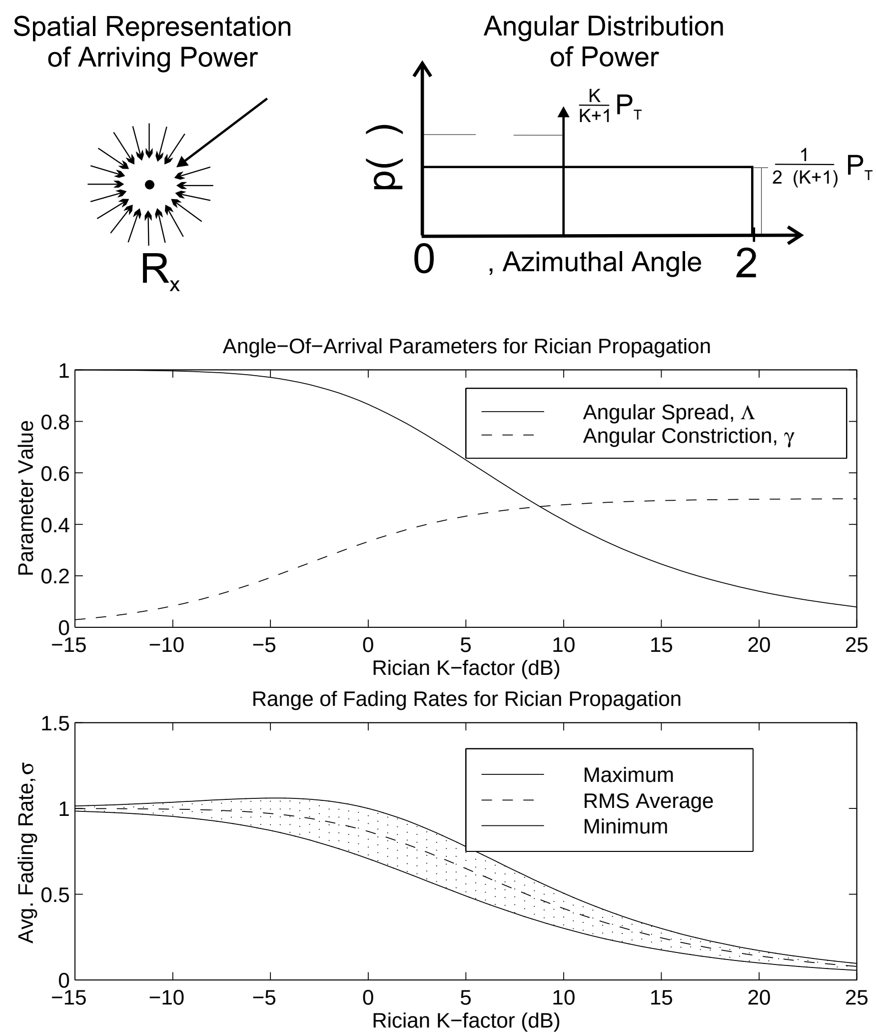


Figure 5.8: Rician propagation model.

## 5.5 Chapter Summary

This chapter presented the basic definitions and concepts behind modeling the angular distribution of multipath power in space – analysis that is usually performed using an *angle spectrum*. Below is a summary of the key points in this chapter:

- Wavevector, wavenumber, and angle spectrum are all related in the following way:
  - ▷ Any wavevector spectrum for a U-SLAC model may be written as an angle spectrum.
  - ▷ Angle spectra are simpler and more physically intuitive than wavevector spectra.
  - ▷ A wavenumber spectrum for a particular orientation in space may be derived from a wavevector or an angle spectrum.
- The following statement uses duality to summarize fading rate variance:

  *The* **(temporal, frequency, spatial)** *fading rate variance of a channel – a measure of fluctuation – is directly proportional to the RMS* **(Doppler, delay, wavenumber)** *spread squared.*

- A shape factor is a geometrical characteristic of the angle spectrum which relates to the wavenumber spread of an azimuth propagation model.
  - ▷ *Angular spread*, $\Lambda$, describes concentration of multipath power in one azimuthal direction and is related to the average wavenumber spread in a local area.
  - ▷ *Angular constriction*, $\gamma$, describes concentration of multipath power in two azimuthal directions and is related to how much a wavenumber spread depends on orientation.
  - ▷ *Direction of maximum fading*, $\theta_{\max}$, describes the azimuthal orientation for which the wavenumber spread is maximized.
- Shape factor theory may be applied to any number of channel models, including
  - ▷ a simple two-wave model
  - ▷ a diffuse azimuthal sector of arriving multipath power
  - ▷ a diffuse double-sector of arriving multipath power
  - ▷ a Rician channel with a specular component and diffuse, omnidirectional power

This chapter – much like the ones before it – has focused on the theory and definitions used to characterize the wireless radio channel. Subsequent topics will deal more with applications in wireless communications that involve the measurement and performance of a channel.

## 5.A Derivation of Shape Factors

The power spectral density (PSD) of a baseband complex received voltage signal is related to the angular distribution of multipath power [39]:

$$S_{\tilde{h}}(k) = \frac{2\pi}{\sqrt{k_{\max}^2 - k^2}} \left[ p\left(\theta_R + \cos^{-1}\frac{k}{k_{\max}}\right) + p\left(\theta_R - \cos^{-1}\frac{k}{k_{\max}}\right)\right], \text{ for } |k| \leq k_{\max} \quad (5.41)$$

where $\theta_R$ is the azimuthal direction of travel and $p(\cdot)$ is the angular distribution of impinging multipath power. The value $k_{\max}$ is the maximum wavenumber, which is equal to $2\pi/\lambda$.

The second moment of the fading process is given by the following integration [20]:

$$\sigma_r^2 = \frac{1}{2\pi} \int_{-k_{\max}}^{k_{\max}} (k - \bar{k})^2 \, S_{\tilde{h}}(k) \, dk \quad (5.42)$$

where $\bar{k}$ is the centroid of the PSD:

$$\bar{k} = \frac{1}{2\pi F_0} \int_{-k_{\max}}^{k_{\max}} k \, S_{\tilde{h}}(k) \, dk \quad (5.43)$$

$F_0$ is defined by Eqn (5.24) – this is really just the average power of the process.

Now insert Eqn (5.43) into Eqn (5.42), making the change of variable $\theta = \theta_R \pm \cos^{-1}\frac{k}{k_{\max}}$, where the $+$ and $-$ signs correspond to the left and right terms of $p(\cdot)$, respectively, of Eqn (5.41). After rearranging the limits of integration, the equation for $\sigma_r^2$ becomes

$$\sigma_r^2 = \frac{F_0 k_{\max}^2}{2} - \frac{k_{\max}^2}{F_0}\left[\int_0^{2\pi} p(\theta)\, \cos(\theta_R - \theta)\, d\theta\right]^2 + \frac{k_{\max}^2}{2}\left[\int_0^{2\pi} p(\theta)\, \cos[2(\theta_R - \theta)]\, d\theta\right] \quad (5.44)$$

Consider a complex Fourier expansion of $\sigma_r^2$ with respect to $\theta_R$:

$$\sigma_r^2 = \frac{1}{2\pi}\mathrm{Real}\left\{\sum_{n=0}^{\infty} A_n \exp(-jn\theta_R)\right\} = \frac{A_0}{2\pi} + \frac{1}{2\pi}\mathrm{Real}\left\{A_2 \exp(-j2\theta_R)\right\} \quad (5.45)$$

All of the $A_n$ are zero for odd $n$. This is because $\sigma_r^2(\theta_R) = \sigma_r^2(\theta_R + \pi)$; that is, a 180° change in the direction of mobile travel should produce identical statistics. Furthermore, Eqn (5.44) has no harmonic content with respect to $\theta_R$ for $n > 2$. Solving for the only two remaining complex coefficients produces

$$A_0 = \int_0^{2\pi} \sigma_r^2 \, d\theta_R = \pi k_{\max}^2 \left[F_0 - \frac{|F_1|^2}{F_0}\right] = \pi k_{\max}^2 \Lambda^2 \mathrm{E}\left\{\left|\tilde{h}(r)\right|^2\right\} \quad (5.46)$$

$$A_2 = 2\int_0^{2\pi} \sigma_r^2 \, \exp(j2\theta_R)\, d\theta_R = \pi k_{\max}^2 \left[F_2 - \frac{F_1^2}{F_0}\right] = A_0 \gamma \exp(j2\theta_{\max}) \quad (5.47)$$

where $\Lambda$, $\gamma$, and $theta_{\max}$ are the three basic spatial channel parameters defined in Eqn (5.25)-Eqn (5.27). If these two coefficients are placed back into Eqn (5.45), the end result is the relationship for $\sigma_r^2$ in Eqn (5.28).

For a mobile receiver, it is often convenient to measure the fading rate variance in terms of change per unit time instead of distance. If the mobile receiver operates in an otherwise static channel, then the mean-squared time rate-of-change is equal to $\sigma_r^2$ multiplied by the squared velocity of the receiver.

# Chapter 6

# Rayleigh Fading Channel Statistics

This chapter presents statistical techniques for characterizing small-scale envelope fading of *Rayleigh* channels as a function of time, space, and frequency. Statistics such as level-crossing rates, average fade duration, and correlation properties all impact the end-to-end performance of a wireless communication system. The basic mathematical analysis of this chapter shows that most of these statistics may be characterized in terms of the *spectrum spreads* of the channel and, in the case of spatial selectivity, the *shape factors* of the wireless channel. An outline of the contents of this chapter are listed below:

- Section 6.1 : analyzes the Rayleigh level-crossing problem
- Section 6.2 : studies autocovariance as a functions of time, space, and frequency
- Section 6.3 : revisits classical spatial channel models using shape factors
- Section 6.4 : summarizes key concepts

The techniques of this chapter may be extended to non-Rayleigh fading situations, although the mathematics quickly becomes intractable outside the Rayleigh case. For the sake of simplicity, all of the illustrations in this chapter will involve the diffusely propagating multipath waves of Rayleigh fading.

## 6.1 The Level-Crossing Problem

A PDF is useful for describing the total time a received signal envelope falls beneath a certain threshold – perhaps a signal-to-noise or signal-to-interference ratio threshold that is acceptable to a communications link. The PDF however, does not answer questions about *how often* the envelope drops below a threshold and *how long* does the envelope spend below this threshold. Such statistics are vital to the performance of error-correction coding, spatial diversity, frequency hopping, or any other wireless communication technique affected by second-order fading statistics.

### 6.1.1 Level-Crossing Rate

For a stochastic process as a function of time, the *level-crossing rate* is defined as the average number of crossings per second that the process drops beneath a specified threshold level. The level-crossing rate, $N_t$, for any general process may be calculated from the joint PDF of envelope, $R$, and its first time derivative $\frac{dR}{dt}$:

$$N_t = \int_0^\infty \dot{\rho} f_{R\dot{R}}(R, \dot{\rho}) d\dot{\rho} \tag{6.1}$$

The value $R$ is the envelope threshold of interest and $f_{R\dot{R}}(\rho, \dot{\rho})$ is the joint envelope and time-derivative of envelope PDF.

One of the convenient aspects of Rayleigh fading processes is the relatively simple formula for the joint PDF in Eqn (6.1). For a Rayleigh process, the time-derivative of envelope follows a Gaussian distribution that is independent of the Rayleigh-distributed envelope PDF. The joint PDF for this case may be written as

$$f_{R\dot{R}}(\rho, \dot{\rho}) = \underbrace{\frac{2\rho}{P_{\text{dif}}} \exp\left(-\frac{\rho^2}{P_{\text{dif}}}\right)}_{f_R(\rho)} \underbrace{\frac{1}{\sigma_t\sqrt{\pi}} \exp\left(-\frac{\dot{\rho}^2}{\sigma_t^2}\right)}_{f_{\dot{R}}(\dot{\rho})} \tag{6.2}$$

where $P_{\text{dif}}$ is the average power of the signal and $\sigma_t^2$ is the temporal fading rate variance, as discussed in Section 5.2.1. Recall also that we may express the temporal fading rate variance using the fundamental spectrum spread theorem of Section 5.2.2.

$$\sigma_t^2 = P_{\text{dif}} \sigma_\omega^2 \tag{6.3}$$

where $\sigma_\omega$ is the RMS Doppler spread. Using this result, the joint PDF in Eqn (6.2), and the original level-crossing rate equation of Eqn (6.1), we may write the final Rayleigh fading level-crossing rate expression as

$$N_t = \frac{\sigma_\omega}{\sqrt{\pi}} \rho_{\text{rms}} \exp\left(-\rho_{\text{rms}}^2\right) \tag{6.4}$$

where $\rho_{\mathrm{rms}}$ is the envelope threshold normalized against the RMS envelope value ($\rho_{\mathrm{rms}}^2 = R^2/P_{\mathrm{dif}}$).

### 6.1.2 Average Fade Duration

The calculation of the *average fade duration* statistic is similar to the level crossing rate. The average fade duration is the amount of time that a received envelope spends underneath a threshold level, once the envelope has crossed that level. For a given threshold level $R$, the average fade duration, $\bar{t}$, is calculated by the following:

$$\bar{t} = \frac{1}{N_t} \int_0^R f_R(\rho) d\rho \tag{6.5}$$

For the temporal Rayleigh fading case, the average fade duration is given by

$$\bar{t} = \frac{\sqrt{\pi}}{\sigma_\omega \rho_{\mathrm{rms}}} \left[\exp\left(\rho_{\mathrm{rms}}^2\right) - 1\right] \tag{6.6}$$

The average fade duration is useful for describing the "burstiness" of bit errors in a temporal fading channel and may be used for interleaving designs.

> *Note: Averages vs. Distributions*
>
> Notice that we are focusing on the *average* level-crossing rate and fade duration. According to Rice's pioneering work, the averages for these quantities have closed-form solutions [25]. Closed-form solutions for the exact *distribution* of fade durations, however, were only possible by making over-simplifying assumptions. To date, effective analytical treatment of the distribution of Rayleigh fades is an unsolved problem in wireless communications.

### 6.1.3 Level Crossing in Frequency

Traditionally, most level crossing analysis is performed on time-varying fading channels. However, for a fixed static channel, we may also define level crossing rates in terms of crossings-per-frequency. Applying duality ($\sigma_\omega \longrightarrow 2\pi\sigma_\tau$), we may write the level-crossing rate for frequency selective channels as

$$N_f = 2\sqrt{\pi}\sigma_\tau \rho_{\mathrm{rms}} \exp\left(-\rho_{\mathrm{rms}}^2\right) \tag{6.7}$$

where $\sigma_\tau$ is the delay spread. Eqn (6.7) is an excellent measure of the frequency selectivity of a dispersive wireless channel.

Likewise, an *average fade bandwidth*, $\bar{f}$, may also be calculated in terms of the delay spread. Applying duality produces the following expression:

$$\bar{f} = \frac{\exp\left(\rho_{\mathrm{rms}}^2\right) - 1}{2\sqrt{\pi}\sigma_\tau \rho_{\mathrm{rms}}} \tag{6.8}$$

The average fade bandwidth is a useful parameter for wireless systems that employ frequency-hopping. In such systems, successive frequency hops should, on average, change the transmitted carrier frequency in excess of the average fade bandwidth to maintain an acceptable signal-to-noise ratio.

### 6.1.4 Level Crossing in Space

Following in the footsteps of the frequency analysis, it is also possible to do a level crossing analysis on a static narrowband received envelope as a function of space. Once again, applying duality ($\sigma_\omega \longrightarrow \sigma_k$) produces an expression for the level crossing rate in units of *crossings per unit distance*,

$$N_r = \frac{\sigma_k}{\sqrt{\pi}} \rho_{\mathrm{rms}} \exp\left(-\rho_{\mathrm{rms}}^2\right) \tag{6.9}$$

and also for the *average fade distance*,

$$\bar{r} = \frac{\sqrt{\pi}}{\sigma_k \rho_{\mathrm{rms}}} \left[\exp\left(\rho_{\mathrm{rms}}^2\right) - 1\right] \tag{6.10}$$

Both the spatial level crossing rate and the average fade distance depend on the wavenumber spread, $\sigma_k$.

The expressions in Eqn (6.9) and Eqn (6.10) may also be written in terms of shape factors. By recognizing the relationship between wavenumber spread and the multipath shape factors of Eqn (5.28), we can write new equations for spatial level-crossing rate and average fade length:

$$N_r = \frac{\sqrt{2\pi}\Lambda\rho_{\mathrm{rms}}}{\lambda} \sqrt{1 + \gamma\cos\left[2(\theta_R - \theta_{\max})\right]} \exp\left(-\rho_{\mathrm{rms}}^2\right) \tag{6.11}$$

$$\bar{r} = \frac{\lambda\left[\exp\left(\rho_{\mathrm{rms}}^2\right) - 1\right]}{\sqrt{2\pi}\rho_{\mathrm{rms}}\Lambda\sqrt{1 + \gamma\cos\left[2(\theta_R - \theta_{\max})\right]}} \tag{6.12}$$

where $\lambda$ is the wavelength of propagation and $\theta_R$ is the azimuthal orientation.

## 6.2 Envelope Unit Autocovariance

Recall that the unit autocovariance of a received envelope as a function of time, frequency, or space determines the coherence of a wireless channel. The unit autocovariance functions developed in this section may be used to develop analytical expressions for coherence time, bandwidth, and distance.

### 6.2.1 Temporal Unit Autocovariance

The unit autocovariance of a time-varying stochastic process may be computed by subtracting the mean-value from the autocorrelation and normalizing the result. The autocorrelation, in turn, is calculated from its Doppler spectrum by performing an inverse Fourier transform. For the complex time-varying channel, $\tilde{h}(t)$, this natural progression is illustrated below:

$$S_{\tilde{h}}(\omega) \xrightarrow{\substack{\text{Fourier}\\ \text{Transform}}} C_{\tilde{h}}(\Delta t) \xrightarrow{\text{Normalize}} \varrho_{\tilde{h}}(\Delta t) \tag{6.13}$$

Thus, if the Doppler spectrum of $\tilde{h}(t)$ is known, it is possible to calculate the unit autocovarriance, $\varrho_{\tilde{h}}(\Delta t)$.

The Doppler spectrum for received *envelope*, $S_R(\omega)$, however, is extremely difficult to calculate – even if we know the *channel* Doppler spectrum, $S_{\tilde{h}}(\omega)$. We would like to use a similar method,

$$S_R(\omega) \xrightarrow{\substack{\text{Fourier}\\ \text{Transform}}} C_R(\Delta t) \xrightarrow{\text{Normalize}} \varrho_R(\Delta t) \tag{6.14}$$

but this is extremely difficult since the act of taking an envelope of a random process is a highly nonlinear operation.

Rather than develop an expression for envelope unit autocovariance directly (which itself requires approximations), we will use the approximate analytical technique developed in Appendix 6.A. This technique produces an expression for envelope unit autocovariance based *solely* on the RMS spectral spread of the process. For the temporal envelope unit autocovariance, $\varrho_R(\Delta t)$, the technique produces the following expression:

$$\varrho_R(\Delta t) \approx \exp\left(-\frac{23}{2\pi^2}\sigma_\omega^2\,\Delta t^2\right) \tag{6.15}$$

where $\sigma_\omega$ is the RMS Doppler spread. Adapted from the original technique in [43], Eqn (6.15) produces near-exact values for unit autocovariance over the most useful range of the function – when $\Delta t$ is small. Despite the approximations used to construct Eqn (6.15), it only becomes inaccurate after a duration, $\Delta t$, in which the time-varying envelopes have become decorrelated. Therefore, Eqn (6.15) is extremely useful for engineering wireless modem designs that are affected by temporal correlation.

We may also note that, with an expression for envelope unit autocovariance, we may now provide a formal expression for *temporal coherence*. The value *coherence time*, $T_c$, is the duration over which the envelope of a temporal fading channel appears to be a constant, as discussed in Section 2.2. Another way of stating this definition is that coherence time, $T_c$, is the value of separation time, $\Delta t$, for which time-varying envelopes become *decorrelated*.

Defined in this manner, the exact coherence time for a time-varying channel will depend on how strictly the engineer chooses to define "decorrelated". A strict definition of coherence time may arise if we require the signal envelope to be 90% correlated ($\varrho_R(T_c) = 0.90$). A more relaxed decorrelation standard will lead to a larger $T_c$. Unless specified otherwise, this work will use the quantity $\exp(-1)$ to describe envelopes that have sufficiently decorrelated. In fact, the time that satisfies this definition is often called the *correlation time* in statistics [18]. Therefore, our generic formal definition for coherence time becomes

$$T_c = \frac{2\pi}{\sqrt{46}\sigma_\omega} = \frac{1.08}{\sigma_\omega} \tag{6.16}$$

Note that this definition of coherence time depends solely and inversely on the RMS Doppler spread, $\sigma_\omega$. The other fine details and structure of the Doppler spectrum, $S_{\tilde{h}}(\omega)$, do not greatly effect temporal channel coherence. Note that this independence is noted and empirically proven by Fleury in [44].

> *Note: Temporal Rayleigh Fading*
>
> For fixed, narrowband receivers, temporal fading in a wireless channel is due to the motion of scatterers. Rayleigh fading as a function of time requires temporally diffuse propagation, which physically means that the propagation environment consists of numerous scatterers, *all of which are in motion.* One such scenario occurs often for mm-wave propagation through a rain storm, where drops of water scatter radio waves to the receiver [45]. However, most cases of temporal Rayleigh fading in terrestrial wireless propagation are due to receivers *moving* through small-scale spatial Rayleigh fading. Recognize, therefore, that *temporal* Rayleigh fading in the absence of receiver (or transmitter) motion, is much more rare than *frequency* or *spatial* Rayleigh fading.

### 6.2.2 Frequency Unit Autocovariance

Once again, applying duality to the temporal analysis produces similar expressions for frequency unit autocovariance. Realizing that $\sigma_\omega \longrightarrow 2\pi\sigma_\tau$ and $\Delta t \longrightarrow \Delta f$, the envelope unit autocovarriance as a function of frequency separation becomes

$$\varrho_R(\Delta f) \approx \exp\left(-46\sigma_\tau^2\, \Delta f^2\right) \tag{6.17}$$

where $\sigma_\tau$ is the RMS delay spread. Again, note the independence of the approximate unit autocovariance in Eqn (6.17) on fine structure of the delay spectrum, $S_{\tilde{h}}(\tau)$; only the RMS delay spread is needed to characterize the small-$\Delta f$ correlation behavior.

Our formal definition for *coherence bandwidth*, $B_c$, will be based on the frequency separation $\Delta f$ that drives the envelope unit autocovariance in Eqn (6.17) to a level of $\exp(-1)$. Following this definition,

$$B_c = \frac{1}{\sqrt{46}\sigma_\tau} = \frac{1}{6.78\sigma_\tau} \tag{6.18}$$

Note how similar this definition of coherence bandwidth is to the arbitrary rule-of-thumb:

$$B_c \approx \frac{1}{5\sigma_\tau} \tag{6.19}$$

which was discussed in Section 2.4.4.

### 6.2.3 Spatial Unit Autocovariance

Of course, the correlation analysis must include the spatial unit autocovariance in order to be complete. Applying the duality results $\Delta t \longrightarrow \Delta r$ and $\sigma_\omega \longrightarrow \sigma_k$, we obtain

$$\varrho_R(\Delta r) \approx \exp\left(-\frac{23}{2\pi^2}\sigma_k^2\, \Delta r^2\right) \tag{6.20}$$

where $\sigma_k$ is the RMS wavenumber spread. *Coherence distance*, $D_c$, is the separation distance in space over which a fading channel appears to be unchanged. Using our general correlation criterion for channel coherence, $\varrho_R(D_c) = \exp(-1)$, the expression for coherence distance becomes

$$D_c = \frac{2\pi}{\sqrt{46}\sigma_k} = \frac{1.08}{\sigma_k} \tag{6.21}$$

Note the insensitivity of this expression to the fine structure of the wavenumber spectrum $S_{\tilde{h}}(k)$. Only the RMS wavenumber spread is important.

Multipath shape factor theory may be applied to Eqn (6.20) to generate equivalent envelope unit autocovariance functions that depend on the geometrical properties of multipath angle-of-arrival. Futhermore, the shape factor theory allows us to study correlation properties as a function of azimuthal orientation, $\theta_R$, in space instead of one-dimensional position:

$$\varrho_R(\Delta r, \theta_R) \approx \exp\left(-23\Lambda^2\left[1 + \gamma\cos(2[\theta_R - \theta_{\max}])\right]\left[\frac{\Delta r}{\lambda}\right]^2\right) \tag{6.22}$$

Eqn (6.22) allows us to estimate the envelope correlation between two points in space separated by a distance $\Delta r$ along an azimuthal direction $\theta_R$. The orientation-dependent coherence distance is

$$D_c(\theta_R) = \frac{\lambda}{\Lambda\sqrt{23(1+\gamma\cos[2(\theta_R - \theta_{\max})])}} \tag{6.23}$$

There are few rules-of-thumb for channel coherence in the literature, other than the case of omnidirectional diffuse propagation ($\Lambda = 1$, $\gamma = 0$). A convenient definition for the coherence distance, $D_c$, is the value that satisfies the equation $\rho_{\text{rms}}(D_c) = 0.5$ [46]. The classical value for coherence distance in an omnidirectional Rayleigh channel is given by

$$D_c \approx \frac{9\lambda}{16\pi} \tag{6.24}$$

where $\lambda$ is the wavelength of radiation. Using the generalized autocovariance function of Eqn (6.22) with this criterion for correlation leads to the definition:

$$D_c(\theta_R) \approx \frac{\lambda\sqrt{\ln 2}}{\Lambda\sqrt{23(1+\gamma\cos[2(\theta_R - \theta_{\max})])}} \tag{6.25}$$

For omnidirectional propagation, Eqn (6.25) differs from Eqn (6.24) by only -3.0% [41].

### 6.2.4 Joint Unit Autocovariance

With the increased focus on *space-time coding* techniques, wireless researchers may find it helpful to characterize a joint unit autocovariance for received envelope as a function of spatial *and* frequency separation. For modest bandwidth systems, it is sufficient to treat spatial and frequency decorrelation as independent phenomena. Therefore, the joint unit autocovariance, $\varrho_R(\Delta f, \Delta r)$, may be written as the product of the individual unit autocovariances [11]:

$$\varrho_R(\Delta f, \Delta r) \approx \varrho_R(\Delta f)\varrho_R(\Delta r) \tag{6.26}$$

Eqn (6.26) describes how the received envelope changes as a function of frequency separation, $\Delta f$, and spatial separation $\Delta r$. Plugging in Eqn (6.17) and Eqn (6.20) into Eqn (6.26) produces:

$$\varrho_R(\Delta f, \Delta r) \approx \exp\left(-\frac{23}{2\pi^2}\left[4\pi^2\sigma_\tau^2\,\Delta f^2 + \sigma_k^2\,\Delta r^2\right]\right) \tag{6.27}$$

Of course, shape factors may be applied to better understand the spatial correlation properties as a function of displacement and orientation. The final unit autocovariance for space-frequency varying envelopes becomes

$$\varrho_R(\Delta f, \Delta r, \theta_R) \approx \exp\left(-46\sigma_\tau^2\,\Delta f^2 - 23\Lambda^2\left[1+\gamma\cos(2[\theta_R - \theta_{\max}])\right]\left[\frac{\Delta r}{\lambda}\right]^2\right) \tag{6.28}$$

Eqn (6.28) may prove invaluable for describing correlation properties (and, hence, performance) of wireless systems that have large bandwidths and multiple transmitter-receiver antennas. The powerful approximations help characterize the complicated phenomenon of joint space-frequency fading.

> *Note: Trying to be Like Einstein*
>
> The name *space-time coding*, which has been applied liberally to describe any next-generation technologies involving time-domain signal coding used in conjunction with multiple transmitter and receiver antennas, may lead to confusion when viewed from a channel modeling perspective. The *time* in space-time (and the *temporal* in the adjective form spatio-temporal) often refers to what we have called the delay dependency, $\tau$, instead of the time dependency, $t$. Rather than use *space-delay coding*, perhaps those that coined the terms could not resist borrowing some of the inspiring terminology from general relativity theory.

## 6.3 Revisiting Classical Spatial Channel Models

This section shows several examples of how level-crossing rate, average fade duration, and unit autocovariance relationships derived using shape factors compare to three well-known cases of propagation that have analytical solutions [20].

### 6.3.1 Classical Spatial Channel Models

The first case of multipath propagation corresponds to a narrowband receiver operating in a local area with multipath arriving from all directions, such that the angular distribution of power, $p(\theta)$, is a constant. The receiver antenna is assumed to be an omnidirectional whip, oriented perpendicular to the ground. Due to the vertical electric-field polarization of the whip antenna, this propagation scenario is referred to as the $E_z$-case [13].

The second two cases correspond to the same narrowband receiver in the same omnidirectional multipath channel, but with a small loop antenna mounted atop the receiver such that the plane of the loop is perpendicular to the ground. The antenna pattern of the small loop antenna attenuates the arriving multipath such that the angular distribution of power becomes

$$p(\theta) = A \sin^2 \theta \tag{6.29}$$

where $A$ is some arbitrary gain constant. Unlike the omnidirectional $E_z$-case, the statistics of this propagation scenario will depend on the direction of travel by the receiver. The $H_x$-case will refer to a receiver traveling in a direction perpendicular to the main lobes of the loop antenna pattern ($\theta = 0$). The $H_y$-case will refer to a receiver traveling in a direction parallel to the main lobes ($\theta = \frac{\pi}{2}$). Figure 6.1 illustrates the $E_z$, $H_x$, and $H_y$ cases for the modeled receiver antennas.

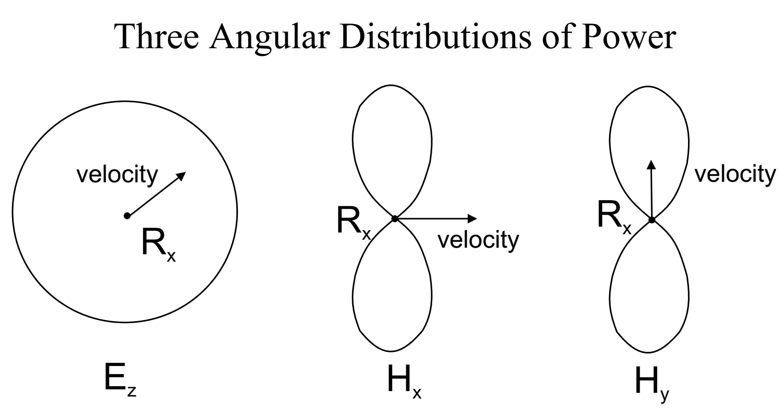


Figure 6.1: Three different multipath-induced mobile-fading scenarios.

### 6.3.2 Channel Model Solutions

The first step is to calculate the three spatial parameters from the angular distribution of power, $p(\theta)$, using Eqn (5.25)-Eqn (5.27). The spatial parameters for the $E_z$-case are $\Lambda = 1$, $\gamma = 0$, and $\theta_{\max} = 0$. Since this case is omnidirectional, the angular spread is at a maximum ($\Lambda = 1$) and the angular constriction is at a minimum ($\gamma = 0$). For the $H_x$- and $H_y$-cases, the spatial parameters are $\Lambda = 1$, $\gamma = \frac{1}{2}$, and $\theta_{\max} = \frac{\pi}{2}$. Since the impinging multipath have no clear bias in *one* direction, the angular spread is at a maximum just like the $E_z$-case. However, there is clearly a bias in *two* directions, resulting in an increased angular constriction of $\gamma = \frac{1}{2}$.

After substitution of these parameters into Eqn (6.11) along with the appropriate direction of mobile travel, the level-crossing rates for the three cases become

$$E_z: \quad N_t = \frac{\sqrt{2\pi} v \rho_{\text{rms}}}{\lambda} \exp\left(-\rho_{\text{rms}}^2\right) \tag{6.30}$$

$$H_x: \quad N_t = \frac{\sqrt{\pi} v \rho_{\text{rms}}}{\lambda} \exp\left(-\rho_{\text{rms}}^2\right) \tag{6.31}$$

$$H_y: \quad N_t = \frac{\sqrt{3\pi} v \rho_{\text{rms}}}{\lambda} \exp\left(-\rho_{\text{rms}}^2\right) \tag{6.32}$$

Note that, although we are studying spatial selectivity, we use the classical literature convention of studying a *temporal* level-crossing rate, $N_t$, by making the substitution $r = vt$, where $v$ is the speed of the mobile receiver. The corresponding average fade durations are

$$E_z: \quad \bar{t} = \frac{\lambda}{\sqrt{2\pi} v \rho_{\text{rms}}} \left[\exp\left(\rho_{\text{rms}}^2\right) - 1\right] \tag{6.33}$$

$$H_x: \quad \bar{t} = \frac{\lambda}{\sqrt{\pi} v \rho_{\text{rms}}} \left[\exp\left(\rho_{\text{rms}}^2\right) - 1\right] \tag{6.34}$$

$$H_y: \quad \bar{t} = \frac{\lambda}{\sqrt{3\pi} v \rho_{\text{rms}}} \left[\exp\left(\rho_{\text{rms}}^2\right) - 1\right] \tag{6.35}$$

These expressions exactly match the original solutions presented by Clarke in [13].

Now substitute the channel shape factors into the approximate spatial autocovariance functions in Eqn (6.22). The results for the three cases are

$$E_z: \quad \varrho_R(\Delta r) = \exp\left[-23\left(\frac{\Delta r}{\lambda}\right)^2\right] \tag{6.36}$$

$$H_x: \quad \varrho_R(\Delta r) = \exp\left[-11.5\left(\frac{\Delta r}{\lambda}\right)^2\right] \tag{6.37}$$

$$H_y: \quad \varrho_R(\Delta r) = \exp\left[-34.5\left(\frac{\Delta r}{\lambda}\right)^2\right] \tag{6.38}$$

These three functions are compared to their more rigorous analytical solutions in Figure 6.2 through Figure 6.4. Note that all three model the spatial autocovariance function consistent with the approximation made in the derivation of Eqn (6.22). The behavior is nearly exact for values of $\Delta r$ equal to or less than a correlation distance.

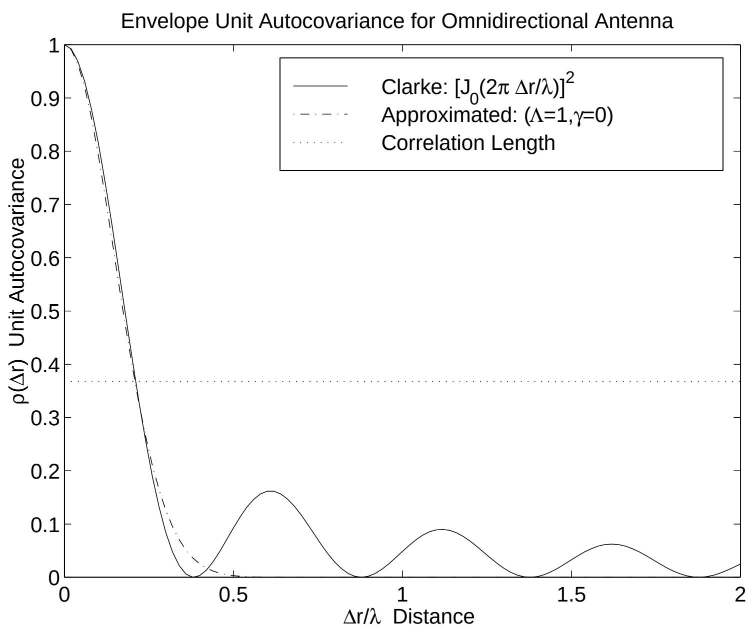


Figure 6.2: Comparison between Clarke theoretical and approximate envelope autocovariance functions for $E_z$-case.

### 6.3.3 Additional Comments

The shape factor technique for finding fading statistics is an intuitive way to relate the physical channel characteristics to the fading behavior. In the previous examples, the spatial parameters may be calculated analytically or even estimated intuitively by simply looking at the distributions of multipath power in Figure 6.1. The use of spatial parameters to find level crossing rate, average fade duration, and spatial autocovariance is quite simple when compared to the full analytical solutions of the $E_z$-, $H_x$-, and $H_y$-cases presented in [20]. The proposed solution is also more comprehensive. For example, once the shape factors have been found, Eqn (6.11), Eqn (6.12), and Eqn (6.22) provide statistics for *all* directions of travel for the $H_x$- and $H_y$-cases, and not just specific directions such as $\theta_R = 0$ or $\theta_R = \frac{\pi}{2}$. Thus, specific fading behaviors for various directions of receiver motion are modeled easily.

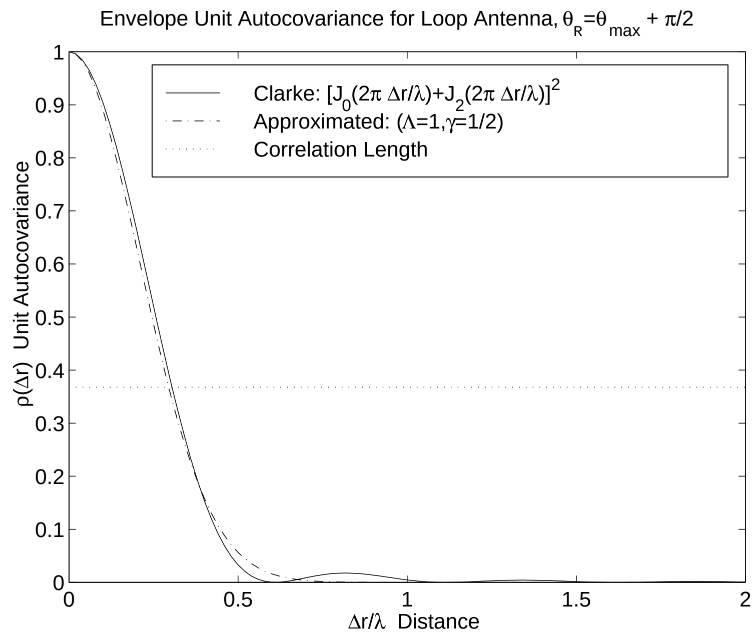


Figure 6.3: Comparison between Clarke theoretical and approximate envelope autocovariance functions for $H_x$-case.

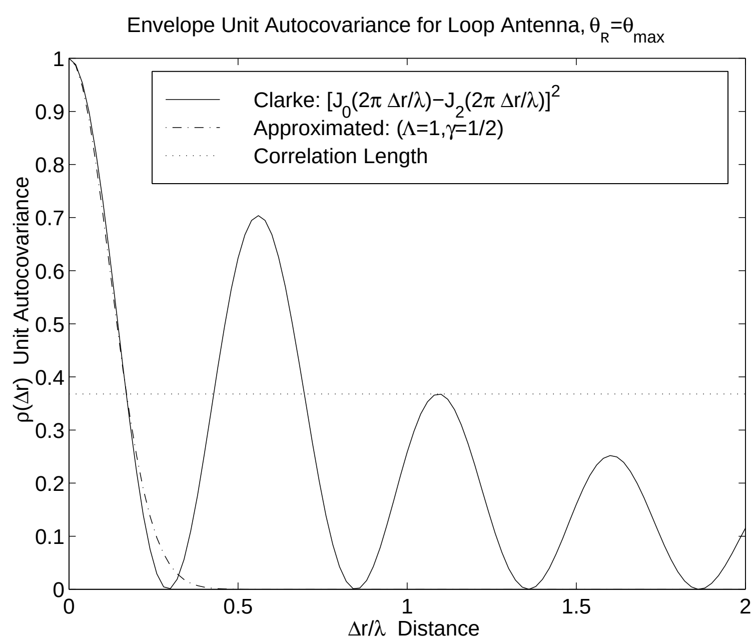


Figure 6.4: Comparison between Clarke theoretical and approximate envelope autocovariance functions for $H_y$-case.

The solution form of Eqn (6.11), Eqn (6.12), and Eqn (6.22) reveals an interesting property about statistics in Rayleigh-fading channels. Since the three shape factors only depend on low-order Fourier coefficients, many of the second-order statistics of Rayleigh-fading channels are insensitive to the higher-order multipath structure. The general biases of angular spread and angular constriction truly dominate the space and time evolution of these fading processes.

## 6.4 Chapter Summary

This chapter presented a number of second-order fading statistics involving the envelopes of Rayleigh fading channels. Below is a summary of the key points of the chapter:

- Level-crossing statistics for Rayleigh fading channels are solely dependent on RMS spectrum spreads.
  - ▷ The *level-crossing rate* describes how often an envelope threshold is crossed.
  - ▷ The *average fade duration* describes how often a signal spends below a threshold, once crossed.
  - ▷ Level-crossing statistical expressions found for one channel dependency lead to expressions for all dependencies if duality is applied.
- Correlation statistics for Rayleigh fading channels may calculated from RMS spectrum spreads as well.
  - ▷ The resulting unit autocovariance functions are approximate, but they characterize the correlation behavior over the most important regions of the function.
  - ▷ Formal definitions for coherence time, bandwidth, and distance may be based on these unit autocovariance functions.
  - ▷ Using our unified approach, *joint* space-frequency autocovariance functions are also easy to approximate.
- The use of *shape factors* in our statistics allows characterization of level crossing rate, average fade length, and spatial unit autocovariance that depends solely on several geometrical properties of multipath angle-of-arrival. Shape factor expressions match well with several analytical baseline cases of multipath propagation.

Many of the statistics discussed in this chapter have useful applications in the design and performance prediction of wireless modems. Designs involving frequency-hopping, diversity, space-time coding, adaptive equalization, interleaving, or error correction coding all require knowledge of these received envelope statistics.

## 6.A Approximate Spatial Autocovariance Function

Unit autocovariance of a WSS time-varying signal envelope process, $R(t)$, is defined as follows [47]:

$$\varrho_R(\Delta t) = \frac{\overbrace{\mathrm{E}\left\{R(t)R(t+\Delta t)\right\}}^{C_R(\Delta t)} - \left(\mathrm{E}\left\{R\right\}\right)^2}{\mathrm{E}\left\{R^2\right\} - \left(\mathrm{E}\left\{R\right\}\right)^2} \tag{6.39}$$

We may express $\varrho_R(\Delta t)$ as the following Mclaurin series:

$$\varrho_R(\Delta t) = \sum_{n=0}^{\infty} \frac{\Delta t^{2n}}{(2n)!} \left.\frac{d^{2n}\varrho_R(t)}{dt^{2n}}\right|_{t=0} \tag{6.40}$$

Eqn (6.40) contains only even powers of $\Delta t$ since any real autocovariance function is an even function. The differentiation of an autocorrelation function satisfies the following relationship [21]:

$$\left.\frac{d^{2n}C_R(\Delta t)}{d\Delta t^{2n}}\right|_{\Delta t=0} = (-1)^n \mathrm{E}\left\{\left(\frac{d^n R(t)}{dt^n}\right)^2\right\} \tag{6.41}$$

and is useful for re-expressing the Mclaurin series:

$$\begin{aligned}
\varrho_R(\Delta t) &= 1 + \frac{\sum\limits_{n=1}^{\infty} \frac{(-1)^n \Delta t^{2n}}{(2n)!} \mathrm{E}\left\{\left(\frac{d^n R(t)}{dt^n}\right)^2\right\}}{\mathrm{E}\left\{R^2\right\} - \left(\mathrm{E}\left\{R\right\}\right)^2} \\
&= 1 - \frac{\mathrm{E}\left\{\left(\frac{dR(t)}{dt}\right)^2\right\}}{2\left[\mathrm{E}\left\{R^2\right\} - \left(\mathrm{E}\left\{R\right\}\right)^2\right]} \Delta t^2 + \cdots
\end{aligned} \tag{6.42}$$

For an envelope that follows a Rayleigh PDF, the denominator of Eqn (6.42) evaluates to

$$\mathrm{E}\left\{R^2\right\} - \left(\mathrm{E}\left\{R\right\}\right)^2 = \left(1 - \frac{\pi}{4}\right) P_{\mathrm{dif}} \tag{6.43}$$

Rayleigh fading processes also have the following unique property [41]:

$$\begin{aligned}
\mathrm{E}\left\{\left(\frac{dR(t)}{dt}\right)^2\right\} &= \frac{1}{2}\mathrm{E}\left\{\left|\frac{d\tilde{h}(t)}{dt}\right|^2\right\} \\
&= \frac{1}{2}\sigma_t^2 \\
&= \frac{1}{2}\sigma_\omega^2 P_{\mathrm{dif}}
\end{aligned} \tag{6.44}$$

Now consider $\varrho_R(\Delta t)$ approximated by an arbitrary Gaussian function and its Mclaurin expansion:

$$
\begin{aligned}
\varrho_R(\Delta t) &\approx \exp\left[-a\Delta t^2\right] \\
&\approx \sum_{n=0}^{\infty} \frac{(-1)^n a^n}{n!} \Delta t^{2n} \\
&\approx 1 - a\Delta t^2 + \cdots
\end{aligned} \tag{6.45}
$$

A Gaussian function is chosen as a generic approximation to the true unit autocovariance since it is a convenient and well-behaved correlation function. The appropriate constant $a$ is chosen by setting equal the second terms of Eqn (6.42) and Eqn (6.45), ensuring that the behavior of both autocovariance functions is identical for small $\Delta t$:

$$
a = \frac{1}{2\pi^2} \underbrace{\left[\frac{2\pi^2}{4-\pi}\right]}_{\approx 23.00} \sigma_\omega^2 \tag{6.46}
$$

Therefore, the approximate unit autocovariance depends only on the RMS Doppler spread.

# Chapter 7

# Spatio-Temporal Measurements

In the coming age of high wireless data demand and increased frequency congestion, technologies involving wideband modulation schemes [48], smart antennas [1], and space-time coding [3, 49] promise to squeeze every drop of capacity out of a wireless data link. Unfortunately, these new technologies have grown at a rate that exceeds our general knowledge of the spatio-temporal wireless channel. Without sufficient knowledge of the channel, the performance of new spatial and wideband signaling techniques is impossible to gauge for a particular radio environment.

This chapter presents the results of a wideband, *peer-to-peer* channel measurement campaign at a wireless carrier frequency of 1920 MHz conducted on the campus of Virginia Tech in November of 1999. In the peer-to-peer configuration, both transmitter and receiver operate at a height of roughly 1.5m above ground (head-level). This configuration would be common for portable, handheld communication devices that operate in mobile ad-hoc networks serving teams of students, soldiers, businessmen, or emergency rescue workers. Below is a summary of the chapter:

- Section 7.1 : discusses previous measurement campaigns in the research literature
- Section 7.2 : overviews the measurement campaign procedure and methodology
- Section 7.3 : presents channel parameters as calculated from measurements
- Section 7.4 : summarizes the key results

The results, as well as the novel measurement technique itself, may prove extremely useful to future propagation studies and peer-to-peer wireless modem design efforts.

## 7.1 Previous Measurement Campaigns

This section discusses the primary contributions of this measurement campaign. Previous results for angular and delay dispersion are compared to values obtained in our campaign.

### 7.1.1 Contribution of this Work

In this paper, peer-to-peer channel statistics for 12 local areas are derived from over 5000 ultra-wideband power delay profile (PDP) snapshots taken by a spread-spectrum sliding correlator channel sounder with 140 MHz of radio frequency bandwidth. This measurement campaign is unique and valuable for the following reasons:

- Joint statistics involving multipath delay dispersion and angle dispersion have been measured at each local area.

- A variety of transmitter-receiver configurations – outdoor-to-outdoor, outdoor-to-indoor, and indoor-to-indoor – were measured.

- This paper introduces a new spatial probing technique that uses directional antennas and mechanical positioning, as opposed to antenna arrays. The new technique facilitates wider-band spatial channel sounding at potentially any carrier frequency in the UHF, microwave, or mm-wave bands.

- The spatial channel parameters are calculated in terms of multipath *shape factors*, one of the first such applications of the theory described in [41].

The results should prove valuable to designers of high-capacity wireless modems and future joint spatio-temporal channel measurement campaigns.

### 7.1.2 Comparison to Other Measurement Campaigns in the Literature

The first documented attempt to measure both angle-of-arrival and time-delay of mobile radio multipath components was made by Japanese researchers Ikegami and Yoshida [50]. More recent spatio-temporal results have been published in [51] and [52], although these research papers measure only a few locations and are meant largely to prove new techniques and concepts in spatio-temporal channel measurement. Pedersen, et. al. have also published delay and azimuthal dispersion results for base station antennas in urban areas [53]. Beyond these publications, the joint spatio-temporal characteristics for most types of radio channels are not conclusively measured.

While the bands around 1920 MHz has been measured extensively for cellular and PCS applications, measurements previously reported in the literature involve transmitters at least 5 meters above the ground – still much higher than a genuine peer-to-peer environment. The range of peer-to-peer outdoor delay spreads presented in this paper are much lower than typical delay spreads measured for mobile radio macrocells (2-3 $\mu$s, [54]) and are more similar to PCS microcell measurements (mean of 137 ns [55]). This is expected since the peer-to-peer mode of propagation is much more lossy than macrocellular configurations since both transmitter and receiver are close to the ground, buried within building, foliage, and terrain clutter.

Our campaign finds a similar range of outdoor RMS delay spreads (17 ns to 219 ns) to those reported by Patwari, et. al. in [56] (25 ns to 333 ns). Unlike the measurements in [56], this paper directly measures the angles-of-arrival of multipath components. Thus, delay dispersion (Section 7.3.1), angle dispersion (Section 7.3.2), and joint angle-delay statistics (Section 7.3.3) are presented for all indoor and outdoor measurement locations.

For indoor receiver locations, our measurements exhibit much lower RMS delay spreads (27-45 ns) than the outdoor locations. Devasirvatham, et. al. corroborates this result in an exhaustive indoor measurement campaign that shows delay spreads are less than 100 ns for indoor office buildings [57]. Woodward, et. al. present a set of measurements at 2.4 GHz that record angle-of-arrival and delay statistics for outdoor-to-indoor configurations. In an urban building, they show low values of RMS delay spread (mean 37 ns) but high values of RMS azimuth angle spread (89° which is 86% of the RMS azimuth spread for the uniform Clarke model) [58]. This compares favorably to our range of outdoor-to-indoor delay spreads 27-44 ns and our angle spread values which show angles-of-arrival spread out from 73-98% of the uniform Clarke model.

## 7.2 Overview of Measurement Campaign

This section provides a general overview of the measured locations, channel sounding hardware, and measurement technique used throughout the campaign.

### 7.2.1 Measured Locations

The measurement campaign was performed during November of 1999 on the campus of Virginia Tech. A total of 12 locations were measured during this campaign using the peer-to-peer configuration of transmitter and receiver antennas (both set 1.5m height above ground).

The first set of 6 measurements were outdoor-to-outdoor locations which emphasized long-distance, obstructed links with up to 1km of transmitter-receiver (TR) separation distance. The signal had to propagate over irregular campus terrain which included hills, multi-story buildings, and leafless trees.

Then, 3 indoor-to-indoor locations were measured inside a four-story office building. The same transmitter – placed inside a fourth-floor office – was used for all 3 indoor-to-indoor measurements. One receiver location was measured on the same floor as the transmitter, on the opposite side of the building. Another receiver location was measured on the ground floor, on the same side of the building as the transmitter. A third location was measured on a different floor than the transmitter *and* on the opposite side of the building.

Finally, 3 outdoor-to-indoor locations were measured using a transmitter placed 330m away from the four-story office building. One receiver location was measured on the ground floor, on the same side of the building as the transmitter. Another receiver location was measured on the fourth floor, also on the same side of the building as the transmitter. A third location on the back side of the building was measured as well. A graphical summary of the 6 indoor local area configurations may be found in Figure 7.1.

### 7.2.2 Channel Sounding Hardware

A spread spectrum sliding correlator approach was used to sound the channel (see [59] for a description). A transmitted carrier frequency of 1920 MHz was used throughout the campaign. The transmitted spread spectrum signal had a radio frequency (RF) bandwidth of 200 MHz, allowing for theoretical resolution of multipath with as little as 10ns of propagation delay. In practice, the resolution was slightly worse since we filtered the signal with a 140 MHz passband filter to remain within our licensed band of 1850-1990 MHz. Since this is an active PCS band in the U.S., the interference rejection capability of the sliding

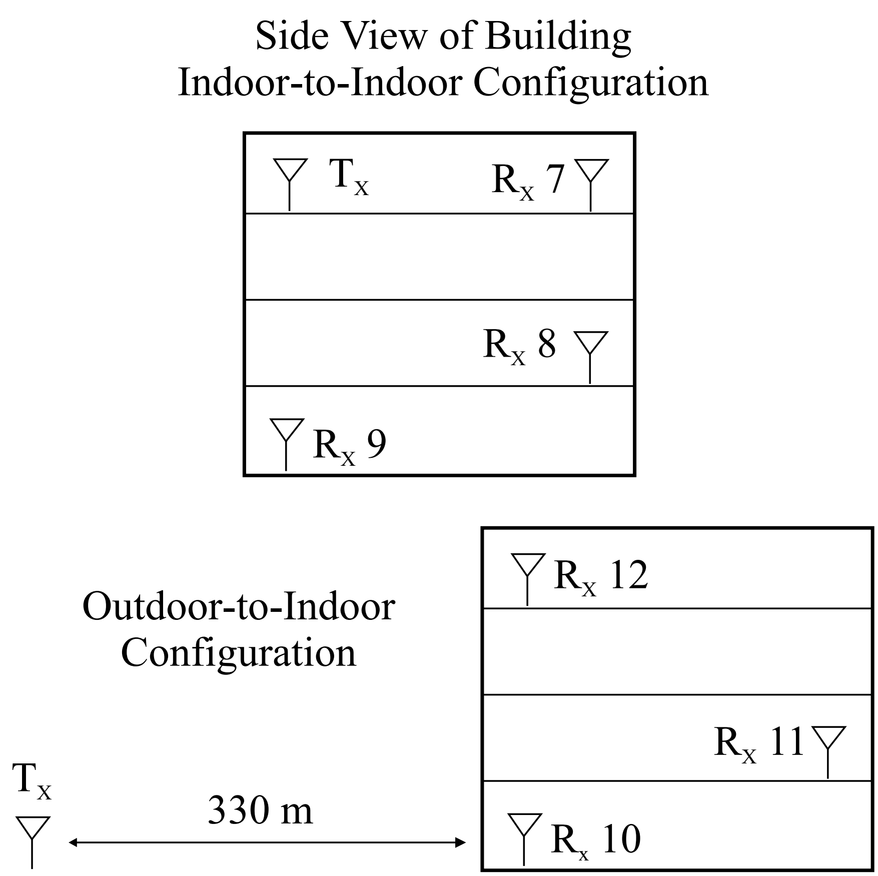


Figure 7.1: The transmitter-receiver configurations for the 6 local areas measured indoors.

correlator was particularly useful.

In order to send the channel sounding signal through the lossy peer-to-peer environment, the transmitter used a 20-watt wideband RF amplifier. Special precautions were taken to control the temperature of the RF hardware and to limit human RF exposure. Back-to-back system calibrations were performed on the transmitter and receiver units at the beginning and end of each measurement day to ensure system stability.

### 7.2.3 Automated Antenna Positioning

These measurements used a precise automated positioning system to place the receiver antenna along a linear track and, for a directional antenna, to orient the antenna with respect to azimuth. The antenna platform is positioned using stepper motors that drive a rotating table and a long serpentine-drive track. The positioning error for placement along the track is $\pm 10\mu$m and for rotation about an axis is $\pm 0.01°$ .

A laptop computer simultaneously coordinated the movement and rotation of the receiver antenna and the data acquisition from the channel sounder. This system was used to take two types of measurement sequences: *track measurements* and *rotational measurements*.

**Track Measurements:** For the track measurement sequence, an omnidirectional antenna is mounted atop the positioning table. Two linear track measurements are performed, each using different track orientations. The first orientation aligns the track along an axis (referred to as the $x$-axis) parallel to the direction of the transmitter location. The second orientation aligns the track along an axis (referred to as the $y$-axis) transverse to the direction of the transmitter location. The orientations are depicted in Figure 7.2. For each linear track measurement, snapshots of the channel PDP are taken along the length of the measurement track (about 9 wavelengths at 1920 MHz). Each PDP snapshot is spaced 0.25 wavelengths apart, producing a total of 36 snapshots per linear track measurement. Thus, a measurement along two orthogonal tracks produces a total of 72 PDP snapshots. A photograph of a track measurement is shown in Figure 7.3.

**Rotational Measurements:** The second measurement sequence at a location is a rotational measurement using a directional antenna. PDP snapshots are recorded from the channel sounder as the test antenna is rotated in steps across the entire horizon in evenly-spaced $10°$ increments. Thus, a single sweep in the rotational measurement results in a total of 36 PDP snapshots. The antenna platform is then moved along the track by 2.67 wavelengths (0.42 meters) and another series of 36 rotational PDP snapshots are recorded.

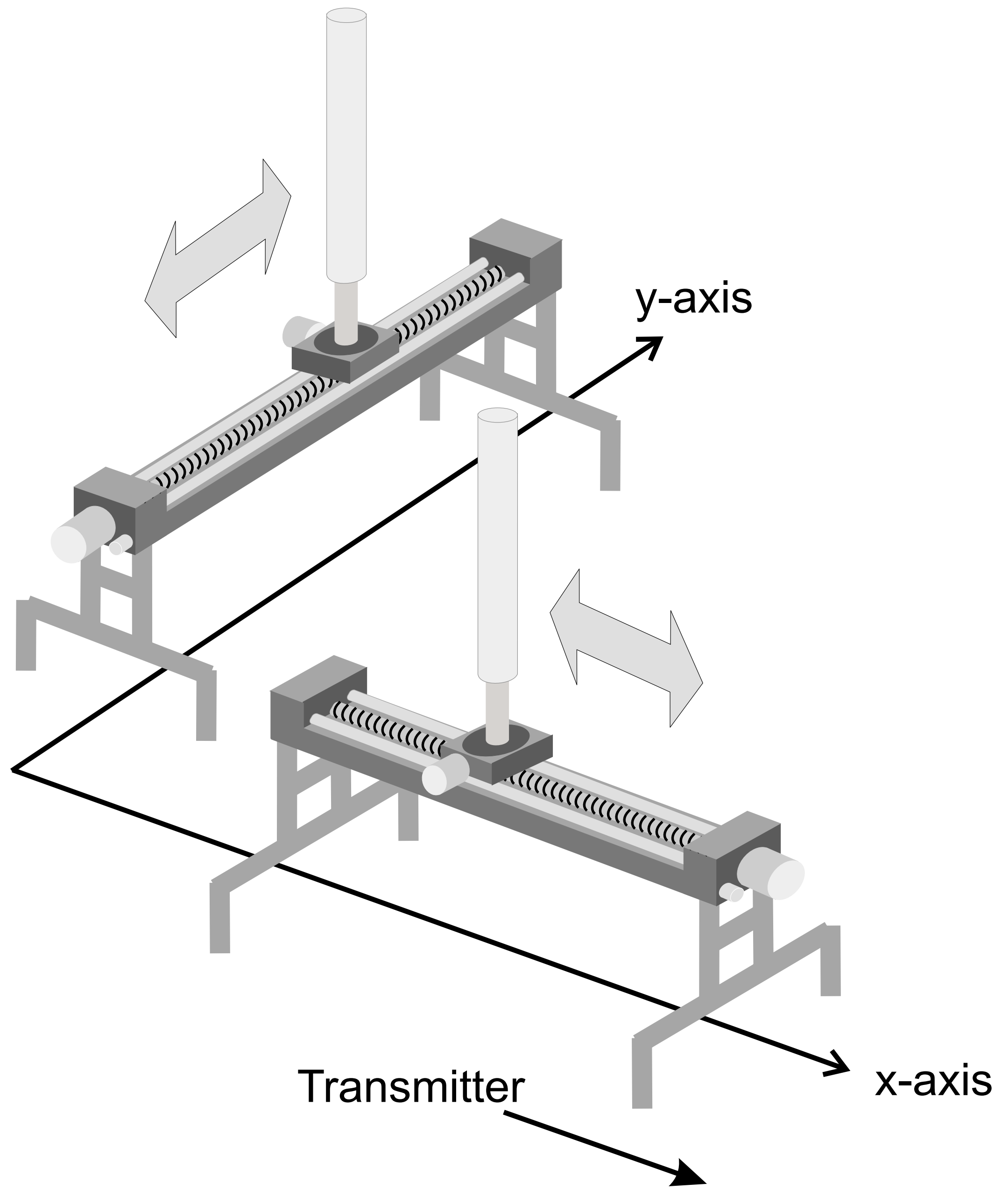


Figure 7.2: In a local area, power delay profiles are measured along two orthogonal linear tracks using an omnidirectional antenna.

Figure 7.3: A track measurement is made with an omnidirectional antenna in a campus parking lot.

This procedure is repeated until a fourth rotational measurement is made. Figure 7.4 illustrates this sequence of measurements. In all, the rotational measurement sequence results in a total of 144 PDP snapshots. A photograph of a rotational measurement is shown in Figure 7.5.

### 7.2.4 Antenna Specifications

All antennas used during this campaign had sufficient bandwidth over the 1850-1990 MHz frequencies to transmit and receive the wideband spread spectrum signal without distortion in space or time. An omnidirectional PCS base station antenna made by Andrew Corporation was used at the transmitter. This antenna had a gain of 8 dBi along the horizon – the direction of peak gain for the elevation pattern. This same type of antenna was also used at the receiver for the track measurements.

The rotational measurements used a directional horn antenna. The horn antenna had a gain of 15 dBi and a half-power beamwidth of 30° . All antennas used at the receivers are elevated to 1.5m height using poly-vinyl chloride masts to minimize scattering from the positioning track to the receiver antenna.

### 7.2.5 Sources of Error in the Experiment

Great care was taken to minimize (but not necessarily remove) the primary sources of error in this experiment. These sources of error are

- **Channel Transients:** Objects moving within the channel during the acquisition time of a PDP may distort the channel measurements. This effect is most pronounced outdoors, where even a slight breeze will rustle the leaves of trees and introduce small-but-noticeable fluctuations to all of the measured multipath components. In November, however, all of the deciduous trees had lost their leaves so this effect was largely absent from the data set in this paper.

- **Self-Scattering Effects:** A large number of people and measurement equipment in the immediate area of the receiver may scatter multipath power to the receiver antenna that would be unrealistic for a real-life scenario. To remove this effect from each of the measurements, all personnel were evacuated from the immediate receiver area, the channel sounding hardware was kept as low to the ground as possible, and the receiver antenna was elevated above the positioning system so as to operate in an area of uncluttered free space.

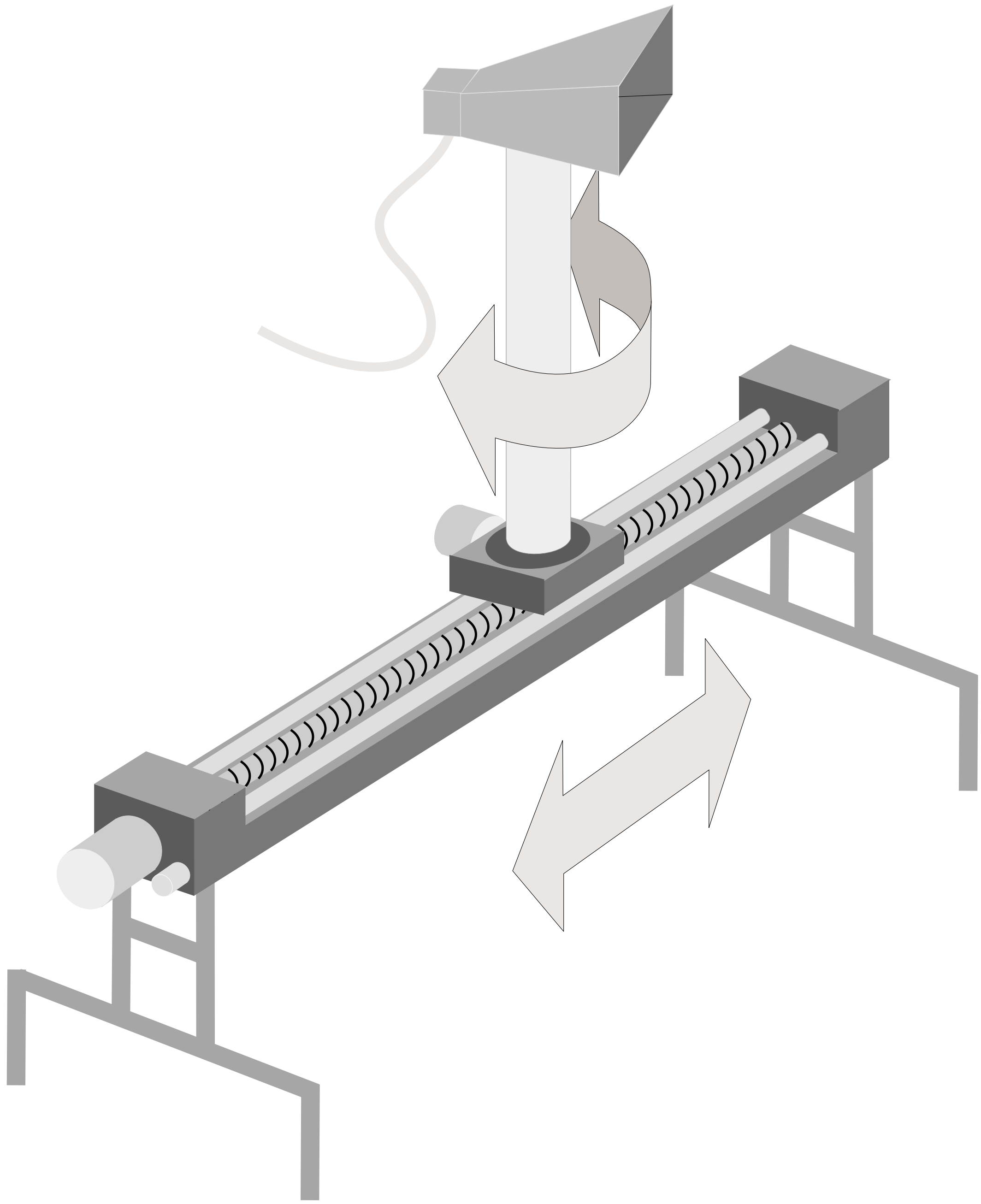

Figure 7.4: In a local area, power delay profiles are measured by spatially averaging angular sweeps with a directional antenna.

Figure 7.5: A rotational measurement is made with a directional horn antenna in the lobby of an office building.

- **Finite Sampling:** Due to finite sampling of PDP snapshots in a local area, all dispersion statistics derived from these measurements will be approximate. However, no single delay statistic presented in this paper was calculated from fewer than 36 PDP snapshots and no single angle-of-arrival statistic from fewer than 144 snapshots. The large number of snapshots per statistic produces reliable results.

## 7.3 Results

This section presents the delay dispersion, angle dispersion, and joint angle and delay statistics calculated from the measurement campaign. For a mathematical description and explanation of each channel parameter discussed, refer to Appendix 7.A.

### 7.3.1 Delay Dispersion Results

Table 7.1 records all of the dispersion results for the 12 measured locations. This table records delay spread, centroid jitter, centroid standard deviation, timing jitter, and timing standard deviation for PDP's measured along orthogonal tracks. The results are calculated from the numerous series of PDP snapshots calculated during a track measurement. One such collection of snapshots is illustrated in Figure 7.6.

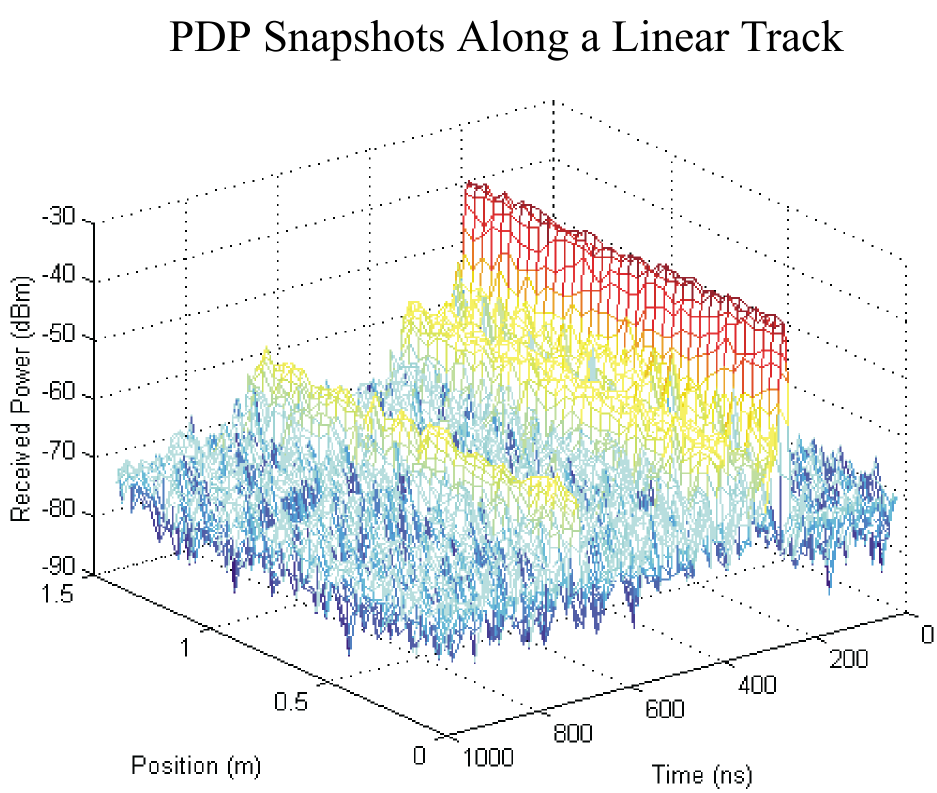


Figure 7.6: A series of PDP snapshots along a track, measured with an omnidirectional receiver antenna.

For outdoor-to-outdoor links, the delay spreads in Table 7.1 range as low a 17 ns to as high as 219 ns. Low values for delay spread are found at location 4, the only line-of-sight link in the outdoor-to-outdoor measurements, as well as locations 5 and 6. It should be

Table 7.1: Summary of dispersion statistics calculated from track measurements.

| | Parallel Track | | | | | Transverse Track | | | | |
|---|---|---|---|---|---|---|---|---|---|---|
| Location | Delay Spread | Centroid Jitter | Centroid Std. Dev. | Timing Jitter | Timing Std. Dev. | Delay Spread | Centroid Jitter | Centroid Std. Dev. | Timing Jitter | Timing Std. Dev. |
| 1 | 164 ns | 118 ns | 34 ns | 128 ns | 37 ns | 138 ns | 95 ns | 22 ns | 146 ns | 30 ns |
| 2 | 196 | 89 | 22 | 90 | 20 | 148 | 101 | 23 | 101 | 26 |
| 3 | 185 | 115 | 23 | 53 | 13 | 219 | 84 | 24 | 71 | 18 |
| 4 | 55 | 17 | 4 | 24 | 6 | 22 | 15 | 4 | 20 | 5 |
| 5 | 51 | 38 | 11 | 51 | 12 | 40 | 25 | 7 | 35 | 9 |
| 6 | 25 | 8 | 2 | 16 | 4 | 17 | 6 | 2 | 10 | 3 |
| 7 | 30 | 33 | 8 | 13 | 4 | 29 | 26 | 6 | 18 | 4 |
| 8 | 45 | 29 | 5 | 24 | 6 | 45 | 29 | 7 | 20 | 5 |
| 9 | 44 | 40 | 11 | 25 | 6 | 42 | 31 | 8 | 25 | 6 |
| 10 | 28 | 10 | 2 | 25 | 6 | 31 | 47 | 12 | 39 | 11 |
| 11 | 35 | 37 | 10 | 46 | 10 | 44 | 46 | 12 | 44 | 12 |
| 12 | 43 | 39 | 9 | 40 | 8 | 27 | 31 | 7 | 31 | 7 |
| Average | 75 | 48 | 12 | 44 | 11 | 67 | 45 | 11 | 47 | 11 |
| Std. Dev. | 62 | 36 | 9 | 32 | 9 | 62 | 30 | 7 | 39 | 8 |

noted that the values in Table 7.1 are comparable to delay spreads measured by Patwari in [56] (from 25 ns to 333 ns), despite the increased average link distances. In fact, the correlation between delay spread and TR separation is weak. For example, the longest obstructed link – location 5 with 910 m of TR separation – has one of the smallest delay spreads at an average of 46 ns.

Delay spreads for indoor receivers demonstrate much more homogeneous behavior, independent of whether the transmitter is indoors or outdoors. The twelve indoor delay spreads (2 for each track for locations 7-12) fall within a 27-45 ns range. Thus, a much simpler equalizer may be used if the radio is guaranteed to be operating indoors.

A final observation should be made about the variability of the delay spread about its mean value within a local area. The value *Timing Jitter* represents the difference between the smallest and largest delay spreads measured along a track. The value *Timing Standard Deviation* measures the mean-squared variation about the average delay spread in a local area. Both Timing Jitter and Timing Standard Deviation measure the variability of delay spread within a local area, but the Timing Standard Deviation may appear to be a better measure of typical behavior since it de-emphasizes the extreme cases of measured delay spread (see Appendix 7.A). However, as Table 7.1 shows, the Timing Jitter is almost always related to the Timing Standard Deviation by a factor of 4. This relationship is completely independent of delay spread or measurement environment. A similar relationship holds between the Centroid Jitter and the Centroid Standard Deviation.

### 7.3.2 Angle Dispersion Results

A number of other multipath parameters may also be calculated from the measured track and rotational data. Table 7.2 records transmitter-receiver separation distance, path loss with respect to 1m free space, the angular spread, and the peak multipath direction of arrival. An example of a measured angle-delay profile is shown in Figure 7.7.

One trend that is apparent from Table 7.2 is in the peak direction of multipath arrival. This parameter measures the direction in azimuth that the horn antenna was pointing when the maximum total power was received. According to Table 7.2, the peak direction of multipath arrival is almost always in the direction of the transmitter (corresponding to $0^\circ$). This is true even for obstructed receiver locations. The one exception in Table 7.2 is location 9, where the peak direction of multipath arrival is $140^\circ$. However, location 9 is an indoor location corresponding to an indoor transmitter that is nearly directly above the receiver, with two floors in between. Given this unique location, the deviation from the trend is understandable. This property of the peak multipath arrival angle implies the

Table 7.2: Summary of spatial multipath parameters calculated from spatially-averaged azimuthal sweeps of a horn antenna.

| Location | Path Loss w.r.t. 1m FS | TR Sep Dist. | Angular Spread | Angular Constriction | Angle of Max. Fading | Peak Mult. Arrival |
|---|---|---|---|---|---|---|
| 1 | 90 dB | 770 m | 0.82 | 0.69 | 44° | 0° |
| 2 | 51 | 550 | 0.65 | 0.44 | -63° | 0° |
| 3 | 39 | 240 | 0.91 | 0.51 | 36° | 20° |
| 4 | 81 | 585 | 0.52 | 0.77 | 89° | 0° |
| 5 | 72 | 910 | 0.46 | 0.70 | 76° | -10° |
| 6 | 83 | 410 | 0.36 | 0.76 | 85° | 0° |
| 7 | 70 | 29 | 0.73 | 0.52 | 84° | -10° |
| 8 | 82 | 33 | 0.74 | 0.50 | 30° | 30° |
| 9 | 76 | 15 | 0.90 | 0.33 | -74° | 140° |
| 10 | 65 | 340 | 0.78 | 0.72 | 85° | 0° |
| 11 | 84 | 365 | 0.86 | 0.19 | -46° | 10° |
| 12 | 85 | 340 | 0.98 | 0.42 | -38° | -50° |
| Average | 73 | – | 0.73 | 0.55 | – | 11° |
| Std. Dev. | 15 | – | 0.19 | 0.19 | – | 43° |

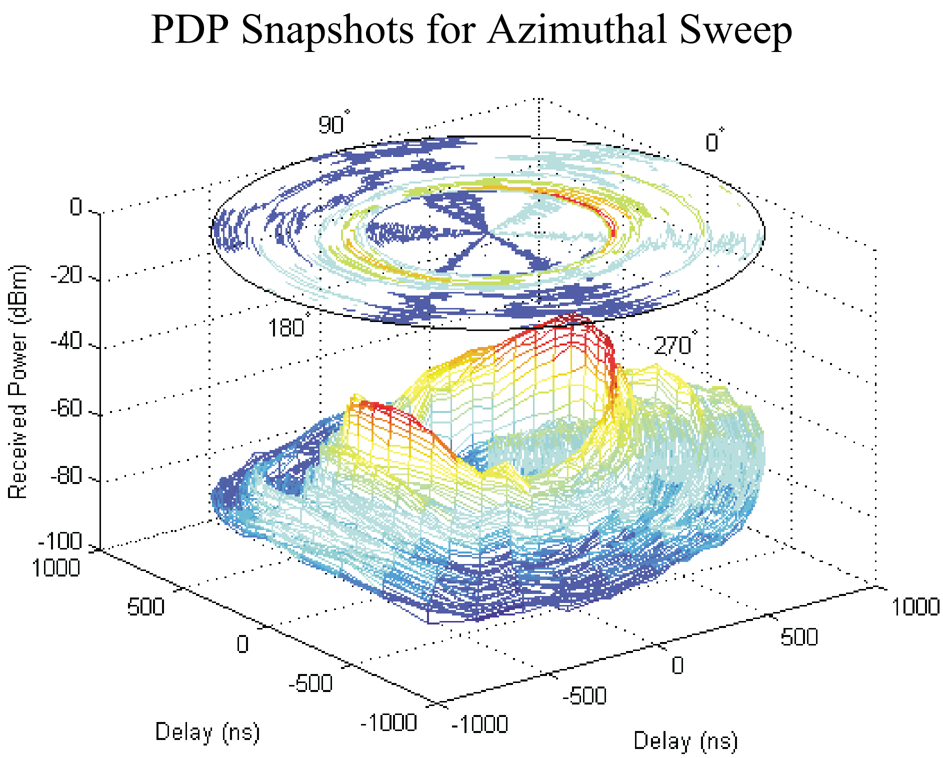


Figure 7.7: A local area angle-delay spectrum as measured from a set of rotational measurements.

effectiveness of simple direction-finding algorithms.

Another trend may be observed in the angular spread data. For indoor receivers at locations 7-12, the angular spread falls within the range 0.73-0.98. Thus, indoor angular spread values are almost always near the maximum value of 1.00. For outdoor receivers at locations 1-6, the angular spread falls within a lower range of 0.36-0.91. Thus, an omnidirectional fading model for narrowband fading such as the Clarke model in [13] is not accurate for long-distance peer-to-peer links. The increase in angular spread indoors as opposed to outdoors may be explained by the increased density of scatterers (doors, walls, shelves, etc.) in all directions in an indoor environment.

Still another trend may be observed in the angular constriction data. From Table 7.2, we see that the average value for angular constriction, $\gamma$, is 0.55. This fairly large value indicates that multipath power is clustering about a few directions instead of being uniformly spread out. This is another indication that idealized, uniform multipath models may not characterize the spatial fading behavior for the peer-to-peer channel.

### 7.3.3 Joint Angle-Delay Statistics

The graph in Figure 7.8 shows angular spread vs. delay spread for the 12 measured local areas. We would expect that higher delay spreads indicate more multipath components from a larger variety of scattering mechanisms; under these circumstances, the angular spread should increase as well. While counterexamples certainly exist, most of the measured points in Figure 7.8 follow this basic trend.

Note that the *rate* at which angular spread increases as a function of delay spread depends heavily on whether the receiver is indoors or outdoors. To study this effect quantitatively, we propose the following empirical guideline for angular spread, $\Lambda$, as a function of delay spread, $\sigma_\tau$:

$$\Lambda \approx \exp\left(-\frac{\sigma_c}{\sigma_\tau}\right) \tag{7.1}$$

The critical delay spread, $\sigma_c$, is the key parameter in Eqn (7.1) for determining the rate of angular spread increase. The critical delay spread may be calculated using linear regression on a set of measurement points, $(-\ln\Lambda, \frac{1}{\sigma_\tau})$. The six indoor points produce a critical delay spread value of 7.4 ns, while the six outdoor points produce a much larger $\sigma_c$ of 32.5 ns. Plots of Eqn (7.1) for these two critical delay spreads are shown in Figure 7.8.

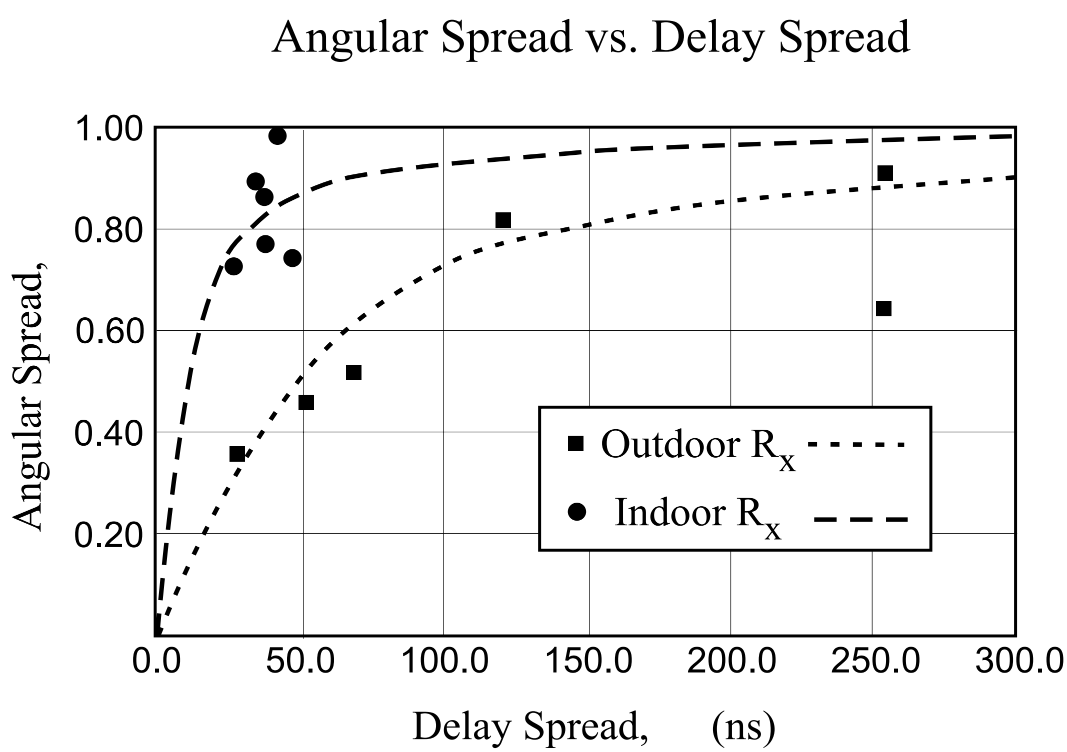


Figure 7.8: The trend between angle spread and delay spread for indoor and outdoor receivers.

## 7.4 Conclusions

This chapter presented a novel technique and quantitative results for measuring 1920 MHz peer-to-peer spatio-temporal radio channels. Angle and delay dispersion data were recorded for outdoor-to-outdoor, outdoor-to-indoor, and indoor-to-indoor transmitter-receiver configurations. This data set illuminates many of the following previously unmeasured, hypothetical trends in the peer-to-peer radio channel:

1. RMS delay spread for outdoor-to-outdoor channels locations is an order of magnitude lower than PCS macrocellular radio channels, primarily due to the reduced transmitter antenna height.

2. RMS delay spread for outdoor-to-indoor and indoor-to-indoor channels drops to around 35ns – much lower than the outdoor-to-outdoor case.

3. Angular spread as measured at the receiver is higher for indoor receivers and lower for outdoor receivers.

4. A distinct, quantified trend emerged that shows how angular spread increases as delay spread increases.

5. Angular *constriction* is relatively high for all peer-to-peer channels, indicating that much of the multipath power is arriving from several discrete directions in azimuth instead of across a smooth, wide continuum of azimuthal angles.

These quantified data trends will help engineers develop new spatio-temporal channel models and design wireless modems for radios operating in the peer-to-peer network configuration.

## 7.A Description of Measured Parameters

This appendix defines the terminology and parameters used in the analysis of the wideband, space-varying channels. The appendix provides a quick, comprehensive summary of all measured parameters and terminology.

### 7.A.1 Noncoherent Channel Measurements

The wideband radio channel is measured as a function of space in this campaign using a *single-channel, noncoherent receiver*. Below is a list of terminology used to describe the types of channels measured during this campaign.

**Channel Impulse Response (CIR):** The CIR is the complex baseband representation of the radio channel, $\tilde{h}(\tau, \vec{r})$. The CIR varies as a function of time-delay, $\tau$, and vector position of receiver antenna in space, $\vec{r}$. If a directional antenna is used at the receiver, the CIR may also depend on the azimuthal orientation of the antenna, $\theta$.

**Power Delay Profile (PDP):** A noncoherent channel measures a PDP instead of a CIR. The PDP has units of *power time*$^{-1}$ and is defined as the magnitude-squared of the CIR:

$$p(\tau, \vec{r}) = |\tilde{h}(\tau, \vec{r})|^2 \tag{7.2}$$

Written without a $\theta$-dependence, it may be assumed that Eqn (7.2) represents a measurement with an omnidirectional antenna.

**Power Angle Profile (PAP):** The PAP is the spatial equivalent of a PDP. The PAP has units of *power radian*$^{-1}$ and is defined as

$$p(\theta, \vec{r}) = |\tilde{h}(\theta, \vec{r})|^2 \tag{7.3}$$

Written without a $\tau$-dependence, Eqn (7.3) represents the angle-of-arrival characteristics of a narrowband channel.

**Angle-Delay Profile (ADP):** When a directional antenna at position, $\vec{r}$, and azimuthal orientation, $\theta$, is connected to a wideband noncoherent channel sounder, an ADP is measured. The ADP is defined as

$$p(\tau, \theta, \vec{r}) = |\tilde{h}(\tau, \theta, \vec{r})|^2 \tag{7.4}$$

### 7.A.2 Power Spectra

When power delay or angle profiles are linearly averaged in space, an estimate of a *power spectrum* is produced. Averaging various power profiles will produce the following power spectra:

**Delay Spectrum:** Spatially averaging a collection of PDP's measured within the same local area produces an estimate for the delay spectrum, $S_{\tilde{h}}(\tau)$, of the channel:

$$S_{\tilde{h}}(\tau) \cong \frac{1}{N}\sum_{i=1}^{N} p(\tau, \vec{r}_i) \tag{7.5}$$

where $\{\vec{r}_i\}$ is the set of measurement positions. The delay spectrum characterizes the frequency selectivity of the stochastic, time-varying radio channel [60].

**Angle Spectrum:** Spatially averaging a collection of PAP's measured within the same local area produces an estimate for the angle spectrum, $S_{\tilde{h}}(\theta)$, of the channel:

$$S_{\tilde{h}}(\theta) \cong \frac{1}{N}\sum_{i=1}^{N} p(\theta, \vec{r}_i) \tag{7.6}$$

The angle spectrum characterizes the spatial selectivity of the stochastic, space-varying radio channel [39, 41].

**Angle-Delay Spectrum:** Spatially averaging a set of full ADP's within the same local area produces an estimate for the joint angle-delay spectrum, $S_{\tilde{h}}(\tau, \theta)$:

$$S_{\tilde{h}}(\tau, \theta) \cong \frac{1}{N}\sum_{i=1}^{N} p(\tau, \theta, \vec{r}_i) \tag{7.7}$$

This joint power spectrum characterizes the full spatio-temporal randomness radio channel.

Note that the use of power spectra in channel modeling assumes radio channels that are wide-sense stationary in space and frequency over basic intervals of interest. The frequency interval of interest is the *RF bandwidth* of the transmitted signal and the spatial interval of interest is the *local area*. Definitions for the coherence bandwidth and the coherence distance of a fading radio channel are based on delay and angle spectra, respectively.

### 7.A.3 Time Delay Parameters

A number of delay dispersion parameters are measured in this campaign and reported in this paper. Each parameter is calculated for a measured local area and is defined below:

**Centroid, $\bar{\tau}$:** The centroid is the *first moment* of a delay spectrum. The $n$th moment of a spectrum is defined as

$$\overline{\tau^n} = \frac{\int\limits_{-\infty}^{+\infty} \tau^n S_{\tilde{h}}(\tau)\, d\tau}{\int\limits_{-\infty}^{+\infty} S_{\tilde{h}}(\tau)\, d\tau} \tag{7.8}$$

Thus, the centroid is Eqn (7.8) evaluated for $n = 1$.

**RMS Delay Spread, $\sigma_\tau$:** The RMS delay spread is the *second centered moment* of a delay spectrum, defined mathematically as

$$\sigma_\tau = \sqrt{\overline{\tau^2} - (\overline{\tau})^2} \tag{7.9}$$

The RMS delay spread is related to the frequency selectivity of a wideband multipath channel [61].

**Centroid Jitter:** If the centroid were calculated from a single PDP instead of the delay spectrum using the definition in Eqn (7.8), then each local area would have a set of centroids as a function of space, $\{\overline{\tau}(\vec{r}_i)\}$. The *centroid jitter* is the maximum centroid value minus the minimum centroid value measured in the same local area. This value measures range of possible centroid fluctuations within a local area.

**Centroid Standard Deviation:** This measure is defined similar to centroid jitter except it is the standard deviation of the set of centroids, $\{\overline{\tau}(\vec{r}_i)\}$, measured within the same local area. This measure is less sensitive to pathological instances of centroid measured at one or two points.

**Timing Jitter:** This parameter, defined by Devasirvatham in [62], is based on the set of instantaneous RMS delay spreads, $\{\sigma_\tau(\vec{r}_i)\}$, calculated from PDP's in a local area. The timing jitter is the maximum delay spread minus the minimum delay spread measured in the same local area. This value measures the range of possible RMS delay spread fluctuations within a local area.

**Timing Standard Deviation:** This measure is defined similar to timing jitter except it is the standard deviation of the set of RMS delay spreads, $\{\sigma_\tau(\vec{r}_i)\}$, measured within the same local area. This measure is less sensitive to pathological instances of RMS delay spread measured at one or two points.

### 7.A.4 Angle-of-Arrival Parameters

There are also several angular dispersion parameters that are measured in this campaign and reported in this paper. Each parameter is also calculated for a measured local area and defined below:

**Peak Angle of Arrival, $\theta_{\mathbf{peak}}$:** This parameter, calculated from the estimate of angle spectrum $S_{\tilde{h}}(\theta)$, is the azimuthal angle in which the largest average multipath power is received.

**Angular Spread, $\Lambda$:** This parameter ranges between 0 and 1 and describes how multipath power concentrates about a single direction-of-arrival in space, with 0 denoting perfect concentration in one direction and 1 representing no clear directional bias in arriving multipath power. The angular spread is calculated from complex Fourier coefficients of the angle spectrum:

$$F_n = \int_0^{2\pi} S_{\tilde{h}}(\theta) \exp(jn\theta)\, d\theta \tag{7.10}$$

and is mathematically defined as [40]:

$$\Lambda = \sqrt{1 - \frac{|F_1|^2}{F_0^2}} \tag{7.11}$$

This definition of angular spread is directly related to spatial selectivity in a narrowband multipath channel: larger values of angular spread imply higher spatial selectivity [63].

**Angular Constriction, $\gamma$:** This parameter also ranges between 0 and 1 and describes how multipath power concentrates about two directions-of-arrival in space, with 1 denoting perfect concentration in two directions and 0 representing no clear bias in two directions. The angular constriction is mathematically defined as [63]:

$$\gamma = \frac{|F_2 F_0 - F_1^2|}{F_0^2 - |F_1|^2} \tag{7.12}$$

Angular constriction is also directly related to spatial selectivity in a narrowband multipath channel: larger values of angular constriction imply spatial selectivity in a local area that is *anisotropic*, depending on the orientation of movement in space.

**Angle of Maximum Fading, $\theta_{\mathbf{max}}$:** This parameter represents the azimuthal direction in space that a receiver must move to experience the maximum possible spatial selectivity. It is defined to be

$$\theta_{\max} = \frac{1}{2}\arg(F_2 F_0 - F_1^2) \tag{7.13}$$

# Chapter 8

# Conclusions

This dissertation has presented a broad overview of stochastic local area channel modeling techniques. This work may be divided into roughly two parts. The first part, Chapter 2-Chapter 3, outline the basic theory and physics required to develop local area channel models that vary as a function of time, frequency, and space. The second part, Chapter 4-Chapter 7, presents many applications of this theoretical and physical framework. Applications include

- development of small-scale fading distributions
- characterization of multipath using shape factors
- development of spatio-temporal second-order channel statistics
- presentation of results from a spatio-temporal measurement campaign

Each of these applications represents a unique, original contribution to the field of channel modeling research.

There is still a tremendous amount of research to be done in the field of stochastic local area channel modeling. The theoretical framework presented in this work will serve, hopefully, as a springboard for future ideas and applications of basic channel modeling theory.

## 8.1 Future Areas of Research

Let us now close with the 5 key areas of future research in the area of stochastic local area channel modeling. Any number of these areas are capable of generating valuable dissertation topics for researchers.

### 8.1.1 Theoretical Framework

The basic theoretical framework in this dissertation deals with a unified description of wireless channels as a function of time, frequency, and position in space. There are two additional dependencies that must be added to complete the treatment:

**Transmitter Position:** The spatial position dependence that has been discussed in this work is the position of the *receiver* antenna. The most sophisticated spatial treatment of the wireless channel, however, should also include the *transmitter* antenna as well. Thus, we could write a more complete spatio-temporal channel model as

$$\tilde{h}(f, t, \vec{r}_{\mathcal{R}}, \vec{r}_{\mathcal{T}})$$

where $\vec{r}_{\mathcal{R}}$ is receiver position and $\vec{r}_{\mathcal{T}}$) is transmitter position in 3D space. This framework would allow a more in-depth study of *multiple-input, multiple-output* (MIMO) space-time coding techniques.

**Antenna Orientation and Polarization:** Another interesting addition to the theoretical framework could be the introduction of directional antennas capable of arbitrary orientation in space. While characterization of channels with directional receiver antennas is possible under the existing framework, a key assumption is that the orientation of the antenna in space remains constant. If the antenna is allowed to rotate in azimuth or tilt in space, the gain and polarization interaction with the antenna and the impinging multipath waves will change dramatically. An excellent example this type of treatment may be found in [64].

### 8.1.2 Specific Analytical Problems

The solid theoretical framework provided in the beginning chapters should provide the impetus for higher-level analytical work in channel modeling theory. Three novel examples of analytical "discoveries" that directly result from the theoretical framework were already presented: 1) the TIP PDF, 2) shape factor theory, and 3) a more powerful analysis of the level-crossing problem and unit autocovariance for Rayleigh channels. Numerous others are also possible.

For example, additional analytical research could be performed on fading PDF's, including improved representations of the TIP PDF. Deriving level-crossing statistics for Rician channels is another excellent example of much-needed analytical research. Developing unit autocovariance expressions for non-Rayleigh channels is yet another example of an unsolved problem in channel modeling, although Karasawa, et. al. have recently made some impressive progress in [65]. All of these analytical problems have more than just scholarly value, too. Their solutions directly impact the design and performance of many types of wireless technologies.

### 8.1.3 Applications to Wireless Technology

There are numerous sophisticated technologies that are ushering in the new era of broadband wireless communications that have channel-dependent performance. Exciting contributions are possible by relating basic channel statistics to the performance of these new technologies. For example, space-time coding techniques are related to spatial correlation properties which, in turn, are related to the shape factors of the multipath channel [3]. Thus, a researcher who couches the performance of space-time systems in terms of multipath geometry stands to make a tremendous contribution to wireless communications. Likewise, new broadband transmission schemes such as *orthogonal frequency division multiplexing* (OFDM) are directly affected by the second-order statistics of fading as a function of frequency [48]. A researcher who couches the performance of OFDM systems in terms of frequency level-crossing rates or correlation properties will have a powerful research legacy in wireless.

### 8.1.4 Measurement Theory

Of course, countless more spatio-temporal measurement campaigns could be performed to augment our current understanding of wireless channels in a variety of environments and transmitter-receiver configurations. Moreover, the theory of channel measurement itself could be made more rigorous. The science of channel measurement too often is dominated by ad-hoc experimentalists who measure first and ask questions later. Invention of new techniques and rigorous statistical analysis of existing methodologies are needed. The spatial probing system and analysis in Chapter 7 is just the proverbial "tip of the iceberg".

### 8.1.5 Computer Simulation

Throughout this treatment, an important topic – computer simulation of spatio-temporal channels – has been intentionally omitted. This omission was not meant to diminish the importance of simulation research. Rather, the science of computer modeling is a potentially rich and rewarding field that deserves a *tremendous* amount of detail and exposition for proper treatment. Many dissertations could be written about using the general theory developed in this work to reconstruct realistic spatio-temporal channels in the laboratory to assist wireless modem design efforts.

# Chapter 9

# Vitae

Gregory David Durgin was born in Baltimore, MD, on October 23, 1974. He received the B.S.E.E. and M.S.E.E. degrees from Virginia Tech in 1996 and 1998, respectively. He is currently working toward the Ph.D. degree at the Mobile and Portable Radio Research Group (MPRG) at the same university as a Bradley Fellow.

Since 1996, he has been a Research Assistant at MPRG, where his research focuses on radio wave propagation, channel measurement, and applied electromagnetics. He has published (as a student) 14 technical papers in international journals and conferences and 1 book chapter. He also serves regularly as a consultant to industry.

Student research awards have included the following: 1998 Blackwell Award for best graduate research presentation in the Electrical and Computer Engineering Department at Virginia Tech, 1998 Stephen O. Rice Prize as a coauthor with Theodore S. Rappaport and Hao Xu for best original paper published in IEEE Transactions on Communications, 1999 Student Paper Prize for PIMRC 99, held in Osaka, Japan.

# Bibliography

[1] L.C. Godara, “Applications of Antenna Arrays to Mobile Communications, Part I: Performance Improvement, Feasibility, and System Considerations,” *Proceedings of the IEEE*, vol. 85, no. 7, pp. 1031–1060, July 1997.

[2] J.H. Winters, “Smart Antennas for Wireless Systems,” *IEEE Personal Communications*, vol. 1, pp. 23–27, Feb 1998.

[3] G.J. Foschini, “Layered Space-Time Architecture for Wireless Communication in a Fading Environment When Using Multi-Element Antennas,” *Bell Labs Technical Journal*, pp. 41–59, Autumn 1996.

[4] P.A. Bello, “Characterization of Random Time-Variant Linear Channels,” *IEEE Transactiona on Communications Systems*, pp. 360–393, Dec 1963.

[5] H. Suzuki, “A Statistical Model for Urban Radio Propagation,” *IEEE Transactions on Communications*, vol. 25, no. 7, pp. 673–680, July 1977.

[6] A.J. Coulson, A.G. Williamson, and R.G. Vaughan, “A Statistical Basis for Lognormal Shadowing Effects in Multipath Fading Channels,” *IEEE Transactions on Communications*, vol. 46, no. 4, pp. 494–502, April 1998.

[7] M.D. Yacoub, “Fading Distributions and Co-Channel Inteference in Wireless Systems,” *Radio Science*, vol. 42, no. 1, pp. 150–158, Feb 2000.

[8] L.W. Couch, *Digital and Analog Communication Systems*, Macmillan Publishing Company, New York, 4th edition, 1993.

[9] T.M. Cover and J.A. Thomas, *The Elements of Information Theory*, John Wiley & Sons, Inc., New York, 1991.

[10] T.S. Rappaport, *Wireless Communications: Principles and Practice*, Prentice-Hall Inc., New Jersey, 1996.

[11] B.H. Fleury, "First- and Second-Order Characterization of Direction Dispersion and Space Selectivity in the Radio Channel," *IEEE Transactions on Information Theory*, vol. 46, no. 6, pp. 2027–2044, Sep 2000.

[12] P. Green Jr., "Radar Astronomy Measurement Techniques," Tech. Rep., MIT Lincoln Lab., Dec 1962.

[13] R.H. Clarke, "A Statistical Theory of Mobile-Radio Reception," *Bell System Technical Journal*, vol. 47, pp. 957–1000, 1968.

[14] P.A. Bello, "Time-Frequency Duality," *IEEE Transactions on Information Theory*, vol. IT-10, pp. 18–33, Jan 1964.

[15] G.S. Brown, "Analytical Electromagnetics (EE 6114): Course Notes," Tech. Rep., Virginia Tech, Fall 1998.

[16] M. Born and E. Wolf, *Principles of Optics: Electromagnetic Theory of Propagation, Interference, and Diffraction of Light*, Pergamon Press, New York, 6th edition, 1980.

[17] J.A. Ogilvy, *Theory of Wave Scattering from Random Rough Surfaces*, Adam Hilger, Philadelphia, 1991.

[18] G.S. Brown, "Rough Surface Scattering (EE 6104): Course Notes," Tech. Rep., Virginia Tech, Fall 1997.

[19] J.F. Ossanna, "A Model For Mobile Radio Fading Due to Building Reflections: Theoretical and Experimental Fading Waveform Power Spectra," *Bell System Technical Journal*, pp. 2935–2971, Nov 1964.

[20] W.C. Jakes, Ed., *Microwave Mobile Communications*, IEEE Press, New York, 1974.

[21] A. Papoulis, *Probability, Random Variables, and Stochastic Processes*, McGraw Hill, New York, 3rd edition, 1991.

[22] G.D. Durgin, T.S. Rappaport, and H. Xu, "Radio Path Loss and Penetration Loss Measurements in and around Homes and Trees at 5.85 GHz," *IEEE Transactions on Communications*, vol. 46, no. 11, pp. 1484–1496, Nov 1998.

[23] A. Abdi and S. Nader-Esfahani, "A General PDF for the Signal Envelope in Multipath Fading Channels Using Laguerre Polynomials," in *IEEE VTS 46th Vehicular Technology Conference*, Atlanta GA, May 1996, pp. 1428–1432.

[24] W.R. Bennett, "Distribution of the Sum of Randomly Phased Components," *Quarterly Journal of Applied Mathematics*, vol. 5, pp. 385–393, April 1948.

[25] S.O. Rice, "Mathematical Analysis of Random Noise," *Bell System Technical Journal*, vol. 23, pp. 282–332, July 1944.

[26] S.O. Rice, "Mathematical Analysis of Random Noise (continued)," *Bell System Technical Journal*, vol. 24, pp. 46–156, Jan 1945.

[27] M. Abramowitz and I.A. Stegun, Eds., *Handbook of Mathematical Functions*, Dover Publications, Inc., New York, 9th edition, 1970.

[28] I.S. Gradshteyn and I.W. Ryzhik, *Table of Integrals, Series, and Products*, Academic Press, New York, 5th edition, 1994.

[29] G.D. Durgin, T.S. Rappaport, and D.A. de Wolf, "More Complete Probability Density Functions for Fading in Mobile Communications," *49th IEEE Vehicular Technology Conference*, vol. 2, pp. 985–989, May 1999.

[30] W.D. Rummler, R.P. Coutts, and M. Liniger, "Multipath Fading Channel Models for Microwave Digital Radio," *IEEE Communications Magazine*, vol. 24, no. 11, pp. 30–42, Nov 1986.

[31] J.W. Nicholson, "Generalisation of a Theorem Due to Sonine," *Quarterly Journal of Pure and Applied Mathematics*, vol. 48, pp. 321–329, 1920.

[32] J.D. Parsons, *The Mobile Radio Propagation Channel*, John Wiley & Sons, New York, 1992.

[33] D.O. Reudink, "Properties of Mobile Radio Propagation Above 400 MHz," *IEEE Transactions on Vehicular Technology*, Nov 1974.

[34] S.O. Rice, "Statistical Properties of a Sine Wave Plus Random Noise," *Bell System Technical Journal*, vol. 27, no. 1, pp. 109–157, Jan 1948.

[35] M. Nakagami, "The m-Distribution – A General Formula of Intensity Distribution of Rapid Fading," in *Statistical Methods in Radio Wave Propagation*, W.C. Hoffman, Ed. Pergamon, Elmsford, NY, 1960.

[36] A.J. Coulson, *Characterization of the Mobile Radio Multipath Fading Channel*, Ph.D. thesis, University of Auckland, New Zealand, August 1998.

[37] W.R. Braun and U. Dersch, "A Physical Mobile Radio Channel Model," *IEEE Transactions on Vehicular Technology*, vol. 40, no. 2, pp. 472–482, May 1991.

[38] H. Stark and J.W. Woods, *Probability, Random Processes, and Estimation Theory for Engineers*, Prentice Hall, New Jersey, 2nd edition, 1994.

[39] M.J. Gans, "A Power-Spectral Theory of Propagation in the Mobile Radio Environment," *IEEE Transactions on Vehicular Technology*, vol. VT-21, no. 1, pp. 27–38, Feb 1972.

[40] G.D. Durgin and T.S. Rappaport, "A Basic Relationship Between Multipath Angular Spread and Narrowband Fading in a Wireless Channel," *IEE Electronics Letters*, vol. 34, no. 25, pp. 2431–2432, 10 Dec 1998.

[41] G.D. Durgin and T.S. Rappaport, "Theory of Multipath Shape Factors for Small-Scale Fading Wireless Channels," *IEEE Transactions on Antennas and Propagation*, vol. 48, no. 5, pp. 682–693, May 2000.

[42] G.D. Durgin and T.S. Rappaport, "Three Parameters for Relating Small-Scale Temporal Fading to Multipath Angles-of-Arrival," in *PIMRC '99*, Osaka Japan, Sep 1999, pp. 1077–1081.

[43] G.D. Durgin and T.S. Rappaport, "Effects of Multipath Angular Spread on the Spatial Cross-Correlation of Received Voltage Envelopes," in *49th IEEE Vehicular Technology Conference*, Houston TX, May 1999, vol. 2, pp. 996–1000.

[44] B.H. Fleury, "An Uncertainty Principle for WSS Processes and Its Application to WSSUS Systems," *IEEE Transactions on Communications*, vol. 44, no. 12, pp. 1632–1634, Dec 1996.

[45] H. Xu, T.S. Rappaport, R.J. Boyle, and J.H. Schaffner, "38 GHz Wideband Point-to-Multipoint Radio Wave Propagation Study for A Campus Environment," in *IEEE 49th Vehicular Technology Conference*, Houston TX, May 1999.

[46] R. Steele, *Mobile Radio Communications*, IEEE PRESS, 1994.

[47] A.M.D. Turkmani, A.A. Arowojolu, P.A. Jefford, and C.J. Kellett, "An Experimental Evaluation of the Performance of Two-Branch Space and Polarization Diversity Schemes at 1800 MHz," *IEEE Transactions on Vehicular Technology*, vol. 44, no. 2, pp. 318–326, May 1995.

[48] Y. Wu and W.Y. Zou, "Orthogonal Frequency Division Multiplexing: A Multi-carrier Modulation Scheme," *IEEE Transactions on Consumer Electronics*, vol. 41, no. 3, pp. 392–399, Aug 1995.

[49] A.R. Calderbank, G. Pottie, and N. Seshadri, "Cochannel Interference Suppression Through Time/Space Diversity," *IEEE Transactions on Information Theory*, vol. 46, no. 3, pp. 922–932, May 2000.

[50] F. Ikegami and S. Yoshida, "Analysis of Multipath Propagation Structure in Urban Mobile Radio Environments," *IEEE Transactions on Antennas and Propagation*, vol. 28, pp. 531–537, July 1980.

[51] J. Fuhl, J.-P. Rossi, and E. Bonek, "High-Resolution 3D Direction-of-Arrival Determination for Urban Mobile Radio," *IEEE Transactions on Antennas and Propagation*, vol. 45, no. 4, pp. 672–682, April 1997.

[52] J.-P. Rossi, J.-P. Barbot, and A.J. Levy, "Theory and Measurement of the Angle of Arrival and Time Delay of UHF Radiowaves Using a Ring Array," *IEEE Transactions on Antennas and Propagation*, vol. 45, no. 5, pp. 876–884, May 1997.

[53] K.I. Pedersen, P.E. Mogensen, and B.H. Fleury, "A Stochastic Model of the Temporal and Azimuthal Dispersion Seen at the Base Station in Outdoor Propagation Environments," *IEEE Transactions on Vehicular Technology*, vol. 49, no. 2, pp. 437–447, March 2000.

[54] S.Y. Seidel, T.S. Rappaport, S. Jain, M.L. Lord, and R. Singh, "Path Loss, Scattering, and Multipath Delay Statistics in Four European Cities for Digital Cellular and Microcellular Radiotelephone," *IEEE Transactions on Vehicular Technology*, vol. 40, no. 4, pp. 721–730, Nov 1991.

[55] M.J. Feuerstein, K.L. Blackard, T.S. Rappaport, S.Y. Seidel, and H.H. Xia, "Path Loss, Delay Spread, and Outage Models as Functions of Antenna Height for Microcellular System Design," *IEEE Transactions on Antennas and Propagation*, vol. 43, no. 3, pp. 487–498, Aug 1994.

[56] N. Patwari, G.D. Durgin, T.S. Rappaport, and R.J. Boyle, "Peer-to-Peer Low Antenna Outdoor Radio Wave Propagation at 1.8 GHz," in *49th IEEE Vehicular Technology Conference*, Houston TX, May 1999, vol. 1, pp. 371–375.

[57] D.M.J. Devasirvatham, R.R. Murray, and C. Banerjee, "Time Delay Spread Measurements at 850 MHz and 1.7 GHz Inside a Metropolitan Office Building," *IEE Electronics Letters*, vol. 25, no. 3, pp. 194–196, 2 Feb 1989.

[58] G. Woodward, I. Oppermann, and J. Talvitie, "Outdoor-Indoor Temporal & Spatial Wideband Channel Model for ISM Bands," in *49th IEEE Vehicular Technology Conference*, Houston TX, May 1999, pp. 136–140.

[59] W.G. Newhall, K. Saldanha, and T.S. Rappaport, "Using RF Channel Sounding Measurements to Determine Delay Spread and Path Loss," *RF Design*, pp. 82–88, Jan 1996.

[60] G.D. Durgin and T.S. Rappaport, "Spatial Channel Modeling for Wireless Communications," in *Wireless Communications for the New Millenium*, S. Sampei, Ed. Kluwer, Tokyo, 2000.

[61] J.C.-I. Chuang, "The Effects of Time Delay Spread on Portable Radio Communications Channels with Digital Modulation," *IEEE Journal on Selected Areas in Communications*, vol. SAC-5, no. 5, pp. 879–889, June 1987.

[62] D.M.J. Devasirvatham, "A Comparison of Time Delay Spread and Signal Level Measurements Within Two Dissimilar Office Buildings," *IEEE Transactions on Antennas and Propagation*, vol. AP-35, no. 3, March 1987.

[63] G.D. Durgin and T.S. Rappaport, "Level Crossing Rates and Average Fade Duration of Wireless Channels with Spatially Complicated Multipath," in *Globecom '99*, Brazil, Dec 1999.

[64] R.G. Vaughan, "Pattern Rotation and Translation in Uncorrelated Source Distributions for Multiple Antenna Beam Design," *IEEE Transactions on Antennas and Propagation*, vol. 46, no. 7, pp. 982–990, July 1998.

[65] Y. Karasawa and H. Iwai, "Formulation of Spatial Correlation Statistics in Nakagami-Rice Fading Environments," *IEEE Transactions on Antennas and Propagation*, vol. 48, no. 1, pp. 12–18, Jan 2000.